



**A University of Sussex DPhil thesis**

Available online via Sussex Research Online:

<http://sro.sussex.ac.uk/>

This thesis is protected by copyright which belongs to the author.

This thesis cannot be reproduced or quoted extensively from without first obtaining permission in writing from the Author

The content must not be changed in any way or sold commercially in any format or medium without the formal permission of the Author

When referring to this work, full bibliographic details including the author, title, awarding institution and date of the thesis must be given

Please visit Sussex Research Online for more information and further details

# **Regulatory Analysis of *Fgf3* and *Fgf10* and the Role of Retinoids in their Control**

---

Stephanie Cadot

Submitted for the degree of PhD

University of Sussex

March 2013

# DECLARATION

---

I, Stephanie Cadot, hereby declare that this thesis has not been and will not be, submitted in whole or in part to another University for the award of any other degree. However, the thesis incorporates to the extent indicated below\*, material already submitted as part of required course work and for the degree of:

Master in Biology at University Joseph Fourier, Grenoble (2008)

\*Figure 3.9 includes previously submitted pictures of 7.75, 9.5 and 10.5dpc embryos

\*Figure 4.10 is a previously submitted schematic

\*Figure 4.11 is a modified version of a previously submitted result figure

# ABSTRACT

---

With 9 million people in the UK alone suffering from deafness or hearing impairment, there is a concerted effort to develop effective treatments. To address this, one strategy is to recruit mechanisms naturally occurring during inner ear development, but this first requires a clear picture of the normal molecular mechanisms underlying this developmental process.

Fibroblast growth factors (FGFs) are short-range extracellular signalling molecules, with *Fgf3* and *Fgf10* already shown to be critical for the earliest event of inner ear induction. Interestingly these ligands are also expressed in the inner ear itself, and mutations in both *Fgf3* and *Fgf10* have independently been linked to sensorineural deafness in humans. This project is focused on unravelling the molecular mechanisms controlling their expression in the inner ear.

Bioinformatic analysis of the *Fgf3* and *Fgf10* enhancer regions revealed the presence of putative binding sites for retinoic acid (RA). RA is a key signalling molecule in inner ear development with both excess and deficit leading to inner ear abnormalities. First, a novel, non-invasive method of RA administration via sugar pellet was tested and proved to be an efficient and reliable alternative to gavage. Using an *Fgf3-lacZ* reporter mouse, the effects of RA excess on *Fgf3* expression were investigated in detail. In addition, preliminary studies of the effects of RA on *Fgf10* were also carried out. Both *Fgf3* and *Fgf10* were downregulated with high doses of RA, confirming previous in vitro studies. In addition, detailed analysis of *Fgf3-lacZ* embryos exposed to RA revealed that downregulation critically depends on the dose and time of administration.

To further explore other direct regulators of *Fgf10* expression, additional reporter constructs were also generated for functional analysis in mouse and in chick. To date, analysis of electroporated chick embryos shows that ear specific *Fgf10* regulation may not be conserved between these two species.

# TABLE OF CONTENTS

---

<b>ABBREVIATIONS</b>	<b>12</b>
<b>1 INTRODUCTION</b>	<b>13</b>
1.1 Ear structure and function .....	14
1.2 Development of the mammalian inner ear .....	22
1.3 The role of FGFs in inner ear development .....	31
1.4 Retinoic acid signalling .....	39
1.5 Other putative upstream regulators of <i>Fgf10</i> .....	49
1.6 Treating hearing impairment .....	52
1.7 Project aims .....	54
<b>2 MATERIAL AND METHODS</b>	<b>55</b>
2.1 Mouse genotyping .....	55
2.2 Retinoic acid administration to pregnant mice .....	59
2.3 Staining embryos for $\beta$ -Galactosidase activity .....	62
2.4 Histological methods .....	63
2.5 General DNA manipulation .....	63
2.6 Reporter vectors .....	71
2.7 <i>Fgf10</i> reporter constructs .....	74
2.8 In situ hybridization .....	78
2.9 Immunohistochemistry .....	81
2.10 Chick otic vesicle electroporation .....	82
2.11 Mouse pronuclear injections .....	83

<b>3</b>	<b>RETINOID CONTROL OF FGF3 EXPRESSION</b>	<b>85</b>
3.1	Development of an improved method for RA administration .....	86
3.2	Validation of the new protocol for administering RA using sugar pellets .....	87
3.3	<i>Fgf3</i> expression in 9.5dpc embryos exposed to RA at 7.75dpc .....	91
3.4	RA-induced downregulation of <i>Fgf3</i> expression is maintained at 10.5dpc .....	99
3.5	Semi-quantitative analysis of downregulation of otic <i>Fgf3</i> expression .....	101
3.6	<i>Fgf3</i> expression in 9.5dpc embryos exposed to RA at 8.5dpc .....	104
3.7	Generation of RA-induced phenotypes in other organ systems .....	109
3.8	<i>Fgf3/Fgf10</i> crossregulation .....	111
<b>4</b>	<b>INVESTIGATING FGF10 TRANSCRIPTIONAL REGULATION</b>	<b>115</b>
4.1	The endogenous <i>Fgf10</i> expression pattern .....	115
4.2	Generation of <i>Fgf10</i> -reporter constructs for analysis in mice .....	118
4.3	Candidate upstream regulators of <i>Fgf10</i> expression .....	132
4.4	Reporter constructs to investigate <i>Fgf10</i> regulation by the <i>Ngn1</i> pathway ...	140
4.5	Generation and analysis of an <i>Fgf10</i> -reporter transgenic mouse line .....	153
4.6	Investigation of mouse <i>Fgf10</i> regulation in the chick inner ear .....	157
4.7	Regulation of <i>Fgf10</i> by retinoic acid .....	169
<b>5</b>	<b>DISCUSSION</b>	<b>172</b>
5.1	Regulation of <i>Fgf3</i> by retinoids .....	172
5.2	Regulatory analysis of <i>Fgf10</i> .....	192
5.3	Conclusion .....	202
	<b>APPENDIX</b>	<b>204</b>
	<b>BIBLIOGRAPHY</b>	<b>222</b>

# TABLE OF FIGURES

---

Figure 1.1 Gross anatomy of the ear .....	15
Figure 1.2 Structure of the inner ear .....	18
Figure 1.3 Transduction of sound-induced vibration into neural signals .....	20
Figure 1.4 <i>Fgfs</i> expression during inner ear induction in mouse .....	24
Figure 1.5 A model of otic patterning and axis specification .....	24
Figure 1.6 Inner ear development .....	28
Figure 1.7 FGFs signalling .....	33
Figure 1.8 Retinoic acid signalling .....	40
Figure 1.9 RA synthetic/catabolic enzymes and nuclear receptors distribution in the developing inner ear .....	40
Figure 1.10 Differential effects of RA on hindbrain signalling .....	46
Figure 1.11 Conceptual drawing of a normal, damaged and repaired organ of Corti...	53
Figure 2.1 Genotyping of <i>Fgf10</i> knockout embryos .....	56
Figure 2.2 pZsGreen1-1 vector .....	72
Figure 2.3 pDsRed-Express2-1 vector .....	72
Figure 2.4 PCR primers location within the 7.0kb <i>Fgf10</i> upstream region .....	74
Figure 3.1 Dose-dependant embryo malformations following RA administration via sugar pellets .....	89
Figure 3.2 Analysis of <i>Fgf3-lacZ</i> expression pattern in 9.5dpc embryos following administration of increasing doses of RA at 7.75dpc .....	92
Figure 3.3 Effect of RA on otic <i>Fgf3</i> expression following administration at 7.75dpc...	96
Figure 3.4 Early time course of <i>Fgf3-lacZ</i> expression .....	98
Figure 3.5 Effects of RA exposure at 7.75dpc on 10.5dpc embryos .....	100
Figure 3.6 Image analysis of <i>Fgf3</i> expression in the 9.5dpc otic vesicle exposed to increasing doses of RA at 7.75dpc .....	102
Figure 3.7 Effects of RA administration after hindbrain patterning .....	105

Figure 3.8 Image analysis of <i>Fgf3</i> expression in the 9.5dpc otic vesicle exposed to increasing doses of RA at 8.5dpc .....	108
Figure 3.9 Generation of identical RA phenotypes using gavage or sugar pellets in other organ systems .....	110
Figure 3.10 Wholemout analysis of early <i>Fgf3-lacZ</i> expression in a <i>Fgf10</i> null background .....	113
Figure 3.11 Analysis of early <i>Fgf3-lacZ</i> expression on sections in a <i>Fgf10</i> null background .....	113
Figure 4.1 Early <i>Fgf10</i> mRNA expression in the developing mouse embryo .....	117
Figure 4.2 Schematic of the <i>Fgf10</i> upstream region and constructs generated .....	119
Figure 4.3 The 7F7R- <i>DsRed</i> reporter construct .....	120
Figure 4.4 Reconstruction of the 7F7R enhancer .....	122
Figure 4.5 Modification of the pDsRed-Express2-1 reporter vector .....	124
Figure 4.6 The 7F3F-3R7R- <i>ZsGreen</i> reporter construct .....	125
Figure 4.7 Generation of a 7F7R enhancer specifically deleted from 3F3R .....	127
Figure 4.8 The 7F3F and 3R7R- <i>DsRed</i> reporter constructs .....	129
Figure 4.9 Generation of the 7F3F- <i>DsRed</i> construct .....	130
Figure 4.10 Generation of the 3R7R- <i>DsRed</i> construct .....	131
Figure 4.11 Generation and trial of <i>Gata3</i> riboprobes .....	134
Figure 4.12 Early pattern of <i>Gata3</i> expression in the developing inner ear .....	136
Figure 4.13 Presence of conserved putative binding sites for neurogenic factors upstream <i>Fgf10</i> .....	138
Figure 4.14 Comparative analysis of <i>NeuroD</i> and <i>Fgf10</i> expression in wholemout in situ mouse embryos at 9.5dpc and 10.5dpc .....	138
Figure 4.15 The Neuro2.5- <i>DsRed</i> reporter construct .....	140
Figure 4.16 Generation of a Neuro2.5- <i>DsRed</i> reporter construct .....	142
Figure 4.17 The Neuro1.1- <i>DsRed</i> reporter construct .....	144
Figure 4.18 Generation of a Neuro1.1- <i>DsRed</i> reporter construct .....	145
Figure 4.19 The 3F-Neuro- <i>DsRed</i> reporter construct .....	148
Figure 4.20 Generation of 3F-Neuro- <i>DsRed</i> construct .....	149
Figure 4.21 The 7F-Neuro- <i>DsRed</i> reporter construct .....	151
Figure 4.22 Generation of 7F-Neuro- <i>DsRed</i> construct .....	152

Figure 4.23 Genotyping and in vivo analysis of 7F7R- <i>DsRed</i> transgenic mice .....	154
Figure 4.24 MiniBglobin- <i>ZsGreen</i> and MiniZsGreen- <i>DsRed</i> reporter vectors .....	159
Figure 4.25 Electroporation of mouse <i>Fgf10</i> constructs in chick using a dual reporter system .....	161
Figure 4.26 Regulation of <i>Fgf10</i> mouse enhancers in chick .....	164
Figure 4.27 Effect of exogenous RA administration on <i>Fgf10</i> expression .....	170
Figure 5.1 Effects of RA and FGFs signalling on the expression of anterior and posterior otic genes .....	182
Figure 5.2 Model of exogenous retinoic acid effect on otic patterning .....	189
Figure S1 Annotated sequence of the 7.4kb upstream <i>Fgf10</i> .....	204

# TABLE OF TABLES

---

Table 2.1 Set of primers used for the genotyping of the 4 transgenic mice lines used in this study .....	56
Table 2.2 PCR conditions for <i>LacZ</i> genotyping .....	57
Table 2.3 Standard PCR conditions .....	58
Table 2.4 PCR reaction mix for genotyping of <i>Fgf10<sup>neo</sup></i> embryos .....	58
Table 2.5 Reaction mix for blunting using T4 DNA polymerase .....	64
Table 2.6 Plasmid dephosphorylation reaction mix .....	65
Table 2.7 Typical ligation set up .....	67
Table 2.8 List of primers used to generate <i>Fgf10</i> enhancer fragments .....	74
Table 2.9 Conditions used for 3R7R fragment amplification with Phusion .....	75
Table 2.10 Reaction mix used for 3R7R fragment amplification .....	75
Table 2.11 Conditions used for 7F3F and Neuro2.5 fragments amplification with Expand Long Template .....	76
Table 2.12 Reaction mix used for 7F3F and Neuro2.5 fragments amplification .....	76
Table 2.13 Conditions used for Neuro1.1 amplification with Phusion .....	77
Table 2.14 Reaction mix used for Neuro1.1 fragment amplification .....	77
Table 2.15 Riboprobe synthesis .....	78
Table 2.16 Riboprobe purification by precipitation in Lithium Chloride .....	79
Table 3.1 Range of doses used to investigate the role of RA in the development of different organ systems .....	87
Table 3.2 Incidence of phenotypes and changes in <i>Fgf3</i> expression with increasing dose of RA administered at 7.75dpc and 8.5dpc .....	90
Table S1 Range of <i>all-trans</i> retinoic acid doses administrated to pregnant mice via gavage or intraperitoneal injections (IP) in the study of various organs systems .....	212

# DEDICATION

---

In loving memory of

**Seth Saunders**

1986-2011

# ACKNOWLEDGEMENTS

---

I would like to thank the people who gave me the opportunity to carry out the work reported in this thesis. First, I would like to thank Sussex University for supporting me through my first 3 years of PhD with a GTA studentship. I would also like to thank my supervisor, Mark Maconochie, for his support, especially during the last months of my experimental work, and for his critical reading and suggestions on this thesis. I am also grateful to Androulla Economou for her help and advices, in particular with the chick electroporations.

I would also like to thank other researchers and students working in the laboratory during my PhD for their help and friendship: Vassilis, Preeti, Fara, Maria and Prathu; or in adjacent laboratory: Richard, Julia and Nicola. I would also like to express my thanks to Vince Edwards for excellent animal husbandry and his help with mouse handling; and I am also grateful to all the undergraduate students who made my teaching duty really enjoyable with their kindness and enthusiasm.

I am also grateful to all of the teachers and teaching assistants who communicated me their passion for science during my degree in France: Francois Cretin, Remy Sadoul, Rabah Iratni, Claire Vourc'h, Thierry Gauthier and Anne-Laure Mahul.

I want to thank as well all the people I have been working with at American Express during the writing of my thesis for their cheerful company: Sarah, Elodie, Ndjimi, Pat, Vero, Aylin, William, Adrien, Ben, Jerome, Laurent, Donald, Elias, Emma... to name just a few. I would have never finished that thesis without all your positive energy! I also want to thank my team leader Yves Tillieux for his flexibility when I needed last minute days off to finish my thesis.

To finish I am obviously grateful to my family and friends for their understanding and support throughout the years; and to David Sheppard for proofreading my thesis.

# ABBREVIATIONS

---

AP	antero-posterior
bHLH	basic helix-loop-helix
BM	basilar membrane
bp	base-pair(s)
CNS	central nervous system
dpc	days post-coitum
DV	Dorso-ventral
EAM	external auditory meatus
FGF	fibroblast growth factor
FGFR	fibroblast growth factor receptor
Hb	hindbrain
HC	hair cells
heSC	human embryonic stem cells
HSPG	heparan sulfate proteoglycan
kb	kilobases
Ngn1	neurogenin 1
nt	neural tube
OC	otic cup
OP	otic placode
OV	otic vesicle
PCR	polymerase chain reaction
PK	proteinase K
PNS	peripherious nervous system
r	rhombomere
RA	retinoic acid
RALDH	retinaldehyde dehydrogenase
RAR	retinoic acid receptors
RARE	retinoic acid responsive element
RoDH	retinol dehydrogenase
RTK	receptor tyrosine kinase
Scc	semi-circular canal
scn	superior cervical nerve
VAD	vitamine A deficient

# 1

## INTRODUCTION

---

Hearing loss is one of the most common sensory deficits with over 200 million people worldwide suffering from deafness or experiencing severe hearing impairment either induced or inherited. In the UK alone, 1 in 850 children is born with significant sensorineural deafness (Fortnum et al., 2001) and in Europe, roughly 30% of men and 20% of women suffer from presbycusis, or age-related, bilateral hearing loss (ARHL), by age 70 years, with a loss of 30 dB or more. These numbers keep increasing as people age, with 55% of men and 45% of women by age 80 years suffering from ARHL (Roth et al., 2001). Presbycusis in the aged has been correlated with a decreased quality of life and depression (Mulrow et al., 1990), and hearing loss in children has been shown to affect behaviour, confidence and social integration (Moeller, 2007). Furthermore, hearing loss costs billions in healthcare each year (Frisina, 2009; Shield, 2006). Thus in addition to the challenges faced every day by people affected to adapt to this sensory deficit, hearing loss has serious financial consequences for everyone.

Current treatment options for hearing impairment, such as hearing devices (aids) and cochlear implants, do not restore hearing to a normal level ([www.nidcd.nih.gov](http://www.nidcd.nih.gov)) and thus more effective treatments need to be found. One alternative long-term strategy is to recruit biological mechanisms naturally occurring during inner ear development, but this first requires a clear picture of the normal molecular mechanisms underlying this

developmental process. Fibroblast growth factors (FGFs) are short-range extracellular signalling molecules, with *Fgf3* and *Fgf10* already shown to be critical for the earliest events of inner ear induction (Alvarez et al., 2003; Zelarayan et al., 2007). In addition, they are also expressed in the inner ear itself (Ohuchi et al., 2005; Pauley et al., 2003; Powles et al., 2004) and mutations in both *Fgf3* and *Fgf10* have independently been linked to sensorineural deafness in human (Shams et al., 2007; Tekin et al., 2008). This thesis addresses the lack of knowledge regarding the molecular mechanisms controlling their expression in the inner ear.

## **1.1 Ear structure and function**

For someone able to perceive, interpret and appreciate sounds every day, hearing may feel like a rather banal phenomenon; but it actually depends on really complex mechanisms that are presented in this section. To start with, we first need to define how 'hearing' happens. A sound is essentially a longitudinal wave causing an oscillation of pressure or vibrations of air molecules (Purves and Williams, 2001). The concept of 'noise' or the concept of 'talking' only exists because we come naturally equipped with a transducer that converts these mechanical waves into neural signals that can be interpreted by the auditory cortex. But how does this actually happen? Mechanical waves will undergo multiple modifications before being processed by the brain to extract the useful information from the original signal. Most of these modifications will occur in the ear that itself is composed of 3 distinct parts; the outer ear, the middle ear and the inner ear (Figure 1.1), and thus their characteristics and functions are presented below.

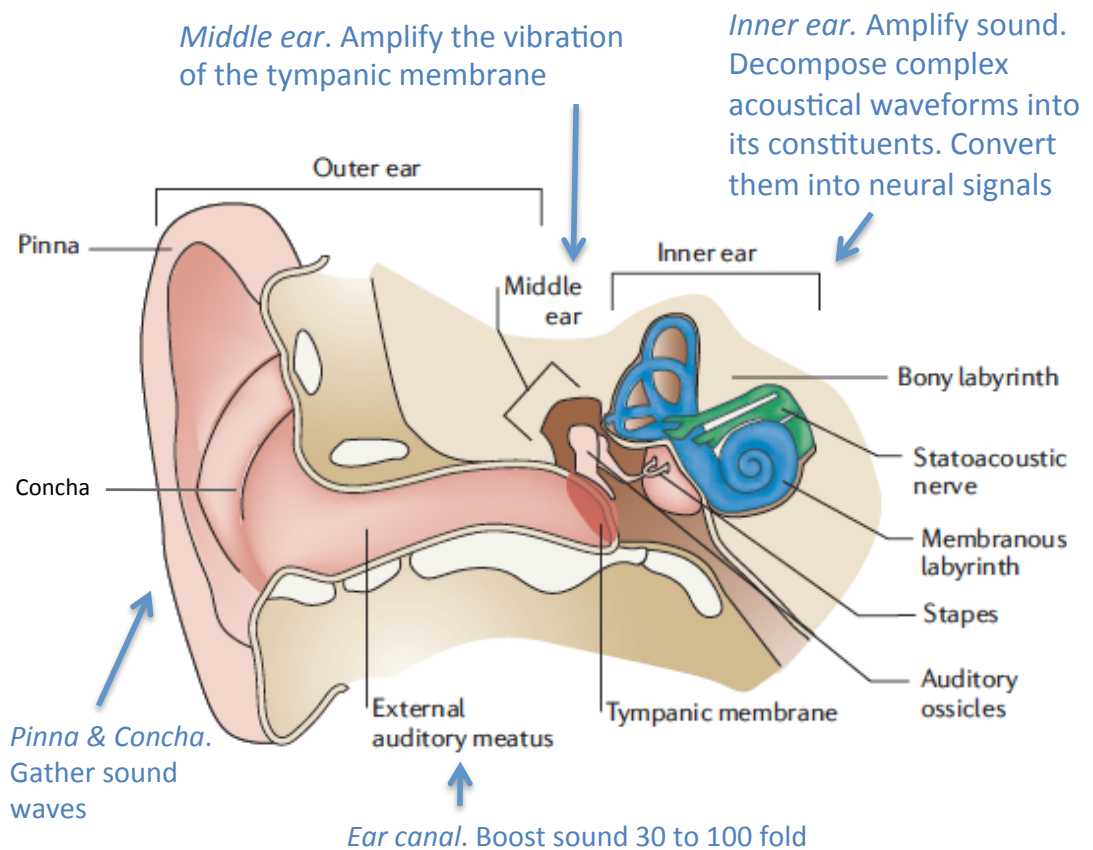


**Figure 1.1 – Gross anatomy of the ear.** The ear is composed of the outer ear, middle ear and inner ear. The outer ear can be subdivided into the pinna, concha and external auditory meatus (or ear canal) and is separated from the middle ear by the tympanic membrane. The pinna and concha gather sound wave and focus them on the ear canal that boosts sound up to 100 fold, causing the tympanic membrane to vibrate. The middle ear transmits and amplifies the movement of the tympanic membrane to the inner ear through a lever system consisting of 3 interconnected auditory ossicles. The cochlea amplifies and decomposes these complex acoustical waveforms into their constituents. These are then transduced to electrical energy in cochlear hair cells and transmitted to the brain via the statoacoustic nerve. Adapted by permission from Macmillan Publishers Ltd: Nature Reviews Neuroscience (Kelley, 2006), copyright (2006)

### **1.1.1 The outer ear**

The outer ear can be subdivided into the pinna, the concha and the external auditory meatus (EAM) or ear canal (Figure 1.1). Each of these parts plays a specific and important role in hearing. The pinna and the concha gather sound waves and participate in their localisation. The ear canal boosts the sound 30- to 100-fold for frequencies around 3kHz and focuses it on the tympanic membrane. The tympanic membrane is composed of two apposed epithelia; one provided by the external ear meatus and the other by the middle ear cavity. A fibrous layer located between these two epithelia gives the membrane consistency and elasticity (Mallo, 2001). This thin membrane is stretched between the air compartments of the outer and middle ear (Figure 1.1), causing it to vibrate in reaction to the acoustic pressure wave that impinges on it (Purves and Williams, 2001).

### **1.1.2 The middle ear**

The airborne sound-induced vibrations captured by the external ear then need to be transmitted to the inner ear, where they will be converted into neural signals that can be interpreted by the auditory cortex. The middle ear not only transfers sound pressure waves to the inner ear but it also matches the relatively low impedance airborne sounds to the higher impedance fluid of the inner ear and enhances important frequencies (Pickles, 1988). The middle ear transmits the vibrations of the tympanic membrane to the inner ear through a lever system consisting of three small, interconnected, skeletal elements or auditory ossicles: the malleus, incus and stapes (Figure 1.1). The malleus provides the physical link between the ossicle chain and the tympanic membrane. The incus then makes the link between the body of the malleus

and a small head in the middle of the stapedial arch. The stapes eventually provide the connection of the ossicles to the inner ear. Due to this spatial arrangement, vibration of the tympanic membranes results in a piston-like movement of these ossicles, which in turn initiates waves in the inner ear fluids (the inner ear compartments and the consequences of these waves are described in section 1.1.3). Without the ossicles, only a small portion of sound would reach the inner ear (Kurokawa et al. 1995). As well as transferring sound energy from the outer to the inner ear, the middle ear therefore plays a significant role in amplifying the vibrations set up on the tympanic membrane. This role in amplification is estimated to increase by 200-fold the pressure measured at the tympanic membrane (Mallo, 2001; Purves and Williams, 2001)

### ***1.1.3 The inner ear***

The inner ear is arranged as a highly complex membranous labyrinth encased in the petrous part of the temporal bone in the skull. The inner ear can be functionally subdivided into two regions: the vestibule and the cochlea (Figure 1.2). Both of these divisions of the inner ear contain regions of sensory hair cells. Hair cells act as mechanotransducers that are connected to the auditory and vestibular nuclei of the brain, through bipolar neurons. The vestibule is located dorsally and is responsible for the sense of motion and gravity (Alsina et al., 2009). The cochlea, which is located ventrally, is the most critical structure in the auditory pathway. Not only does the cochlea amplify the incoming sound wave but it also acts as a mechanical frequency analyser, by decomposing complex acoustical waveforms into its constituents, before converting them into neural signals (Alsina et al., 2009).

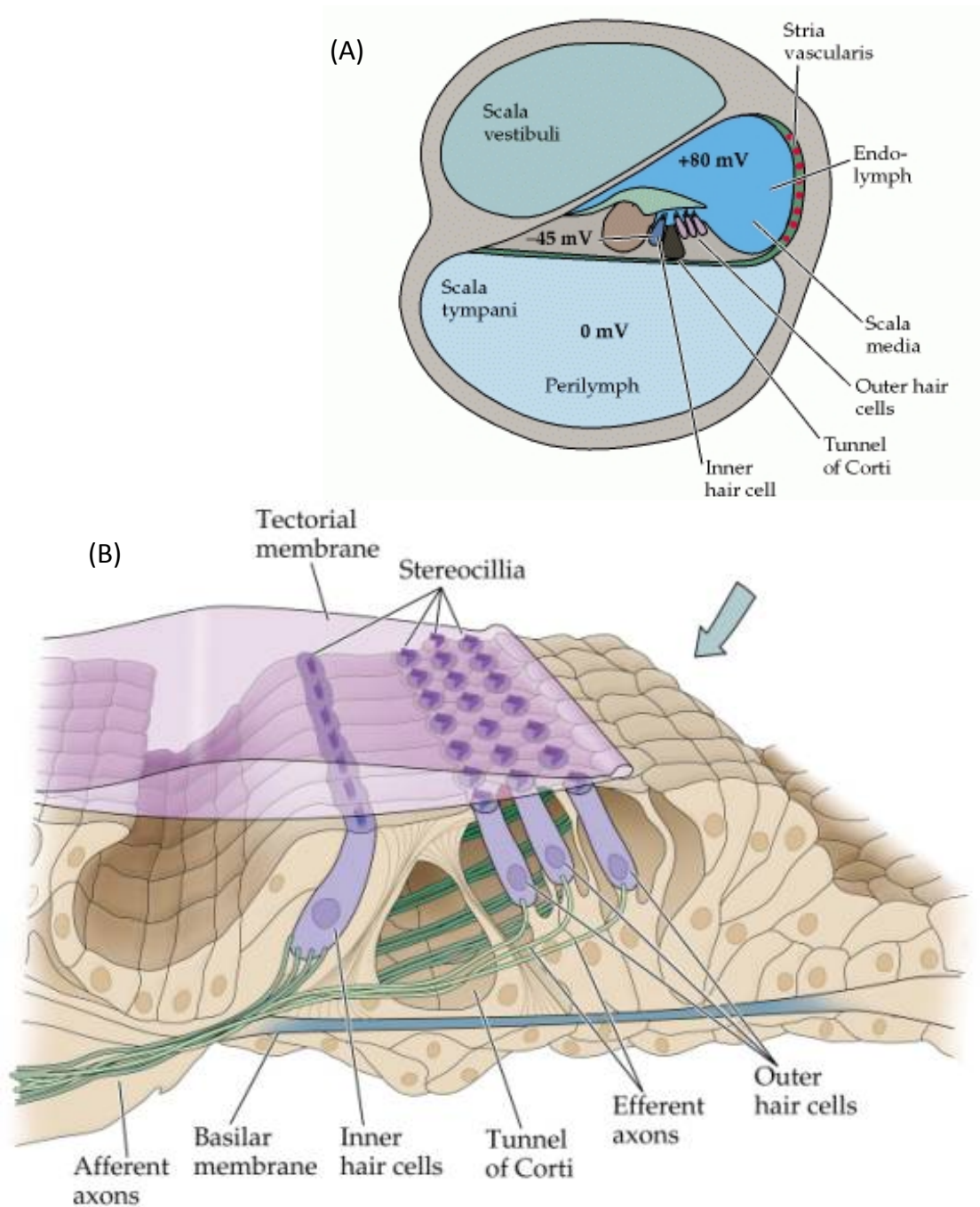


**Figure 1.2 Structure of the Inner Ear.** The inner ear can be subdivided into two functionally distinct regions : the vestibule and the cochlea. (A) A cross-section of the cochlea reveals three fluid-filled chambers. The organ of Corti that is responsible for hearing runs within the scala media. (B) The organ of Corti is composed of a tectorial membrane in which are embedded the stereocilia of the sensory hair cells, laying on top of another important membrane, the basilar membrane. [Purves \(2001\) Neuroscience](#)

Thus, along the cochlea, different frequencies are detected and corresponding signals are sent to the auditory centres for processing.

### **Structural organization of the mammalian cochlea**

In mammals, the cochlea is a small, coiled structure; making 2.75 turns around its axis in human (Kingsley, 1999). The number of turns varies according to the species. The cochlea consists of three fluid-filled chambers arranged in a parallel spiral. Two of these chambers, the scala vestibuli and the scala tympani, run on each side of the scala media or cochlear duct. The organ responsible for hearing (the organ of Corti) runs within the cochlear duct (Figure 1.2). The organ of Corti is composed of a basilar membrane upon which lay several layers of epithelial cells, and apically, several rows of hair cells. Sensory hair cells are the mechanotransducer cells, and display stereocilia on their apical surface that are embedded in the overlying tectorial membrane (Figure 1.2). The scala vestibuli and tympani join at the apical end of the cochlea so that the fluid movement, triggered by the oval window through vibration of the stapes, eventually causes the round window located at the basal end of the scala tympani to bulge out at the end of the passage of the travelling wave. The vibrations or travelling waves are subsequently translated into a shearing motion between the basilar membrane (BM) and the overlying tectorial membrane (TM) of the organ of Corti (Figure 1.3). The stereocilia located at the apical end of the hair cells contains transducer/ion channels that open when they are stretched, leading to a voltage change across the hair cell membrane. Action potentials generated travel through the bipolar neurons linking the hair cells to the brain, where the signal is processed and perceived (Purves and Williams, 2001; Vander et al., 2001).

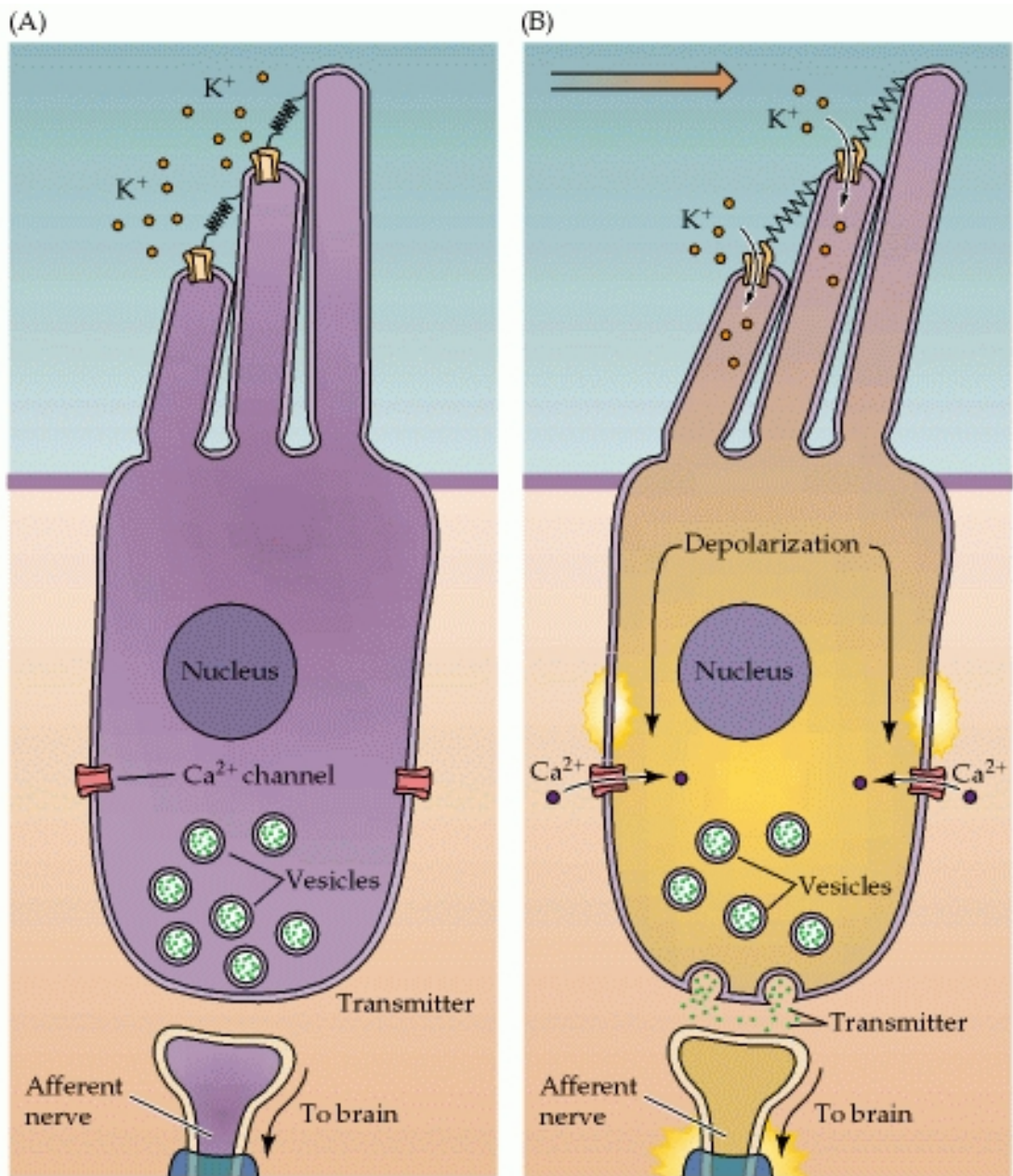


**Figure 1.3 Transduction of sound-induced vibrations into neural signals.** (A) Travelling waves result into shearing motion between the tectorial and basilar membrane. This shearing force bends the stereocilia of the hair cells. (B) Deflection of the stereocilia leads to the opening of ion channels, depolarization of the hair cell, release of neurotransmitter onto the nerve endings of auditory neurons and generation of action potential. [Purves \(2001\) Neuroscience](#)

The morphology and structure of the basilar membrane (BM) varies along the cochlea, from wide and flexible apically to small and stiff basally. These differences in stiffness and size result in different positions of the BM vibrating maximally with different stimulus frequencies: the BM resonates to low frequency at its wide, flexible apex and high frequencies at its thin, stiff base (Patuzzi, 1996). Therefore a complex sound composed of different frequencies will lead to a pattern of BM vibration equivalent to the superposition of vibrations generated by the individual tones composing it. The BM is said to be tonotopically organized (Purves and Williams, 2001).

### **The vestibular system**

The vestibular system is composed of a series of interconnected canals (Figure 1.2), the semi-circular canals (scc) link to two additional chambers, the utricle and saccule (Purves and Williams, 2001). Within these regions are located five sensory patches of hair cells, cristae in the ampulla of each scc and 2 otolith organs or maculae, located in the utricle and the saccule (Figure 1.6). Similarly to cochlear hair cells, all the vestibular sensory epithelia send neural signal to the brain, via the movement of their stereocillia, leading to the transduction of currents (Kingsley, 1999). The nature of the message to the brain is different though, with the vestibular system allowing interpreting of linear acceleration and head position. These signals are integrated in the brainstem nuclei with visual cues to maintain balance.

## **1.2 Development of the mammalian inner ear**

The entire mammalian inner ear, with all its different specialised cell types such as hair cells and neurons, derive from a patch of cranial ectoderm called the otic placode. This patch invaginates to first form the otic cup and subsequently the otic vesicle. This initially simple hollow vesicle then undergoes a series of complex remodelling to eventually give rise to the highly sophisticated adult inner ear. This section describes in more details the process of inner ear formation along with the signalling mechanisms involved.

### ***1.2.1 Formation of the preplacodal domain***

Several lines of evidence, morphological, experimental and molecular, suggest that all craniofacial sensory organs belong to a group of related structures, the sensory placodes, that all originate from the 'preplacodal region' (Ohyama et al., 2007; Streit, 2007). Morphologically, regions from which the sensory placode will originate appear like a continuous thickened band of ectoderm in mice, human and amphibians (Ohyama et al., 2007). In addition, transplantation experiments show that this thickened region is competent to form multiple placodes (Jacobson, 1963). Furthermore, the preplacodal domain is characterized by a particular set of molecular markers; and alteration of the expression of these genes results in variation in the size of the preplacodal domain (Glavic et al., 2004).

According to this model, the first step toward inner ear formation is to form the preplacodal domain, a region of competence for all the sensory placode. The second

step is the induction of a 'pre-otic field' within the preplacodal domain. As development proceeds, the preplacodal region gets gradually divided into smaller domains, in response to specific molecular signals (Streit, 2007). The 'pre-otic field' is subsequently refined into the otic placode and surrounding epidermis (Ohyama et al., 2007)

### **1.2.2 Inner Ear Induction**

The induction of the inner ear, that is to say the specification of one particular patch of cranial ectoderm as otic, depends on FGF signalling from the surrounding hindbrain, mesoderm and endoderm. The identity and source of FGFs may vary from species to species but they always play a central role in the induction of the otic placode (Ohyama et al., 2007).

The induction of the inner ear can be subdivided into 3 steps with regard to the dynamic expression of *Fgf3*, *Fgf8* and *Fgf10* during this process (Figure 1.4; reviewed in Schimmang, 2007). Step 1 - expression of *Fgf8* and *Fgf10* in the lateral plate mesoderm (that will later give rise to the heart) at 8dpc marks the start of the induction process. Step 2 - *Fgfs* starts to be expressed in neural tissues as evidenced by *Fgf3* expression in the hindbrain and preplacodal domain (Wright and Mansour, 2003), *Fgf10* expression in the hindbrain (Alvarez et al., 2003), and transient *Fgf8* expression in the preplacodal ectoderm (Lahder et al., 2005). *Fgf8* is also transiently detected in the pharyngeal endoderm (Lahder et al., 2005). Step 3 marks the completion of placode formation.

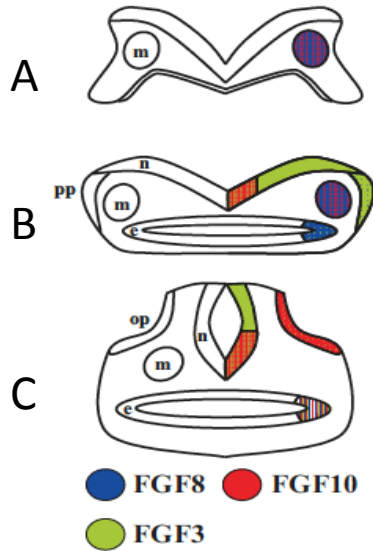


**Figure 1.4 *Fgfs* expression during inner ear induction in mice.** (A) During the 1<sup>st</sup> step of the induction process, *Fgf8* and *Fgf10* are expressed in the mesoderm. (B) The 2<sup>nd</sup> step of induction is characterized by the onset of *Fgfs* expression in neural tissues, with *Fgf3* and *Fgf10* expression in the hindbrain. *Fgf3* also starts to be expressed in the preplacodal ectoderm and *Fgf10* in the endoderm. (C) Finally, during the 3<sup>rd</sup> step of induction the otic placode is fully formed and start invaginating. At this stage *Fgf3* and *Fgf10* are still expressed in the hindbrain and *Fgf10* is now expressed in the otic placode. In addition all three *Fgfs* are expressed in the endoderm. Abbreviations: *m*, mesoderm; *n*, neural tube; *op*, otic placode; *pp*, preplacodal domain. Reproduced from (Schimmang, 2007) with permission from The International Journal of Developmental Biology (Int. J. Dev. Biol.) (2007) Vol 51: 473-481

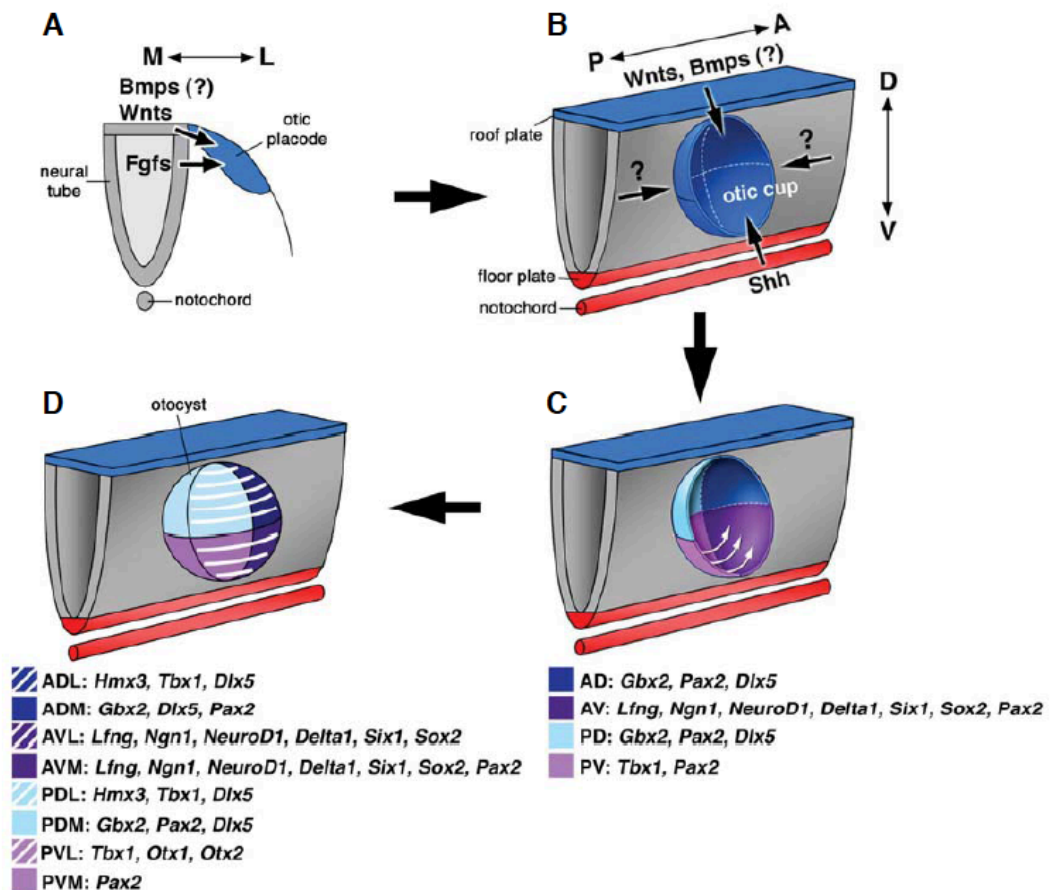


**Figure 1.5 A model on otic patterning and axis specification.** (A) Otic placode is induced by *Fgfs*, *Wnts* and possibly *Bmps* signalling from the hindbrain and surrounding tissues. (B,C) The invaginating otic placode receives AP (*Wnts*, *Bmps*) and DV signals (*Shh*) from surrounding tissues. AP specification is thought to involves the induction of *Tbx1* in the posterior otic cup. *Tbx1* may in turn restrict the anterior neurosensory region that is characterized by the expression of *Ngn1*, *NeuroD* and *Lfng*. Postero-ventral cells then migrates to form most of the lateral wall, with the exception of the anterior neurosensory domain. (D) The lateral wall continues receiving AP and DV signals is subdivided in domains characterized by the expression of specific genes. Abbreviations: *M*, medial; *L*, lateral; *A*, anterior; *P*, posterior; *D*, dorsal; *V*, ventral. Reproduced from (Bok, 2007) with permission from The International Journal of Developmental Biology (Int. J. Dev. Biol.) (2007) Vol 51: 521-533

*Fgf8* expression disappears from the preplacodal domain with only a few transcripts still expressed in the ventral surface ectoderm, pharyngeal endoderm and mesoderm (Lahder et al., 2005). Shortly before placode invagination, *Fgf3* is now detected in the pharyngeal endoderm, as well as in rhombomeres 5 and 6 (r5-r6) and in the otic placode (Mahmood et al., 1996). *Fgf10* also starts to be expressed in the invaginating placode at this stage, as well as in the pharyngeal endoderm with *Fgf3* and *Fgf8* (Pirvola et al., 2000; Alvarez et al., 2003; Wright and Mansour., 2003).

### **1.2.3 Patterning and axis specification**

As the otic ectoderm becomes specified, it starts expressing specific combinations of genes (Figure 1.5; reviewed in Bok et al., 2007). The earliest molecular markers of the otic placode in mice are *paired box* genes (*Pax*); *Pax8* is expressed first (Ohyama and Groves, 2004), shortly followed by *Pax2* (Oywama et al., 2007). Importantly, early molecular asymmetries prefigure axis formation, with for instance expression of several neurosensory markers in the anterior region of the invaginating otic placode: *Fgf10*, *Lunatic Fringe* (*Lfng*), *Neurogenin1* (*Ngn1*) and *NeuroD* (Bok et al., 2007). In the posterior region of the otocyst, expression of *Tbx1* delimits the neurogenic domain. However, this pattern of expression is only prefiguring future axis formation, not determining it, as evidenced by otic transplantation studies in chick that showed that despite a clear molecular patterning, otic vesicle transplanted in the wrong orientation adopt the correct antero-posterior (AP) identity (Wu et al., 1998). What are the signals responsible for conferring this AP axial identity to the otic placode? Due to its crucial role in inner ear induction, and its arrangement in rhombomeres each expressing a particular set of gene, the hindbrain seems a good candidate. However, hindbrain

rotation experiments in chick that switched the position of rhombomeres 5 and 6 (r5 and r6) did not affect the AP identity of the inner ear (Bok et al., 2005). AP axis formation is discussed further in later sections of this thesis (see section 5.1.5).

The inner ear is also divided into different domains along its dorso-ventral (DV) axis, with the dorsal region of the otic vesicle that will give rise to the vestibular structures and the ventral region that will give rise to the auditory component of the inner ear. Proper formation of these two different structures depends on the establishment of the dorso-ventral axis. Here again each compartment is characterised by a different set of molecular markers (Figure 1.5), for the vestibular system it for instance includes *Dlx5* (Distal-Less homeobox 5), *Hmx3* (H6 family homeobox 3) and *Gbx2* (Gastrulation brain homeobox 2), and for the auditory system *Lfng* (Lunatic Fringe), *Ngn1* (Neurogenin1), *NeuroD1*, *Sox2* (Sex Determining Region Y-Box 2) and *Six1* (Sine Oculis Homeobox Homolog 1)(Fekete and Wu, 2002). As for the AP axis, the onset of gene expression is not concomitant with the establishment of the DV axis. The lack of correlation between gene expression pattern and axis formation is consistent with the AP axis being established before the DV axis, whereas molecular marker expression appears at the same time along the AP and DV axis (Wu et al., 1998)

In contrast to what has been shown for the AP axis, transplantation experiments in chick embryos where the hindbrain is rotated in VD instead of DV orientation results in the expression of several ventral genes including *NeuroD* dorsally, whereas the expression of dorsal gene such as *Gbx2* is abolished (Bok et al., 2005). This demonstrates that the establishment of the DV axis depends on hindbrain signalling

and is thought that the effects of the hindbrain on DV axis formation are partly mediated by *Sonic Hedgehog (Shh)* signalling from the floor plate/notochord and *Wnt* signalling from the dorsal neural tube (Figure 1.5; reviewed in Bok et al., 2007).

Along these molecular changes, morphological changes also happen; starting with a thickening of the otic placode (Figure 1.6) at 8.0dpc (days post coitum). Half a day later the otic placode already starts to invaginate and will have formed a hollow vesicle by 9.5dpc. At this stage, the first sign of elongation can also be seen, which correspond to the future endolymphatic duct (Reviewed in Romand et al., 2006). The first neuroblastes also start delaminating from the antero-ventral wall of the otic vesicle (OV) (Figure 1.6) and can be identified by the expression of specific neuronal markers such as *NeuroD* (Romand et al., 2006). By 10.5dpc, the endolymphatic duct can now be observed dorsally (Figure 1.6) and morphogenesis of the cochlea, vestibular canals, utricule and saccule also starts. These will adopt a more mature appearance by 12.5dpc and eventually reach their almost adult form at 17.5dpc (Figure 1.6). Interestingly, the otic epithelium gives rise to a wide spectrum of specialised cell types including epithelial, neural, sensory and supporting cells, thus providing the major contribution to inner ear cells. Additional cells are however provided by melanocytes (in the stria vascularis) and Schwann cells; the vestibulo-acoustic ganglion also partly originates from neural crest cells (Alsina et al., 2009).

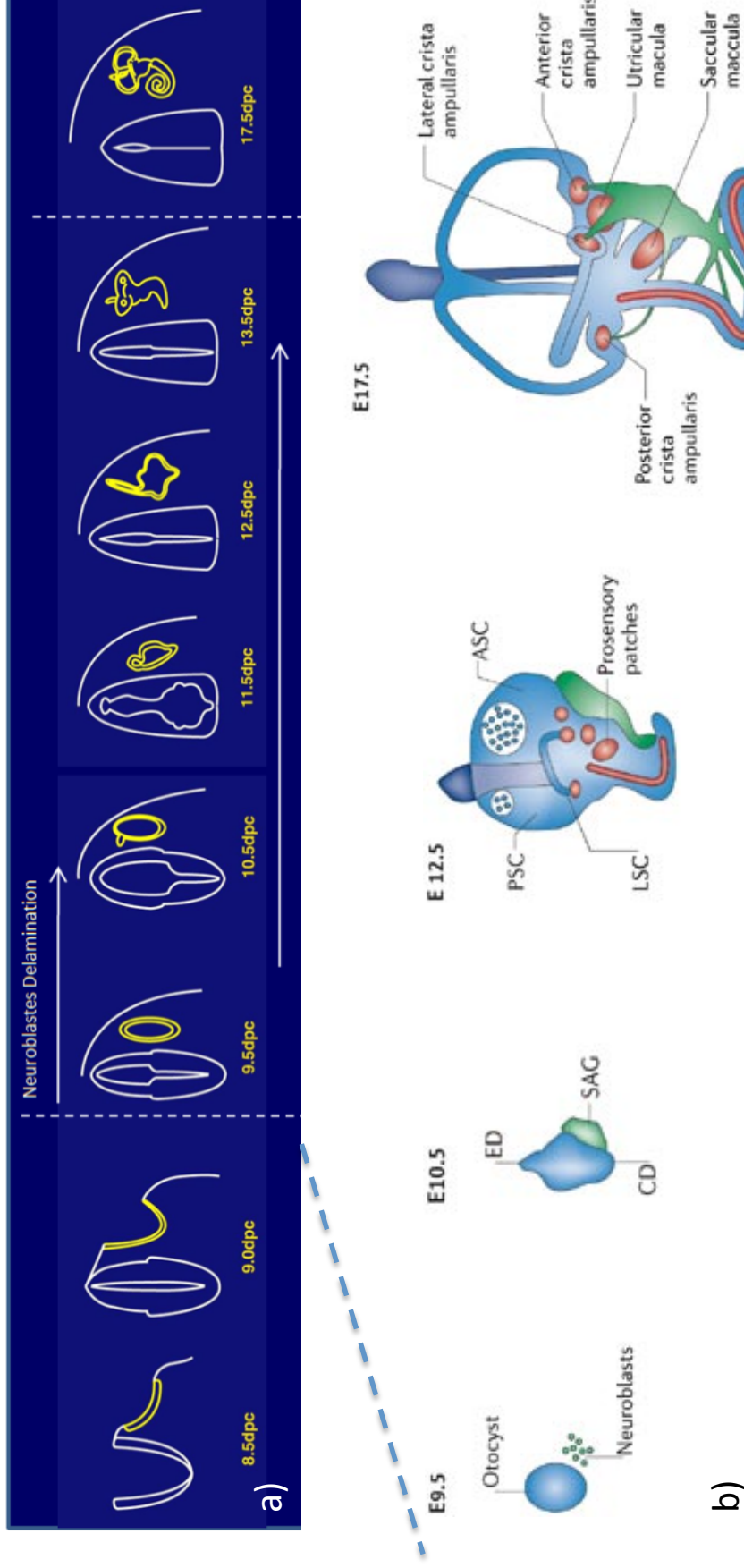


**Figure 1.6 Inner ear development.** a) Cross-section showing the development of the inner ear in relation to the hindbrain: The inner ear arises from a simple patch of ectoderm that thickens to form the otic placode at 8.0dpc. At 8.5dpc, the placode starts to invaginate and will have formed a hollow vesicle by 9.5dpc. At this time, neuroblasts also start delaminating from the antero-ventral wall of the otic vesicle. The otic vesicle will then undergo morphogenesis to give rise to almost all inner ear cell types b) Details of inner ear morphogenesis and sensory organ location. Adapted by permission from Macmillan Publishers Ltd: Nature Reviews Neuroscience (Kelley, 2006), copyright (2006)

#### **1.2.4 Molecular basis of inner ear morphogenesis**

Most inner ear structures consist in both sensory and non-sensory regions and reciprocal interactions between these sensory and non-sensory tissues is thought to coordinate the morphogenesis of these regions during inner ear development (Bok et al., 2007). One example of such molecular interplay between a sensory and non-sensory compartment involves *Fgf10* and its receptor, *Fgfr-2(IIIb)*. *Fgf10* is expressed in the presumptive sensory domain, whereas *Fgfr-2(IIIb)* is expressed in a complimentary pattern into the non-sensory epithelium (Pirvola et al., 2000). Interestingly, despite being expressed exclusively in non-sensory epithelia, targeted mutation of *Fgfr-2(IIIb)* resulted in a dysgenesis of the cochleovestibular labyrinth as well as in defects in sensory patches and vestibulo-acoustic ganglion formation; in addition to the defects in the non-sensory epithelium. Since the lack of *Fgfr-2(IIIb)* cannot explain by itself defects in areas where it is not expressed, we might assume that what is lacking in these organs/tissues, is a signal normally generated in response to FGFR-2(IIIb) activation by ligand binding (Bok et al., 2007).

#### **Cochlea formation**

The cochlear duct forms in the postero-lateral wall of the otic vesicle and descend ventro-medially. It then extends and coils to 1 and  $\frac{3}{4}$  turns in mice. Initially thick and wide, it is thought to reach its final shape via convergent extension along its axis (Bok et al., 2007; Chacon et al., 2012). Proper development of the cochlear duct depends on the coordination of numerous factors, such as *Pax2* and *Otx1* that play a critical role in cochlea formation by regulating differential proliferation and growth (Burton et al. 2004). Thus, targeted mutation of *Otx1* mutation results in abnormal growth and

coiling and *Pax2* null mutations results in agenesis of the cochlea and of the auditory ganglion (Burton et al., 2004). Tissue-specific deletion of *Tbx1* in the mesenchyme also results in malformation of the cochlear duct (Xu et al., 2007), demonstrating that changes in the expression of gene in the mesenchyme can also cause defects in the inner ear epithelium, probably as a result of abnormal epithelial/mesenchymal interactions. This further supports the hypothesis that the formation of the different components of the inner ear is interdependent.

### **Crista and canal formation**

The semicircular canals are induced in the dorso-lateral region of the otic vesicle. Crista and canal formation involves *Bmp4* and *Fgf10* signalling in a 'canal genesis zone' adjacent to the presumptive crista. Targeted inactivation of *Fgf10* in mice results in abnormal crista development and absence of semi-circular canals (Pauley et al., 2003). Interestingly gain of function experiments using *Fgf10* loaded beads in chick embryos, suggest that *Fgf10* also promotes canal formation (Chang et al., 2004). Thus, in addition to its crucial role during inner ear induction, *Fgf10* appears to also be involved in later morphogenetic events.

### **1.3 The role of Fgfs in Inner ear development**

Fibroblast growth factors (FGFs) are short-range extracellular signalling molecules that control normal development of the mammalian embryo in a large number of different developmental contexts and their role during the induction of the otic placode was already introduced in section 1.2.2. The characteristics of FGF signalling and its role during inner ear development are presented in more details in the following sections.

#### **1.3.1 The Fibroblast Growth Factors family**

The fibroblast growth factor protein was described for the first time more than 40 years ago, when it was found to be mitogenic for cultured fibroblasts (Gospodarowicz and Moran, 1975). So far, a total of 22 *Fgfs* have been reported following the sequencing and bioinformatic analysis of the human and mouse genomes. Human and mouse *Fgfs* are homologous in sequence, share similar binding specificities to receptors and can be classified into subgroups according to their structure, biochemical properties and expression (Bottcher and Niehrs, 2005; Guillemot and Zimmer, 2011). Most *Fgfs*, including *Fgf3*, *Fgf8* and *Fgf10*, are classical short-range extracellular signalling molecules acting in an autocrine and/or paracrine fashion by interacting with receptors present in the membrane of the target. There are however two other subsets of *Fgfs* with different properties. *Fgf15/19*, *Fgf21* and *Fgf23*, comprise a second subset that acts in long-distance signalling, in a manner similar to endocrine factors that regulate metabolism, and thus display 'hormone-like' properties. A third subset, including *Fgf11* to *Fgf14*, are not secreted and do not activate FGF receptors, but instead interact with voltage gated channels or localize to

the nucleus (Itoh and Ornitz, 2008). With all these different functions it comes as no surprise that members of the FGF family control normal development of the mammalian embryo in almost all developmental contexts.

Members of the first and best characterised subset of FGF signalling molecules, that display short-range ligand-receptor interactions, were in particular shown to be critical for early inner ear development, with *Fgf3*, *Fgf10* and *Fgf8* all collaborating in the earliest events of inner ear induction (Zelarayan et al., 2007). Therefore the characteristics of the receptors with which they interact, as well as the downstream signalling pathways they activate, are discussed in more detail in the next section.

### **1.3.2 *Fgfs* signalling**

The FGF ligands signal through cognate FGF receptors (FGFRs) that compose a subfamily of receptor tyrosine kinases (RTKs). There are 4 different FGF receptors in vertebrates, FGFR1 to 4 that all exist in multiple isoforms due to alternative splicing and that exhibit different FGF-binding specificities (Zhang et al. 2006; Guillemot, 2011). Interaction of FGFs with their receptors is also strongly influenced by cofactors such as heparan sulfate proteoglycans (HSPGs), which are also considered low affinity receptors (Sugaya, 2008). FGFRs are single spanning transmembrane proteins with an extracellular domain composed of three immunoglobulin-like loops that bind the FGF ligand (Figure 1.7). The intracellular domain has tyrosine kinase activity that interacts with intracellular substrates and signal transduction molecules (Bottcher and Niehrs, 2005).

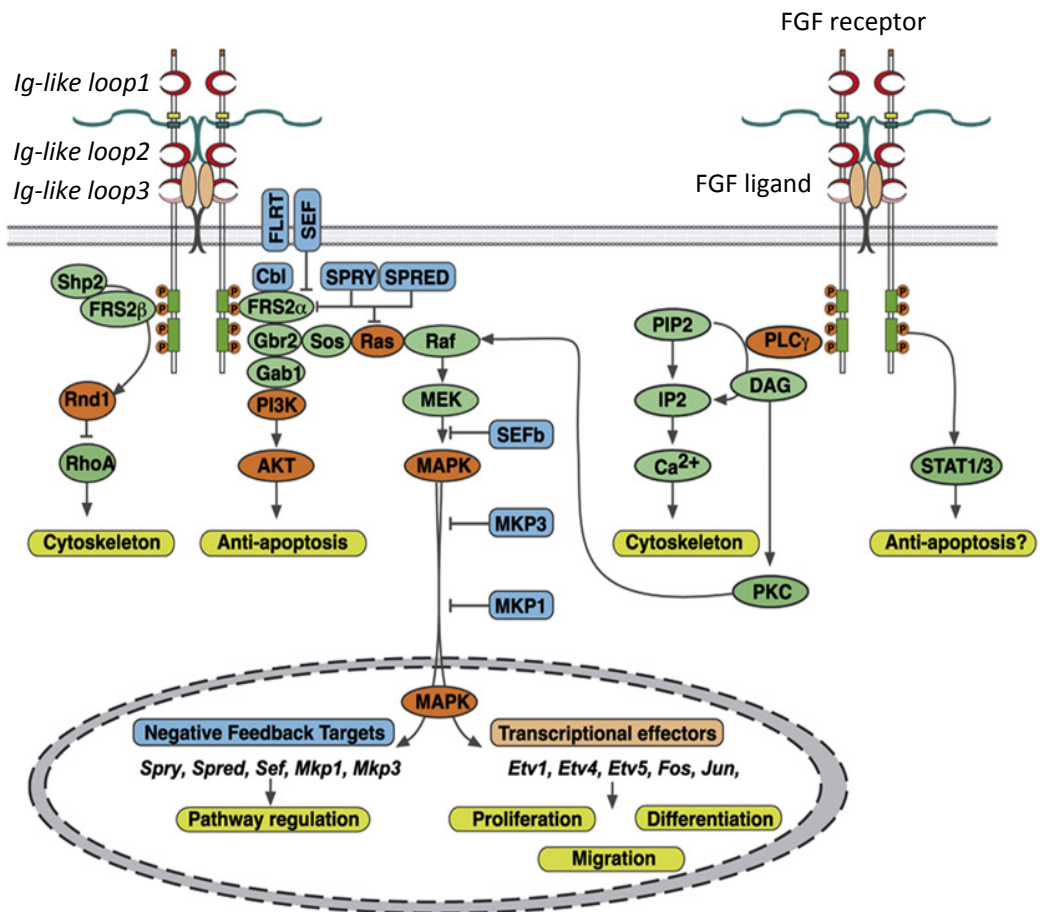


**Figure 1.7 Fgfs signalling.** Dimerisation of the FGF receptor following FGF binding results in autophosphorylation of tyrosine kinase residues. Phosphorylated residues attract proteins such as FRS2, PLC $\gamma$  or STAT1/3, resulting in the recruitment and assembly of signalling complexes. Fgfs signalling is involved in numerous events such as cytoskeleton dynamic, apoptosis and cell proliferation, differentiation and migration. Fgfs signalling also auto-regulates itself via the activation of several feedback inhibitors such as *Sef* and *Sprouty*. Reprinted from Neuron, 71, (Guillemot et al., 2011). From Cradle to Grave: The Multiple Roles of Fibroblast Growth Factors in Neural Development, 574-588, Copyright (2011), with permission from Elsevier

Binding of FGFs to their respective FGFR, triggers the dimerisation of the receptors, which results in the auto-phosphorylation of a number of tyrosine kinase residues. Phosphorylation of FGFR intracellular domain leads to the recruitment and assembly of signalling complexes (Figure 1.7). One of the proteins recruited by FGFR phosphorylation is FGFR substrate 2 (FRS2), which then allows the recruitment of Grb2, SOS and eventually the activation of an important protein, Ras, which then goes on and phosphorylates MAPK ERK, thus turning on the pathway of the same name (Figure 1.7). G Ras plays a critical role in controlling cell growth and differentiation via the activation or upregulation of several transcription factors such as *Ets* proteins, *AP1*, *Gata*, *c-myc* and CREB. Thus, deregulation of this pathway is usually associated with the development of cancer (De Luca et al., 2012). Under normal conditions, this pathway regulates itself, via the activation of several feedback inhibitors such as *Sef* and *Sproutys* (Figure 1.7). FGF signalling can also activate the phosphoinositide-3 kinase pathway, which in turn activate the serine/threonine kinase Akt/protein kinase B. This pathway is also involved in the regulation of cell survival and growth and associated with cancer when misregulated. JAK-STAT pathway is another downstream target of FGF3 signalling and is for instance involved in limb growth, and blood cell differentiation (Gilbert, 2006).

FGF signalling has been shown to be important for many cellular roles that are important in development, such as animal-vegetal pole specification in *Xenopus* (Kumano et al., 2001); maintenance of the stem zone during posterior axial elongation in chick and mouse (Dorey and Amaya, 2010); induction of the peripheral nervous system (PNS), patterning of the neural primordium, proliferation of neural progenitors,

neuronal migration, axon navigation, synaptogenesis (Streit et al., 2007; Guillermot and Zimmer, 2011); differentiation, apoptosis, cell adhesion and cell survival (Bottcher and Niehrs, 2005)

### **1.3.3 *Fgfs and inner ear induction***

The dynamically changing patterns of *Fgf3*, *Fgf8* and *Fgf10* at the time of otic placode induction (described in section 1.2.2) suggest they are important factors in this process. In agreement with that hypothesis, the sufficiency of *Fgfs* to ectopically induce the otic placode has been demonstrated for *Fgf10*, where its misexpression in the hindbrain leads to ectopic vesicle formation next to r3-r5 (Alvarez et al, 2003). Misexpression of *Fgf3* also leads to the generation of ectopic otic vesicle but with a lower occurrence than *Fgf10* (Alvarez et al., 2003).

Requirement for FGF signalling was first assessed in single mutants. Targeted inactivation of *Fgf3* resulted in almost half the embryos not presenting any phenotype. Remaining embryos were affected in various degrees and developmental abnormalities included poorly coiled and swollen cochlear duct, lack of endolymphatic duct and sac, and abnormal fusion/truncation of the vestibular canals (Alvarez et al., 2003; Wright and Mansour, 2003). *Fgf10* null embryos were also analysed. The sacculle and cochlea were smaller but otherwise unchanged. However the posterior canal system and the crista were completely lacking (Pauley et al., 2003). Furthermore, targeted mutation of *Fgfr-2(IIIb)*, the receptor through which both *Fgf3* and *Fgf10* signal to their target cells, lead to even more developmental abnormalities, such as severely disrupted cochleovestibular membranous labyrinth, absence of

endolymphatic duct, and non sensory epithelium, sensory patches and vestibulo-cochlear ganglion staying at rudimentary stage (Pirvola et al., 2000).

#### **1.3.4 *Fgfs in inner ear morphogenesis***

It is now well established that redundant FGF signalling from tissues surrounding the future otic placode is required for inner ear induction (see section 1.2.2). But is it the only role for FGF signalling during inner ear development? Interestingly *Fgf3* and *Fgf10* are also expressed within the developing inner epithelium itself at later stages, with their expression overlapping in the antero-ventral wall of the otic vesicle. This antero-ventral domain is thought to be the proneurosensory region that will later give rise to all the sensory patches and neurons of the inner ear (Pirvola et al., 2000), suggesting *Fgf3* and *Fgf10* may play a role in later aspects of development, such as inner ear neurogenesis.

A brief review of the literature indeed revealed some circumstantial evidence for the role of FGF signalling in neurogenesis. According to a review (Sanchez-Calderon et al., 2007), *Fgf2*, *Fgf3*, *Fgf8*, *Fgf10* and *Fgf19* have been shown to participate in otic neurogenesis (Adamska et al., 2001; Alsina et al., 2004; Wright and Mansour, 2003). For instance in chick, ectopic expression of *Fgf3* in combination with *Fgf2* resulted in an enlarged vestibulo-acoustic ganglion (Adamska et al., 2001), suggesting a potential involvement of *Fgf3* in ganglion formation. In addition, overexpression of *Fgf10* in chick gives rise to a larger number of cells expressing the neurogenic markers *NeuroD* and *NeuroM* (Alsina et al., 2004), whereas targeted mutation of *Fgf10* in mice results in a reduction in the number of otic neurons (Pauley et al., 2003). Mutation of *Fgfr-*

*2(IIIb)*, the receptor used both by *Fgf3* and *Fgf10*, also lead to the failure of forming a vestibulo-acoustic ganglion (Pirvola et al., 2000). Furthermore, *Fgf10* is involved in neurogenesis in other organ systems. In particular, in the mouse forebrain, *Fgf10* has been shown to promote the maturation of glial cells and the initiation of neurogenesis (Sahara and O'Leary, 2009). *Fgf10* was also shown to promote synaptogenesis in chick motoneuron cultures (Umemori et al., 2004). All together these suggest that FGF signalling is not only important for inner ear induction, but actually plays a role in every aspect of inner ear development, including neurosensory development.

This hypothesis is further supported by a recent study (Chen et al., 2012), where human Embryonic Cells (heSCs) cultured with both *Fgf3* and *Fgf10* gave rise to two types of otic progenitors, that were then able to differentiate in vitro into auditory neurons and hair-cell-like cells.

### **1.3.5 *Fgfs* redundancy and compensation mechanisms**

As explained above, *Fgf3* and *Fgf10* are both expressed in the prosensory domain of the developing otic vesicle and they have been showed to play crucial roles in numerous aspects of inner ear development. However, surprisingly, *Fgf10* null mice only display mild defects in inner ear morphogenesis and innervation (Wright and Mansour, 2003) and only around 50% of *Fgf3* null mice display a phenotype (Alvarez et al., 2003). Since *Fgf3* and *Fgf10* signal through the same *Fgfr-2(IIIb)* receptor this suggests that the two Fgfs may compensate for each other. Such a phenomenon may be masking further roles of *Fgf10* and/or *Fgf3* in later events of inner ear development within the otic epithelium, suggesting a comparative study of both these factors is

required to get the whole picture of *Fgfs* control of inner ear development. Importantly, both *Fgf3* mutations and *Fgf10* mutations have separately been reported to underlie sensorineural deafness in humans (Shams et al., 2007; Tekin et al., 2008). This demonstration of *Fgf3* and *Fgf10* roles in deafness in mice and humans, makes it timely to establish a more detailed picture of their expression and regulation during inner ear development.

To investigate the regulation of *Fgf* signalling regulation during development, a bioinformatic analysis of the 7.4kb region upstream *Fgf10* was performed. It revealed the presence of several putative binding sites for transcription factors and other signalling complexes involved in inner ear development, such as retinoic acid (RA), GATA3, NEUROD, NEUROGENIN1 and NSCL1 (Appendix Figure S1). The *Fgf3* enhancer also contains 7 putative RA binding sites, including one that was shown to bind RA in vitro (Frenz et al., 2010). The next sections present in more detail these candidates for *Fgf3/10* regulation in the inner ear.

## 1.4 Retinoic Acid signaling

Retinoic acid (RA) is a small lipophilic molecule, derived from the breakdown of vitamin A. The circulating form of vitamin A (retinol) is taken up into cells by diffusion across the cell membrane, where it is converted into RA by two oxidative reactions (Figure 1.8). The first reaction involves alcohol dehydrogenase and retinol dehydrogenase (RoDH) that convert the physiologically inactive retinol into retinal. The second reaction involves members of the retinaldehyde dehydrogenase family (RALDH1, 2, 3 and 4) that converts retinal into either *all trans*-RA or *9-cis* RA. RA then exerts its effects by binding to two families of nuclear receptors, the RARs ( $\alpha$ ,  $\beta$  and  $\gamma$ ) and the RXRs ( $\alpha$ ,  $\beta$  and  $\gamma$ ). RARs and RXRs can form both homodimeres and heterodimeres. Complex formed by the RA ligand and these receptors then directly regulate gene expression via binding to RA-binding sites (RAREs) located on the DNA regulatory sequences of RA's target genes (Figure 1.8).

Normal embryonic development depends on homeostatic concentrations of RA with both excess and deficiency resulting in developmental anomalies (McCaffery et al., 2003) and thus RA signalling must be tightly controlled. First of all RA signalling depends on the availability of vitamin A, as shown for instance by the study of Vitamin A Deficient (VAD) quails (Kil et al., 2005).

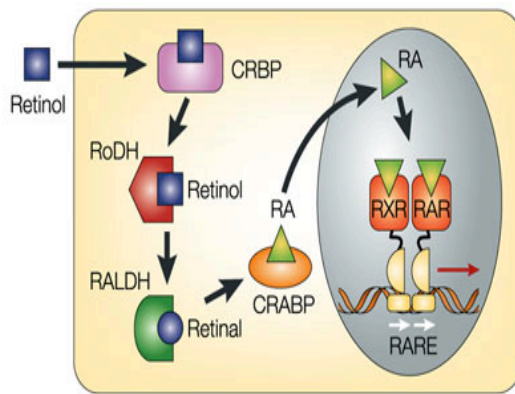


**Figure 1.8 Retinoic acid signalling.** RA is a small lipophilic molecule derived from the breakdown of the vitamin A (retinol). The vitamin A is taken up into the cells and then converted into retinal by retinol dehydrogenases (RoDHs). The retinal is later converted into *all-trans* RA or *9-cis*-RA by retinol dehydrogenases (RALDHs). (CRBP/CRABP are cellular retinol/RA binding proteins that are thought to be involved in regulating the concentration of RA). RA binds to nuclear receptors (RXR, RAR) and these complexes regulate gene expression by binding to RA responsive sites (RAREs).

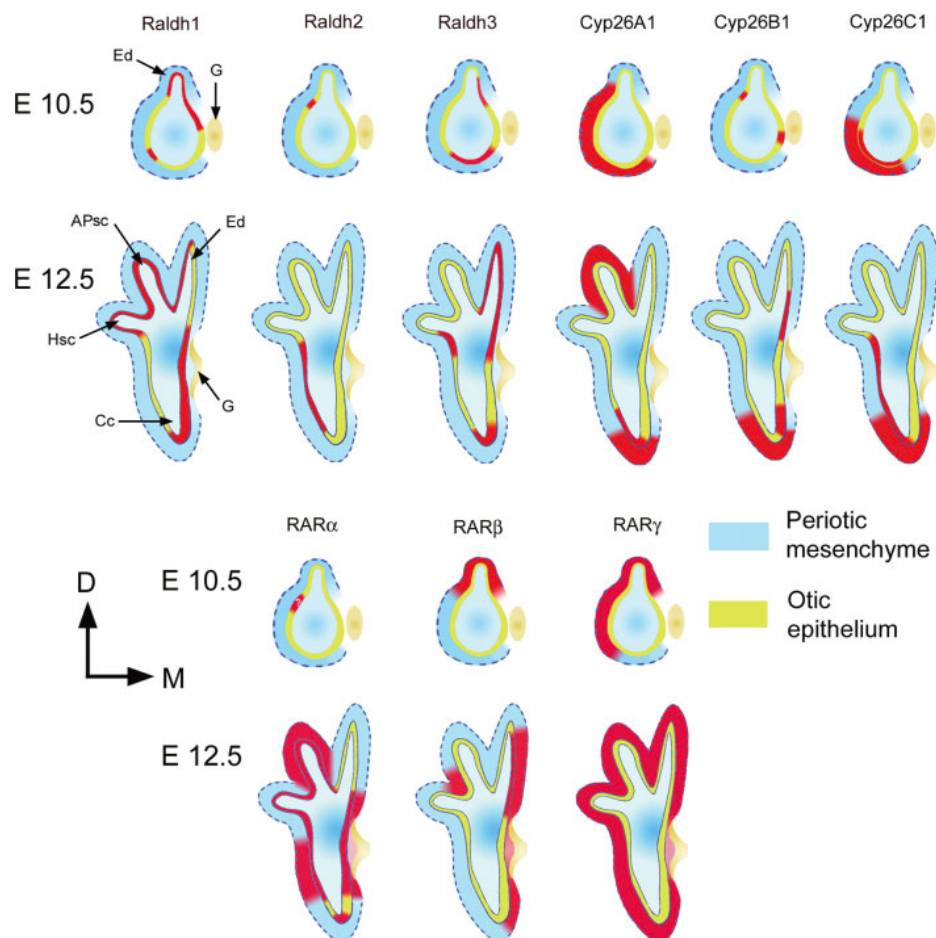


**Figure 1.9 RA synthetic/catabolic enzymes and nuclear receptors distribution in the inner ear.** RA synthetic (RALDHs) and catabolic enzymes (CYP26) are restricted to a specific region of the otic epithelium/periotic mesenchyme. At 10.5dpc, *Cyp26* expression are predominantly expressed in the latero-ventral mesenchyme, and *Raldhs* in the dorso-medial otic epithelium. At 12.5dpc, *Raldhs* and *Cyp26* continue to have a rather complementary pattern, with the exception of some overlapping region of expression, for instance in the ventral region. RA nuclear receptors RAR $\alpha$ , $\beta$  and  $\gamma$  are also expressed in specific regions of the otic epithelium and/or periotic mesenchyme. At 10.5dpc, they are predominantly restricted to a dorso-lateral region. At 12.5dpc, their expression encompasses more inner ear domains. *Abbreviations:* Ed, endolymphatic duct; G, vestibulo-acoustic ganglion; Apsc, anterior and posterior semi-circular canals; Hsc, horizontal semi-circular canal; Cc, cochlear duct. Reproduced from (Romand et al., 2006) with permission from John Wiley and Sons. Copyright © 2006 Wiley Periodicals, Inc.

Similarly to its active metabolite, RA, both deficiency and excess of Vitamin A itself also results in congenital malformations (Zile, 1998) as shown through the shortening of the caudal hindbrain in VAD rat embryos (White et al., 2000) and craniofacial abnormalities in mice and rats fed with excess RA (Alles and Sulik, 1992; Emmanouil-Nikoloussi et al., 2000). However, excess of dietary vitamin A has less dramatic consequences than RA excess or Vitamin A deficiency, since the availability of RA synthesizing enzymes will be a limiting factor in the generation of RA from the ingested vitamin A.

This illustrates that at the level of the organism, the first element of control of RA signalling is the biosynthesis step to produce RA. A second element of control that is common to all chemical/biochemical reactions is the half-life of the active molecule and the time taken before RA becomes degraded. In the case of a biological metabolite like RA, degradation is a crucial regulatory control mechanism rather than just loss of activity. Control of degradation is ensured by three members of the cytochrome P450 superfamily CYP26A1, CYP26B1 and CYP26C1 (Rhinn and Dolle, 2012; Romand et al., 2006). Homeostatic supply of RA in the embryo is thus tightly controlled by precise stage and –tissue-specific expression of both synthesizing (RALDHs) and degradation enzymes (CYP26). Interestingly, and consistent with their essential regulatory role to ensure the appropriate local RA concentrations, synthesizing and degrading enzymes are expressed in a mostly complementary pattern in the developing inner ear (Figure 1.9; Romand et al., 2006). This control of RA signalling is in addition to spatiotemporal control of receptor expression that comes as a last step in the signalling cascade

through which RA regulates gene expression through DNA binding as a RA/RAR/RXR complex.

The crucial functions of RA signalling during vertebrate development were first inferred by studying the teratogenic effects of excess RA, either indirectly by dosing pregnant mice or directly in chick embryo using RA-soaked beads (reviewed in Rhinn and Dolle, 2012). These experiments revealed profound craniofacial malformations illustrating that RA is a key signalling molecule in vertebrates (Yasuda et al., 1986). Later it was shown that excess RA affects a wide range of organ systems such as the hindbrain (Marshall et al., 1992), forebrain (Simeone et al., 1995), heart (Wasiak and Lohnes, 1999), limb (Kochhar et al., 1984), eye (Sulik et al., 1995) palate (Dempsey and Trasler, 1983) and the ear (Frenz et al., 1996). The study of VAD (Vitamin A deficient) quails and mouse knockout for RA receptors then showed that lack of RA, similarly to excess of RA, lead to developmental abnormalities. Mutant analysis and subsequent phenotypes affecting all the above organ systems revealed RA is an essential morphogen for normal embryonic development, with the lack of RA resulting in developmental defects (reviewed in Rhinn and Dolle, 2012). Interestingly, due to its broad spectrum of effects in embryonic development, RA has been referred to as ‘a master differentiation factor’ (Romand et al., 2006). This highlights the likelihood that RA will either control a large number of developmental genes, or some of the key developmental genes that are used in a large number of developmental contexts (such as the *Hox* genes for instance in patterning multiple developmental fields – limb, hindbrain, gut), in order to have such extensive effects in so many organs (reviewed in Romand et al., 2006). Elucidating the identity of the genes acting downstream of RA in

the different tissues is the first step toward understanding how RA controls development.

#### ***1.4.1 RA signaling in the developing hindbrain***

Although RA exerts its effects in multiple tissues, the molecular mechanisms underlying embryonic development normally controlled by RA in the developing hindbrain are specifically discussed in more detail here for two major reasons. First, the hindbrain is one of the organs/tissues where the effects of RA excess and deficiency have been best described at a molecular level, making the hindbrain a paradigm for understanding RA regulatory effects (reviewed in Rhinn and Dolle, 2012). Second, inner ear induction and cochlear coiling, two major inductive events in the developing inner ear, have been shown to be dependent on signalling from the hindbrain. Thus, any RA-induced changes in hindbrain patterning (described below) are potentially likely to indirectly influence inner ear development (Frenz et al., 2010). Clearly then, an understanding how RA affects hindbrain patterning will be crucial in the interpretation of phenotype and gene expression changes following aberrant RA signalling.

Hindbrain development involves the generation of 7 (mammalian) or 8 (avian) transient neuroepithelial compartments called rhombomeres (r), which all have a distinct molecular identity according to their position along the AP axis (Kiecker and Lumsden, 2005) and are units of cell lineage restriction. Rhombomere formation leads to the generation of specific molecular patterns along the hindbrain that vary at different axial levels. Therefore rhombomeres can be each characterized by a specific

combination of *Hox* gene expression. Disruption of this pattern of expression by exposure to excess vitamin A was first demonstrated 40 years ago (Morriss, 1972). In mouse embryos exposed to RA at 7.75dpc, at a stage before hindbrain patterning, the hindbrain appears shortened and adopts a r4-like identity according to molecular markers (Morriss-Kay et al., 1991). Interestingly, studies of embryos deficient in RA, such as VAD quails embryos (Gale et al., 1999), and also more recently VAD rat (White et al., 2000) also showed misspecification of the caudal hindbrain, where the region from r4 to r8 is transformed into an enlarged r3, while more anterior rhombomeres extended posteriorly (reviewed in Rhinn and Dolle, 2012). Thus, correct hindbrain patterning requires RA concentrations along the anterior-posterior axis to be at a specific equilibrium (homeostatic), with excess RA affecting the rostral hindbrain and RA deficiency affecting the caudal hindbrain. This suggested the existence of a spatially controlled RA gradient in the hindbrain, with specific concentrations of RA specifying different rhombomere compartments. This RA gradient hypothesis assumes the somitic mesoderm up to and including the 1<sup>st</sup> somite is the main source of RA in the hindbrain region due to its high concentration in RALDH2 (one of the enzyme involved in the 2<sup>nd</sup> step of RA biosynthesis from vitamin A). RA is then envisaged to diffuse from this source creating a gradient with high caudal RA concentration and low rostral concentrations. This hypothesis gained further support from the work of dissecting the regulatory pathway controlling *Hox* and other segmentally expressed genes in the hindbrain that were used as molecular markers for the RA excess and deficiency studies (Glover et al., 2006).

However, RALDH2 is not the only enzyme involved in RA biosynthesis and in addition, the specificity of RA concentration at a particular level is not determined by its synthesis alone, but rather by the equilibrium between synthesis and degradation. Thus, on top of this RA gradient that was so far presented like a passive mechanism, is likely superimposed an active process, which maintains and refines this gradient along the hindbrain through the specific expression of synthesizing and catabolizing enzymes. The highly dynamic expression of the RALDH5 and CYP26 genes in the hindbrain during its formation is in agreement with this hypothesis (Glover et al., 2006).

### **The effect of timing of RA administration on hindbrain patterning**

The teratogenicity described thus far in RA excess experiments is a consequence of administration at 7.75dpc, prior to hindbrain patterning, but interestingly the effects of RA were also studied by administering RA following hindbrain patterning, at 8.5dpc. Are homeostatic concentrations of RA only required during hindbrain formation or could excess RA also disrupt the patterning of the hindbrain after it has been specified? In other words, is the hindbrain pattern e.g. *Hox* code plastic? In embryos exposed to RA at 8.5dpc there was no apparent change of brain morphology (Wood et al., 1994) but further detailed molecular analysis revealed the change in expression of some molecular markers, with r2 ectopically expressing *Hoxb2* and *Hoxb1* (Figure 1.10; Morriss-Kay et al., 1991). The combined expression of these two genes is normally found in r4, suggesting that r2 had adopted a r4-like identity following RA administration after hindbrain patterning (Morriss-Kay et al., 1991). However, the *Hox* gene expression pattern of other rhombomeres and in particular r4 and r5, from which

emanate the inner ear inductive signals, appears unaltered. This is thus strikingly different from embryos exposed to RA at 7.75dpc, which all displayed a highly disrupted hindbrain identity (Figure 1.10). This difference between embryos exposed to RA prior to, or after, hindbrain patterning will thus likely play a major factor in differentiating direct and indirect effects of RA on the developing otocyst and on the control of otic gene expression.

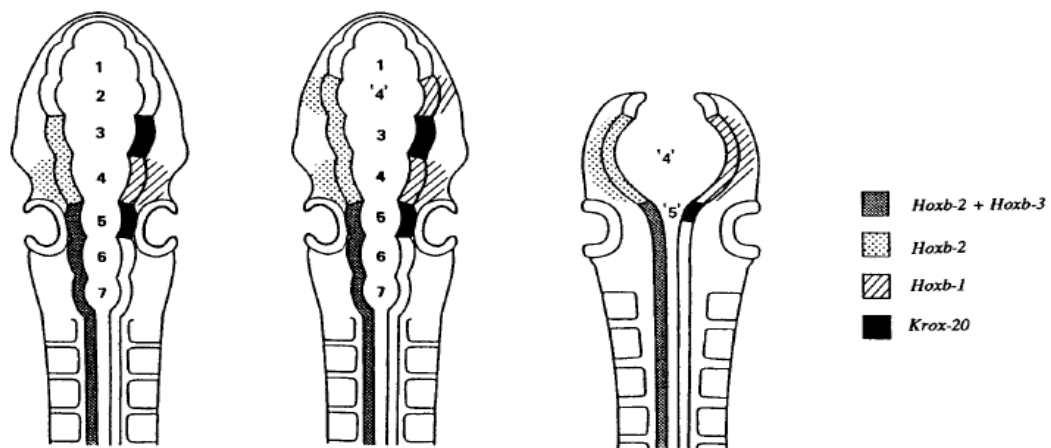


**Figure 1.10 Differential effects of retinoic acid on hindbrain patterning.** In control embryos the hindbrain is characterized by the expression of specific gene combinations along the antero-posterior axis. For instance rhombomere 4 (r4) is characterized by the expression of *Hoxb-2* and *Hoxb-1*. In embryos exposed to RA at 8.5dpc, after hindbrain patterning. Hindbrain formation is almost unaltered apart from r2 adopting a r4 like identity, with the misexpression of *Hoxb-2* and *Hoxb-1*. In embryos exposed to RA at 7.75dpc, prior to hindbrain patterning, the hindbrain appears shortened and adopt an r4 identity (adapted from Wood, 1994)

### **1.4.2 Effects of RA on the developing inner ear**

Inner ear development also requires optimal homeostatic concentrations of RA with both excess and deficiency leading to inner ear dysmorphogenesis – a so-called “Goldilocks” phenomenon (Frenz et al., 2010). Interestingly, the developing inner ear epithelium itself contains all the elements of the RA pathway, with RALDH, RAR/RXR and CYP26 expression distributed according to a dynamic and restricted pattern (Romand et al., 2006). Thus, in addition to the RA diffusing from the somatic mesoderm, *in situ* sources of RA synthesis in the inner ear epithelium are also likely to play a role in inner ear development. To summarize, there are two sources of RA: RA from the somitic mesoderm may affect the inner ear directly, but also indirectly through reprogramming the hindbrain, and a second source of RA within the otic epithelium itself that may affect inner ear development directly.

Although some ear abnormalities have been reported among the multiple craniofacial abnormalities mentioned in early RA teratogenic studies in mice (Yasuda et al., 1986) and humans (Lammer et al., 1985), the first conclusive demonstration of a role for RA in inner ear development was in cochlear cultures. In these *in vitro* experiments, exposure to excess RA during early postnatal development lead to the development of supernumerary rows of hair cells, suggesting RA may play a crucial role in cochlear hair cell differentiation (Kelley et al., 1993). Detailed *in vivo* studies of the effects of excess RA on the inner ear have subsequently revealed a number of developmental anomalies of the inner ear (Frenz et al., 1998; Frenz and Liu, 2000; Frenz et al., 2010; Frenz et al., 1996). For instance, the otic vesicle seemed shifted anteriorly in some 9.5dpc embryos (Frenz et al., 1996). At 11.5dpc, developing inner ears displayed elongating ovoid

shapes with almost half of them lacking the vestibulo-acoustic ganglion and endolymphatic duct. At 13.5dpc, in RA-treated embryos the developing inner ears showed an uncoiled rudimentary cochlear projection and the vestibular portion of the ear was disorganised; e.g. a common utriculo-saccular space in more than half of the ears analysed. In addition, the pattern of capsular chondrogenesis was irregular, and the vestibulo-acoustic ganglion was highly reduced or even absent, with a lack of neuritic projections to the cochlea (Frenz et al., 1996). Similar defects are observed in human embryos following exposure to RA during the first trimester of pregnancy, and these have been linked to sensorineural deafness (Lammer et al., 1985).

Interestingly, these defects mimic some of the phenotypes observed in *Fgf3* and *Fgf10* knockout mice. For instance, anomalies of the inner ear in *Fgf3* null mice includes a failure of endolymphatic duct formation and reduced cochlear coiling (Wright and Mansour, 2003), whereas anomalies of the inner ear in *Fgf10* null mice includes agenesis or reduction of the semi-circular canals and their innervations (Pauley et al., 2003). Interestingly, alterations in *Fgf3* expression in the brain had previously been reported in mice in which RA signalling is impaired by the target mutation of *Raldh2* (Niederreither et al., 1999) and in mice exposed to excess RA (Mahmood et al., 1996). *Raldh2* null mice present segmentation defects and altered gene expression in the posterior hindbrain, including downregulation and lack of proper restriction of *Fgf3* (Niederreither et al., 1999). In mouse embryos exposed to excess RA at 7.75dpc, *Fgf3* expression in the caudal hindbrain/rostral hindbrain was patchy, irregular and more extensive than normal. Upregulation of *Fgf3* expression at the midbrain/hindbrain junction, along with ectopic expression in the midbrain, were also reported following

RA administration at 8.25dpc (Mahmood et al., 1996). All together, this suggests that *Fgf3*, and perhaps also *Fgf10*, may be downstream targets through which RA exerts its effects during development. Given the importance of RA signalling and *Fgf3* in, not only inner ear development, but in human deafness, a thorough investigation of how RA leads to dysmorphology is required.

## **1.5 Other putative upstream regulators of *Fgfs* signalling**

### **1.5.1 *Gata3***

Members of the GATA family are transcription factors that bind to a consensus 'GATA' DNA-motif (A/T-GATA-A/G). Six factors (GATA1-6) have been identified in vertebrates. These factors are, similar to members of the FGF family, involved in cell-fate specification as well as cell differentiation, proliferation and motility during development (Patient and McGhee, 2002). Interestingly, two family members, *Gata2* and *Gata3*, are expressed in inner ear (Lillevali et al., 2006). Their expressions initially overlap in the mouse otic vesicle (around 9.5–10.5dpc) but become increasingly distinct during subsequent development with *Gata2* being mainly expressed in the nonsensory areas of the vestibular epithelium, whereas *Gata3* expression is confined to the sensory domains and is restricted to the cochlea by 18.5dpc (Lillevali et al., 2004). Mutation in either *Gata2* (Haugas et al., 2010) or *Gata3* (Lillevali et al., 2006) results in inner ear abnormalities.

*Gata3*, which is expressed throughout the otic placode at 8.5dpc, is one of the earliest markers of the inner ear (Lawoko-Kerali et al., 2002). Its expression has also been reported later on in the migrating auditory neuroblasts (Lawoko-Kerali et al., 2004). *Fgf10* also appears to be expressed in the delaminating neuroblasts (Pauley et al., 2003) although it has not yet been determined whether it is expressed in the auditory or vestibular neuroblasts only or in both types. *Gata3* is known to regulate multiple events during inner ear development with *Gata3* deficiency leading to severe abnormalities during otic placode invagination. The utricle, cochlea and endolymphatic duct are also strongly reduced in *Gata3* null embryos, suggesting *Gata3* also plays an important role in later morphogenetic events (Karis et al., 2001; Lillevali et al., 2006). In addition, *Gata3* is also thought to be involved in cochlear hair cell development and neurogenesis (Karis et al., 2001). The molecular basis of the defects observed in *Gata3* deficient inner ears are not yet understood, but the loss of *Fgf10* expression in otic epithelium and auditory ganglion suggests *Gata3* may be an important regulator of FGF signalling during development (Lillevali et al., 2006). In silico analysis of the *Fgf10* enhancer reveals the presence of putative GATA3 binding sites (Ohuchi et al., 2005) and GATA3 was shown to transactivate a *Fgf10* reporter construct in vitro in NIHT3T3 fibroblaste cell line (Lillevali et al., 2006). All together these data suggest that *Fgf10* is one of the targets through which *Gata3* exerts its effect on inner ear development. However the nature of this regulation – direct or indirect – is still to be determined. Although the transactivation experiment could suggest a direct regulation, there is no evidence that this occurs in vivo in inner ear cells.

### **1.5.2 The Neurogenin Pathway**

*Ngn1* and *NeuroD* are proneural genes that encode transcription factors of the basic Helix-Loop-Helix (bHLH) class and bind to a common DNA sequence called the E-box sequences (Abello and Alsina, 2007). The term proneural relate to their role in neurogenesis.

In vertebrate, inner ear neurogenesis first involves the specification of a proneural field characterised by the expression of *Ngn1* in the antero-ventral wall of the otic placode. Following *Ngn1* expression, the expression of *NeuroD1* is switched on and neuroblasts start to delaminate and differentiate. Members of the FGF family (*Fgf3*, *Fgf8* and *Fgf10*) are also expressed in the antero-ventral area and might be involved in the recruitment of cells into the neurosensory lineage (Abello and Alsina, 2007).

Functional analysis of *Ngn1* and *NeuroD* mutants suggests they are sufficient for neurogenesis, with *Ngn1* being involved in neuronal determination, and *NeuroD* being involved in neuronal differentiation and survival (reviewed in Abello and Alsina, 2007). In *Ngn1* mutant the proximal cranial sensory ganglia are lost (Ma et al., 2000) whereas ectopic neurons form in *Xenopus* if *Ngn1* is overexpressed (Perron et al., 1999). Disruption of *NeuroD* function also results in a severe loss of sensory neurons associated with the inner ear (Kim et al., 2001) as well as in the formation of ectopic hair cells within the auditory ganglia (Jahan et al., 2010). Interestingly, mutations in either *Ngn1* or *NeuroD* also affect the formation of the organ of Corti that is shortened in both mutants and presents multiple (ectopic) rows of hair cells (HC) (Fritzscht et al.,

2011). Thus, these two genes seem to play a crucial role both in neuron and hair cell formation.

These roles of *Ngn1* and *NeuroD* in the antero-ventral wall of the otic vesicle (Bok et al., 2007), where *Fgf10* is also expressed (Pauley et al., 2003; Abello and Alsina, 2007), suggest that these members of the *Neurogenin* pathway represent good candidates for regulating *Fgf10* expression in vivo.

## 1.6 Treating hearing impairment

How could we use the mechanisms naturally occurring during development to restore hearing? To illustrate that, a schematic example of a damaged organ of Corti is presented in Figure 1.11. In such case, the hair cells are lost and progressively replaced by epithelial cells. The idea is that if we could expose this damaged epiderm to the same set of signals allowing the differentiation of hair cells and neurons during embryogenesis then we may be able to force the differentiation of new hair cells to replace the one that had been lost. This could be done by direct delivery of the gene required for hair cell and neuron differentiation to the epiderm or, as depicted in Figure 1.11, by grafting cells that were induced to differentiate as hair cells/neurons in vitro beforehand (Brigande and Heller, 2009).

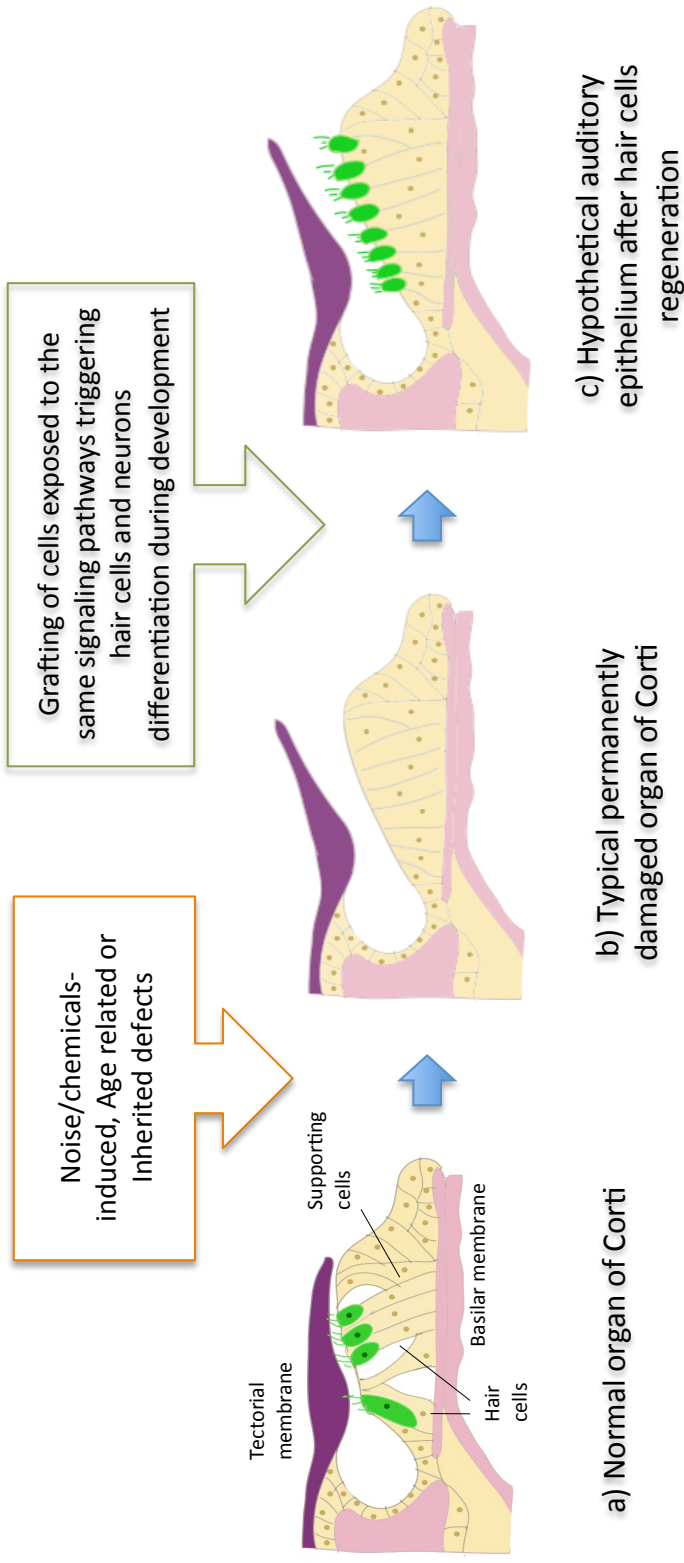


**Figure 1.11 Conceptual drawings of a normal, damaged and repaired organ of Corti.** (a) In the normal organ of Corti, mechanotransduction of sounds depends on the presence of functional hair cells (HC) in connection with bipolar auditory neurons. (b) Typically, damages of the organ of Corti results in the loss of HC and neurons innervating them as well as de-differentiation of supporting cells. Generic hair cells (HC) could be generated in vitro via exposure of embryonic stem cells to the same signaling pathways triggering HC and neuron differentiation during otic development. (c) Hypothetical implantation of the generic hair cells in the damaged otic epithelium and reformation of neuronal connection. It is unclear whether appropriate connection with the tectorial membrane will reform too ([Brigande et al. 2009](#)).

Such changes in the identity of differentiated cells are not just speculation; they have been achieved in vitro. Six years ago already, Shinya Yamanaka (Nobel Prize 2012) and Kazutoshi Takahashi turned differentiated fibroblasts into pluripotent cells in vitro by exposing them to a combination of only 4 genes: *Oct4*, *Sox2*, *Klf4* and *c-Myc* (Takahashi and Yamanaka, 2006). This demonstrates that a couple of key genes can have a tremendous effect on cell differentiation. Even more recently, human embryonic stem cells induced in vitro to differentiate into auditory neuron progenitors were shown to restore auditory evoked responses when transplanted in gerbils' cochlea (Chen et al., 2012). Interestingly, hair cell and auditory neuron-like features had been induced by exposure to *Fgf3* and *Fgf10*, putting these two genes in the regulatory pathway(s) controlling hair cell and neuron differentiation.

## 1.7 Project aims

In this project I thus took *Fgf3* and *Fgf10* as a starting point from which to investigate the network involved in hair cell and neuron formation. Bioinformatic analysis of *Fgf3/10* genomic regions revealed the presence of putative binding sites for retinoic acid (RA). However the spatial and dose-dependent effects of RA on *Fgf3/Fgf10* expression in vivo are unknown. Thus a major focus of this study was to investigate whether abrogated *Fgf3/10* signalling could in part explain the genesis of RA-induced inner ear phenotypes. In addition, this study also looked to investigate regulatory mechanisms underlying normal *Fgf10* expression in the inner ear during embryogenesis.

## 2

# MATERIAL AND METHOD

## 2.1 Mouse Genotyping

### 2.1.1 Transgenic mouse lines and primers used for genotyping

Four different genetically modified mouse strains/lines were used in this study:

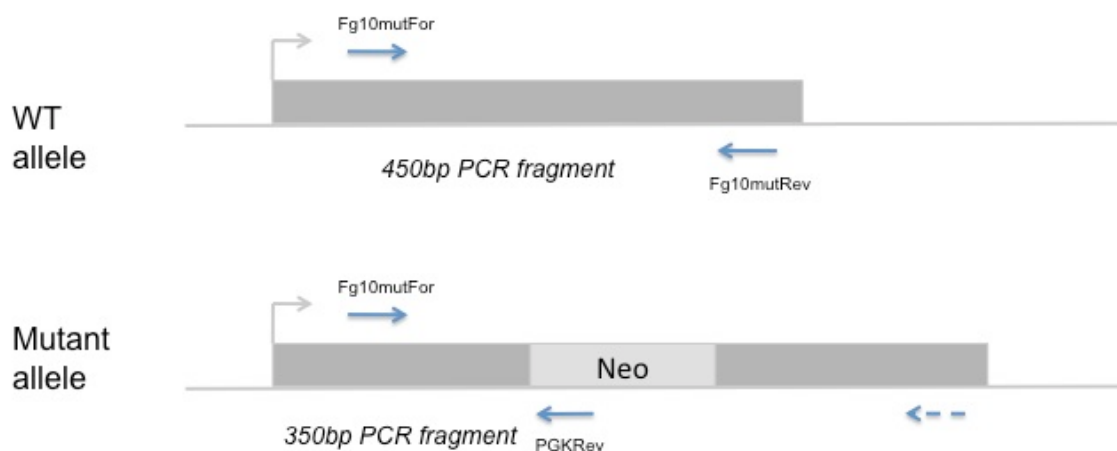
- (i) An *Fgf3-lacZ* reporter line that has been previously described (Powles et al., 2004) and is able to recapitulate *Fgf3* pattern of expression in all endogenous domains of *Fgf3* expression, with the exception of rhombomeres 5 and 6.
- (ii) An *Fgf10* mutant mouse line where a PGK-*neo* cassette had been inserted in reverse orientation in the *Fgf10* coding region (Min et al., 1998).
- (iii) An *Fgf10*-reporter line (3f3r-*ZsGreen*) able to recapitulate the endogenous pattern of *Fgf10* expression in the inner ear and that was generated in the laboratory during the course of this study as part of an independent project (Economou et al., 2013).
- (iv) A second *Fgf10*-reporter line (7f7r-*DsRed*) generated as part of this project and hypothesized to contain all enhancers' elements required to recapitulate the full pattern of *Fgf10* expression.

Each of these transgenic lines was genotyped by PCR amplification using one of the set of primers listed in Table 2.1.

**Table 2.1 – Set of primers used for the genotyping of the 4 transgenic mouse lines used in this study**

Transgenic mice line	Forward primer	Reverse primer
<b><i>Fgf3-lacZ</i></b>	5'-GCGACTTCCAGTTCAACATC-3'	5'-CTGGAATTCGCCGATACTG-3'
<b><i>Fgf10neo</i></b>	5'-TCCAGCTGTCTCTGCCTCGCAG-3'	5'-GGAGAACAGCAGCCTTCTCCAGCGGACA-3' 5'-CATCTGCACGAGACTAGTGAGACGTGC-3'
<b>3F3R-ZsGreen</b>	5'-GGAGATGACCATGAAGTACCGCATGG-3'	5'-GCTTGTGCTGGATGAAGTGCCAGTC-3'
<b>7F7R-DsRed</b>	5'-GCGATCGCAGGAAAGTGCCTAGGCT-3'	5'-GCTTGATGACGTTCTCAGTGCTATCCATGG-3'

Genotyping of *Fgf10* mutant embryos required making the difference between embryo homozygous or heterozygous for the mutation. *Fgf10*<sup>+/-</sup> and *Fgf10*<sup>-/-</sup> and WT embryos were identified using a set of three different primers (See Table 2.1 and Figure 2.1).

**Figure 2.1 – Genotyping of mouse embryos homozygote, heterozygote or wild-type for the *Fgf10* mutation.**

Annealing of *Fgf10* forward and reverse primers (blue arrows) to the wild-type *Fgf10* allele gives rise to a 450bp DNA fragment following PCR amplification. In the mutant allele a *Neo* cassette inserted in reverse orientation results in the *Fgf10* forward primer (blue arrow in broken line) to be 1.8kb apart from the *Fgf10* reverse primer. This 1.8kb fragment cannot be generated under the PCR conditions used for genotyping. However the second forward primer (indicated in italic in Table 2.1), in combination with the *Fgf10* reverse primer, results in the generation of a 350bp DNA fragment. Thus, wild-type alleles are predicted to amplify a 450bp fragment, whereas in the presence of the mutant allele a 350bp fragment is amplified. This permitted the identification of wild-type (one band of 350bp), homozygous (one band of 450bp) and heterozygous (two bands of 350 and 450bp) mutants.

### 2.1.2 DNA preparation from mouse ear notches

DNA was prepared from ear notches by digestion at 55°C overnight in 400µg/ml proteinase K (PK) in 20µL ear notch buffer (20mM Tris-Cl pH8.0, 10mM EDTA). The next day 180µL of ddH<sub>2</sub>O was added to the mix and the PK was heat inactivated at 95°C for 15min. 1-2µL of DNA solution was then used to set up PCR reactions.

### 2.1.3 PCR conditions

Typically PCR conditions were similar to the one used for *lacZ* genotyping (Table 2.2) with the exception of the annealing temperature that was 70.6°C for *Fgf10neo*, 65.5°C for 3F3R-*ZsGreen* and 63°C for 7F7R-*DsRed* PCR reactions were set up as described in table 2.3 with the exception of *Fgf10neo* genotyping, due to the presence of 3 primers instead of 2 (table 2.4)

**Table 2.2 PCR conditions for *LacZ* genotyping**

Description	Temperature	Time	Cycles
<b>Initial denaturation</b>	95°C	2min	1
<b>Denaturation</b>	95°C	30s	
<b>Annealing</b>	59°C	30s	x 35
<b>Elongation</b>	72°C	1min	
<b>Final Elongation</b>	72°C	2min	1
<b>Hold</b>	6°C	--	

Table 2.3 Standard PCR reaction mix

Reagents	V (in $\mu\text{L}$ )
<b>Ultra-pure water</b>	7.8
<b>10x buffer</b>	2.0
<b>2.5 mM dNTPs</b>	2.0
<b>Forward primer</b>	0.5
<b>Rev primer</b>	0.5
<b>Mg<sup>2+</sup></b>	4.0
<b>DMSO</b>	1.0
<b>DNA Taq polymerase</b>	0.2
<b>DNA</b>	2.0
<b>TOTAL</b>	20.0 $\mu\text{L}$

Table 2.4 - PCR reaction mix for genotyping of *Fgf10neo* embryos

Reagents	V (in $\mu\text{L}$ )
<b>Ultra-pure water</b>	6.8
<b>10x buffer</b>	2.0
<b>2.5mM dNTPs</b>	2.0
<b><i>Fgf10</i>MutFor</b>	1.0
<b><i>Fgf10</i>MutRev</b>	0.5
<b>PGKRev (315)</b>	0.5
<b>Mg<sup>2+</sup></b>	4.0
<b>DMSO</b>	1.0
<b>DNA Taq polymerase</b>	0.2
<b>DNA</b>	2.0
<b>TOTAL</b>	20.0 $\mu\text{L}$

### **2.1.4 Confirmation of *in vitro* genotyping results**

Whenever possible, PCR results were confirmed *in vivo* by analyzing reporter gene expression, or, through the visualization of morphological features of mutants, such as the lack of limb bud in *Fgf10*<sup>-/-</sup> mice that is detectable by 10.5dpc. Additionally, male homozygotes for a specific reporter gene were bred and identified as those giving rise to litters where all the embryos express the transgene when backcrossed to wild-type females. Ideally, each male should have been tested 13 times, because if out of 13 litters all embryos carry the transgene, then the probability the male is heterozygous is less than one in a thousand; as determined by a Chi-squared test with a Yates correction factor of 0.5 ([www.informatics.jax.org](http://www.informatics.jax.org)). However with just 5 litters for each male we can already be 95% confident that they were homozygotes. In addition, all *Fg3-lacZ* embryos (as presented in Chapter 3) showed visible X-GAL staining, with the exception of one (Figure 3.5G) for which genotype was further confirmed by a PCR on its yolk sac.

## **2.2 Retinoic Acid Administration to pregnant mice**

### **2.2.1 Preparation of chocolate/sugar pellets**

**Chocolate pellets.** To prepare chocolate pellets, chocolate spread (regular chocolate spread for human consumption available from supermarkets, 1.25g) was mixed with 800ml water and 5.6g icing sugar. Using a 10.0ml syringe, small pellets of around 50-150mg weights were made and allowed to set at 4°C on plastic Petri dishes. Experimental results (see section 3.1) showed that ideal size pellets weighed between 70 and 110mg for complete ingestion.

**Sugar pellets.** Writing icing sugar (Dr.Oekter brand) was used directly to make pellets in a Petri dish with setting at 4°C. Although this was not statistically tested, mice seemed to show a preference toward the green-coloured pellets during control feeding experiments with sugar only, and thus the green icing sugar was then preferentially used to generate RA-laced pellets. This apparent preference was based on the shorter time between exposure to the pellet and consumption by the mice (n=6). Since mice have next to no colour perception but a particularly developed sense of smell, this putative preference is more likely be due to the green paste scent.

**Retinoic acid-laced chocolate/sugar pellets.** To make retinoic acid (RA)-laced pellets, all-trans retinoic acid powder (Sigma) was added either to the chocolate mix or to icing sugar and mixed thoroughly until homogenous. The yellow RA powder is particularly easily visible when mixed with green icing sugar making it easy to monitor for homogenous RA mixing. Pellets were then left to set at 4°C for 2 hours before being transferred to -20°C where they were stored for up to a week without any noticeable decrease in efficiency (judged by reproducible generation of phenotypes). RA concentrations in the sugar/chocolate mix was adjusted according to the desired administration dose, ranging from 4.5mg/kg to 25mg/kg, in order to keep the pellets in the optimal size range of 70-110mg final pellet weight.

### **2.2.2 RA administration to mice via chocolate/sugar pellets**

*Fgf3-lacZ* homozygous males were crossed with wild-type females and pregnant mice were identified by the presence of a vaginal plug. RA administration was performed according to the protocol already described in detail elsewhere (Cadot et al., 2012). Briefly, for inner ear analysis, pregnant mice of mean weight of 25g received a dose of 0mg, 4.5mg, 6mg, 7mg, 8mg, 10mg or 25mg/kg RA mixed in either a chocolate or sugar pellet of the appropriate size either at 4pm on day 7 of gestation (for administration at 7.75dpc) or at 10:30am on day 8 of gestation (for administration at 8.5dpc). For doses of 2x25mg/kg of RA, time of exposure was 10:30am and 2:30pm on day 8. Clean cages without sawdust or bedding were used to allow visualization of pellet ingestion. These mice were then humanely killed by cervical dislocation at 9.5dpc or 10.5dpc as required for analysis, and their embryos processed as described in section 2.3. Embryos were examined on a Zeiss (Thornwood,NY) Stemi SVII stereomicroscope or Nikon (Melville,NY) Steromicroscope. For phenotype analysis of other organ systems, RA doses and timing of administration used were 100mg/kg at 11.5dpc for the limb and palate; and 10mg/kg at 7dpc for the heart. Mice were then humanely killed as described above and embryos examined at 18.5dpc (limb and palate analysis) or 9.5dpc (heart analysis).

### **2.2.3 RA administration via oral gavage**

For administration of RA via oral gavage, all-trans RA (Sigma) was resuspended in sesame seed oil at 5mg/ml and stored in the dark at 4°C until use the next day. For analysis of inner ear phenotypes, pregnant mice of mean weight 25mg received either one dose of 25mg/kg of RA at 10:30am or two consecutive doses of 25mg each at

10:30am and 2:30pm on day 8 as previously described (Frenz et al. 1996). Administration was performed using a blunt feeding needle with terminal ball bearing to reduce oesophageal abrasion. Mice were humanely killed by cervical dislocation at 9.5dpc and embryos processed as described in section 2.3. For limb, palate and heart phenotype analysis, doses and timing of administration were as described in the previous section 2.2.3.

### **2.3 Staining embryos for for $\beta$ -Galactosidase activity**

*Fgf3-lacZ* reporter expression was detected by staining for  $\beta$ -galactosidase activity. Pregnant mice were humanely killed by cervical dislocation and the uterus dissected and chilled immediately on ice in 1X PBS (Phosphate Buffer Saline, pH 7.4). Embryos were carefully dissected out of embryonic membranes and fixed by immersion in LacZ fixative (1% Formaldehyde, 0.2% Gluteraldehyde, 2mM  $MgCl_2$ , 5mM EGTA, 0.02% Nonidet P40 in PBS) for 30 minutes on ice. Embryos were then rinsed in PBS + 0.02% NP40 for three 30 minute washes. Embryos were then incubated overnight, in the dark at room temperature, in LacZ staining solution (5mM  $K_3Fe(CN)_6$ , 5mM  $K_4Fe(CN)_6 \cdot 3H_2O$ , 2mM  $MgCl_2$ , 0.01% sodium deoxycholate, 0.02% NP40) to which had been freshly added 1mg/mL of Xgal (5-bromo-4-chloro-indolyl- $\beta$ -D- galactopyranoside) in DMF (dimethylformamide). After development of the blue signal (around 18hours), embryos were rinsed 3 times in PBS and then post-fixed in 4% PFA (paraformaldehyde in PBS) at 4°C for 45-60min. Embryos were rinsed again 3 times in PBS before taking photographs on a Nikon SMZU stereomicroscope.

## 2.4 Histological methods

Some embryos were selected for further detailed analysis as wax sections. Such embryos, typically 9.5dpc to 11.5dpc in age, were first dehydrated in an increasing ethanol dilution series (25%, 50%, 75%, 95%, 100% x2) using 5 to 10 minute incubations according to their size. Next, embryos were cleared in two changes of HistoClear (National Diagnostic) for 20-45 minute incubation, followed by incubation in molten wax at 55-60°C for 5-30 minutes. Embryos were then transferred to moulds and set at 4°C. 10-20µM thick ribbons were cut on a microtome (Leica RM2135), sections floated on a waterbath and collected on TESPA (3-aminopropyltriethoxysilane) treated slides. For *lacZ* embryos, wax was removed from sections by brief immersion in Histo-Clear, sections rehydrated through a reverse ethanol series (100%, 95%, 70% ethanol and tap water etc) for 3 minute incubations, counterstained in 0.25% eosin for 10 seconds and dehydrated again before mounting in DPX mount. For in situ hybridization (ISH) embryos, sections were washed from the wax by brief immersion in HistoClear and they were mounted in DPX mount without counterstaining.

## 2.5 General DNA manipulation

### 2.5.1 DNA digestion by restriction endonucleases

1 to 10µg of plasmid DNA was digested with 3-5 units/µg of DNA of restriction endonuclease(s), with the appropriate buffer at 1x concentration in a final volume of 20 to 50µL. Buffers and enzymes were in general purchased from New England Biolabs. DNA incubation time varied depending on the purpose of the experiments.

For subsequent cloning, DNA digestions were incubated 1 to 2 hours maximum at 37°C; for minipreps, digestions were incubated for 2 hours to overnight.

### **2.5.2 Blunting DNA fragments**

Typically, fragments were first prepared by restriction endonuclease digestion and the enzyme was first inactivated by denaturation for 20min at 65°C or 80°C according to the endonucleases used (NEB appendix). If the enzymes used could not be heat inactivated, then DNA fragments were purified using the GeneClean kit (section 2.5.5) to purify DNA from a solution. The fill-in reaction using T4 DNA polymerase was then set up as described in table 2.9.

**Table 2.5 Reaction mix for blunting using T4 DNA polymerase**

Reagents	Quantities
<b>Restriction digest or purified DNA fragment</b>	15-47 $\mu$ L
<b>100x BSA</b>	0.5 $\mu$ L
<b>2.5mM dNTPs</b>	2 $\mu$ L
<b>T4 DNA polymerase</b>	1U/ $\mu$ g of DNA
<b>dH2O</b>	up to 50 $\mu$ L

The reaction mix was incubated for 15min at 12°C. The reaction was then stopped by the addition of 100mM of EDTA and heat inactivation of T4 for 20min at 75°C. Fragments were then purified using the GeneClean protocol (section 2.5.5)

### **2.5.3 Plasmid dephosphorylation**

Plasmid dephosphorylation was performed using the CIP alkaline phosphatase from Roche. Following plasmid digestion the DNA fragments to dephosphorylate were incubated for 1 hour at 37°C with 1U of CIP for 1pmol of DNA ends (Table 2.6)

**Table 2.6 Plasmid dephosphorylation reaction mix**

Reagents	Volume
<b>Restriction digest or purified DNA fragment</b>	15-37 $\mu$ L
<b>10X CIP Buffer</b>	5 $\mu$ L
<b>Calf Intestine Phosphatase (CIP)</b>	1U/1pmol of end
<b>dH2O</b>	up to 50 $\mu$ L

The phosphatase reaction was stopped by adding 1/10 vol of 200mM EGTA, followed by heat inactivation for 20min at 65°C. DNA fragments were then run on an agarose gel and purified using the GeneClean kit according to the protocol presented in section 2.5.5.

### **2.5.4 Agarose gel electrophoresis**

Typically 0.5-10 $\mu$ g of DNA fragments were resolved by agarose gel electrophoresis using 0.8-2% agarose gels containing 0.01% (2-5 $\mu$ l/100ml of 10mg/ml stock) ethidium bromide at approximately 75mA for 30-60 minutes. Agarose gels were prepared with, and run into, 1XTAE buffer obtained from freshly diluting 50X TAE buffer stock (40mM Tris Base, 20mM acetic acid, 1mM EDTA, pH 8.4)

### ***2.5.5 Extraction of DNA from agarose gel using the GeneClean protocol.***

DNA for extraction was run on an agarose gel at 0.8-1.5%. The required bands were cut out using a scalpel under long wave UV illumination. Exposure to ultra-violet was kept to a minimum since it is mutagenic for the DNA. DNA was then extracted from the bands using the GeneClean kit with some modifications to the manufacturer instructions. Briefly, gel slices were weighed in 1.5mL Eppendorf tubes. 3X volume 6M NaI (sodium iodide) were added and tubes were put to incubate for 5min at 55°C (or till dissolution of all the gel). 2.5µL of Glass milk were then added and tubes were incubated at room temperature (RT) on roll for 30min (an additional overnight incubation step at 4°C was performed for DNA fragments with sizes inferior to 800bp). Tubes were then centrifuged for 30sec at 13000rpm and supernatants discarded. Pellets were resuspended in 500µL, centrifuged for 5sec at 13000rpm and supernatant discarded. This step was performed a second time, following that, the pellets were centrifuged for 5sec to remove all traces of liquids and dried at 37°C for 5min. Pellets were then resuspended in 10µL of 10mM Tris pH8 and incubated for 1min at RT. Tubes were then centrifuged at full speed for 30sec and supernatants carefully transferred to a 0.5µL Eppendorf. Pellets were resuspended in another 10µL of Tris, incubated for 1min at 55°C and centrifuged at full speed for 30sec. The supernatants were pooled with the previous 10µL in the 0.5µL Eppendorf tube. 1µL of each tube was checked on gel for quantification.

### ***2.5.6 Ligations***

Ligations were usually set up at 3 different vector:insert ratios (Table 2.7), except for ligations known to be particularly efficient and for which only one ligation reaction was

set up at the ratio that seemed the most appropriate. A control without insert also allowed monitoring whether the vector had been fully digested and dephosphorylated when applicable.

**Table 2.7 – Typical ligation reaction set up**

Reagents	1:1	1:2	1:3	1:0
<b>Linearised plasmid</b>	5-50ng			
<b>Insert</b>	5-50ng			NONE
<b>T4 DNA Ligase buffer</b>	1	1	1	1
<b>T4 DNA ligase</b>	0.5	0.5	0.5	0.5
<b>dH2O</b>	up to 10 $\mu$ L			

Ligations were always incubated overnight at 12-16°C and sometimes left to incubate a couple of hours more at 4°C before being transferred at -20°C for storage till transformation.

### ***2.5.7 Generation of supercompetent cells***

The transformation efficiency of supercompetent cells is usually much better than what can be obtained with bacterial cells induced with calcium chloride. In addition, cells could be prepared in bulk and conserved at 4°C for months while being immediately available for transformation at any time. In order to generate supercompetent cells, a SOB plate was streaked with a frozen stock of DH5 $\alpha$  and incubated overnight at 37°C until the colonies were 2-3mm in diameter. The next day, one of these colonies was picked and incubated in 10mL of SOB medium (2% tryptone, 0.5% yeast extract, 10mM NaCl, 2.5mM KCL in dH<sub>2</sub>O) overnight with moderate

agitation (240rpm). On day 3, 4 x 50mL of SOB medium were inoculated with 100-500 $\mu$ L of overnight bacterial culture in a 500mL Erlen. Bacteria were then further incubated with moderate agitation at 37°C until the cell density is  $6.9 \times 10^7$  viable cells/mL, as evidenced by an OD = 0.3-0.4. It usually took 2hours for the bacterial cells to reach this stage. Cultures were then transferred to 50mL Falcon tubes and chilled on ice for 10-15min, before being centrifuged at 4°C for 20min at 3000rpm. Bacterial pellets should stay on ice at all times. Thus, they were quickly and thoroughly drained by inverting the tubes on some paper towels for a few seconds only. Pellets were then resuspended in 1/3 (17mL) of the original culture volume (50mL) in FSB (Frozen Storage Buffer: 10mM potassium acetate, 10% redistilled glycerol, 100mM KCl, 45mM MnCl<sub>2</sub>.4H<sub>2</sub>O, 10mM CaCl<sub>2</sub>.2H<sub>2</sub>O, 3mM HAcOCl<sub>3</sub>) using a 10mL pipette and incubated on ice for 10-15min before being centrifuged again at 4C for 20min at 3000rpm. After thoroughly draining the pellets, cells were resuspended in FSB to 1/12.5 of their original culture volume (thus into 4mL of FSB for an original culture volume of 50mL). 3.5% of DMSO (dimethyl sulfoxide, 140 $\mu$ L) was then squirted into the center of the cell suspension that was immediately swirled for 5-10sec. Tubes were then incubated on ice for 5min, after that a second aliquot of DMSO (140 $\mu$ L) was added, giving a 7% DMSO final concentration. Cells were swirled and incubated on ice again for 10-15min. Cells were then transferred to chilled screw cap tubes to make aliquots of 400-600 $\mu$ L. To finish, they were flash frozen in dry ice or in dry ice/alcohol bath before being transferred to the -80°C fridge for storage. Transformation efficiencies in the different batches of cell thus obtained varied between  $1 \times 10^8$  and  $2.5 \times 10^8$ .

### ***2.5.8 Transformation of supercompetent cells***

One or several supercompetent cell aliquots (according to the number of transformations to perform) were thawed on ice for 10min. In the meantime, 2-4 $\mu$ L of DNA ligations (between 10ng and 80ng of DNA) were added to 50mL falcons chilled on ice. As soon as thawed, 100 $\mu$ L of supercompetent cells were added to each falcon and swirled briefly. After a 30min incubation on ice, the cells with DNA were heat-shocked for 1 min 25sec at 42°C, and then left to rest for 2min on ice. 500 $\mu$ L of SOC (10mM MgCl<sub>2</sub>, 10mM MgSO<sub>4</sub>, 20mM Glucose in SOB medium) was then added to each transformation and the cells were incubated at 37°C with moderate agitation for 1hour. Following that, 100 $\mu$ L of cells were plated on LB plates + 100mg/mL Ampicilline or 50mg/ml Kanamycin depending on the construct being cloned.

### ***2.5.9 Plasmid DNA purification and analysis***

A successful transformation of supercompetent cells with ligations means that a certain number of colonies will have grown on the LB+antibiotic plates that have been incubated overnight. In order to determine whether these colonies have really taken up the DNA construct under investigation, the plasmid DNA needs to be amplified and then extracted from the bacteria for analysis. To do so, up to 24 colonies were used to inoculate each 5mL of LB + antibiotic. Overnight incubation with moderate agitation at 37°C will allow amplification of the plasmid for DNA analysis. The following day, 1.5mL of each miniculture was transferred to a 1.5mL Eppendorf tube and centrifuged for 1min at 13000rpm. The supernatant was discarded and the pellets centrifuged for 30sec more in order to eliminate all traces of LB medium that could interfere with DNA analysis later on. First the pellets were resuspended in 100 $\mu$ L of Solution I (50 mM

Glucose, 25mM Tris-Cl, 0.5mM EDTA in dH<sub>2</sub>O), then 200µL of freshly made Solution II (0.2N NaOH, 1% SDS in dH<sub>2</sub>O) was added and the tubes inverted 6 times each. To finish 150µL of SolIII (3M potassium acetate, 11.5% glacial acid acetic in dH<sub>2</sub>O) was added, the tubes were inverted 6 times again, and then incubated for 5min on ice before being centrifuged again for 5min at 13000rpm. The supernatants were transferred to new tubes and the pellets discarded. Once bacteria have been harvested, and the plasmid released, it has to be precipitated and purified. To do so, 1mL of 100% Ethanol was added to the 1.5mL Eppendorfs. Tubes were inverted several times to mix the DNA with ethanol and then incubated at room temperature for 5min, the time needed for the DNA to precipitate. Tubes were then centrifuged at 13000rpm for 5min and the ethanol discard. DNA pellets were then rinsed with 250µL of 70% ethanol, centrifuged again for 1min to get rid of all traces of ethanol and then dried at 55°C for 10min. Pellets were then resuspended in 20-40µL of TE (pH8) depending on their size.

### **Midipreps**

The plasmid DNA obtained from miniprep extraction is neither pure nor concentrated enough to allow for any experiments to be performed. Large Scale Plasmid Preparations, or Midipreps, thus needed to be performed. To do so 4 x 50mL of LB with the appropriate antibiotic were inoculated with 500µL of miniculture and grown for around 16hours, or till OD = 3. Each 50mL culture was poured into a 50mL Falcon and centrifuged at 3000rpm for 20 minutes at 4°C. Pellets were then processed using the Promega or Roche Midiprep kit according to manufacturer's protocol. DNA was typically resuspended in 200µL of water and its concentration determined using an Eppendorf BioPhotometer.

### **Restriction analysis**

Restriction analysis was usually performed in two steps. First, a screening for DNA fragment of expected construct size versus plasmid alone using an enzyme that cut once in the vector. Second, the identity and orientation of the fragment cloned was confirmed by digesting the clone both with an enzyme cutting in the plasmid, and an enzyme cutting in the insert. Even when an enzyme cutting both in the insert and in the vector was available, thus allowing the identification of positive clones from the first step, at least one more restriction digest was performed to confirm this positive result.

## **2.6 Reporter vectors**

Two reporter vectors were used in this study. pZsGreen 1-1 that encodes an optimized variant of wild-type *Zoanthus* sp. Green fluorescent protein, ZsGreen1 (Figure 2.2) and pDsRed-Express2-1 that encodes DsRed-Express2, a variant of the *Discosoma* sp. Red fluorescent protein, DsRed (Figure 2.3). Both vectors are promotorless and were thus modified by the addition of a  $\beta$ globin promoter.

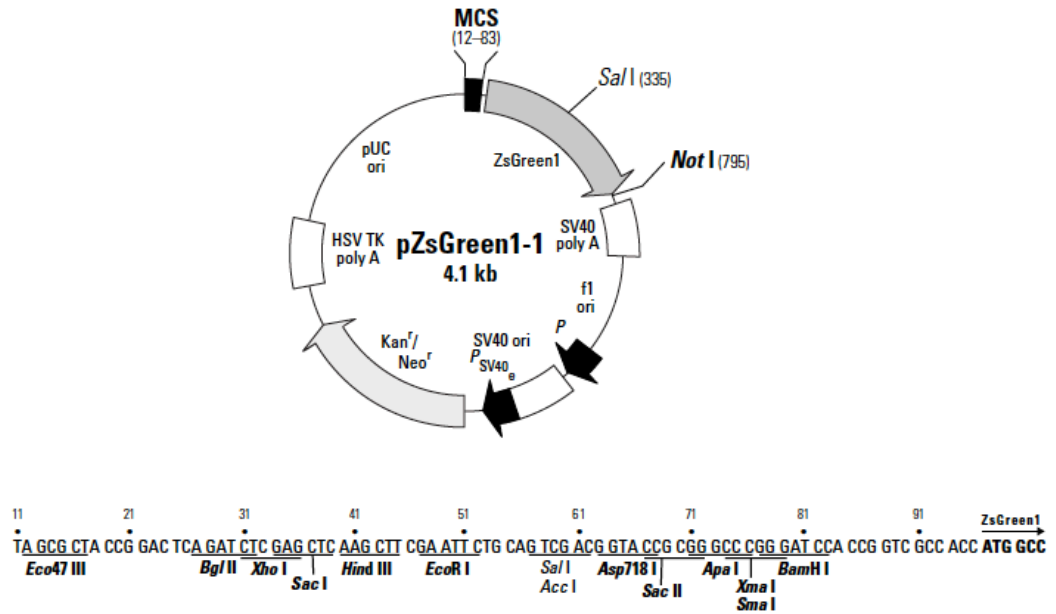


**Figure 2.2 pZsGreen1-1 vector.** Restriction map and multiple cloning site (MCS) of the promoterless ZsGreen1 reporter vector. © Clontech

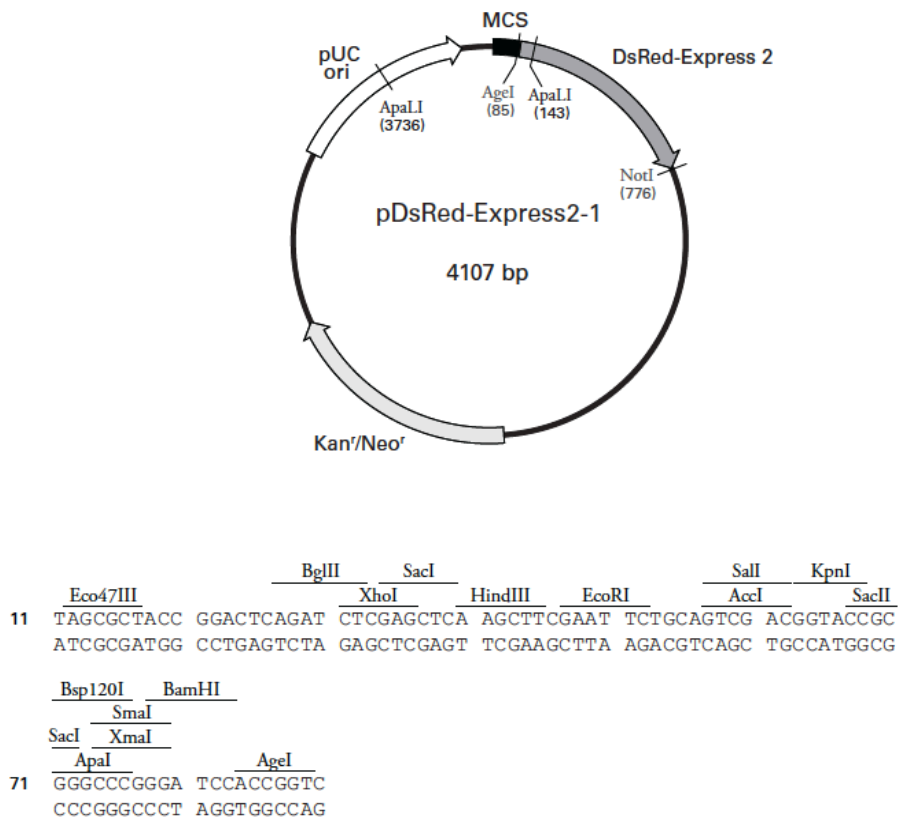


**Figure 2.3 pDsRed-Express 2-1 vector.** Restriction map and multiple cloning site (MCS) of the promoterless DsRed2 reporter vector. © Clontech

### 2.6.1 Reporter vectors used in mice

The pZsGreen vector had been modified prior to the start of this doctoral project with the insertion of a minimal human  $\beta$ globin promoter as a *Bam*HI fragment:

5'GGATCCCCCGGGCTGGGCATAAAAGTCAGGGCAGAGCCATCTATTGCTTACATTTGCTTCTA  
GCCTGCAGGTCGAGGAGCGCAGCCTTCCAGAAGCAGAGCGCGGCCATGGGGGATCC-3'

Black letters represent the human  $\beta$ globin promoter sequence whereas blue letters are plasmid sequences originating from the plasmid from where the promoter was taken out. The TATA box is highlighted in red and the +1 in green. In addition, an *Spe*I restriction site had been generated upstream of the promoter by the cloning of *Spe*I linkers in the *Sma*I restriction site in the MCS. The  $\beta$ globin-pZsGreen1-1 vector has been shown to drive reporter expression in mice if, and only if, a suitable enhancer is cloned upstream (Economou et al., 2012). The pDsRed vector was thus modified similarly, except that *Spe*I linkers were cloned into the *Sal*I restriction site.

### 2.6.2 Reporter vectors used for chick electroporation

Three reporter constructs were used for analysis into chick: mini $\beta$ globin-*ZsGreen*, *CMV-DsRed* and a dual reporter including both mini $\beta$ globin-*ZsGreen* and *CMV-DsRed* in a single construct. The mini $\beta$ globin promoter used in the chick reporter constructs is a shortened version of the one used in mice reporter constructs, where only sequences indispensable for expression have been kept. In particular, plasmid backbone DNA is cut out: 5'GGGCATAAAAGTCAGGGCAGAGCCATCTATTGCTTACA-3'. *CMV-DsRed* contains a chicken  $\beta$ -actin promoter that drives constitutive expression of *DsRed* and was used as a positive control of electroporation.

## 2.7 *Fgf10* reporter constructs

*Fgf10* enhancer fragments were amplified with High Fidelity PCR polymerase using the PCR primers listed in table 2.8. The location of the primers is schematised in Figure 2.4. The generation and cloning of *Fgf10* reporter constructs is detailed in the results (sections 4.2 and 4.4).

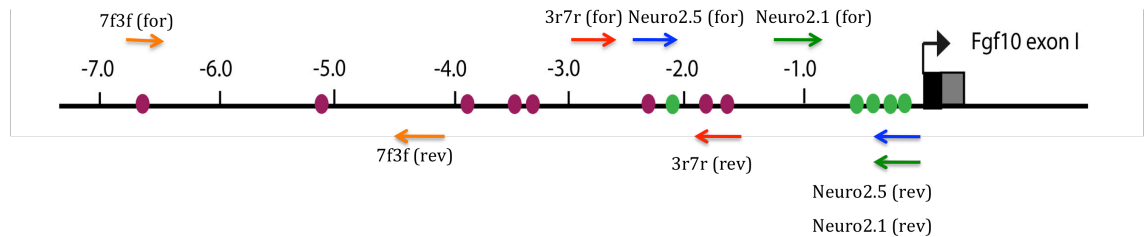


**Figure 2.4 PCR primers location within the 7.0kb *Fgf10* upstream region.** In orange are indicated the primers to amplify the 7f3f fragment while adding *SpeI* and *NdeI* restrictions sites. In red are indicated the primers to amplify the 3r7r fragments while adding *SpeI* and *NdeI* restrictions sites. In blue are indicated the primers to amplify the Neuro2.5 fragment and in green the primers to amplify the Neuro1.1 fragment. Plain red circles mark the position of putative Gata3 binding sites and plain green circles the position of putative binding sites for NGN11, NEUROD or NSCL1.

**Table 2.8 List of primers used to generate *Fgf10* enhancer fragments**

Enhancer fragment	Forward primer	Reverse primer
<b>Neuro2.5</b>	5'-TGTACTGAAACTCTCGGCACTG-3'	5'-AGTGTGGGCTGAAGAAGTGTC-3'
<b>Neuro1.1</b>	5'-TCTGTTCTTGAGAGAGATTTGCC-3'	5'-AGTGTGGGCTGAAGAAGTGTC-3'
<b>7f3f(<i>SpeI</i>/<i>NdeI</i>)</b>	5'-GAGAGAACTAGTACATCAGGGCTACCT GGCAGAGAC-3'	5'-GAGAGACATATGCAGATGCCTTAGTA GCTATGCTCTCTG-3'
<b>3r7r(<i>SpeI</i>/<i>NdeI</i>)</b>	5'-GAGAGACATATGTGTGATGTTCTGTCAC GTTGTTGA-3'	5'-GAGAGAACTAGTCAGAAGAGGATGCTC TGGGCA-3'

\**SpeI* sites are indicated in blue and *NdeI* sites in red

DNA fragments were amplified from mouse genomic DNA or from a FGF10 BAC clone using high-fidelity PCR with Phusion DNA polymerase (Thermoscientific) or Expand

Long Template PCR system (Roche). PCR conditions and reaction mixes are listed in the tables below, 3R7R fragment amplification (Table 2.9 and 2.10), 7F3F and Neuro2.5 fragment amplification (Table 2.11 and 2.12), Neuro1.1 fragment amplification (Table 2.13 and 2.14).

**Table 2.9 Conditions used for 3R7R fragment amplification with Phusion**

Description	Temperature	Time	Cycles
<b>Initial denaturation</b>	98°C	2min	1
<b>Denaturation</b>	98°C	30s	
<b>Annealing</b>	55°C	30s	x 35
<b>Elongation</b>	72°C	30s	
<b>Final Elongation</b>	72°C	10min	1
<b>Hold</b>	6°C	--	

**Table 2.10 Reaction mix used for 3R7R fragment amplification**

Reagents	V (in $\mu\text{L}$ )
<b>Ultra-pure water</b>	11.8
<b>10x HF buffer</b>	2.0
<b>2.5mM dNTPs (200 <math>\mu\text{M}</math>)</b>	2.0
<b>3R7R forward primer (500 <math>\mu\text{M}</math>)</b>	1.0
<b>3R7R reverse primer (500 <math>\mu\text{M}</math>)</b>	1.0
<b>DMSO (3%)</b>	1.0
<b>Phusion DNA polymerase (1U)</b>	0.2
<b><i>Fgf10</i> BAC DNA</b>	1.0
<b>TOTAL</b>	20.0 $\mu\text{L}$

**Table 2.11 Conditions used for 7F3F and Neuro2.5 amplifications with Expand Long Template**

Description	Temperature	Time	Cycles
<b>Initial denaturation</b>	94°C	2min	1
<b>Denaturation</b>	94°C	30s	
<b>Annealing</b>	54°C	30s	x 30
<b>Elongation</b>	68°C	3min 30s	
<b>Final Elongation</b>	68°C	10min	1
<b>Hold</b>	6°C	--	

**Table 2.12 Reaction mix used for 7F3F and Neuro2.5 fragment amplification**

Reagents	V (in $\mu$ L)
<b>Ultra-pure water</b>	14.2
<b>10x buffer2</b>	2.0
<b>2.5 mM dNTPs</b>	1.5
<b>7F3F or Neuro2.5 forward primer</b>	0.6
<b>7F3F or Neuro2.5 reverse primer</b>	0.6
<b>DMSO</b>	0.4
<b>Expand Long Template Polymerase</b>	0.2
<b>Fgf10 BAC DNA</b>	0.5
<b>TOTAL</b>	20.0 $\mu$ L

**Table 2.13 Conditions used for Neuro1.1 amplification with Phusion**

Description	Temperature	Time	Cycles
<b>Initial denaturation</b>	98°C	2min	1
<b>Denaturation</b>	98°C	30s	
<b>Annealing</b>	66°C	30s	x 35
<b>Elongation</b>	72°C	30s	
<b>Final Elongation</b>	72°C	10min	1
<b>Hold</b>	6°C	--	

**Table 2.14 Reaction mix used for Neuro1.1 fragment amplification**

Reagents	V (in $\mu$ L)
<b>Ultra-pure water</b>	21.4
<b>5X GC buffer</b>	8.0
<b>2.5 mM dNTPs</b>	3.2
<b>Neuro1.1 forward primer</b>	2.0
<b>Neuro1.1 reverse primer</b>	2.0
<b>DMSO</b>	1.2
<b>Phusion DNA polymerase</b>	0.4
<b><i>Fgf10</i> BAC DNA</b>	2.0
<b>TOTAL</b>	40.0 $\mu$ L

## 2.8 In situ hybridization

### 2.8.1 Riboprobes synthesis

In situ hybridizations were carried out according to standard methods. Single-stranded DIG-labelled sense and anti-sense *Fgf10*, *Gata3* and *NeuroD* riboprobes were prepared using RNA polymerase T7 and T3. In order to generate riboprobes and sens control, 5µg of cDNA were first digested in a final volume of 50L, and this until full linearization of the construct. Riboprobes synthesis was then performed overnight at 37°C as indicated in table 2.15.

**Table 2.15. Riboprobes synthesis**

Reagents	Volume
<b>Linearised cDNA clone (~1ug)</b>	10µL
<b>10x Transcription Buffer</b>	2.0µL
<b>0.1M DTT</b>	2.0µL
<b>DIG Labelling Mix</b>	2.0µL
<b>RNAsin</b>	0.5µL
<b>T3/T7 polymerase</b>	0.5µL
<b>DEPC H2O</b>	up to 20µL

### 2.8.2 Riboprobes purification

Riboprobes were purified by precipitation in Lithium Chloride in presence of Linearised Acrylamide. For lithium chloride precipitation, the reaction mix shown in table 2.16 was added to the transcription reaction, mixed well and left to precipitate overnight at -80°C. The next day, the samples were centrifuged at full speed for 20min at 4°C. The

supernatants were then removed and replaced with 70% Ethanol. Samples were centrifuged again for 10min at 4°C. After the supernatant was discarded, the pellets were dried at 37°C, and then resuspended in 1X TE.

**Table 2.16 Riboprobes purification by precipitation in Lithium Chloride**

Reagents	Volume
<b>Linearised Acrylamide</b>	1µL
<b>1X TE DEPC</b>	100µL
<b>4M LiCl</b>	10µL
<b>100% Ethanol</b>	300µL

### ***2.8.3 Wholemout In Situ Hybridization protocol***

At the appropriate gestational stage (8.5-11.5dpc), pregnant female mice were humanely killed by cervical dislocation and embryos dissected, rinsed in DEPC-PBS, and fixed at 4°C in 4% PFA in DEPC PBS for 30 minutes to 2 hours, depending on the size of the embryos. Embryos were subsequently rinsed in DEPC-PBS and dehydrated through a methanol series at 4°C (25%, 50%, 75% and 2x100% methanol in PBT (PBS + 0.1% Tween) and stored at -20°C prior to wholemount in situ hybridization.

#### **Pre-treatment and RNA hybridization**

On day 1 of in situ hybridization (ISH), selected embryos were transferred to RNase free 2mL Eppendorf tubes and rehydrated through a methanol serie at RT in 5-10min steps (75%, 50%, 25% methanol) followed by two washes in PBT. Embryos were then incubated at RT for 5 to 20min in 10µg/mL Proteinase K, according to the size of the

embryos. The Proteinase K reaction was stopped by re-fixing the embryos at RT for 20min in fresh 0.2% gluteraldehyde/4% PFA in PBT. Embryos were then washed 3 times in PBT for 5min and twice for 5min in hybridization buffer (50% formamide, 5X SCC pH5, 1% SDS, 50µg/mL yeast DNA, 50µg/mL heparine, 5mM DEPC EDTA, 0.2% Tween, 0.5% CHAPS in dH<sub>2</sub>O). Embryos were then prehybridized for 2 hours in hybridization buffer, and then hybridized overnight at 63°C in hybridization buffer with riboprobe at a concentration of 1µg/mL.

#### **Washes and immunohybridization**

On day 2, the embryos were rinsed twice, incubated for 30min at 68°C in Solution I (50% formamide, 5X SCC pH5, 1% SDS in dH<sub>2</sub>O), and transferred to new 2.0mL Eppendorfs. Embryos were then washed twice for 30min at 65°C in Solution III (50% formamide, 2X SCC pH5, 1% SDS in dH<sub>2</sub>O). Following that, embryos were washed 3 times in 1X TBST (0.14M NaCl, 2.7mM KCl, 1% Tween in dH<sub>2</sub>O) and incubated for 3hours in pre-Ab solution (2% blocking reagent, 10% lamb serum in TBST). They were then incubated overnight at 4°C in pre-Ab solution with riboprobe at a 1/2500 concentration.

#### **Washes and immunodetection**

On day 3, the embryos were transferred to new 2.0mL Eppendorfs and washed in 1X TBST three times for 5min each, and then five times for 1hour at RT. Before initiating the staining reaction embryos were equilibrated in freshly made NTMT (100mM Tris pH9.5, 1.4M NaCl, 50mM MgCl<sub>2</sub>, 0.1% Tween 20 in dH<sub>2</sub>O) via two 20min washes. Embryos were then stained in the dark in NTMT + 4.5µL NBT (nitro-blue tetrazolium

chloride) and 3.5 $\mu$ L BCIP (5-Bromo-4-chloro-3-indolyl phosphate) for 20min on roll and then at 37°C until properly stained. Development of the staining reaction was checked regularly under a Nikon SMZ1500 stereomicroscope. For most embryos further staining in PVA (polyvinyl acetate) was required. Staining reaction was then stopped by three washes in PBT + 1mM EDTA and post-fixed for 1hour in 4% PFA in PBS.

## **2.9 Immunohistochemistry**

Immunolabelling was carried out according to standard methods. Briefly 9.5, 10.5 and 11.5dpc embryos were dissected out of their embryonic membranes and fixed for 1 to 2 hours in 4% PFA. Embryos were then washed 3 times in PBS-1% Triton for 30 minutes each time, before being incubated for 1 hour in block solution (PBS 1% triton + 10% lamb serum + 0.2% sodium azide). An alpha-red primary antibody raised in rat (Chromotek) was used at a 1/1000 in block solution for labelling at 4°C for 2 days with gentle rotation. After several washes in PBS-1% Triton and block solution for 1 hour, the secondary anti-goat antibody was added at a 1/500 dilution in block solution and embryos were incubated for 2 days with gentle rotation at 4°C. Embryos were then washed in PBS-Triton and stored in the dark at 4°C. Photographs were taken using a Nikon AZ100 fluorescent microscope.

## **2.10 Chick otocyst electroporation**

### ***2.10.1 DNA preparation***

The day before electroporating, *Fgf10*-reporter constructs were precipitated overnight in ethanol and resuspended in 20 $\mu$ L of Tris pH7.5 at a concentration of 3-4 $\mu$ g/ $\mu$ L.

### ***2.10.2 Eggs preparation and incubation***

Fertilized eggs were ordered (from Henry Stewart) and stored at 10°C for use within a week. On day 1, eggs were arranged horizontally and incubated at 37°C for around 40hrs or until the embryos reached HH stage 11 (Hamburger and Hamilton, 1992). On day 3, 5-10ml of albumin was removed from the egg with a 10ml syringe needle. Using cellotape, the top of the eggs was then covered to prevent the shell from cracking when cutting out a little re-sealable window on the top of the eggs. This process is called windowing. No more than 5 embryos were windowed at once to prevent embryos from drying out during electroporation. Black ink was injected under the embryo to visualize whether they had reached the appropriate embryonic stage; if not, the egg was resealed using parafilm and left to incubate for few more hours. The incubator was kept humidified with sterile water.

### ***2.10.3 DNA injection and electroporation***

Needles were stored in a square Petri Dish, using stripes of blue tack as needle holders/rests. Injection needles were loaded with DNA/FastGreen mix and held in place on the side of the microscope using blue tack. On the day of electroporation, 2 $\mu$ L of each enhancer constructs (3-4 $\mu$ g/ $\mu$ L) were mixed with 2 $\mu$ L of CMV-*DsRed* control,

and Fast Green was added to the mix at 1/10 volume. When using the dual reporter (which already include an internal CMV-DsRed control), Fast Green was added at 1/10 volume to 4 $\mu$ L of construct. DNA was then mixed and centrifuged at full speed for 30 seconds. The supernatant was transferred to a clean tube and stored on ice until loading of the electroporation needle. Embryos were electroporated with a BTX ECM 830 electroporator with the following settings: Voltage, 15V; Pulse length, 50msec; Pulse number, 5. Following electroporation, eggs were immediately re-sealed with parafilm.

#### ***2.10.4 Chick embryos harvesting and analysis***

12 to 18 hours after electroporation, chick embryos were dissected out of all embryonic membranes and fixed in 4% PFA for 1hour. Photographs were taken with a Nikon AZ100 stereomicroscope and imaged captures using a Nikon Ds-Fi1 digital camera.

### **2.11 Mouse pronuclear injections**

Transgenic mice were generated by Mark Maconochie by pronuclear microinjection of linearised DNA constructs into pronuclei of F2 eggs produced by superovulation of 28-38 day F1 (CBAxC57/BL6) females crossed with F1 stud males as described in Hogan et al., 1994. Injected embryos were then transferred to pseudopregnant F1 (CBAxC57/BL6) females. F1 mice were used because they possess hybrid vigor (Research.jax.org). In particular, they have larger litters and thus produce more eggs for injection and later more transgenic embryos to analyse. They also survive better under stress, such as the one imposed by the transfer of the injected embryos to the

pseudopregnant females. Founder embryos were used to generate stable transgenic lines. Genotyping for the presence of reporter transgenes was performed as described in section 2.1. The embryos examined were F2. Contrary to F1 hybrid, they are genotypically distinct and therefore some variations in phenotypes may be expected.

# RETINOID CONTROL OF FGF3 EXPRESSION

---

Endogenous retinoic acid (RA) plays a key role during inner ear development, with both excess and deficiency of RA resulting in developmental abnormalities (Frenz et al., 2010). RA was first shown to affect ear development in babies born from teenage girls that had been treated for cystic acne with a daily dose of 40mg isotretinoin (13-cis RA) during their pregnancy (Lott et al., 1984). A detailed analysis of RA-induced embryopathy of the mouse inner ear (Frenz et al., 1996) reports a number of anomalies, such as the absence of the endolymphatic duct and vestibulo-acoustic ganglion at 11.5dpc; as well as an uncoiled cochlear duct, abnormal capsule formation and incomplete semicircular duct formation at 13.5dpc. Defective semicircular canal formation was also shown in chick following in ovo implantation of RA-soaked beads (Choo et al., 1998). Interestingly RA also affects cell differentiation in the organ of Corti, with exogenous RA addition resulting in an increase in the number of hair cells and supporting cells (Kelley et al., 1993). The next step in understanding the role of RA in inner ear development is to identify the molecular mechanisms underlying RA-induced inner phenotypes. Interestingly, mutational analysis of *Fgf10* and *Fgf3* report defects similar to the one induced by excess RA, such as abnormal semicircular

formation and innervation was reported in *Fgf10* null mice (Pauley, 2003) and failure to form the endolymphatic duct and reduced cochlear coiling in *Fgf3* mice (Wright and Mansour., 2003). Furthermore in silico analysis of the *Fgf3* enhancer reveals the presence of 7 putative RA responsive elements (RAREs). In this chapter, the spatiotemporal effects of RA on *Fgf3* expression are investigated in detail using an *Fgf3-lacZ* reporter mouse line. Moreover, a new non-invasive method for RA delivery to pregnant mice is designed as an alternative to gavage feeding.

### **3.1 Development of an improved non-invasive method for retinoic acid administration**

Whilst the demonstration had been done that mice would self-administer RA via chocolate pellets, only 50% of mice ate such treats. Furthermore, the time required for the mice to eat the treat ranged from 1 to 4hrs, indicating that improvements were still required for this to represent a routine method of RA application. In order to refine the recipe, pellets of various sizes and of various coating (freshly made RA-free paste or icing sugar) were experimented. These trials revealed that the pellets were more easily ingested when their size was around 70mg. Furthermore, icing sugar coating also increased intake. It became clear that the presence of sugar seemed to positively influence the efficiency of intake, and therefore I decided to try making sugar pellets rather than chocolate pellets. Pellets were prepared using commercially available writing icing sugar and, as suspected, drastically increased the efficiency of self-administration. This then became the routine method used for the outlined below.

### 3.2 Validation of the new protocol for administering RA using sugar/chocolate pellets

After improving the efficiency of the self-administration of pellets above, next the reliability, reproducibility and harmlessness of the vehicle alone were tested. In the pilot experiments carried out during my MSc project, the couple of different RA doses used seemed to give different phenotypes but only one litter was analysed for each dose. Thus to explore any reproducible dose-dependent relationship, a wider range of RA dosing levels was also tested in multiple litters. Firstly, a literature search was carried out to review the range of RA doses used by researchers (Table 3.1, Appendix Table S1, note that references for both tables are in the Appendix), which revealed a very broad range of RA has been used in different contexts.

**Table 3.1** Range of doses used to investigate the role of RA in the development of different organ systems

Dose (mg/kg)	Organ system
<b>Gavage</b>	
0,313-2,5	Eye, craniofacial (Sulik et al., 1995)
5	Pharyngeal arches (Taylor et al., 1995)
10	Palate (Wang et al., 2009), forelimb (Campbell et al., 2004), axial skeleton (Iulianella and Lohnes, 1997), Neural crest (Mallo and Brandlin, 1997; Mulder et al., 2000), heart (Wasiak and Lohnes, 1999), hindbrain (Morris-Kay et al., 1991; Mahmood et al., 1996)
12	Hindbrain ((Morris-Kay et al., 1991; Wood et al., 1994; Mahmood et al., 1996), pharyngeal arches (Mahmood et al., 1996)
3x 12.5	Neural tube closure/NTDs (Ehlers et al., 1992)
20	Limb (Kwasigroch et al., 1984), axial skeleton (Kawanishi et al., 2003), hindbrain (Conlon and Rossant, 1992; Marshall et al., 1992; Folberg et al., 1999), forebrain (Simeone et al., 1995)
25	Neural crest (Mulder et al., 2000), hindbrain (Leonard et al., 1995)
2x 25	Inner ear (Frenz et al., 1996; Frenz and Liu, 2000; Liu et al., 2008)
30	Palate, forelimb (Campbell et al., 2004), axial skeleton (Kawanishi et al., 2003), midbrain, forebrain (Simeone et al., 1995; Avantaggiato et al., 1996; Zhang et al., 2003)
40	Limb (Kwasigroch et al., 1984), axial skeleton (Kawanishi et al., 2003)
50	Neural crest (Mulder et al., 2000), inner ear (Frenz et al., 1996)
60	Palate, forelimb (Campbell et al., 2004), limbs (Anson et al., 1991), pharyngeal arches (Vanmuylder et al., 2004)
70	Palate (Degitz et al., 1998; Zhang et al., 2003)
80	Limb (Kochhar, 1973; Kwasigroch et al., 1984)
100	Palate, forelimb (Campbell et al., 2004; Abbott et al., 2005), limb (Kochhar, 1984; Kwasigroch and Neuberger, 1980; Cusic and Dagg, 1985; Alles and Sulik, 1989; Hayes and Morris-Kay, 2001), palate (Kochhar et al., 1984; Wang et al., 2009), neural crest (Mulder et al., 2000), pharyngeal arches (Abe et al., 2008), heart (Wasiak and Lohnes, 1999)
200	Limb, palate (Kochhar et al., 1984)
<b>IP injection</b>	
1, 3, 5, 7.5	Forelimb (Lee et al., 2006)
12.5	Eye (Ozeki and Shirai, 1998)
30	Neural tube closure/NTDs (Kuno et al., 1999)
50	Forelimb (Shimizu et al., 2007), neural tube closure/NTDs (Dempsey and Trasler, 1983; Kuno et al., 1999)
53	Neural tube closure/NTDs (Kapron-Bras and Trasler, 1988)
70	Heart (Ratajska et al., 2005)

Initially, mice were exposed to what seems to be one of the most common doses used in previous teratogenic studies of the hindbrain (10mg/kg). Excess RA was administered using either gavage or pellet.

Analysis of embryos at 9.5dpc revealed that regardless of the delivery method, a variety of developmental abnormalities similar to what has previously been reported in the literature were generated (Figure 3.1). Malformations include smaller embryos, general truncation of the anterior CNS in 85% (n=13) of the embryos (Figure 3.1A,C,O,N), profound delay in the closure of the anterior neural tube in 54% of the embryos (arrows, Figure 3.1A-D,M-O) and a wavy/crenulated neural tube more posteriorly (asterisks, Figure 3.1B,D,N,P). This demonstrated that similar teratogenic phenotypes could be generated through both conventional gavage feeding and this new system for delivery of RA. Moreover the phenotypes are generated at similar doses through both delivery methods.

Developmental delay and severity of malformations in embryos exposed to 10mg/kg prompted an analysis of RA teratogenicity at lower doses. A dose of 7mg/kg still resulted in craniofacial malformations with in particular a delay in anterior neural tube closure in 90% (n=31) of the embryos (arrows, Figure 3.1E,F,H). However, the dorsal margin of the neural tube were not wavy as in embryo fed with 10mg/kg of RA (asterisks, Figure 3.1B,D,N,P) but instead appeared smooth as in the control embryo. Strikingly, embryo size was also similar to control embryos (Figure 3.1E,H).

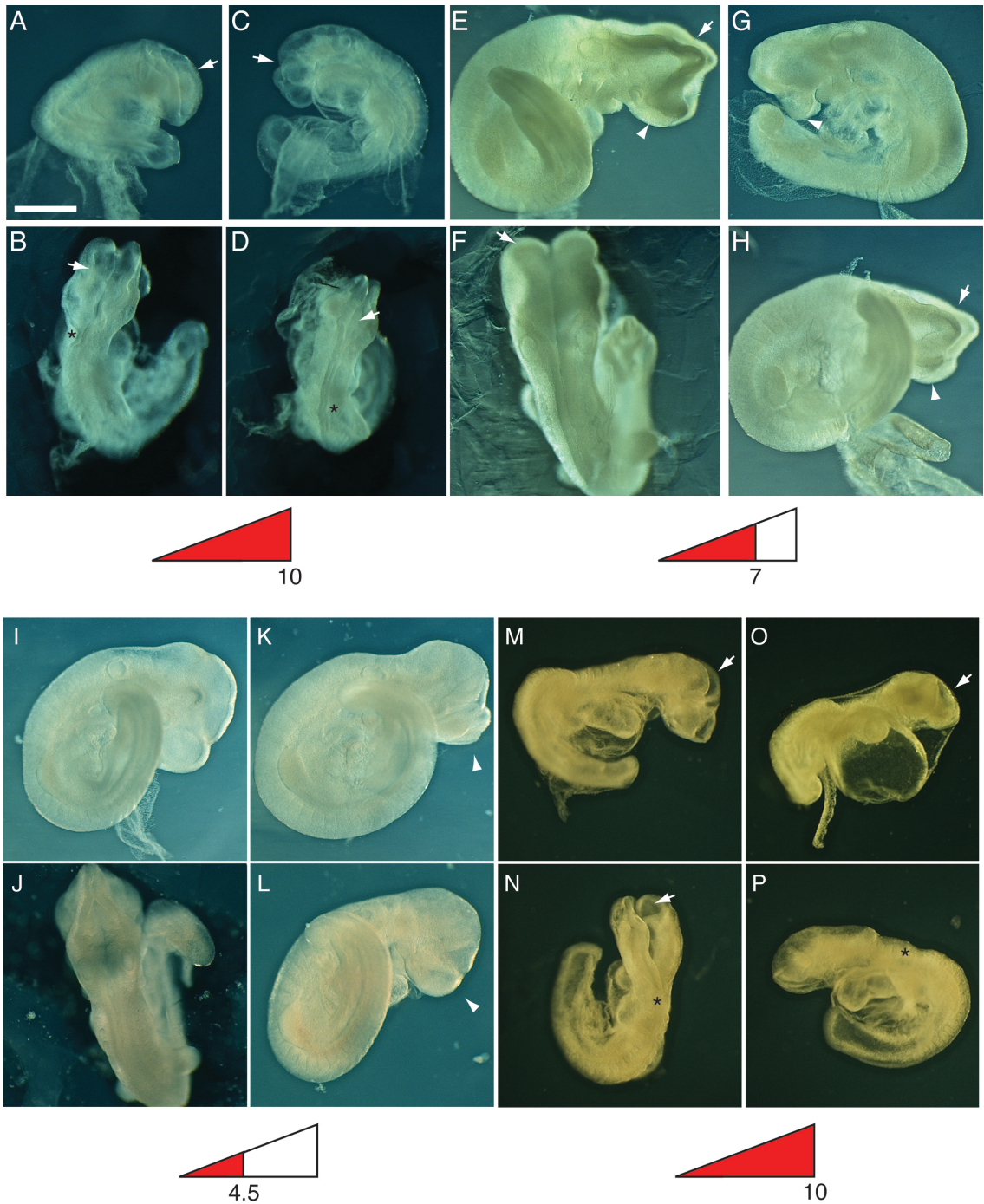


**Figure 3.1 Dose-dependant embryo malformations following RA administration via sugar pellets.** Pregnant mice were fed with RA-laced sugar pellets at 7.75dpc and their litters analyzed at 9.5dpc. Doses were as indicated on the figure : (A-D) 10mg/kg, (E-H) 7mg/kg, (I-L) 4.5mg/kg. Gavage administration was also performed as a control using 10mg/kg (M-P). Increasing RA dose led to an increase in embryo malformations that includes open neural tubes (indicated with arrows), shortened prosencephalon (indicated by arrowheads) and wavy neural tube borders (Indicated by asterisks). Embryos exposed to high doses of RA were also smaller than normal suggesting a developmental delay or growth reduction. Comparison of embryos exposed to RA via sugar pellets or gavage shows that the exact same phenotypes are induced. Scale bar = 500 $\mu$ m. Adapted from (Cadot et al., 2012) Copyright © 2012 Wiley Periodicals. Inc

Furthermore, the anterior truncation only occurred in 19% (n=31) of the embryos with the remaining 81% of embryos displaying a less severe phenotype characterized by a foreshortening of the prosencephalon (arrowheads, Figure 3.1E,G,H). Surprisingly, the incidence of open neural tubes in embryo exposed to 7mg/kg of RA was higher than in embryos exposed to 10mg/kg. However this does not imply neural tube formation was more affected by 7mg/kg of RA as evidence by the sharp decrease in anterior truncation in embryo exposed to this lower dose of exogenous RA (Table 3.2a). Next, an even lower dose of 4.5mg/kg of RA was trialled (Figure 3.1I-L). Only 43% (n=14) of embryos exposed to this dose presented a delay in anterior neural tube closure (Figure 3.1K), none displayed any obvious anterior truncation and 57% of the embryos displaying a normal phenotype (Figure 2.1I,J). Numbers of embryos displaying the different phenotypes are summarised in table 3.2a.

**Table 3.2 Incidence of phenotypes and changes in *Fgf3* expression with increasing RA dose**

<i>Table 3.2a RA administration at 7.75dpc</i>					
Ra dose (/kg)	4.5mg	6mg	7mg	8mg	10mg
<b>Number of embryos analysed</b>	<b>14</b>	<b>23</b>	<b>31</b>	<b>23</b>	<b>13</b>
Anterior truncations	0%	13% (3)	19% (6)	65% (15)	85% (11)
Open neural tube	43% (6)	78% (18)	90% (28)	91% (21)	54% (7)
<b>Number of embryos analysed</b>	<b>7</b>	<b>23</b>	<b>22</b>	<b>29</b>	<b>7</b>
Altered <i>Fgf3</i> spinal cord expression	0%	0%	0%	24% (7)	100%
Altered <i>Fgf3</i> rhombomere boundary	28% (2)	74% (17)	90% (20)	100%	100%
Altered <i>Fgf3</i> otic expression	28% (2)	79% (19)	90% (20)	100%	ND
<i>Table 3.2b RA administration at 8.5dpc</i>					
RA dose (/kg)	4.5mg	8-10mg	25mg	25mg gavage	2x25mg gavage
<b>Number of embryos analysed</b>	<b>10</b>	<b>20</b>	<b>15</b>	<b>16</b>	<b>8</b>
Altered <i>Fgf3</i> otic expression	0%	90% (18)	93% (14)	88% (14)	100% (8)

\*Numbers in parentheses corresponds to number of embryos

In order to confirm that the chocolate/sugar vehicle alone was not responsible for the phenotypes observed, control mice were fed with pellets of 1x, 3x and 5x the amount of unsupplemented vehicle used for RA administration (see Figure 3.2). Since the next experiments would look at the expression of *Fgf3-lacZ*, control embryos presented are expressing this transgene. None of these doses generated any of the abnormalities reported with excess RA, confirming that the teratogenicity presented was due to RA itself and not constituents present in the chocolate paste or writing icing sugar. In addition *Fgf3-lacZ* expression was unaltered.

Taken together, this new method of RA self-administration using sugar pellets seems to be an effective alternative to gavage, with the advantages of not involving any invasive procedures or requiring any animal restraint. In addition, these data showed that the incidence and severity of RA-induced phenotypes is dose-dependent.

### **3.3 *Fgf3*-expression in embryos exposed to RA prior to hindbrain patterning (at 7.75dpc)**

In order to address the spatiotemporal relationship between RA and *Fgf3* expression in the whole embryo, the response of the *Fgf3-lacZ* reporter line to increasing RA concentrations was studied. The data is presented in sections focused on different developing domains: the spinal cord, hindbrain and midbrain, and the otic vesicle.

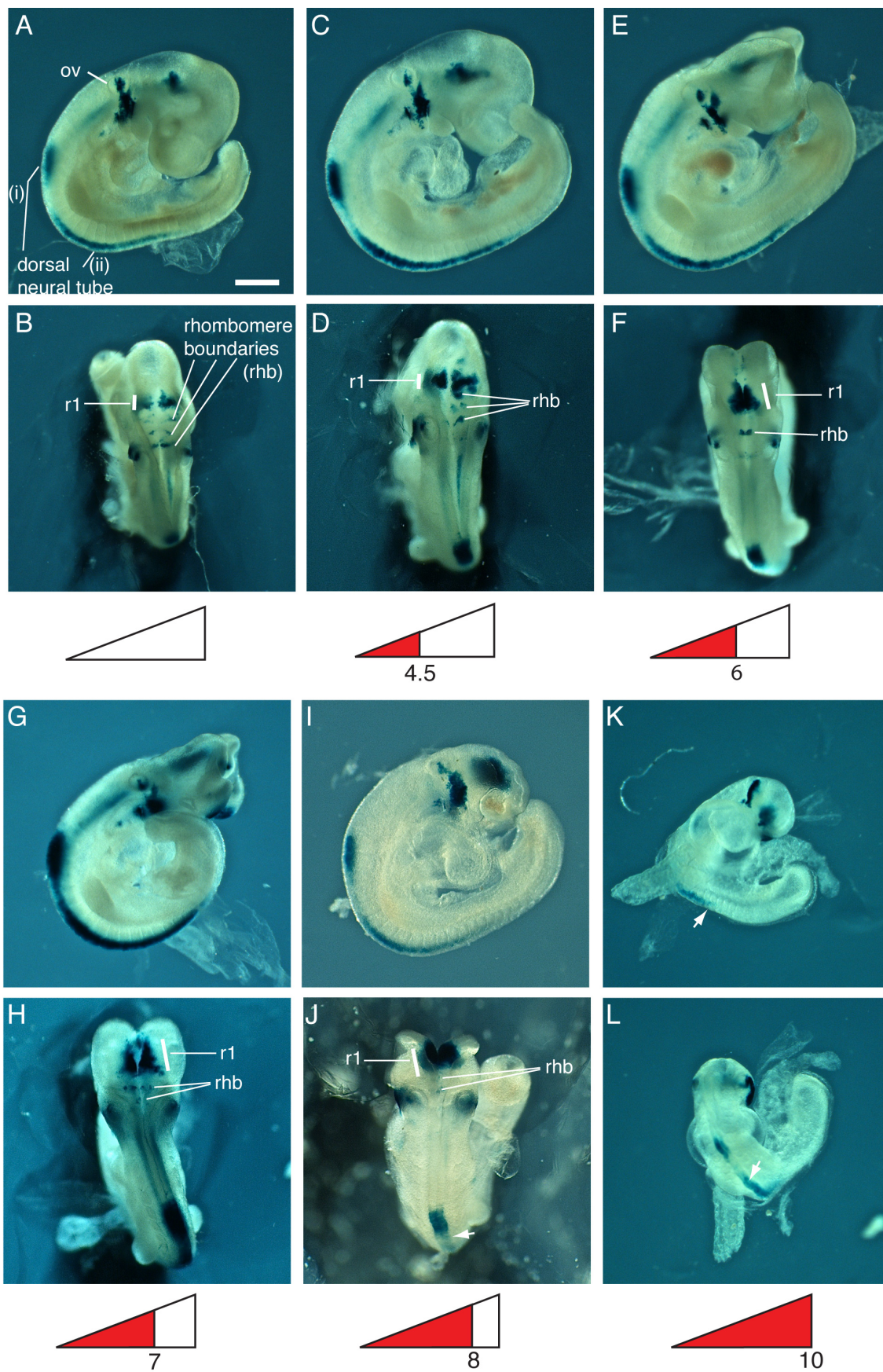
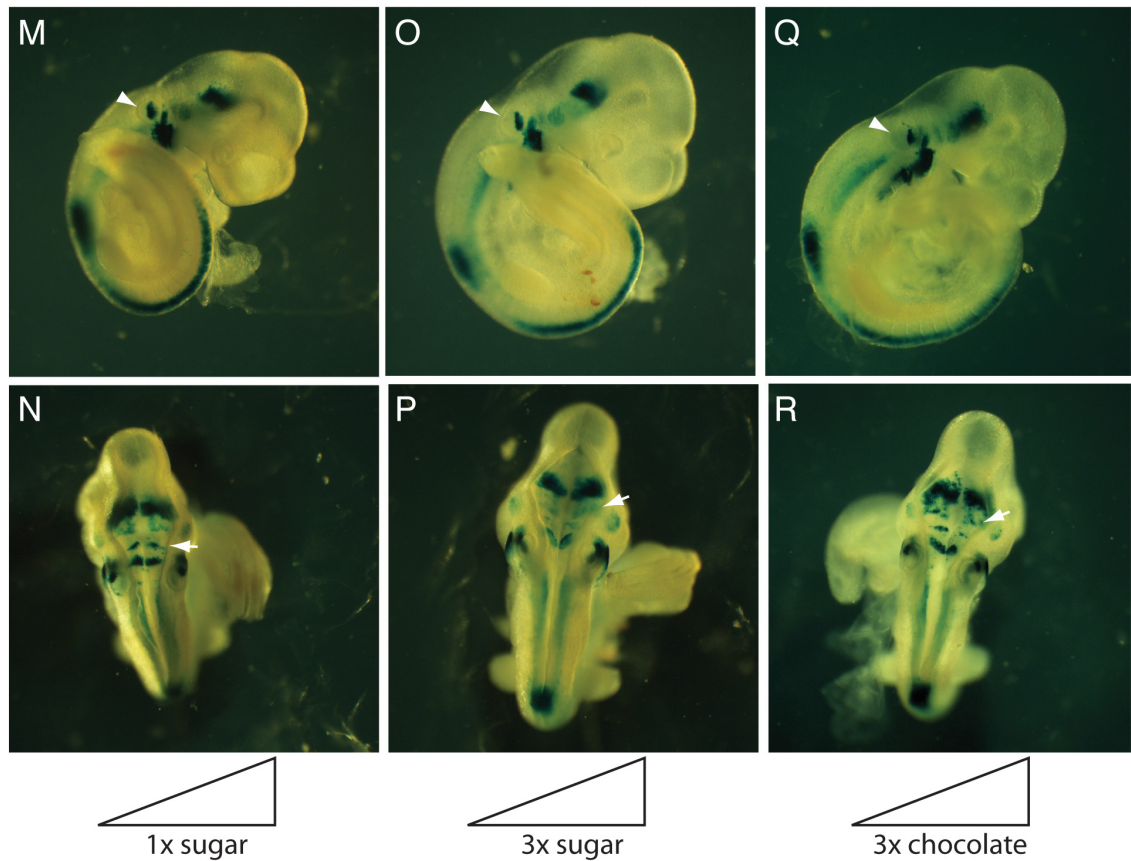


Figure 3.2 (continues)



**Figure 3.2 Analysis of *Fgf3-lacZ* expression pattern in 9.5dpc embryos following administration of increasing RA doses at 7.75dpc.** Lateral and dorsal views of untreated, RA treated and control embryos are shown in consecutive panels. (A,B) Untreated embryos; (C,D) 4.5mg/kg; (E,F) 6mg/kg; (G,H) 7mg/kg; (I,J) 8mg/kg; (K,L) 10mg/kg. Hindbrain *Fgf3* expression is altered from 6mg/kg (F), starting with a loss of rhombomere boundary expression domains. Increasing doses of RA leads to increasing alteration of *Fgf3* expression in the hindbrain, with a complete loss of expression in embryos exposed to 10mg/kg of RA(K,L). *Fgf3* expression in the spinal cord starts becoming weaker and patchy with doses of 8mg/kg (arrows in J) and 10mg/kg (arrows in K,L). Control embryos were treated with 1x sugar (M,N), 3x sugar (O,P), and 3x chocolate (Q,R). None of these doses lead to any developmental abnormalities or alteration of *Fgf3-lacZ* expression either in the otic vesicle (arrowheads in M,O,Q) or in the hindbrain (arrows in N,P,R). Scale bar = 500  $\mu$ m. Adapted from (Cadot et al., 2012) Copyright © 2012 Wiley Periodicals, Inc

### **3.3.1 Spinal cord**

*Fgf3* expression in the spinal cord normally consists of two domains. The first domain is restricted to a small area of dorsal neural tube expression located just anteriorly to the forelimb bud (Figure 3.2 Ai). The second domain is more extensive, starting at the level of the forelimb and spreading posteriorly, approximately until the future hindlimb region (Figure 3.2Aii). *Fgf3* expression in these domains appears unaffected in embryo treated with 4.5mg, 6mg and 7mg/kg of RA (Figure 3.2C,E,G). A dose-dependent downregulation of *Fgf3* was however observed with RA dose of 8mg/kg (Figure 3.2I) and 10mg/kg (Figure 3.2K) of RA. At these higher doses *Fgf3* expression appeared patchy in 24% (n=29) of the embryos exposed to 8mg/kg of RA and 100% of embryos exposed to 10mg of RA (see table 3.2a). It was however spatially restricted to the same area as in control embryos.

### **3.3.2 Hindbrain and midbrain**

The minimal *Fgf3* enhancer used in this study lacks the regulator elements required to drive endogenous *Fgf3* expression in rhombomeres 5 and 6. However, the *Fgf3-lacZ* reporter recapitulates endogenous expression throughout rhombomeres 1 as well as at rhombomere boundaries r2/3, r3/4 and r4/5 at 9.5dpc (Figure 3.2B). *Fgf3* expression in one or more of these rhombomere boundaries was lost when using doses of 6 to 8mg/kg and a complete abolition of boundary expression was observed with 10mg/kg (Figure 3.2L). On the other hand, expression of *Fgf3-lacZ* in rhombomere 1 persists and actually appears more extensive than in the control (compare Figure 3.2B to 3.2F,H,J) apart from a dose of 10mg/kg where expression in all rhombomeres and rhombomere boundaries has disappeared. This is most likely due to the severe

truncation of the anterior neural tube. Alteration of *Fgf3* expression at rhombomeric boundaries was also found to be dose-dependent, with only 28% of embryos with altered rhombomeres boundary expression for a dose of 4.5mg/kg (n=7); 74% for 6mg/kg (n=23); 90% for 7mg/kg (n=22) and 100% for 8-10mg/kg (n=36). Results are summarised in table 3.2a.

### **3.3.3 The developing inner ear/otic vesicle**

The particular focus of this project is the developing inner ear, therefore the detailed effects of RA on *Fgf3* expression in the developing inner ear were also analyzed through both wholemount analysis and sections. Figure 3.3 illustrates sections taken at dorsal, mid and ventral planes through the otocyst, along the horizontal axis, with the exception of the embryo for 10mg/kg. *Fgf3* is normally expressed in the antero-ventral wall of the otic vesicle, extending in the lateral and dorsal domains (Figure 3.3A-Aiii). In embryo treated with 4.5mg/kg of RA this expression was unchanged (Figure 3.3B-Biii). However with doses of 6mg/kg and 7mg/kg it begins to be lost in the dorsal domain of the otic vesicle (Figure 3.3C,D). A few *Fgf3*-expressing cells are highlighted by arrowhead in Ci and Di). At highest RA doses (8-10mg/kg) *Fgf3* expression was totally lost from the dorsal otic domain (Figure 3.3Ei,Fi). The ventral patch of expression is the most persistent and although downregulated for doses of 6 to 8mg/kg, it was never abolished in the embryos presented here (Figure 2.4C,D,Cii,Dii,Ciii,Diii). As noted for the spinal cord and hindbrain, downregulation of *Fgf3* expression in the otic vesicle was dose-dependant: 28% of the embryos exposed to 4.5mg/kg showed an alteration of otic *Fgf3* expression (n=7); this number increases to 74% with a 6mg/kg RA dose (n=23), 90% with 7mg/kg and 100% with 8mg/kg (n=29) (see table 3.2a).

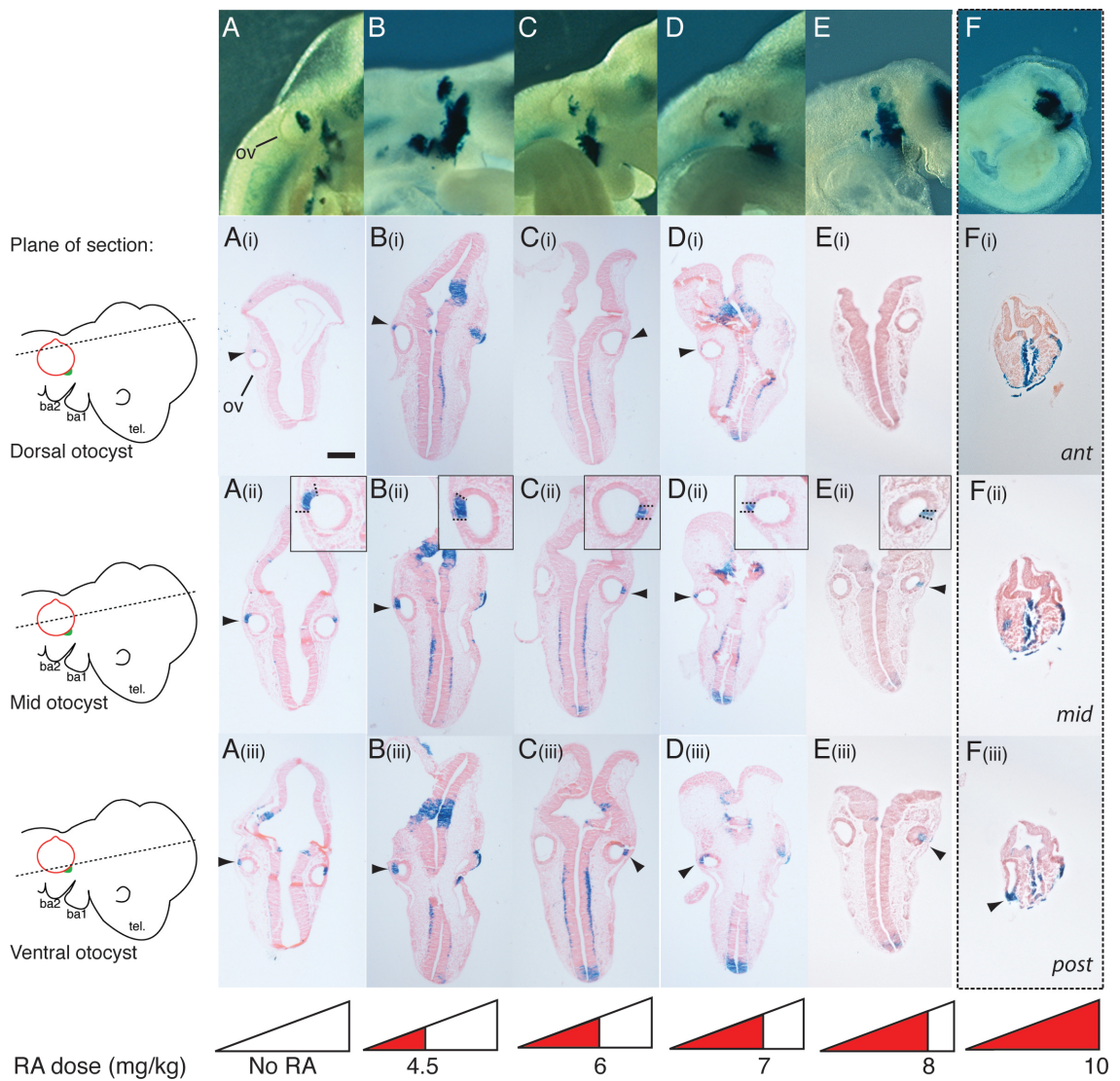


**Figure 3.3 Effects of RA on otic *Fgf3* expression following administration at 7.75dpc.** Lateral views (A-F) and horizontal sections of control and RA-treated embryos are shown in consecutive panels. (A-Aiii) untreated embryos; (B-Biii) 4.5mg/kg; (C-Ciii) 6mg/kg; (D-Diii) 7mg/kg; (E-Eiii) 8mg/kg; (F-Fiii) 10mg/kg. Sections in Fi-Fiii are in the anterior-posterior direction. In control embryos, *Fgf3* expression in dorsal sections is first seen as a small anterior patch (A, Ai). In mid-otic sections, this patch extends laterally (Aii). Higher magnification of the otic vesicle are shown in insets, with the magnified otic vesicle identified by an arrowhead. In embryos treated with 4.5mg/kg of RA this pattern of expression appeared unaffected. However with doses of 6mg/kg and above there is an increasing alteration of otic *Fgf3* expression domain, where expression is lost in dorsal sections (Ci,Di,Ei); and becomes restricted to a smaller and smaller lateral patch on mid-otic sections (Cii,Dii,Eii), thus appearing as lateralized. *Fgf3* expression in the ventral otic vesicle is the most resistant to changes with a slight downregulation and lateralization only visible in embryo treated with 8mg/kg (Eiii). *Ov*, otocyst; *ba*, branchial arches; *tel*, telencephalon. Scale bar = 500  $\mu$ m. Adapted from (Cadot et al., 2012) Copyright © 2012 Wiley Periodicals, Inc

Interestingly, *Fgf3* expression also appeared to become more and more restricted laterally with increasing RA dose, making the domain of *Fgf3* expression in the otic vesicle looks like if it was shifted posteriorly. Whereas in untreated embryos *Fgf3* expression extends laterally from the mid-anterior region of the otic vesicle (inset in Figure 3.3Aii), it was restricted to a small lateral region in embryos exposed to RA (insets in Figure 3.3Cii, Dii, Eii)

The only apparent discrepancy in the results came from embryos exposed to the highest RA dose tested in this experiment (10mg/kg). Here *Fgf3* expression did not seem to be downregulated but instead more strongly expressed than in control. Since the embryos are much smaller in size and present characteristics of earlier stages embryos, I hypothesized that the *Fgf3* expression pattern in the otocyst represents the pattern expected at an earlier stage.

In order to compare expression directly to my own results, a brief time course using the exact same experimental conditions and reagents used for the RA studies (See Figure 3.4) was carried out. During development, a progressive restriction of *Fgf3* expression between 8.5dpc and 10dpc is observed. At first *Fgf3* expression encompasses a large band of surface ectoderm stretching from the invaginating otic cup to the 2<sup>nd</sup> branchial arch (Figure 3.4A). Then this expression starts dividing into two territories (Figure 3.4D) and becomes clearly separated and restricted to smaller regions (Figure 3.4E,F). Comparing the embryo exposed to 10mg/kg of RA in Figure 3.3F and the untreated embryo in Figure 3.4A, the pattern of *Fgf3-lacZ* expression is similar but the otic vesicle size is much larger in the embryo treated with RA.

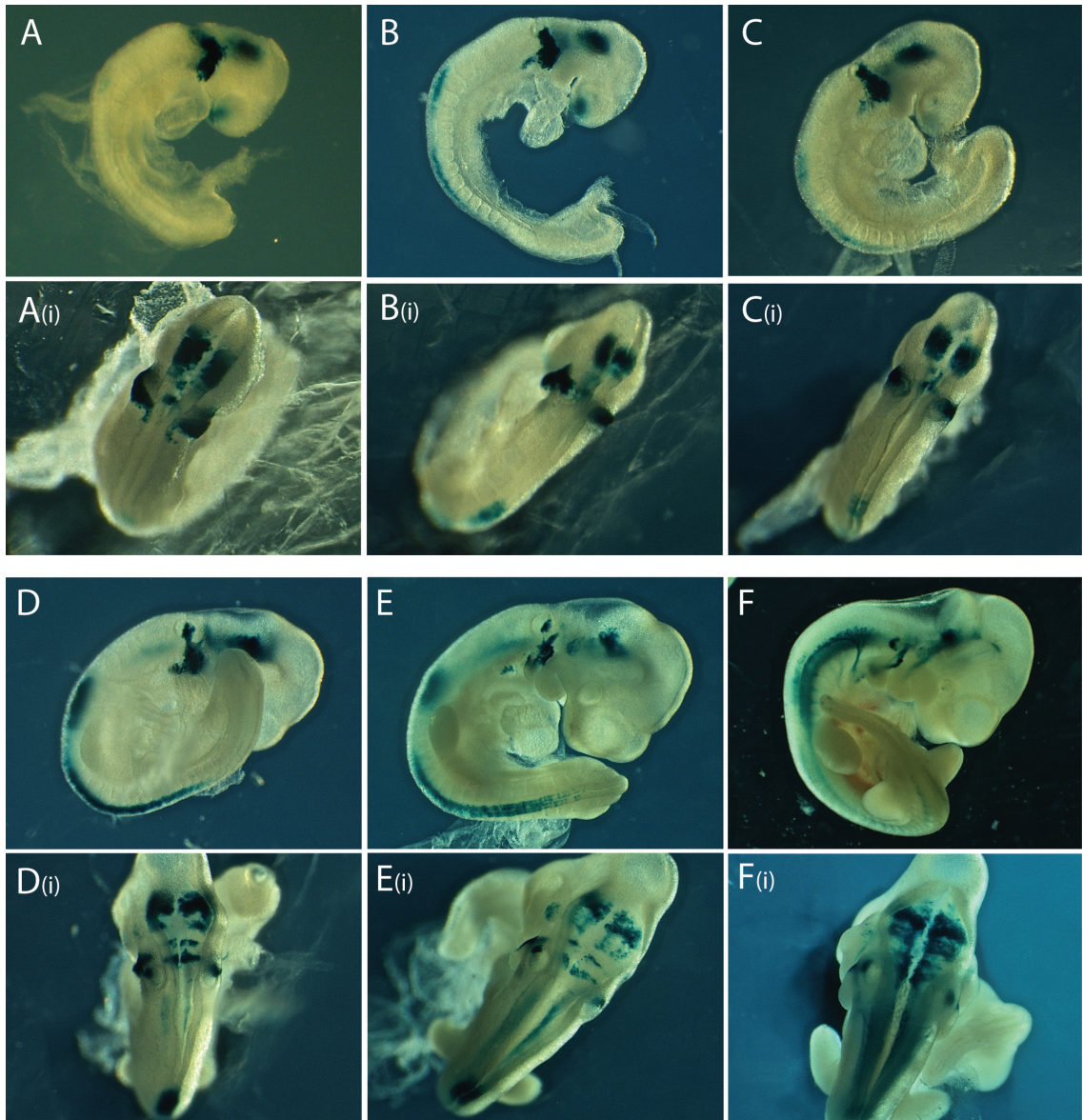


**Figure 3.4 Early-time course of *Fgf3-lacZ* expression.** Lateral and dorsal views of embryos are presented in consecutive panels at the following stages : (A-Ai) 8.75dpc; (B-Bi) 9.0dpc; (C-Ci) 9.25dpc; (D-Di) 9.5dpc; (E-Ei) 10.5dpc; (F-Fi) 11.5dpc. At early stages, *Fgf3* expression encompasses a large band of surface ectoderm, stretching from the invaginating otic cup to the 2<sup>nd</sup> branchial arch (A). This band gets thinner as the embryo develops (B,C) and eventually starts forming two territories (D). At 10.5dpc and 11.5dpc these two domains of expression are now clearly separated (E,F). Adapted from (Cadot et al., 2012) Copyright © 2012 Wiley Periodicals, Inc

Thus the expression with this dose of RA did indeed appear to be similar to that expected at earlier time points, supporting the notion of developmental delay of *Fgf3* at high RA doses.

If embryos are delayed then perhaps analysis after an additional day of utero development (10.5dpc) should allow us to see *Fgf3* expression similar to that of 9.5dpc profile. Therefore embryos exposed to the highest RA dose (10mg/kg) at 10.5dpc; along with embryos exposed to 4.5; 7 and 8mg/kg were analysed at this later time point.

### **3.4 RA-induced downregulation of *Fgf3* expression is maintained at 10.5dpc**

Analysis of the effects of RA at 10.5dpc (Figure 3.5) was consistent with the dose-dependent alteration of *Fgf3* expression reported at 9.5dpc (Figure 3.5). Thus, *Fgf3* expression in the spinal cord was unaffected with RA doses up to 7mg/kg (Figure 3.5C,E) but was strongly downregulated (Figure 3.5I) or even lost in some embryos (Figure 3.5G) with higher doses. At this later stage of development, additional domains of *Fgf3* expression are now visible in the geniculate and superior cervical nerves (gn, scn, Figure 3.5B). These were unaffected by doses of up to 10mg/kg of RA (compare Figure 3.5B,D,F with G,H,J). While the inner ear develops, *Fgf3* domain of expression becomes restricted to the ventral regions of the otic vesicle, to eventually appear as a strong antero-ventral patch of reporter expression at 10.5dpc (Figure 3.5B).

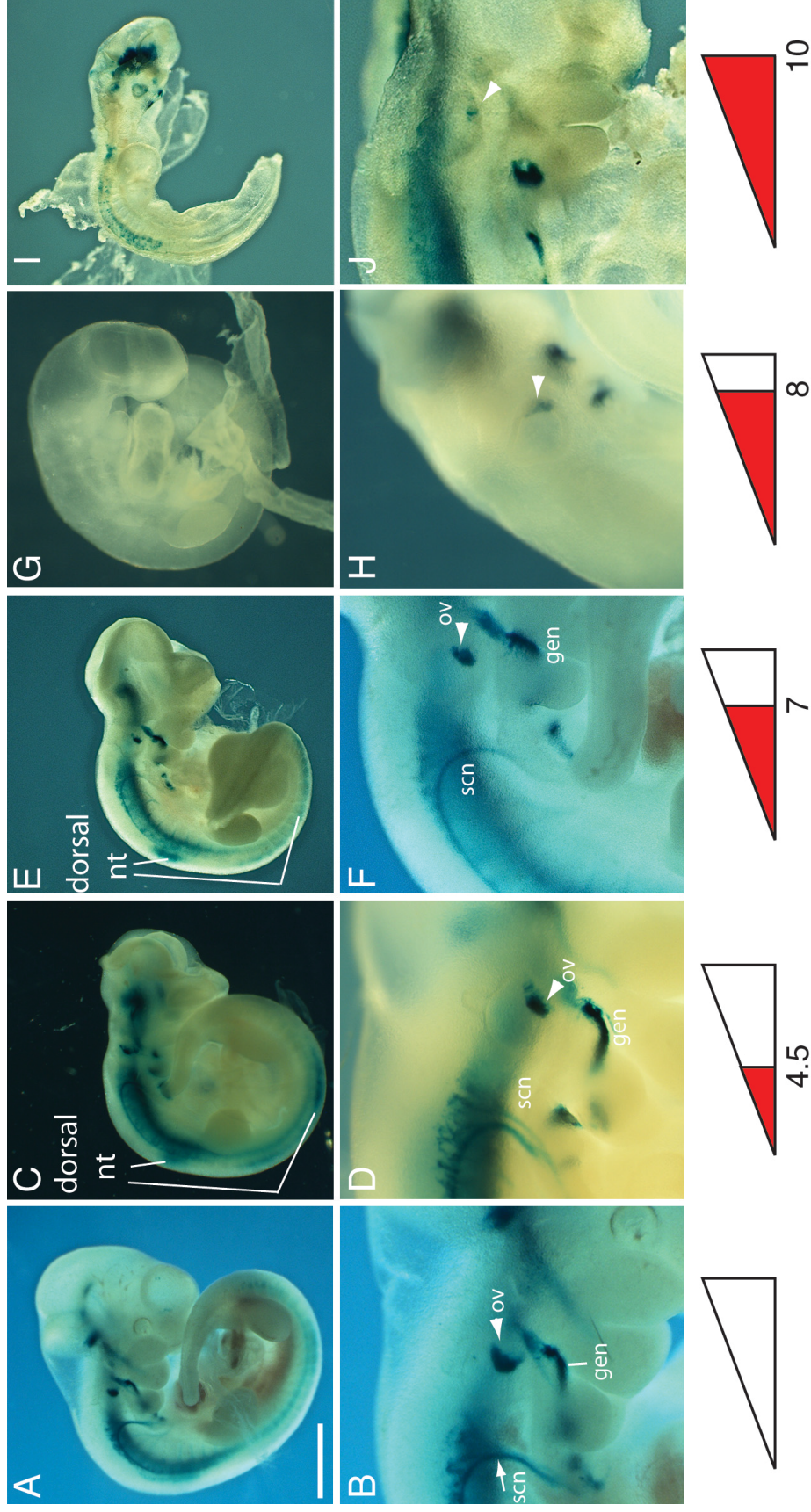


**Figure 3.5 Effects of RA exposure at 7.75dpc on the 10.5dpc embryo** . Lateral views of whole embryos and higher magnification of the otic region of untreated and RA-treated embryos are presented in consecutive panels. (A,B) control embryos; (C,D) 4.5mg/kg; (E,F) 7mg/kg; (G,H) 8mg/kg; (I,J) 10mg/kg. For doses up to 7mg/kg *Fgf3* expression in the CNS was unaltered (C,E). However it was lost in some embryo treated with 8mg/kg of RA (G) and strongly downregulated in other embryos (H,I,J). Otic *Fgf3* expression was also increasingly downregulated with increasing dose of RA (compare arrowheads in B,D,F,H,J). Adapted from (Cadot et al., 2012)  
 Copyright © 2012 Wiley Periodicals, Inc

With RA doses of up to 7mg/kg, this patch of expression was unchanged spatially but it appeared smaller than in control (compare arrowheads in 3.5B with D,H). In embryo treated with a higher RA dose of 8mg/kg, otic *Fgf3* expression was strongly downregulated (arrowhead, Figure 3.5H) or even completely lost in 4 embryos (n=14; Figure 3.5G). Administration of 10mg/kg of RA then gave rise to embryos exhibiting strong developmental abnormalities and developmental delay (Figure 3.5I,J). Some *Fgf3* expression was still detectable but strongly downregulated (Figure 3.5J) or impossible to attribute to any particular structure (Figure 3.5I). This is consistent with otic *Fgf3* expression being downregulated with a 10mg/kg dose of RA, although it could not be observed at 9.5dpc due to the developmental delay.

### **3.5 Semi-quantitative analysis of the dose-dependent downregulation of otocyst expression**

Representative embryos selected after thorough analysis of the data for each dose, and presented in the previous figures, suggested a dose-dependency of *Fgf3* downregulation with increasing RA dose. In order to give more weight to this so far only descriptive demonstration of *Fgf3* dose-dependent downregulation by exogenous RA, a semi-quantitative analysis was performed using the ImageJ software (Rasband, 1997). The otic vesicles were first digitally dissected. To do so, they were observed at high magnification in ImageJ and their areas thoroughly delimited using a tracing tool. Then the area of *Fgf3* expression was delimited using a colour detection tool. The amount of pixels in the total area versus area with *Fgf3* expression was determined.

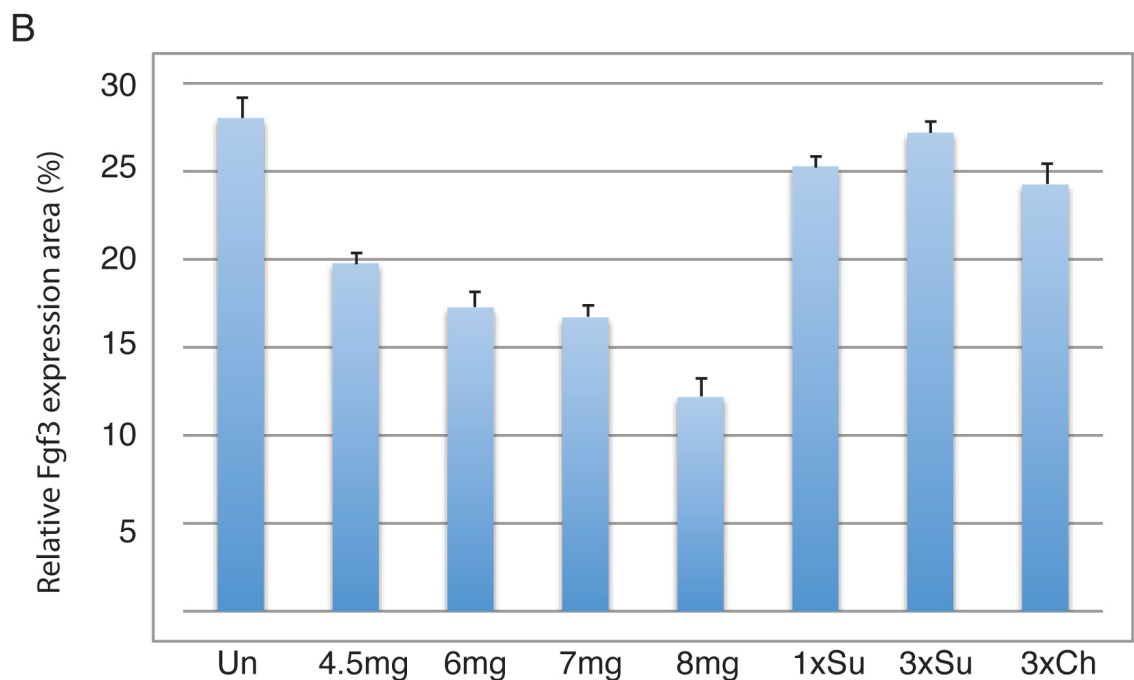
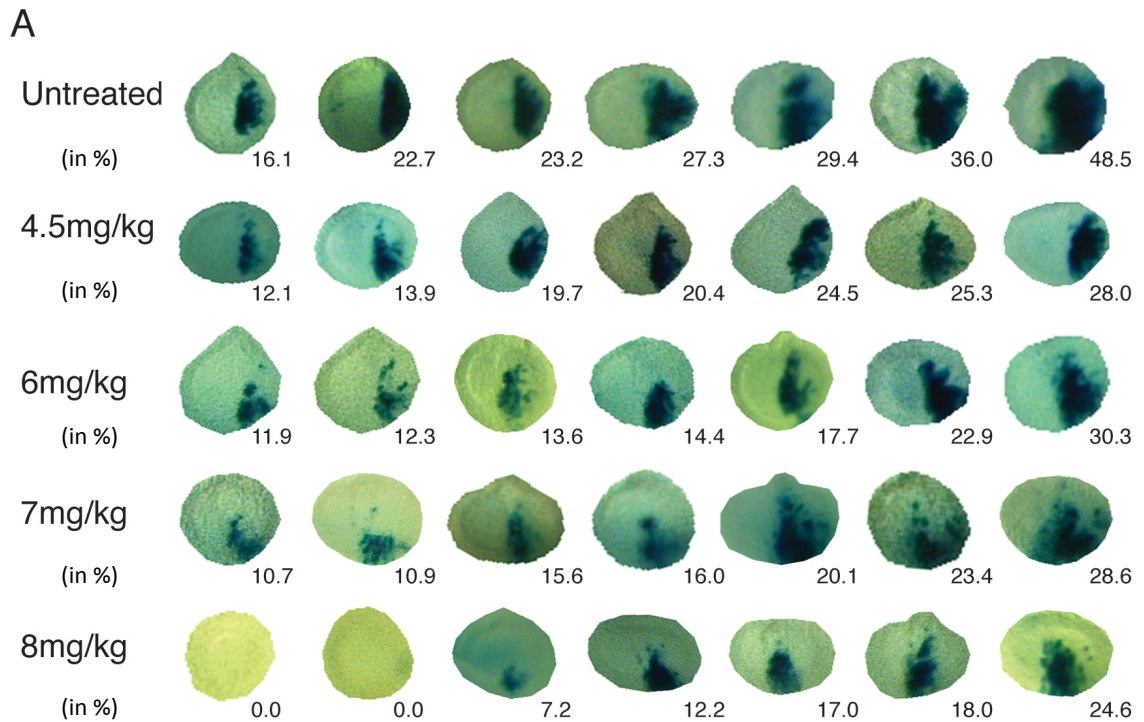


**Figure 3.6 Image analysis of *Fgf3* expression in the 9.5dpc otic vesicle exposed to increasing dose of RA at 7.75dpc.** A) Representative array of digitally dissected otic vesicle from control and RA-treated embryos. The relative area of *Fgf3* expression was determined using the ImageJ software and is shown in subscript as a percentage of the area of the whole otic vesicle. Otic vesicles are not drawn to scale and are all oriented with their anterior pole toward the right. This analysis also illustrate the dose-dependent lateralization of *Fgf3* expression. B) Relative areas of *Fgf3* expression in the analyzed otic vesicles were plotted as a histogram and confirm the dose dependent decrease in *Fgf3* expression with increasing RA dose. Plots of otic *Fgf3* expression area for embryos exposed to 1x sugar (1xSu); 3x sugar (3xSu) and 3x chocolate (3xCh) confirm the specificity of the response to RA. Numbers used in a analysis: untreated n=13; 1xsugar n=4, 3xsugar n=4, 3xchocolate n=6; and RA : 4.5mg/kg n= 10; 6mg/kg n= 13; 7mg/kg n=13; 8mg/kg n=22) Adapted from (Cadot et al., 2012) Copyright © 2012 Wiley Periodicals. Inc

The area of *Fgf3* expression on these 2D images was then calculated as a percentage of the overall otocyst area (see Figure 3.6A for an array of some of the otic vesicles used for analysis). Since in the embryos, the *Fgf3* domain of expression is in 3D and not in 2D, this analysis cannot be viewed as a true quantitative assay. The use of confocal microscopy to obtain real 3D estimates was also explored, but it would have been extremely time consuming to obtain the data for just one otic vesicle, and thus impossible at the scale of the 179 otic vesicles analysed in the timeframe of this study. This 2D analysis is nevertheless useful, as it allows comparing a large number of 9.5dpc embryos exposed to RA with similar and different doses, as opposed to relying exclusively on 1 or 2 representative pictures of embryos for each RA doses to support the results.

This image analysis first revealed that despite variations in the otic domain of *Fgf3* expression using a same dose of RA, there was a clear dose-dependent decrease of *Fgf3* expression with increasing RA doses (Figure 3.6A) The extent of this dose-dependant downregulation is particularly clear when plotted as a histogram (Figure 3.6B). In addition, this analysis confirms that the domain of *Fgf3* otic expression becomes lateralized with increasing doses of RA, thus appearing posteriorly shifted in the otic vesicle (Figure 3.6A).

### **3.6 *Fgf3*-expression in embryos exposed to RA after hindbrain patterning (at 8.5dpc)**

The timing of exposure to exogenous RA has been shown to play a crucial role in the induction of specific phenotypes. Exposure to RA prior to the onset of somatic segmentation (7.75-8.25dpc) results in dramatic alterations of hindbrain patterning, where the shortened hindbrain is converted to a more posterior identity as evidence by the changes in Hox genes pattern of expression (Figure 1.10; Wood et al., 1994; Glover et al., 2006). Since the hindbrain plays a crucial role in inner ear induction and later in the dorso-ventral patterning of the otic vesicle, this suggested that the downregulation of otic *Fgf3* expression reported in embryos exposed to RA at 7.75dpc could merely be due to secondary effects of altered hindbrain patterning.

In order to determine if excess RA could still downregulate *Fgf3* expression in the otic vesicle independently of hindbrain re-patterning, *Fgf3* expression was also analysed in embryos exposed to RA at early somite stage (8.5dpc), a stage where the administration of RA does not alter the posterior hindbrain identity (Wood et al., 1994; Glover et al., 2006; Morriss-Kay et al., 1991). Embryos examined at 9.5dpc (Figure 3.7) presented an increasing downregulation of otic *Fgf3* expression with increasing doses of RA (Table 3.2b), thus showing similarities to what has been seen in embryos exposed to RA at earlier stage. There was however several differences.

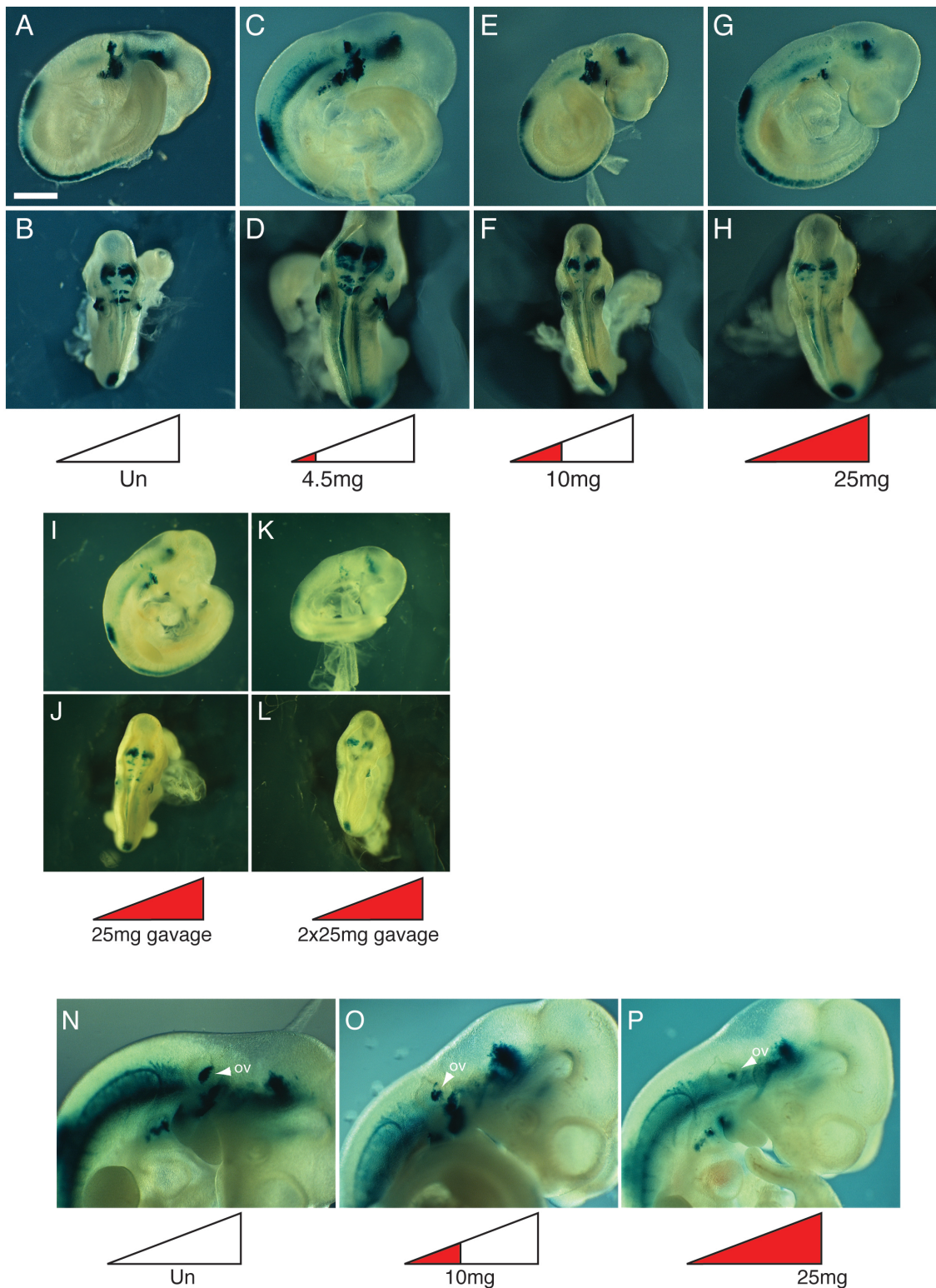


**Figure 3.7 Effects of RA administration after hindbrain patterning.** Lateral and dorsal views of control and RA-treated embryos at 9.5dpc (A-L) and 10.5dpc (N-P). *Fgf3* expression in the CNS was unaltered by RA doses inferior to 25mg/kg, and even then there was only a slight downregulation (G,H,P). In the otic vesicle *Fgf3* expression was downregulated with dose of 8-10mg/kg (E) and even almost completely extinguished with RA dose of 25mg/kg (G). Similar downregulation of otic *Fgf3* expression was observed in 9.5dpc embryos following gavage administration (I-K). Hb, hindbrain; ov, otic vesicle; nt, dorsal neural tube. Scale bar = 500  $\mu$ m. Adapted from (Cadot et al., 2012) Copyright © 2012 Wiley Periodicals, Inc

First of all, alteration of *Fgf3* expression required higher doses of RA, where *Fgf3* expression in the spinal cord and hindbrain was unaffected by doses of 8-10mg/kg, while *Fgf3* expression in the otic vesicle was downregulated (Figure 3.7E,F) but with a lower incidence compared to embryos exposed to a similar dose at 7.75dpc. Even with a dose of 25mg/kg of RA, more than 3 times the dose required to totally extinguish *Fgf3* otic expression in embryo exposed at early somites stages, a couple of *Fgf3*-expressing cell were still visible in the otic vesicle of all but one embryos. Interestingly, in embryos exposed to 10mg/kg of RA the downregulation of *Fgf3* expression was restricted to the otic vesicle, whereas in embryo exposed to 25mg/kg of RA *Fgf3* expression was also lost in the branchial arches, as well as in the surface ectoderm between the OV and the branchial arches (compare Figure 3.7E and G).

A dose of 25mg/kg of RA also seemed to lead to a slight downregulation of *Fgf3* in the hindbrain and spinal cord. *Fgf3* expression appeared unaltered in all area of endogenous expression with a dose of 4.5mg/kg (Figure 3.7C,D), despite the image analysis suggesting a slight downregulation (Figure 3.8). In addition, *Fgf3* seemed to be evenly downregulated throughout the otic domain, rather than predominantly lost in the antero-dorsal region of the otic vesicle, and thus no phenomenon of lateralization of *Fgf3* expression was observed at this stage.

In order to further prove that the novel method of RA administration presented here has no influence on the phenotype, a couple of gavage experiments were also performed using RA doses of 25mg/kg and 2x25mg/kg (Figure 3.7I-L). A dose of 25mg/kg gave results similar to what had been observed when using RA-laced sugar

pellets, where *Fgf3* expression is lost both in the otic vesicle and in the adjacent surface ectoderm, as well as downregulated in the hindbrain and spinal cord (Figure 3.7I,J). Administration of 2 doses of 25mg/kg of RA gave rise to similar phenotypes but with an increasing number of embryos showing complete loss of *Fgf3* expression in the OV (Figure 3.7K,L). Expression in the hindbrain and spinal cord were also more downregulated than with a single shot of 25mg/kg of RA.

An image analysis of the otic vesicle of RA-treated embryo using either self-administration of sugar pellets or gavage was also performed at this stage and data plotted as a histogram (Figure 3.8). A dose dependant downregulation of *Fgf3*-expression in the otic vesicle could be observed, independently of the delivery technique. The incidence of embryos with altered otic expression of *Fgf3* following administration to RA at 8.5dpc is presented in Table 3.2b.

The effects of RA administration at early somitic stage were also analysed at 10.5dpc. Following administration of up to 25mg/kg of RA (Figure 3.7O,P) embryo appeared morphologically similar to control embryos (Figure 3.7N) but *Fgf3* expression started to be downregulated in the otic vesicle of embryos exposed to RA doses 10mg/kg (Figure 3.7O) and was even more downregulated with a dose of 25mg/kg (Figure 3.7P). In addition *Fgf3* expression was lost in the surface ectoderm adjacent to the otic vesicle (Figure 3.7P) as previously reported at 9.5dpc (Figure 3.7G).

Together these data demonstrate that *Fgf3* expression has a different sensitivity to RA after hindbrain patterning.

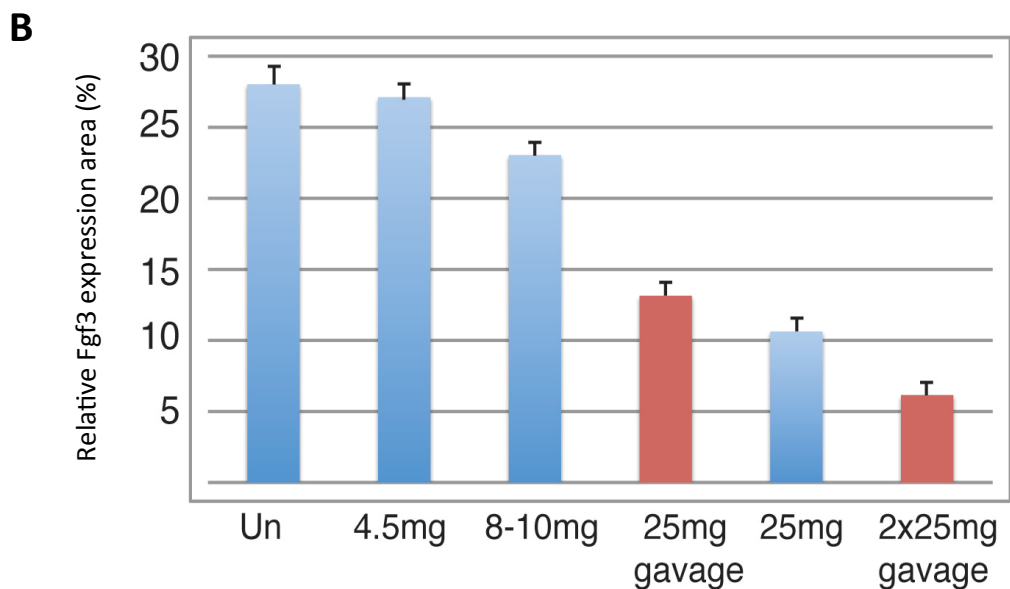
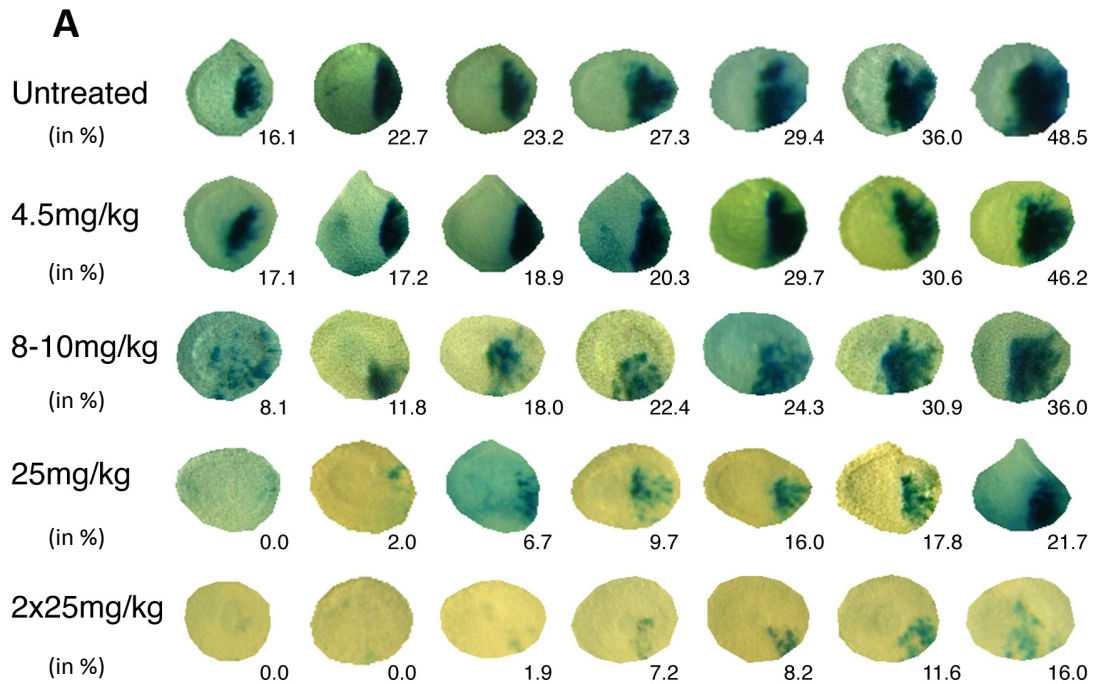


**Figure 3.8 image analysis of *Fgf3* expression in the 9.5dpc otic vesicle exposed to increasing dose of RA at 8.5dpc.** A) Representative array of digitally dissected otic vesicle from control and RA treated embryos. The relative area of *Fgf3* expression was determined using the ImageJ software and is shown in subscript as a percentage of the area of the whole otic vesicle. This analysis illustrates the difference in the alteration of *Fgf3* expression following exposure at 8.5dpc instead of 7.75dpc, with *Fgf3* being downregulated throughout the otic vesicle and not lateralized. B) Otic image analysis plotted as a histogram confirms dose-dependent downregulation of otic *Fgf3* expression following RA administration after hindbrain patterning. Error bars represent standard error to the mean. Numbers used in a analysis: untreated n=13; RA via sugar pellet: 4.5mg/kg n= 18; 8-10mg/kg n= 21; 25mg/kg n=27; and RA via gavage: 25mg/kg n=17; 2x25mg/kg n= 14. Adapted from (Cadot et al., 2012) Copyright © 2012 Wiley Periodicals, Inc

*Fgf3* requires higher dose of RA to be clearly downregulated in a large percentage of embryos: 25mg/kg in early somitic embryos vs. 8mg/kg in presomitic embryos. *Fgf3* expression is also downregulated in the otic vesicle whereas other domain of endogenous expression (CNS) remains unaltered. This contrasts from the concomitant downregulation of *Fgf3* in both the OV and the CNS in presomitic embryos. Importantly, there was a dose-dependent downregulation of *Fgf3* expression in the otic vesicle following administration of RA at the early somatic stage, a stage where the posterior identity of the hindbrain is unchanged by RA. Thus the alteration in *Fgf3* otic pattern of expression is unlikely to be due to secondary effects from the hindbrain. This supports the hypothesis of a direct regulation of *Fgf3* by RA.

### **3.7 Generation of RA phenotypes in other organ systems**

A brief survey of the literature has revealed that RA was playing a crucial role in lots of different organs and tissues of the developing embryo (Table 3.1 and Appendix Table S1). In order to assess whether the novel RA delivery procedure could be used for RA studies in other organ or tissues, the effects of RA administration via sugar pellets and gavage were compared in 3 other organ systems: the limb, the palate and the heart.

Limb abnormalities were previously reported in 100% of the embryos exposed to 100mg/kg of RA at 11.5dpc (Alles and Sulik, 1989). Administration of 100mg/kg of RA either via gavage (n=7) or sugar pellets (n=10) both led to a similar shortening of hindlimbs and forelimbs in all embryos examined (Figure 3.9B,C, compare to untreated 3.9A)

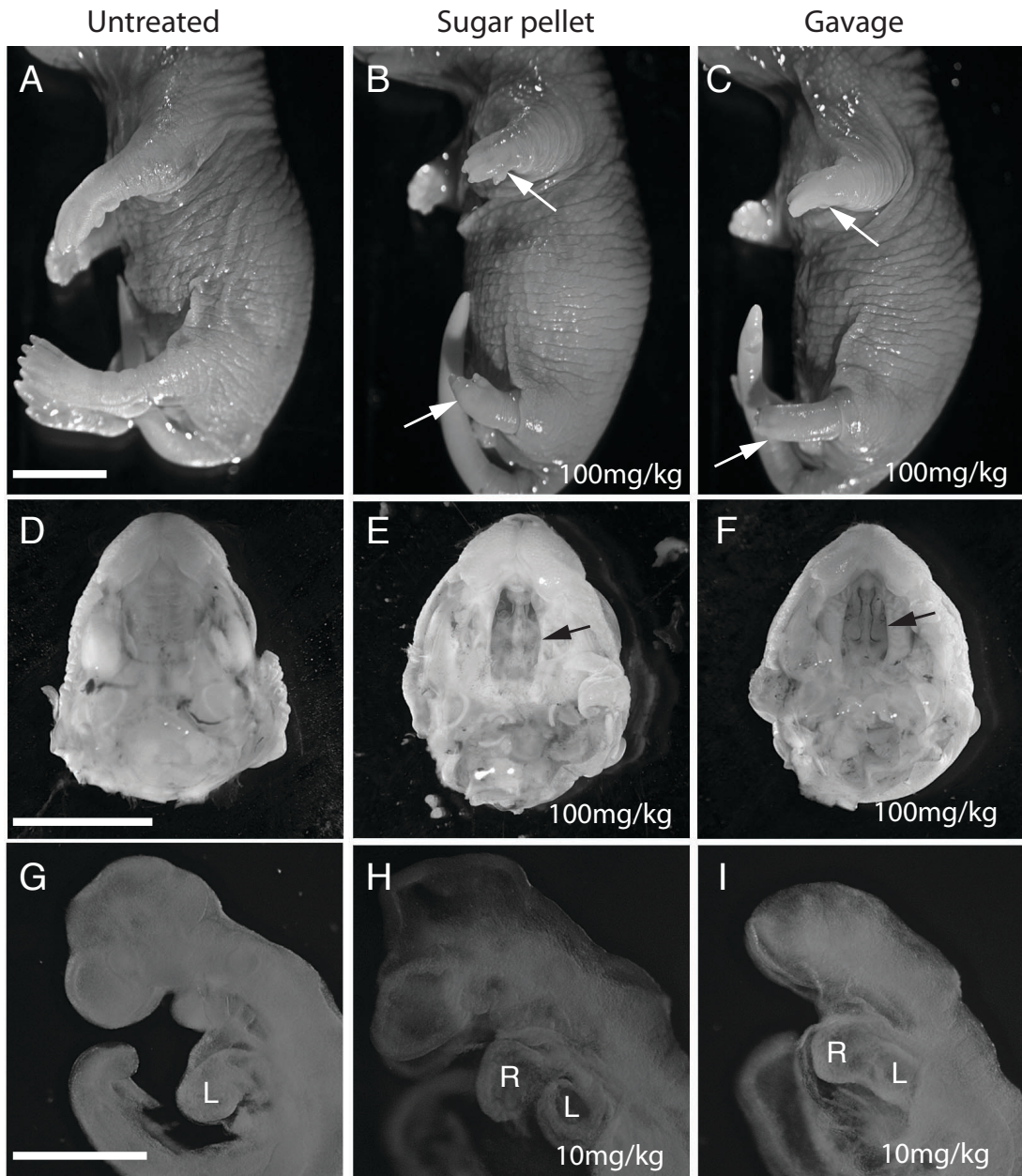


**Figure 3.9 Generation of identical RA phenotypes in other organ systems using sugar pellets.** Administration of 100mg/kg of RA at 11.5dpc results in similar limb reduction anomalies regardless whether pellets or gavage was used as highlighted by white arrows (C,D). Identical cleft palate phenotypes at 18.5dpc were also generated using pellet or gavage (black arrows in E,F). Eventually, similar patterning defects of the heart vesicles were also obtained with pellet (H) and gavage (I). Untreated embryos (A,D,G). Scale bar : (A-F)= 5mm; (G-I) = 500  $\mu$ m. Adapted from (Cadot et al., 2012) Copyright © 2012 Wiley Periodicals. Inc

The palate was the next organ to be trialled. Exposure to excess RA at 11.5dpc has been shown to interfere with the fusion of the palatal shelves, resulting in the development of cleft palate. An RA dose of 100mg/kg has been shown to induce a cleft palate phenotype in 65-82% of embryos (Abbott et al., 2005; Campbell et al., 2004; Kochhar et al., 1984). Administration of 100mg/kg of RA using either gavage (n=4) or sugar pellets (n=5) resulted in cleft palate phenotypes of similar severity in all the embryos examined (Figure 3.9E,F compare with 3.9D).

Finally, heart defects have been reported following RA administration, where the heart presents an aberrant looping with the heart vesicles being arranged as an anterior and a posterior chamber instead of a left and a right chamber (Wasiak and Lohnes, 1999). Administration of 10mg/kg of RA at 7.75dpc resulted in such an aberrant heart vesicles arrangement (Figure 3.8H,I) regardless of the delivery method being gavage (n=5) or sugar pellets (n=13)

All together this shows that RA administration using sugar pellets can be applied to other organ systems than the inner ear.

### **3.8 *Fgf3/Fgf10* cross-regulation**

*Fgfs* cross-regulation has been reported for other *Fgfs* during inner ear induction, with misexpression of *Fgf10* expression in the hindbrain that results in ectopic *Fgf8* expression; and double knock-out of *Fgf3* and *Fgf8* that leads to a downregulation of *Fgf10* expression (Zelarayan et al., 2007). Interestingly *Fgf10* expression was reported

as shifted dorso-medially, along with the vestibulo-acoustic ganglion in *Fgf3* null mice (Hatch et al., 2007). Furthermore, *Fgf3*, *Fgf8*, and *Fgf10* signalling from the hindbrain, endoderm and mesoderm are thought to be able to compensate for each other during inner induction since targeted mutation of *Fgf3* or *Fgf10* alone only lead to variable defects of mouse inner ear morphogenesis, whereas *Fgf3/Fgf10* and *Fgf3/Fgf8* double mutants fail to develop otic vesicles. Interestingly *Fgf10* and *Fgf3* are also expressed in the developing inner ear itself, where their expressions overlap in the antero-ventral wall of the otocyst (Hatch et al., 2007; Pirvola et al., 2000), suggesting that *Fgf3* could also compensate for *Fgf10* deficiency during later stages of development. Functional redundancy could also reflect similar regulatory mechanisms and analysis of this mechanism could improve our understanding of both *Fgf3* and *Fgf10* regulation both individually and together. As it is not clear which mechanisms lead to such compensation, *Fgf3* reporter expression was analysed in an *Fgf10* null mutant background between 7.75dpc and 11.5dpc.

Analysis of wholemount *Fgf3-lacZ* embryos null for *Fgf10* revealed a delay and/or a downregulation of *Fgf3-lacZ* expression in the hindbrain of *Fgf10* knockout embryos (Figure 3.10B) compared to control embryos at the same stage (Figure 3.10A). *Fgf3* expression was also weaker in the hindbrain and midbrain of 9.0 and 9.5dpc *Fgf10* KO embryos (Figure 3.10G,H). However *Fgf3-lacZ* expression appears unaltered at the level of the otic vesicle (Figure 3.10G-K). At 10.5dpc, level of reporter expression in the brain of mutant embryos (Figure 3.10I) is similar to the control (Figure 3.10D) and the *Fgf3-lacZ* expression pattern in the developing inner ear is also conserved; both at this stage and at 11.5dpc (Figure 3.10K).

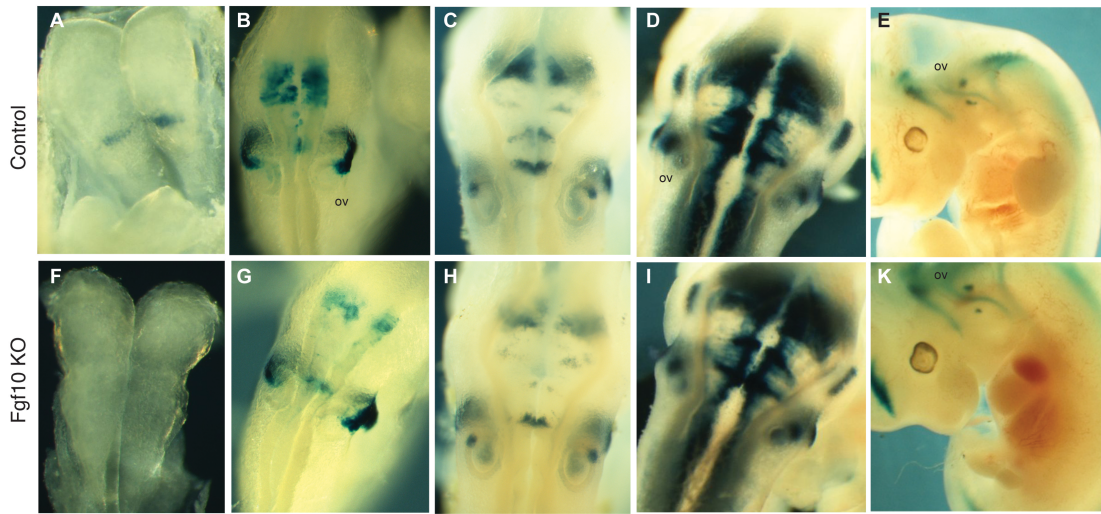


**Figure 3.10 Wholemount analysis of early *Fgf3-lacZ* expression in a *Fgf10* null background.** Lateral and dorsal views are presented in consecutive panels. Embryonic stages are as follow: (A,F) 7.75dpc; (B,G) 9.0dpc; (C,H) 9.5dpc; (D,I) 10.5dpc; (E,K) 11.5dpc. At 7.75dpc, *Fgf3* expression was absent from the brain of *Fgf10* null embryos (F) and also seemed downregulated compared to control up to 9.5dpc (G,H). Hindbrain expression in *Fgf10* null embryos was however similar to control at 10.5dpc (I). Otic expression seems unaltered between 9.0dpc and 11.5dpc.

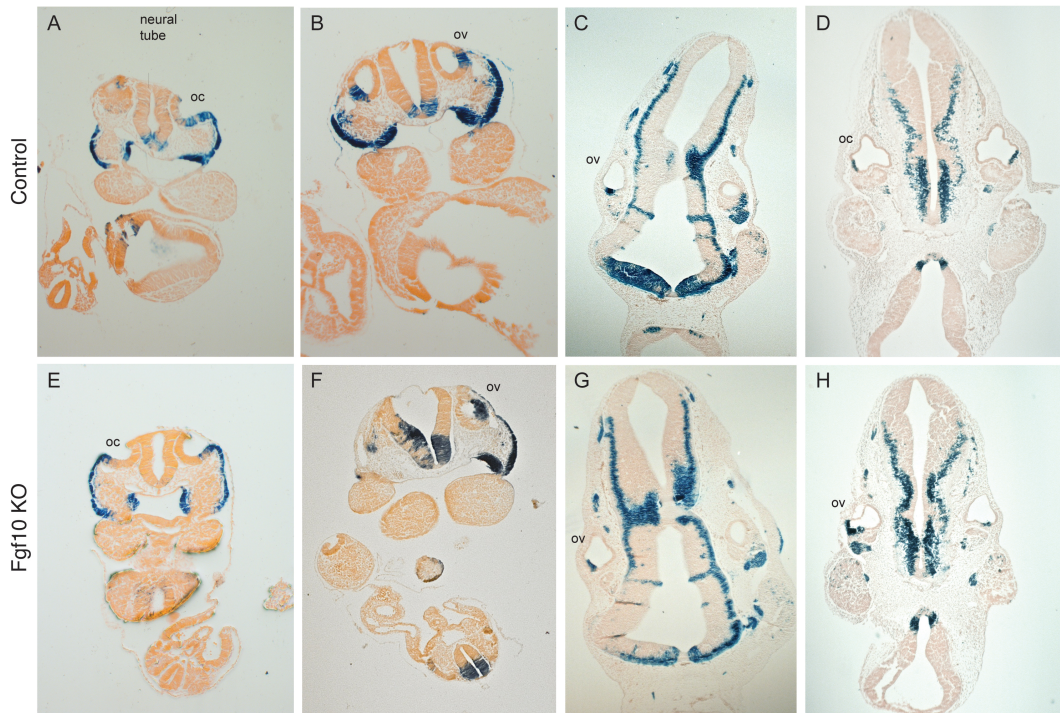


**Figure 3.11 Analysis of early *Fgf3-lacZ* expression on section in a *Fgf10* null background.** Transverse section at the following embryonic stages: (A,E) 9.5dpc; (B,F) 10.5dpc; (C,G) 10.5dpc; (D,H) 11.5dpc.

*Fgf3-lacZ* expression was also analyzed on sections at the level of the otic vesicle. At 8.5dpc *Fgf3-lacZ* expression extends from the middle of the ventral wall of the otic pit and along the surface ectoderm spreading from the otocyst to the 2<sup>nd</sup> branchial arches in control embryo (Figure 3.11A). This pattern of expression was unchanged in mutant embryos (Figure 3.11E). At 9.5dpc *Fgf3* was expressed in the anteroventral wall of the otocyst both in control and *Fgf10* KO embryos (Figure 3.11B,F).

At 10.5dpc, *Fgf3* expression is restricted to a small anteroventral patch (Figure 3.11C); this expression domain was unaltered in *Fgf10* KO embryos despite some morphogenetic anomalies (Figure 3.11G). At 11.5dpc development of the inner ear was clearly abnormal in *Fgf10* mutant embryos (Figure 3.11H) compared to control embryo (Figure 3.11D). However, there were still no significant differences in *Fgf3* expression spatial domains of expression and thus *Fgf3* expression is unaltered in the *Fgf10* KO mutant.

In summary, maintenance of *Fgf3-lacZ* expression in *Fgf10* KO mice shows that *Fgf3* could also compensate for the lack of *Fgf10* expression at later stages of inner ear development. This compensation could happen in several different ways. For instance, *Fgf3* could be overexpressed, resulting in more FGF3 protein produced to interact with FGFR-2(IIIb). Alternatively, more FGF3 protein could also be produced by upregulation at the translation level. The results presented here allow ruling out the first hypothesis since there was no significant upregulation of *Fgf3-lacZ* expression in any of the embryos analysed. Therefore compensation should happen at the FGF3 ligand level, although the exact mechanisms remain to be determined.

## 4

# INVESTIGATING MECHANISMS OF FGF10 TRANSCRIPTIONAL REGULATION

---

In the previous chapter, the regulatory importance of RA in controlling *Fgf3* expression was presented. However, this regulation may be through either direct mechanisms involving one or more of a number of RA response elements, or indirect mechanisms. In addition, the redundant requirements for *Fgf3* and *Fgf10* in inner ear induction and their overlapping expression in the otic epithelium itself was also discussed, and it is of interest that *Fgf3* expression was never lost nor upregulated in *Fgf10* null embryos. This raises the question as to whether these genes share any conserved mechanisms underlying their normal regulation. In order to begin an *Fgf10* regulatory analysis, enhancer elements responsible for controlling normal *Fgf10* expression had first to be identified and cloned.

## **4.1 Investigation of the endogenous *Fgf10* expression pattern**

The *Fgf10* mRNA expression pattern was first analysed using in situ hybridization. As well as providing detailed comparative expression data for comparison to *Fgf3*, such expression data is also essential to evaluate expression of *Fgf10*-reporter constructs, in order to determine whether or not a given construct recapitulates all or only part of

the endogenous *Fgf10* expression pattern. A 500bp fragment from the 5' region of a *Fgf10* cDNA clone was used to synthesize antisense and sense *Fgf10* riboprobes.

Inner ear *Fgf10* expression was first detected around 8.75dpc in the mouse otic placode as a weak anterior patch of staining (Figure 4.1A). This anterior patch of expression becomes more pronounced at the otic cup stage (Figure 4.1B). The *Fgf10* mRNA pattern then starts to slightly change as the otic cup begins to approach closure around 9.5dpc, with *Fgf10* expression now extending more ventrally (Figure 4.1C). Horizontal sections of wholemount embryos hybridized with *Fgf10* antisense riboprobes reveals that this strong antero-ventral patch of expression is located medially, close to the neural tube (Figure 4.1F). 0.25dpc later, additional low level of *Fgf10* expression can be seen throughout the otic vesicle epithelium in addition to the strong patch of anterior expression (Figure 4.1D). *Fgf10* expression is also visible in the vestibulo-acoustic and trigeminal ganglia (see arrows in Figure 4.1E) as well as throughout the developing limb (arrows, Figure 4.1D). At 10.0dpc of development, the extrusion of the endolymphatic duct from the dorso-medial region of the otic vesicle is the first visible sign of inner ear morphogenesis, in combination with the elongation of the otic vesicle along its dorso-ventral axis (Figure 4.1E). *Fgf10* expression remains prominent in the anterior part of the developing inner ear but is also evident as a small posterior patch as well (Figure 4.1E).

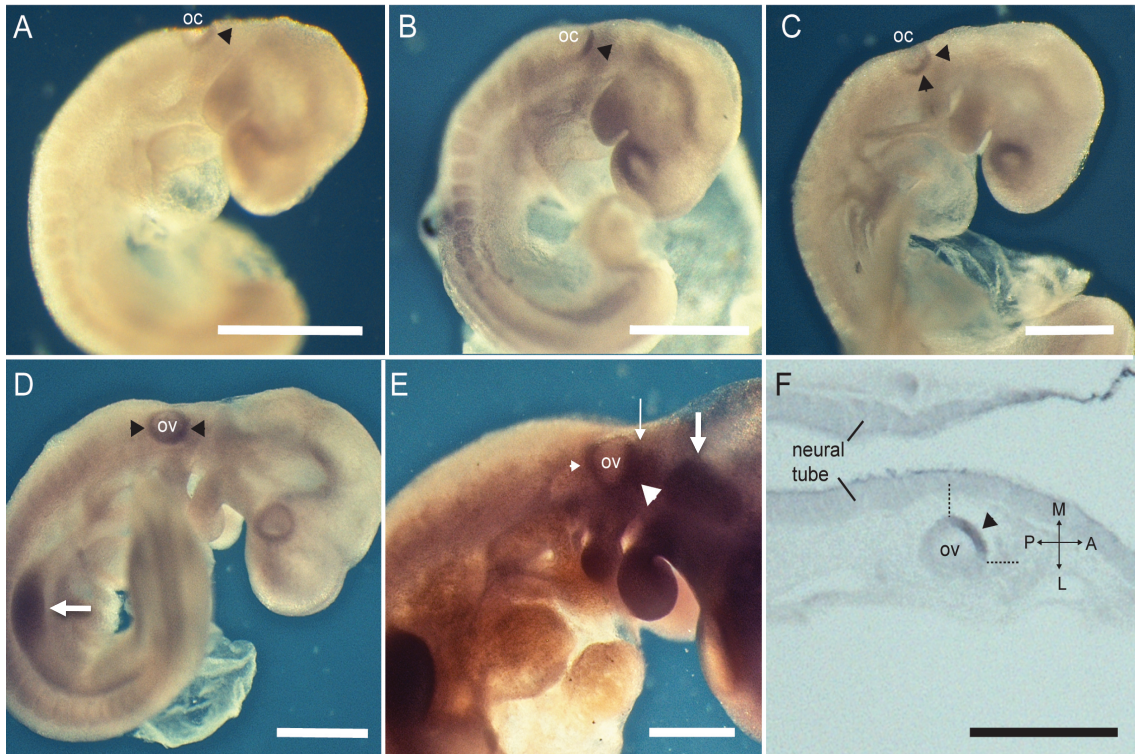


**Figure 4.1 Early *Fgf10* mRNA expression in the developing mouse embryo.** At 8.75dpc *Fgf10* expression is initiated in the anterior part of the otic placode (A). Expression is upregulated at the otic cup stage (B) and start extending ventrally at 9.0dpc (C). At 9.5dpc expression is now visible throughout the epithelium of the closed otic vesicle (D), although still stronger in the antero-ventral region. *Fgf10* is now also expressed in the developing limb (arrow, D). At 10.0dpc *Fgf10* otic expression appears as a strong the anterior patch and a smaller dorsal patch (arrowheads, E). In addition expression is now visible in the developing vestibulo-acoustic ganglion (thin arrow, E) and the trigeminal ganglion (wide arrow, E). Coronal section through wholmount embryos hybridized at 9.5dpc shows localization of *Fgf10* expression in the antero-medial wall of the otic vesicle. Oc, otic cup; ov, otic vesicle. Scale bar 500µm. This figure also appears in (Economou et al., 2013). Copyright © 2012 Elsevier B.V.

## 4.2 Generation of *Fgf10*-reporter constructs for analysis in mice

Contrary to *Fgf3*, an *Fgf10* reporter transgenic line was not available, so the first step was to identify and clone a *cis*-acting DNA sequence able to recapitulate *Fgf10* expression in vivo. An *Fgf10* enhancer with inner ear expression activity had been previously described in (Ohuchi et al., 2005) where a 6.6kb enhancer region upstream *Fgf10* was able to drive *LacZ* reporter expression in all endogenous areas of the inner ear (construct F, Figure 4.2). Interestingly, these authors had also shown that a smaller 800bp fragment within this 6.6kb region (construct 3-1, Figure 4.2) drives *LacZ* expression in more restricted area of the inner ear and also only from a later stage of development than normal endogenous expression. The modularity of *cis*-regulatory control units has been demonstrated in a large number of genes such *Fgf4* (Iwahori et al., 2004), *Ngn1* (Nakada et al., 2004), *Pax2* (Pfeffer et al., 2002), *Dlx* (Park et al., 2004) and *Hox* genes (Tumpel et al., 2002). As well as looking to explore the mechanisms underlying normal *Fgf10* regulation, this project also looked to pursue further the potential for other regulatory modules involved in controlling *Fgf10* inner ear expression. Identification of such regulatory modules controlling *Fgf10* expression in different areas of the inner ear would increase our understanding of *Fgf10* role in the development of each of these regions. Unfortunately, neither Ohuchi's reporter line mice are extant (M.Maconochie personal communication).

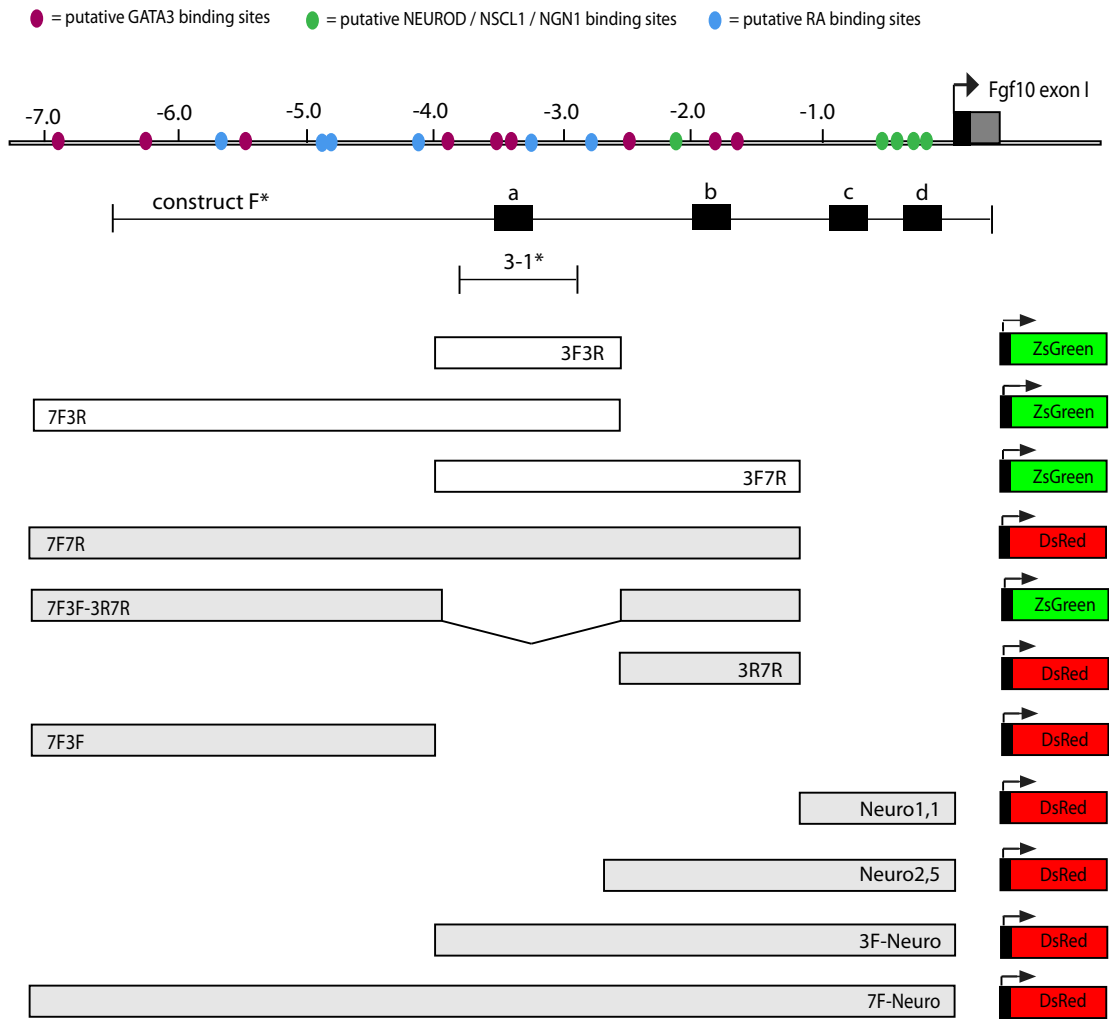


**Figure 4.2 Schematic of the *Fgf10* upstream region and constructs generated.** Location of the *Fgf10* enhancer fragments previously tested in (Ohuchi et al., 2005) are indicated and highlighted with asterisks (construct F and 3-1). Dark boxes a,b,c and d are conserved element, with these 4 regions being highly homologous in mouse, chick and human. The 6.6kb construct F was shown to recapitulate *Fgf10* expression in all endogenous area of expression. The 0.8kb 3-1 construct was shown to drive expression in restricted are of the inner ear only. White boxes represents enhancer fragment cloned prior to the start of this PhD (P.Datta). They were designed based on the location of putative Gata3 binding sites (symbolized as plain red circles). The 1.4kb 3F3R fragment includes the limited ear 800bp enhancer 3-1 and and 7F3R and 3F7R were designed to encompass the entire enhancer region required for full *Fgf10* endogenous expression. Grey boxes are the constructs generated in this project. The 5.6kb 7F7R enhancer was reconstructed using the 7F3R and 3F7R fragments previously obtained by high-fidelity PCR amplification. The 7F3F-3R7R enhancer correspond to 7F7R from which was specifically deleted 3F3R. It was generated in order to determine whether potential ear regulatory elements lying outside 3F3R could be separated as distinct regulatory modules controlling *Fgf10* expression in different location/time than 3F3R. 7F3F and 3R7R were also cloned independently for the same purpose. Four more constructs termed Neuro1.1, Neuro2.5, 3F-Neuro and 7F-Neuro were also generated following bioinformatics analysis of the *Fgf10* enhancer with an updated database that revealed the presence of putative binding sites for members of the *Neurogenin* pathway (NGN1, NEUROD and NSCL1, symbolized as plain green circles). Two different reporter genes were used, *ZsGreen* and *DsRed*, in order to later allow for comparative analysis of the specific expression pattern generated by the different enhancer in a same embryo - the use of two differently colored fluorescent molecules will allow determining area of overlapping expression at the cellular level. Putative binding sites for retinoic acid (RA) are also indicated (plain blue circles).

### 4.2.1 Reconstruction of the full *Fgf10* enhancer

Based on the results described by Ohuchi et al. (2005), a larger fragment was cloned as part of an MSc project in the laboratory (P.Datta). This 1.4kb enhancer (hereafter referred to as 3F3R) that incorporates the limited 800bp 3-1 enhancer (Ohuchi et al., 2005) and additional 5' and 3' sequences was cloned upstream of green fluorescent reporter gene called *ZsGreen* (Figure 4.2). In addition two larger overlapping genomic regions had been amplified (3F7R and 7F3R, Figure 4.2) that together included all the putative GATA3 binding sites thought to be important for *Fgf10* regulation in the inner ear, and were thus predicted to encompass the full *Fgf10* enhancer. In order to recreate a fully functional inner ear enhancer, I first looked to recreate the 5.6kb 7F7R genomic region (Figure 4.3) by ligating together these two 7F3R and 3F7R fragments that had been previously amplified by high fidelity PCR.

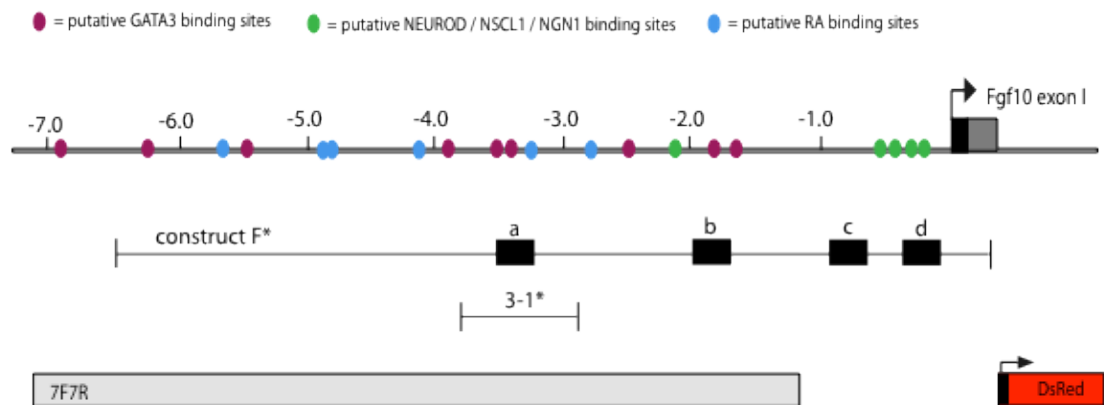


**Figure 4.3 The 7F7R-DsRed reporter construct.** The 5.9kb 7F7R fragment is indicated in grey. Above it, the 7kb upstream *Fgf10* are represented, along with putative binding sites for GATA3 (in red), NEUROD/NSCL1/NGN1 (in green), and retinoic acid (in blue). Enhancer fragments previously tested by Ohuchi (2005) are indicated with asterisks (construct F and 3-1). Dark boxes a, b, c and d are conserved elements, with these 4 regions being highly homologous in mouse, chick and human.

Using the strategy outlined in Figure 4.4a, a *HindII-XbaI* fragment from 3F7R was ligated downstream and contiguous to the endogenous *HindII* site using a *HindIII-HincII* fragment of 7F3R. Successful cloning was confirmed by restriction analysis using (i) digestion with *AflIII* that was predicted to linearise the 8.6kb clone and (ii) a *SpeI* digest that releases the 5.7kb enhancer from the 2.9kb pSK-bluescript backbone (Figure 4.4b).

A reporter system was then chosen. Previously 3F3R had been cloned in a *ZsGreen* reporter construct including a minimal  $\beta$ globin promoter, which is on its own unable to support expression. Fluorescent expression in the inner ear was detected using such a 3f3r-*ZsGreen* construct in transgenic embryos (Economou et al., 2012). This reporter could have been used for 7F7R too, but since the aim of this project was to identify any modular components underlying regulation, for example by comparing the 3F3R and 7F7R reporter patterns, a second fluorescent reporter (*DsRed*) was selected. Thus the experimental design was to enable easy comparison of the patterns of expression generated by the two enhancers in the same embryo.

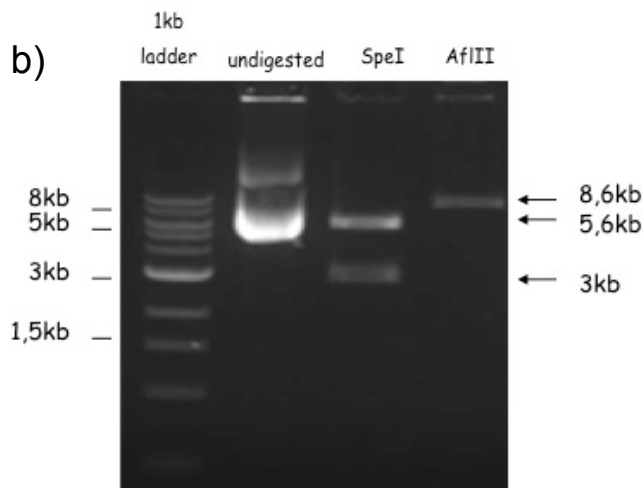
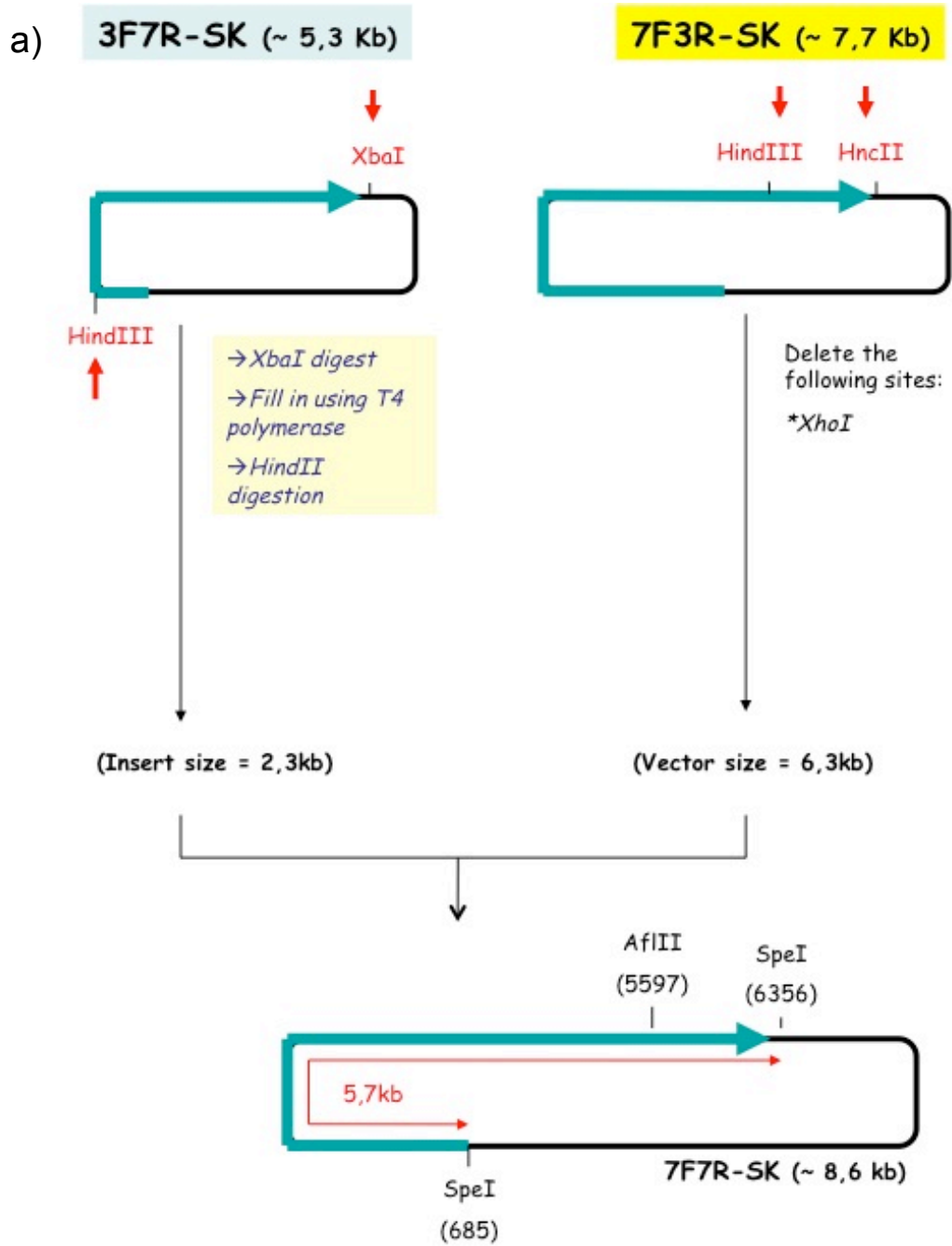


**Figure 4.4 Reconstruction of the 7F7R enhancer.** a) Overview of the cloning strategy used to reconstruct 7F7R. B) Restriction analysis confirms cloning of 7F7R in SK : *AflIII* linearises the 8.5kb clone and *SpeI* releases the 5.6kb enhancer from the 2.9kb pBluescript SK backbone.

A pDsRed expression vector was purchased (Clontech). This clone however did not contain any promoter so first it had to be modified. A human  $\beta$ globin minimal promoter had previously been inserted in front of the promoterless pZsGreen clone and shown to successfully drive reporter expression in mice when in presence of an enhancer (M.Maconochie, personal communication; Economou et al., 2012) and thus the same strategy was adopted.

The 114bp  $\beta$ globin minimal promoter was digested from a *ZsGreen* reporter construct and cloned as a *Bam*HI fragment upstream the *DsRed* reporter gene. In addition, a new *Spe*I restriction site was also incorporated by the insertion of *Spe*I linkers upstream of the promoter to facilitate future cloning (Figure 4.5a). Successful insertion of the  $\beta$ globin promoter was confirmed by digestion with *Bam*HI to release the 114bp promoter from 4.1kb pDsRed vector backbone (Figure 4.5b). In addition, the generation of the *Spe*I restriction was confirmed by successful linearization of the 4.2kb  $\beta$ globin-*DsRed* clone using *Spe*I (Clone1, Fig 4.5c).

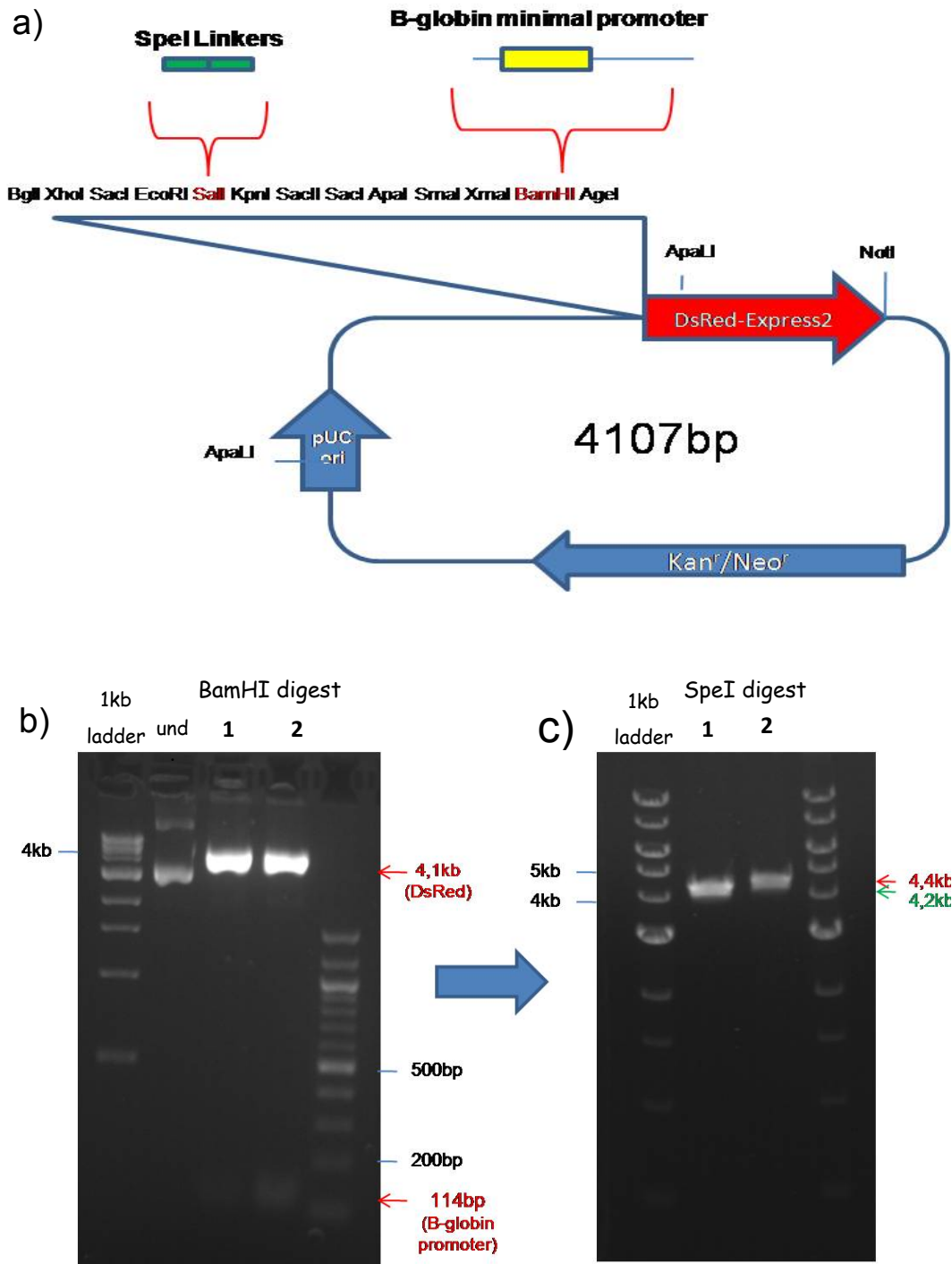


**Figure 4.5 Modification of the pDsRed-Express2-1 reporter vector.** a) Schematic of the pDsRed expression vector (Clontech) and location of *SpeI* linkers and  $\beta$ globin promoter insertion. b) Restriction analysis of two  $\beta$ globin-DsRed positive clones (1 and 2). *Bam*HI digest releases the 114bp promoter. 1.5% agarose gel. c) The generation of a novel *SpeI* restriction sites is confirmed by the linearisation of the clones. Clone 1 is of the expected 4.2kb size, Clone 2 is 0.2kb bigger. Sequencing results showed clone 2 contains 3 repeat of the  $\beta$ globin enhancer, as expected from the amount of DNA recovered at 114bp following *Bam*HI digest (b). und: undigested

#### 4.2.2 Can 'early' and 'late' patterns of *Fgf10* expression be separated?

According to Ohuchi et al. (2005), the full 6.6kb enhancer was able to recapitulate the full endogenous pattern of *Fgf10* expression from 8.75dpc onwards whereas the smaller ~800bp enhancer could only drive *Fgf10* expression in restricted area of the inner ear and from later developmental stages (around 10.5dpc), the "late" pattern. The constructs here 7F7R (5.6kb) and 3F3R (1.4kb) were predicted to mirror these activities.

#### The 7F3F-3R7R construct

In order to determine if 'early' and 'late' patterns can be separated into distinct control elements, a 2<sup>nd</sup> reporter construct encompassing the 5.6kb region but lacking the 1.4kb (3F3R) late element was generated (7F3F-3R7R; Figure 4.6).

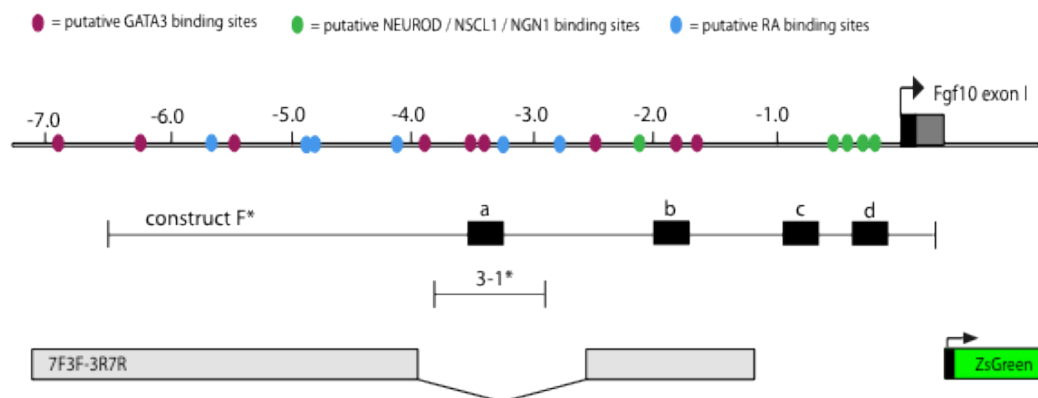


**Figure 4.6 The 7F3F-3R7R-ZsGreen reporter construct.** The 7F3F-3R7R enhancer is indicated in grey. Above it the 7kb upstream *Fgf10* are represented, along with putative binding sites for GATA3 (in red), NEUROD/NSCL1/NGN1 (in green), and RA (in blue). Enhancer fragments previously tested by Ohuchi (2005) are indicated with asterisks (construct F and 3-1). Dark boxes a, b, c and d are conserved elements, with these 4 regions being highly homologous in mouse, chick and human.

To do so, a set of PCR primers were designed to amplify 7F3F and 3R7R, while adding a unique *NdeI* restriction site to the 3' end of the 7F3F fragment, and to the 5' end of the 3R7R fragment. This allowed ligating the two fragments together while specifically excluding the 3F3R enhancer region (Figure 4.7a). *SpeI* sites were also added by PCR in 5' of 7F3F and 3' of 3R7R to facilitate cloning. An overview of the cloning strategy is given in Figure 4.7b. Successful insertion of 7F3F in 3R7R-SK was confirmed by restriction analysis with *BglII* that linearises the 7.2kb 7F3R-3R7R-SK plasmid by cutting once into 7F3F, and using the introduced *NdeI* site that cuts at the junction between 7F3R and 3R7R (Figure 4.7c). The 7F3R-3R7R enhancer was then subcloned as a *SpeI* fragment in the pZsGreen reporter (Figure 4.7e) and cloning confirmed by restriction analysis with *NdeI* that linearises the 8.4kb construct, and *HindIII NdeI* that generates two fragments of 5.4kb and 3kb (Figure 4.7d,e).

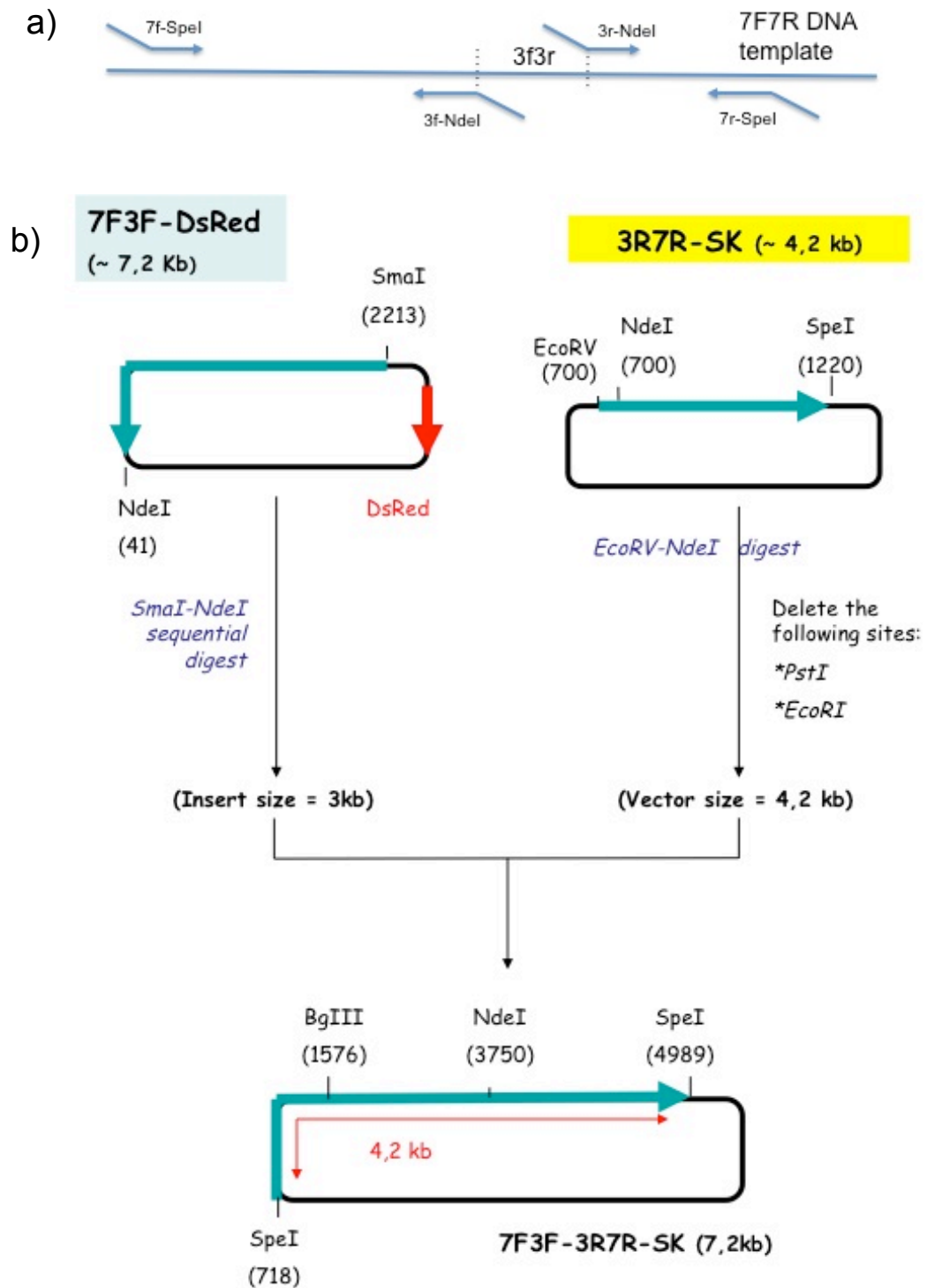


**Figure 4.7 Generation of a 7F7R enhancer specifically deleted from 3F3R.** a) Schematic of the primers used to insert *SpeI* and *NdeI* by high-fidelity PCR. b) Overview of the strategy used to reconstruct 7F3F-3R7R. c) Restriction analysis of 7F3F-3R7R-SK: *BglII* and *NdeI* both linearises the 7.2kb construct. d) Restriction analysis of 7F3F-3R7R-ZsGreen : *NdeI* linearises the 8.4kb construct, and *NdeI/HindIII* double digest generates two fragments of 5.4 and 3kb as expected. e) Schematic map of the 7F3F-3R7R-ZsGreen clone.



## 7F3F and 3R7R constructs

7F3F-DsRed and 3R7R-DsRed constructs (Figure 4.8) were also prepared in order to test whether the region that contains the early pattern of expression can be separated into two distinct regulatory modules. Briefly, 7F3F (Figure 4.9) and 3R7R (Figure 4.10) were cloned as *SpeI-HindIII* fragment in the  $\beta$ globin-*DsRed* reporter. 7F3F cloning was confirmed, with restriction analysis with *HindIII* that linearises the 7.2kb clone and digestion with *BglI* that generates two fragments of 7.2kb and 5kb by cutting once within *DsRed* and once within 7F3F (Figure 4.9b). 3R7R cloning was confirmed by restriction analysis with *BglI* that linearised the 5.4kb clone and *BglI/PvuII* double digest that generates two fragments of 3.1kb and 2.3kb (Figure 4.10b).

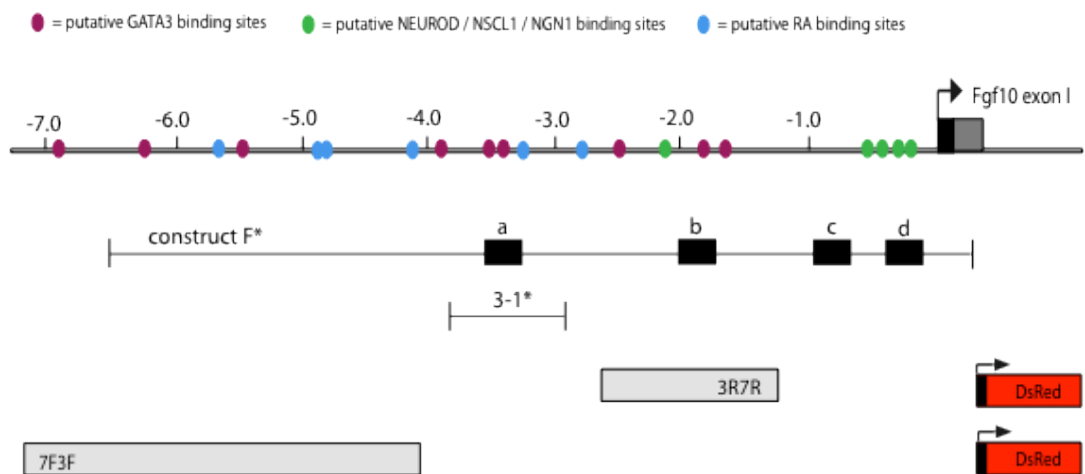


**Figure 4.8 The 7F3F and 3R7R-DsRed reporter constructs.** The 7F3F and 3R7R regions are indicated in grey. Above it the 7kb upstream Fgf10 are represented, along with putative binding sites for GATA3 (in red), NEUROD/NSCL1/NGN1 (in green), and retinoic acid (in blue). Enhancer fragments previously tested by Ohuchi (2005) are indicated with asterisks (construct F and 3-1). Dark boxes a, b, c and d are conserved elements, with these 4 regions being highly homologous in mouse, chick and human.

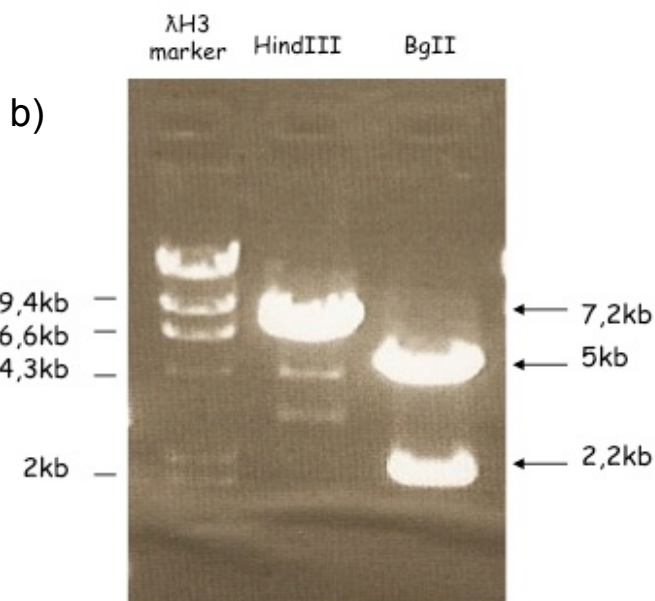
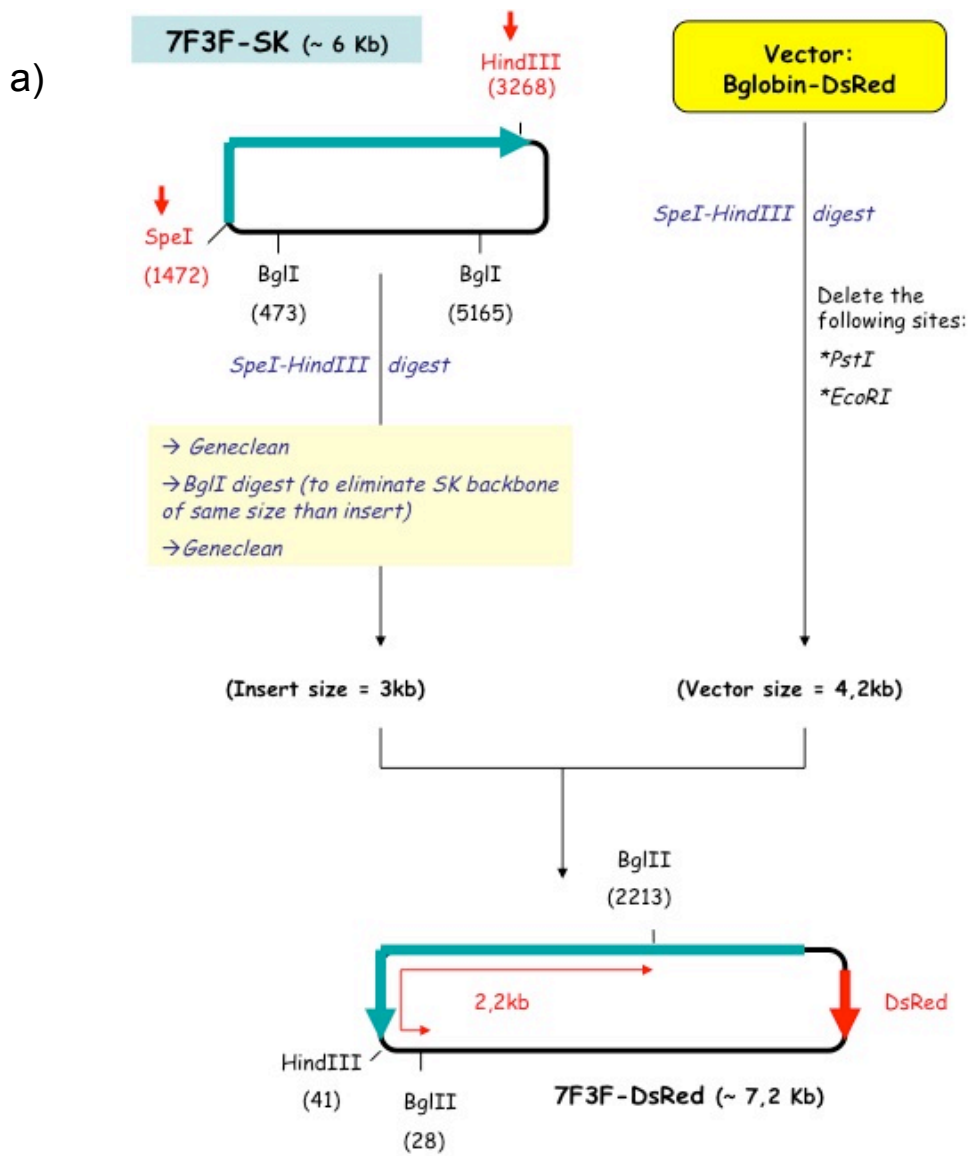


**Figure 4.9 Generation of the 7F3F-DsRed construct.**  
a) Overview of the cloning strategy used to reconstruct 7F3F. b) Restriction analysis confirms cloning of 7F3F in pDSRed : *HindIII* linearises the 7.2kb clone and *BglII* generates two fragments of 5kb and 2.2kb as expected.

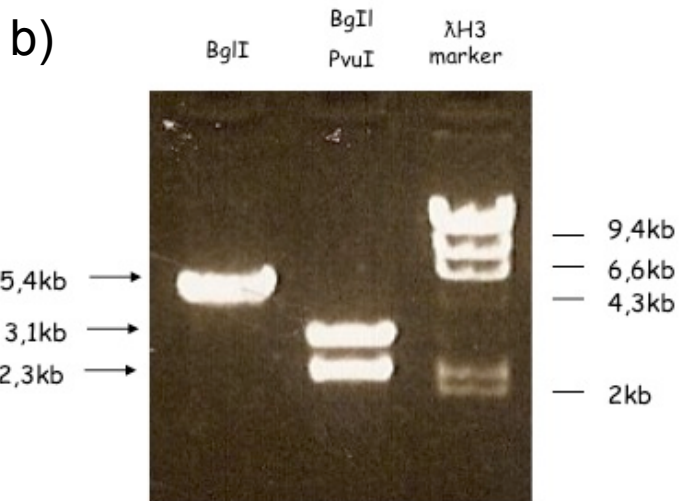
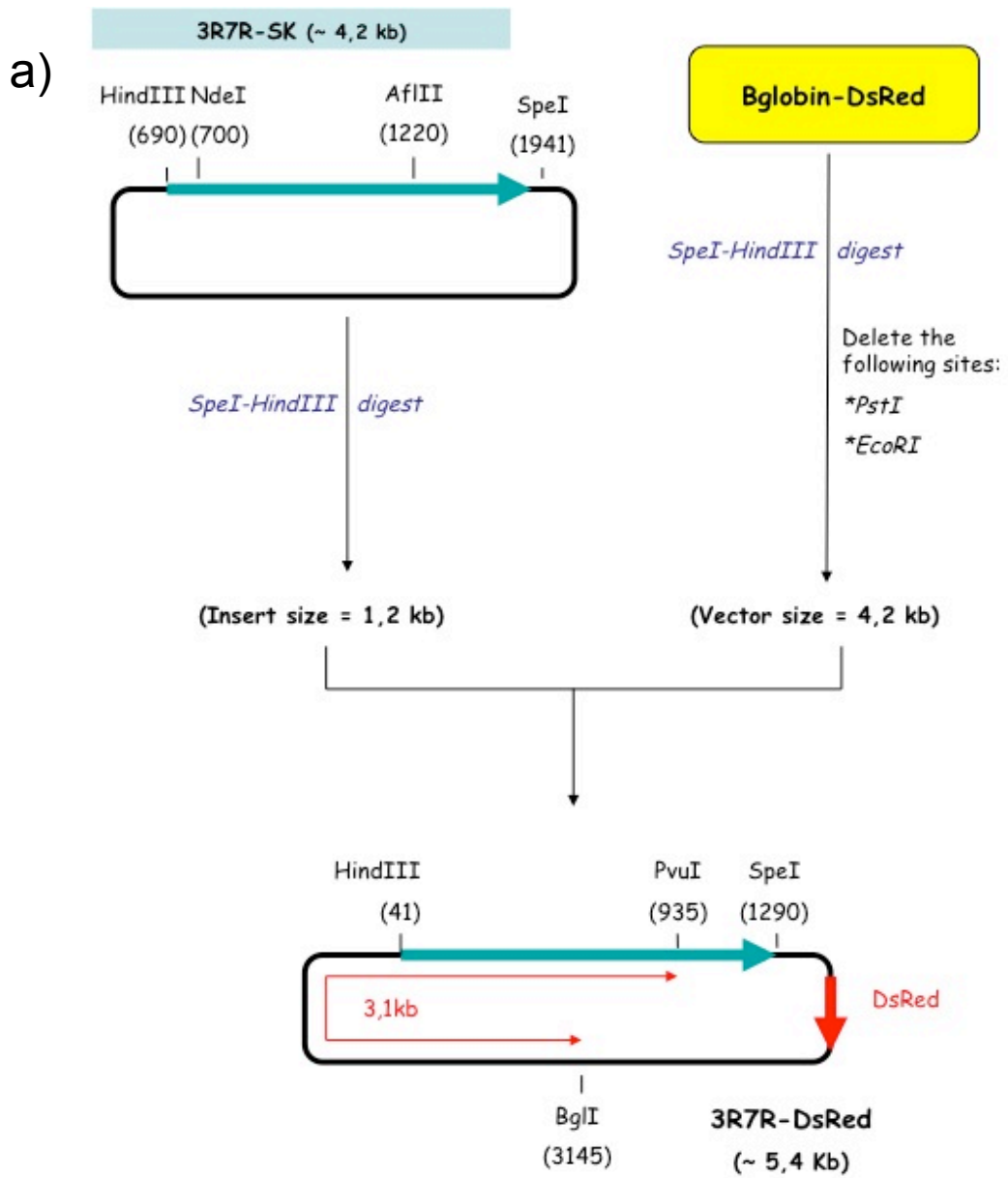


**Figure 4.10 Generation of the 3R7R-DsRed construct.**  
a) Overview of the cloning strategy used to reconstruct 3R7R. b) Restriction analysis confirms cloning of 3R7R in pDSRed : *BglI* linearises the 5.4kb clone and *BglI/PvuI* double digest generates two fragments of 3.1 and 2.3kb as expected.

### 4.3 Candidate upstream regulators of *Fgf10* expression

One of the main objectives of this project was to use an *Fgf10*-reporter transgenic mouse to investigate whether *Fgf10* is, like *Fgf3*, also subject to control by RA. In addition, bioinformatic analysis of the enhancer by Ohuchi (2006) and P.Datta (Msc Thesis 2007, University of Sussex) had also revealed the presence of binding sites for other putative upstream regulators of *Fgf10*, expression such as binding sites for the transcription factor GATA3. In particular, the 'late' 3F3R enhancer contains three GATA3 binding sites (Figure 4.2), and two of which are highly conserved across Mouse, Human and Chick species. This was of particular interest because a relationship between *Gata3* and *Fgf10* had already been suggested in the developing inner ear.

*Fgf10* expression appeared to be either strongly downregulated or not upregulated in the inner ear in *Gata3* mouse mutants (Lillevali et al., 2006). Moreover *Fgf10* appeared to be transactivated by GATA3 in vitro in an NIH3T3 fibroblast cell line (Lillevali et al., 2006). However, evidence for direct regulatory control of *Fgf10* by GATA3 in vivo were lacking, and *Gata3* could instead exert its regulatory control through initiating a cascade of gene transcription prior to an effect on *cis*-acting regulatory regions of *Fgf10* through unknown intermediate(s). In order to investigate whether *Gata3* represented a good candidate for a direct regulator of *Fgf10*, I looked to analyse the expression profile of *Gata3* during early inner ear development.

### ***4.3.1 Is Gata3 expressed at the right time and place to regulate Fgf10 expression in the inner ear?***

In order to confirm that *Gata3* and *Fgf10* are expressed in overlapping areas of the inner ear during early stages of development, comparative *Fgf10* and *Gata3* expression was analysed via non-radioactive in situ hybridization.

#### **Generation of *Gata3* riboprobes**

Firstly, *Gata3* riboprobes were generated. A full-length *Gata3* cDNA including 3' and 5' UTRs was ordered from (Geneservices). Bioinformatics was next used to try and determine which region(s) would be suitable to make riboprobes. Blast analysis of the full length *Gata3* cDNA clone sequence against the mouse genome revealed a 500bp central region highly conserved amongst members of the *Gata3* family (Figure 4.11a) that could potentially hybridise against other GATA family members. This highly conserved region is located between 1.3kb and 1.7kb of the *Gata3* cDNA.

Therefore restriction enzymes were carefully chosen to exclude this conserved region from the region used for generating riboprobes. Two different DNA fragments were chosen for further testing, 750bp in 5' and 450bp in 3' (Figure 4.11a). Successful cloning of the 450bp cDNA fragment in pbluescript was confirmed by restriction analysis with *SacI/NotI* double digest releasing the 450bp riboprobe (Figure 4.11b). Restriction analysis also confirmed the cloning of the 750bp fragment in pbluescript with *EcoRI* linearising the 3.7kb cloner and *EcoRI/BamHI* releasing the riboprobe (Figure 4.11c).

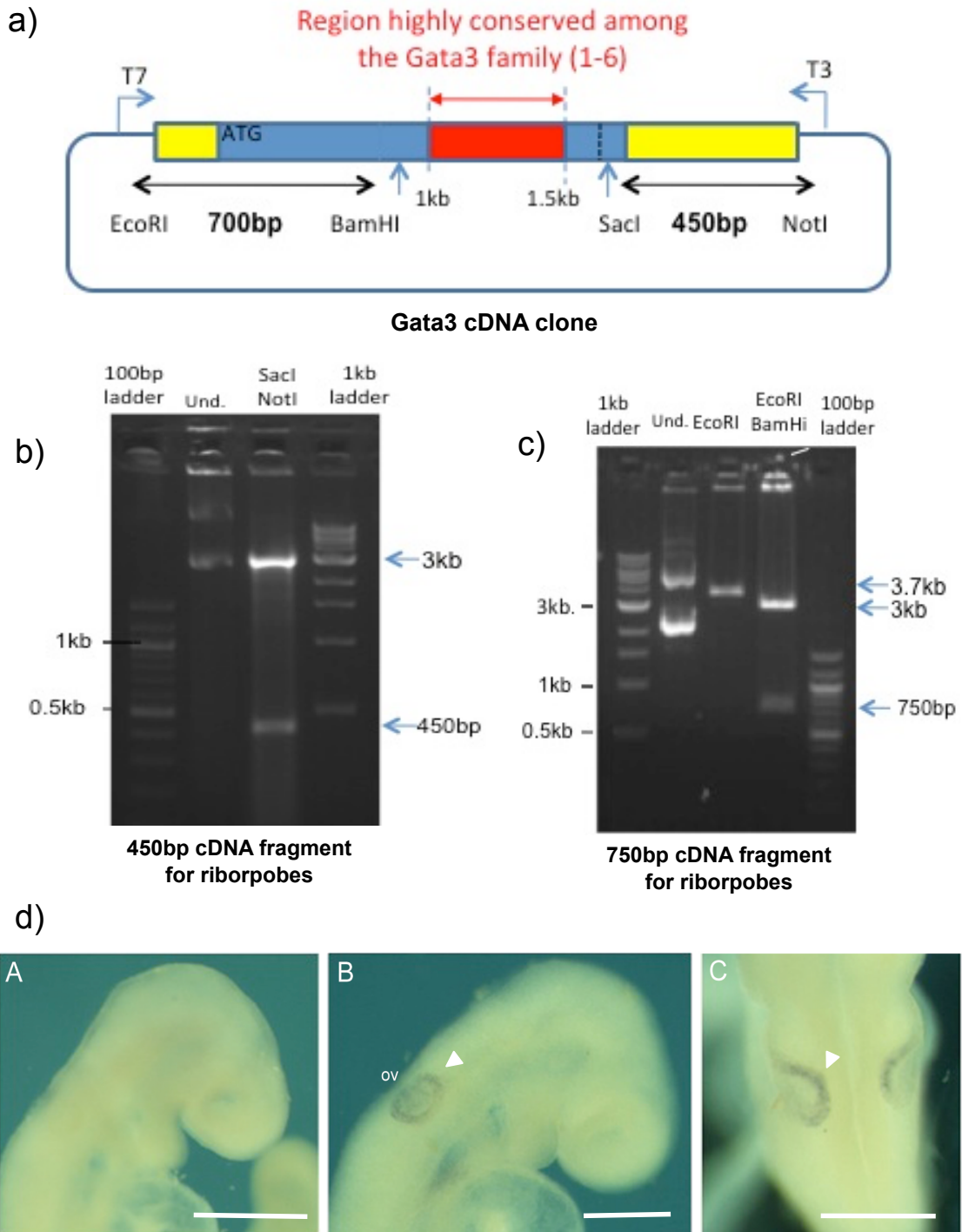


**Figure 4.11 Generation and trial of *Gata3* ribopobes.** a) Schematic of the *Gata3* cDNA highlighting a central region highly conserved among *Gata3* members. Two cDNA fragments excluding this region of homology were selected for subcloning in SK: 750bp in 5' and 450bp in 3'. b) Restriction analysis confirms cloning of the 3' 450bp fragment, with the generation of two fragments of 3kb and 450bp. c) Restriction analysis confirm cloning of the 5' 750bp cDNA fragment, with *EcoRI* linearising the 3.7kb fragment and *EcoRI/BamHI* releasing the 750bp riboprobe. d) In situ hybridization of wholemount embryos at 9.0dpc with *Gata3* sens control probes (A) or antisens ribopobes (B,C) *Gata3* expression in the otic epithelium is prominent dorsally and extends posteriorly, anteriorly and laterally. A dorsal view of the embryos shows the strong dorsal expression in the otic cup. Scale bar = 500µm

The 450bp 3'riboprobe was first tested in mice wholemount in situ. Both sense and antisense probes were prepared and hybridized against 9-9.5dpc embryos. *Gata3* expression was not detected in any of the embryo analysed (data not shown). The 750bp 5'riboprobe was also tested and strong expression in the developing otic vesicle was evident (B, C in Figure 4.11d), with the sense control not giving any signal (A in Figure 4.11d). This probe was thus used to investigate early expression of *Gata3* in wholemount embryos.

### **Analysis of the early pattern of *Gata3* expression**

*Gata3* expression is first visible throughout the anterior most part of the otic placode at 8.75-9dpc (Figure 4.12A); and continues to be expressed here later as placode starts invaginating to form the otic cup (Figure 4.12B). Dorsal view confirms the lack of *Gata3* expression in the latero-medial wall of the otic vesicle (Figure 4.12C). *Gata3* expression can also be seen throughout the otic epithelium as otic cup closes but expression is now considerably weaker in the ventral wall (Figure 4.12D). *Gata3* expression was also detected in the developing vestibulo-acoustic and trigeminal ganglion at 9.5dpc (arrows, Figure 4.12E) and 10.5dpc (Figure 12F). These results compared favourably with the pattern of GATA3 expression previously reported in the inner ear (Lawoko-Kerali et al., 2002)

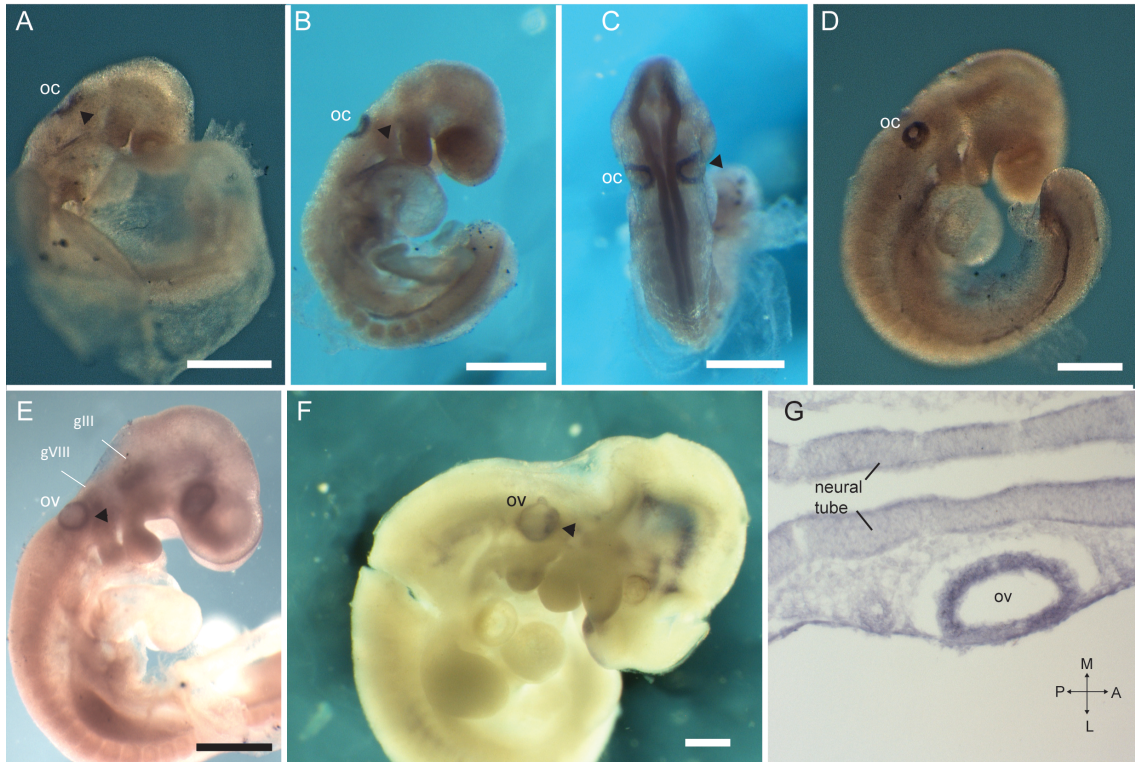


**Figure 4.12 Early pattern of *Gata3* expression in the developing inner ear.** *Gata3* expression is visible throughout the otic placode at 8.75dpc (A). As the placode starts to invaginate, expression is upregulated (B). Dorsal views of the otic cup confirms the pattern of expression noted in Figure 4.8D, with a lack of expression in the lateral wall (C). Strong *Gata3* expression in the developing inner ear with the exception of the latero-medial domain is also seen as the otic is almost closed (D). *Gata3* is still expressed throughout the otic vesicle at 9.5dpc (E). At 10.5dpc *Gata3* expression appears to be restricted to the anterior otic epithelium and developing ganglion (F). Coronal sections of a wholemount embryo hybridized at 9.5dpc confirm expression throughout the otic epithelium. Scale bar = 500 $\mu$ m. This figure also appears in (Economou et al., 2013). Copyright © 2012 Elsevier B.V.

### **Comparison of *Fgf10* and *Gata3* pattern of expression**

At the time of *Fgf10* onset of expression, *Gata3* is already expressed throughout the otic placode and overlaps with *Fgf10* in the anterior region of the otic placode (compare Figure 4.1A and 4.12A). As the otic cup starts to invaginate, both *Gata3* and *Fgf10* are upregulated in the anterior otic epithelium (compare Figure 4.1B and 4.12B). Both *Gata3* and *Fgf10* are preferentially expressed in the antero-medial wall of the otic vesicle (compare Fig 4.1F and 4.12D) with weaker expression in the lateral domain. At 10dpc, *Fgf10* and *Gata3* are both expressed in the anterior wall of the developing inner ear as well as in the trigeminal and vestibulo-acoustic ganglia (compare Figure 4.1E) and 4.12E). Thus, *Gata3* expression overlaps *Fgf10* expression throughout early inner ear development.

### **4.3.2 Are members of the Neurogenin pathway expressed at the right time and place to regulate *Fgf10* expression in the inner ear?**

I was also interested to identify whether there were additional putative *Fgf10* upstream regulators in addition to *Gata3*. Therefore an updated in silico analysis of the 10kb region upstream of *Fgf10* was performed using the Genomatix software ([www.genomatix.de](http://www.genomatix.de)) using the updated databases (2010); and using MatInspector to identify putative transcription factor binding sites. This analysis revealed the presence of a cluster of binding sites for members of the *Neurogenin* pathway (NEUROD1, NSCL1 and NGN1) close to the endogenous *Fgf10* promoter, with some of these sites being conserved in human and/or chicken *Fgf10* upstream regions (Figure 4.13).

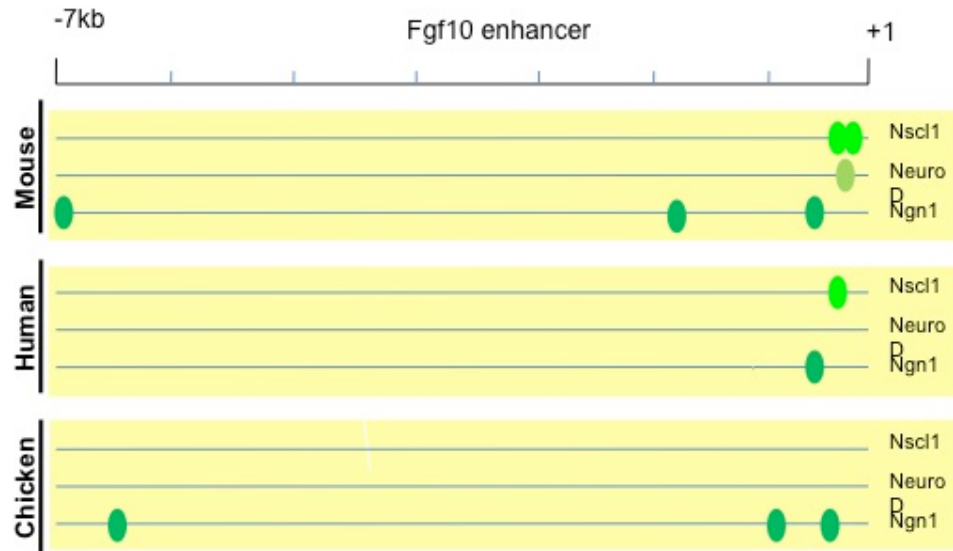


**Figure 4.13 Presence of conserved putative binding sites for neurogenic factors upstream *Fgf10*.** Bioinformatic analysis of the region upstream *Fgf10* revealed a cluster of binding sites for member of the *Neurogenin* pathway (indicated as green dots on the figure). Alignment with the upstream regions of human and chicken *Fgf10* reveals that some of these sites are conserved.

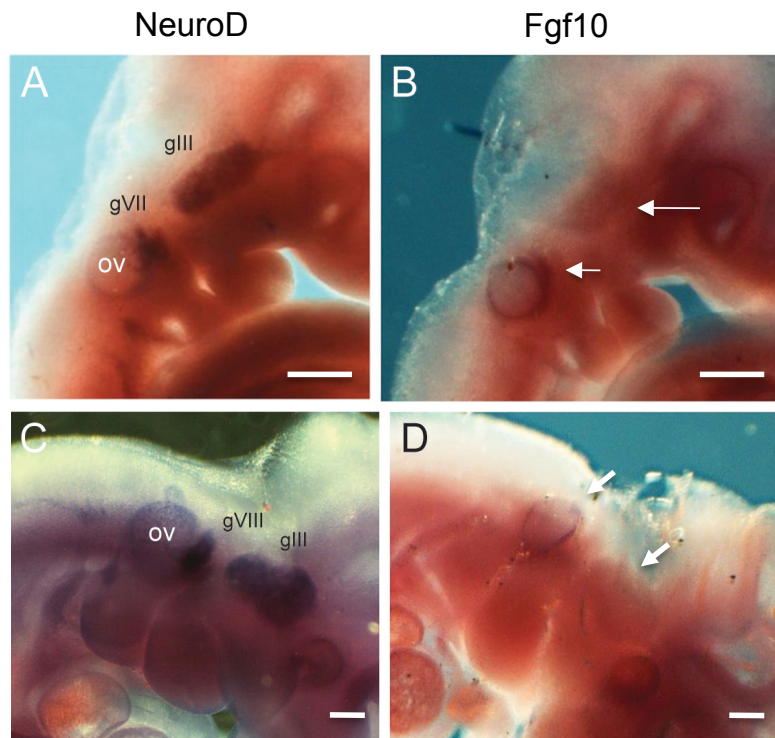


**Figure 4.14 Comparative analysis of *NeuroD* and *Fgf10* expression in whole-mount in situ mouse embryo at 9.5 and 10.5dpc.** *NeuroD* is strongly expressed in the anteroventral wall of the otic vesicle and the forming vestibulo-acoustic (gVIII) and trigeminal (gIII) ganglia at 9.5dpc (A). At this stage, *Fgf10* is also expressed in the anterior wall of the otic vesicle, as well as in developing gVIII and trigeminal ganglia (arrows, B). This pattern of expression is conserved at 10.5dpc. Scale bar = 500µm

Clustering of these sites, together with expression of *Fgf10* in inner ear neurons (Fritzscher et al., 2010) suggest *Fgf10* might be a direct downstream target of the *Neurogenin* pathway. In order to confirm that members of the *Neurogenin* pathway and *Fgf10* are expressed in overlapping areas of the developing inner ear, one member of this pathway, *NeuroD* was chosen for comparative in situ analysis with *Fgf10*.

### **Comparative analysis of *NeuroD* and *Fgf10* expression**

Previously I had isolated and cloned a 500bp *NeuroD* cDNA fragment and shown that probes synthesised from this fragment could successfully detect the early pattern of *NeuroD* expression in mice at 9.5dpc (S. Cadot, Msc Report 2008, University of Sussex). Here wholemount in situ hybridization was carried out using this *NeuroD* riboprobe at 9.5dpc and 10.5dpc. At 9.5dpc, *NeuroD* is strongly expressed in the antero-ventral wall of the otic vesicle as well as in the delaminating neuroblasts populating the vestibulo-acoustic ganglion, as well as the trigeminal ganglion (Figure 4.14A). *Fgf10* is also expressed in the anterior wall of the otic vesicle and in the developing vestibulo-acoustic and trigeminal ganglia (Figure 4.14B). This pattern of expression was conserved at 10.5dpc both for *NeuroD* (Figure 4.14C) and *Fgf10* (Figure 4.14D). Thus at these early stages of inner ear development, *NeuroD* is expressed in the right area to act as a direct upstream regulator of *Fgf10*.

## 4.4 Reporter constructs to investigate *Fgf10* regulation by the *Neurogenin* pathway

The 7F7R enhancer cloned above (section 4.2.1) to reconstruct the “full” *Fgf10* inner ear domain excludes a 1.1kb region proximal to the endogenous promoter (Figure 4.2). The clusters of neurogenic binding sites identified above are localized within this 1.1kb region. Thus, in order to test the regulatory activity of these sites and the potential role of the *Neurogenin* pathway in controlling *Fgf10* expression, additional enhancer-reporter constructs were generated.

### Neuro2.5 construct

Firstly, a 2.5kb enhancer fragment that includes all the putative binding sites for member of the *Neurogenin* family was cloned (Figure 4.15).

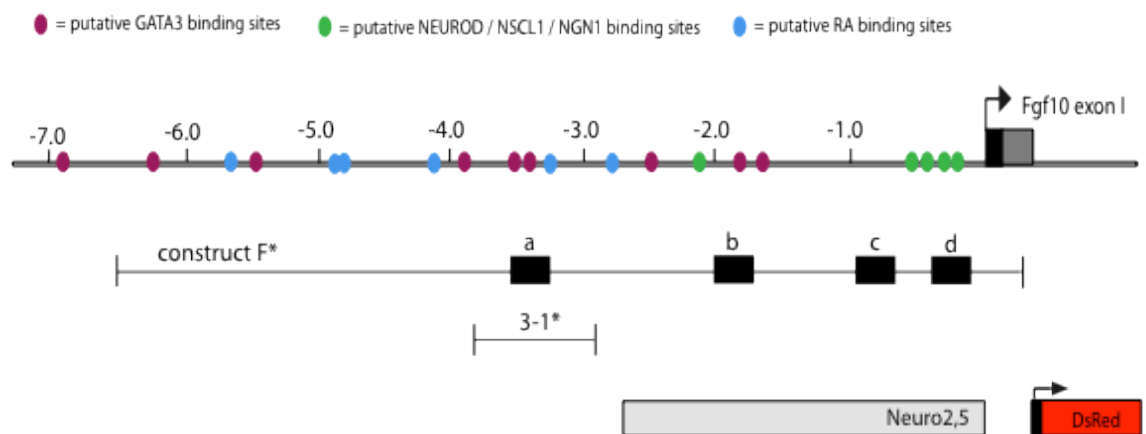


**Figure 4.15 The Neuro2,5-DsRed reporter construct.** The Neuro2,5 enhancer fragment is indicated in grey. Above it, the 7kb upstream *Fgf10* are represented, along with putative binding sites for GATA3 (in red), NEUROD/NSCL1/NGN1 (in green), and RA (in blue). Enhancer fragments previously tested by Ohuchi (2005) are indicated with asterisks (construct F and 3-1). Dark boxes a, b, c and d are conserved elements, with these 4 regions being highly homologous in mouse, chick and human.

Initial and multiple attempts to amplify a 2.5kb fragment from mouse genomic DNA, a fragment overlapping the 7F7R enhancer, containing all the putative neurogenic binding sites, and extending just in front of the promoter, were unsuccessful. Sequence analysis of this region revealed a high GC content of this region that might explain a failure to amplify in such a complex template (genomic DNA). Thus instead an *Fgf10* BAC clone was therefore ordered (Geneservices) in order to provide a more specific template for PCR amplification. Using a high-fidelity DNA polymerase and a buffer special for region riche in GC, this template permitted amplification of a 2.9kb fragment (Figure 4.16a). This Neuro2.5 fragment amplified by PCR happened to have naturally occurring restriction sites at both ends: *EcoRI* in 5' and *SacI* in 3' that permitted directional cloning in SK (Figure 4.16a). Successful cloning was confirmed by restriction analysis (Figure 4.16b). *AflIII* linearised the 5.5kb Neuro2.5-SK clone by cutting at a single site within the *Fgf10* enhancer fragment. An *AflIII/SacI* double digest cuts in both the insert and the pBluescript vector, generating two DNA fragments of 3.7kb and 1.8kb (Figure 4.16b).

Neuro2.5 was then sub-cloned in reverse orientation in pDsRed as an *EcoRI-SacI* fragment (Figure 4.16d). Cloning was confirmed by restriction analysis with *EcoRI*, that linearizes the 6.7kb construct, and *AflIII* that generates two fragments of 4.9kb and 1.8kb by cutting both in Neuro2.5 and in pDsRed (Figure 4.16c). Reverse orientation was chosen because this fragments lies really close to the promoter and could possibly contain part of the *Fgf10* promoter, which could drive reporter gene expression in the absence of suitable enhancer thus compromising the regulatory analysis of *Fgf10*.

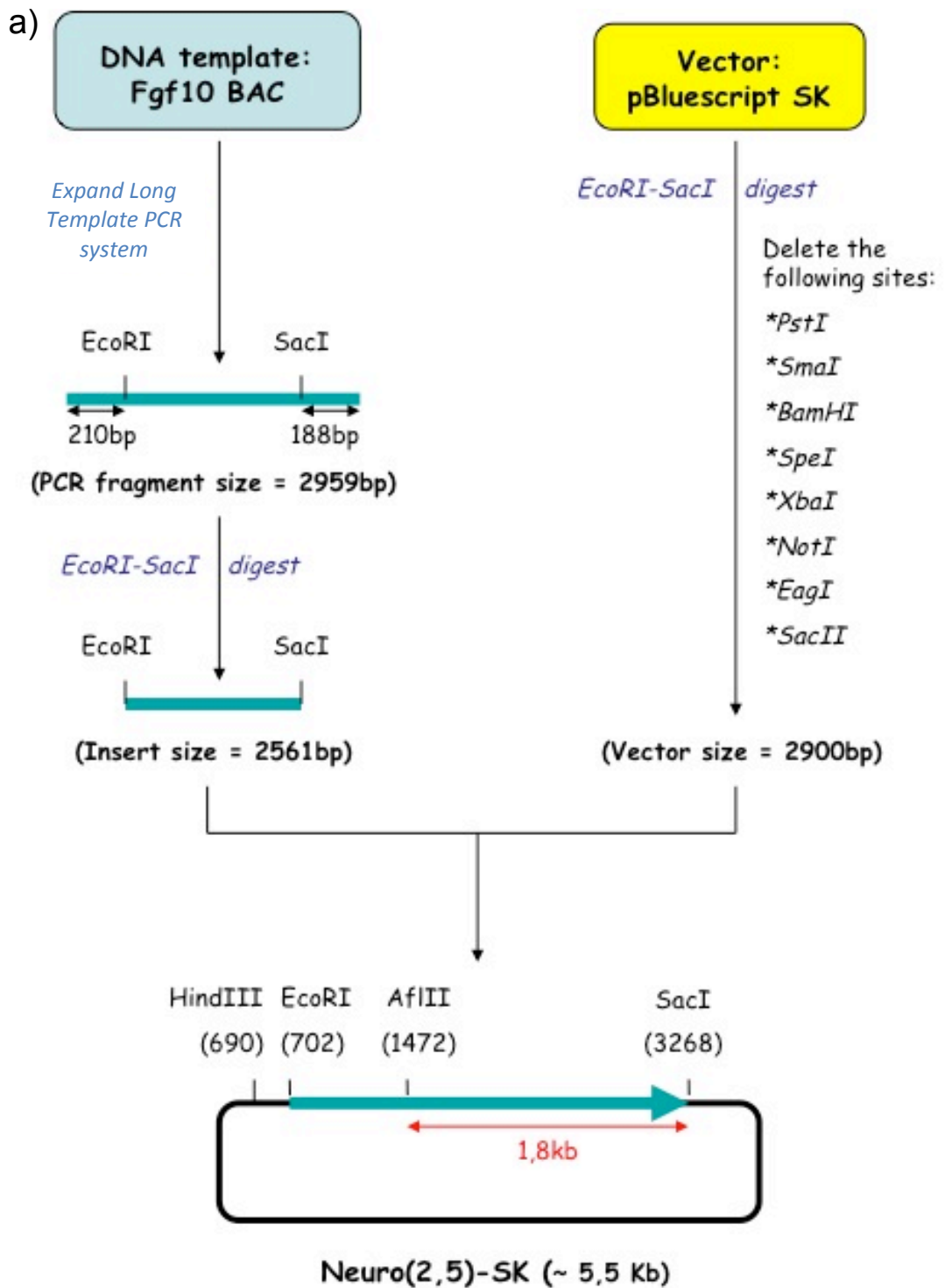


**Figure 4.16 Generation of a Neuro2.5-*DsRed* reporter construct.** a) Overview of the cloning strategy used. Neuro2.5 was amplified by high-fidelity PCR with the primers and PCR conditions as indicated in section 2.7.2. Neuro2.5 naturally contained an *EcoRI* site in 5' and *SacI* site in 3' that were used for cloning in SK. b) Restriction analysis confirms cloning of Neuro2.5 in SK, with *AflII* that generates one 5.5kb fragment and *AflII/SacI* double digest that generates two fragments of 3.7kb and 1.8kb. c) Neuro2.5 was then sub-cloned in reverse orientation in pDsRed and cloning confirmed by restriction analysis with *EcoRI* that linearises the construct and generate a fragment of 6.7kb; and *AflII* that generates two fragment of 4.9 and 1.8kb. d) Schematic of the Neuro2.5-*DsRed* construct

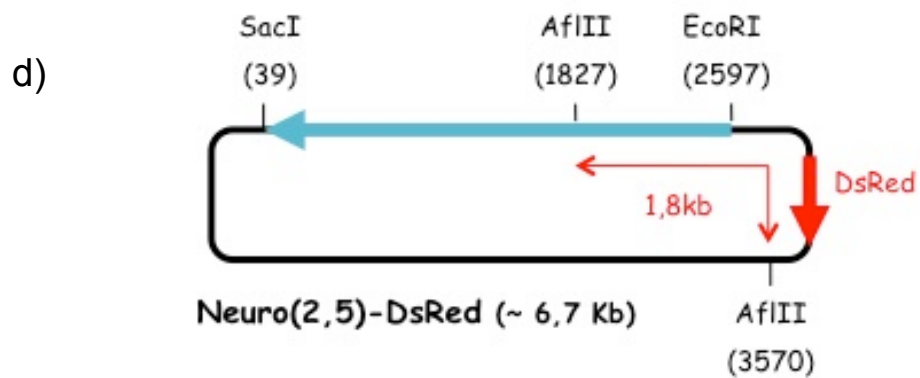
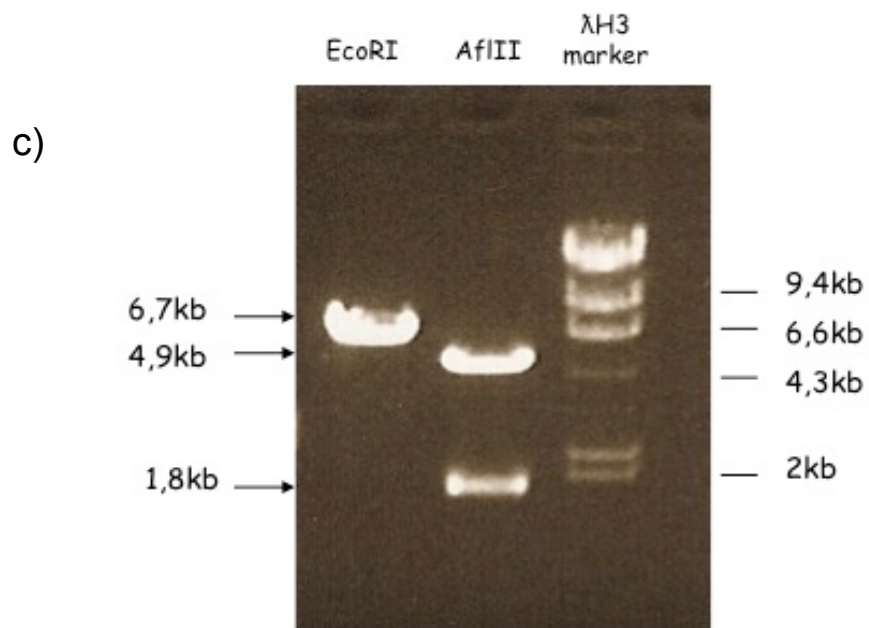
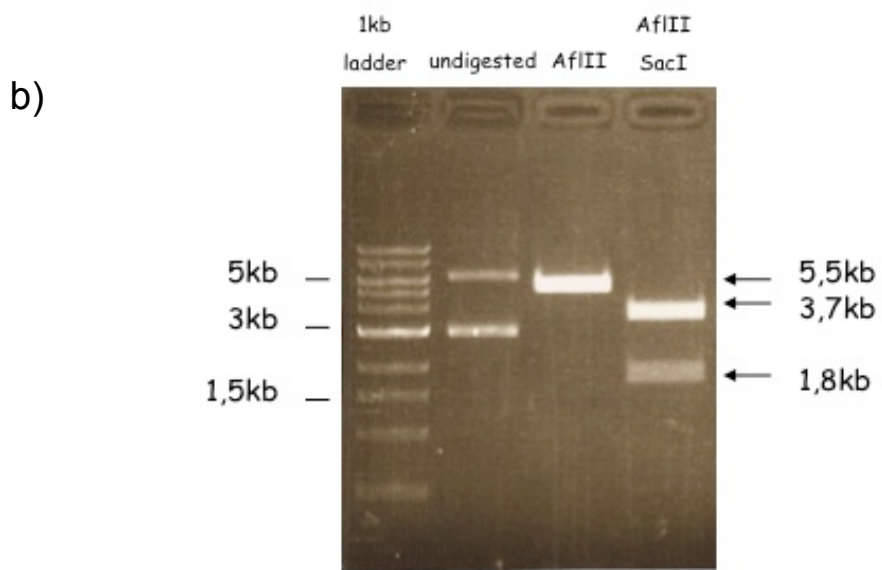
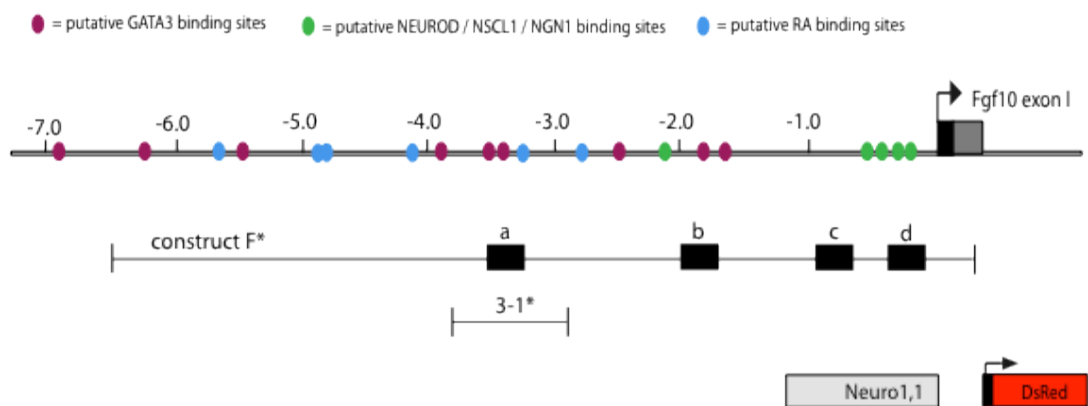


Figure 4.16

### Neuro1.1 construct

In order to determine whether the cluster of neurogenic binding sites on its own could drive *Fgf10* expression, a second fragment (Neuro1.1), which contains only the cluster of neurogenic binding sites close to the promoter, was cloned (Figure 4.17). As for Neuro2.5, Neuro1.1 was first amplified by PCR using again a *Fgf10* Bac as a template. Since the Phusion High-fidelity polymerase used for amplification generates blunt-end and the Neuro1.1 PCR fragment contains a *SacI* restriction site in 3' (Figure 4.18a), Neuro1.1 could then be cloned directionally in pSK. Restriction analysis confirmed cloning, with *SmaI* that linearizes the 4kb fragment and *SacI/HindIII* that releases the 1.1kb enhancer (Figure 4.18b).



**Figure 4.17 The Neuro1,1-DsRed reporter construct.** The Neuro1,1 enhance is indicated in grey. Above it the 7kb upstream *Fgf10* are represented, along with putative binding sites for GATA3 (in red), NEUROD/NSCL1/NGN1 (in green), and retinoic acid (in blue). Enhancer fragments previously tested by Ohuchi (2005) are indicated with asterisks (construct F and 3-1). Dark boxes a, b, c and d are conserved elements, with these 4 regions being highly homologous in mouse, chick and human.

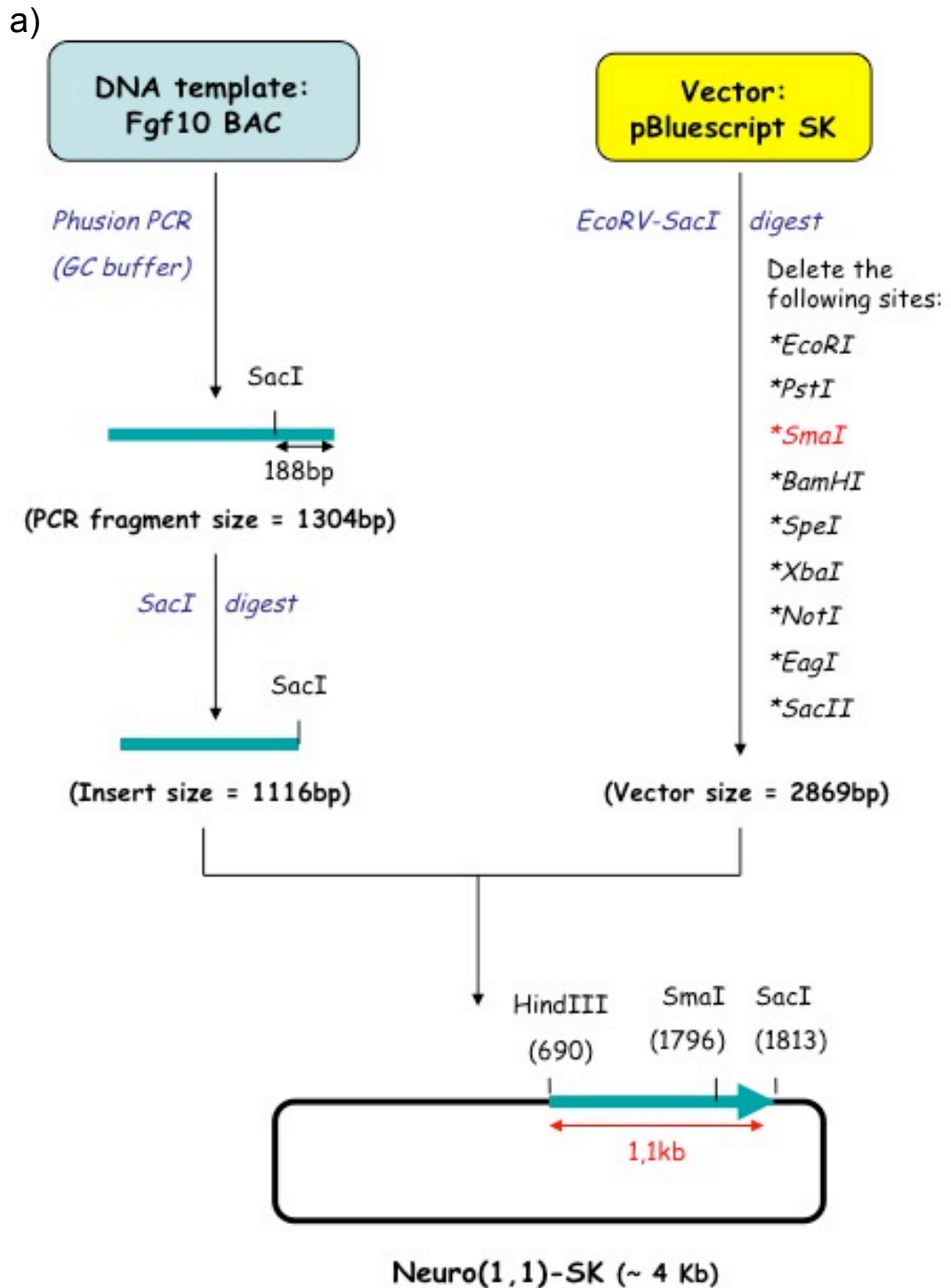


**Figure 4.18 Generation of a Neuro1.1-*DsRed* reporter construct.** a) Overview of the cloning strategy used. Neuro1.1 was amplified by high-fidelity PCR with Phusion. Phusion generates blunt end and thus the 1.1kb fragment was cloned as a *SacI*/blunt fragment into SK digested with *SacI* and *EcoRV*. b) Cloning was confirmed by restriction analysis, with *SmaI* that linearises the 4kb Neuro1.1-SK clone and *SacI*/*HindIII* double digest that releases the 1.1kb neuroenhancer. c) Neuro1.1 was then subcloned in pDsRed in reverse orientation as a *SacI*-*HincII* fragment and cloning confirmed by restriction analysis with both *SmaI* digest and *SacI*/*SacII* digest, both generating two fragments of 4.2kb and 1.1kb.c) Schematic of Neuro1.1-*DsRed* reporter construct

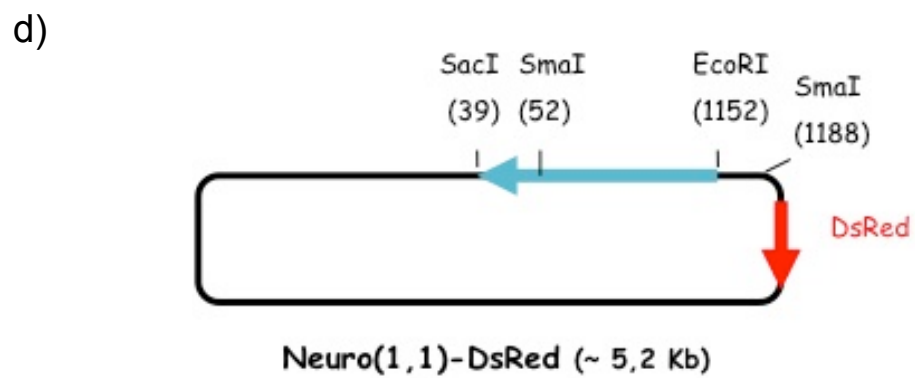
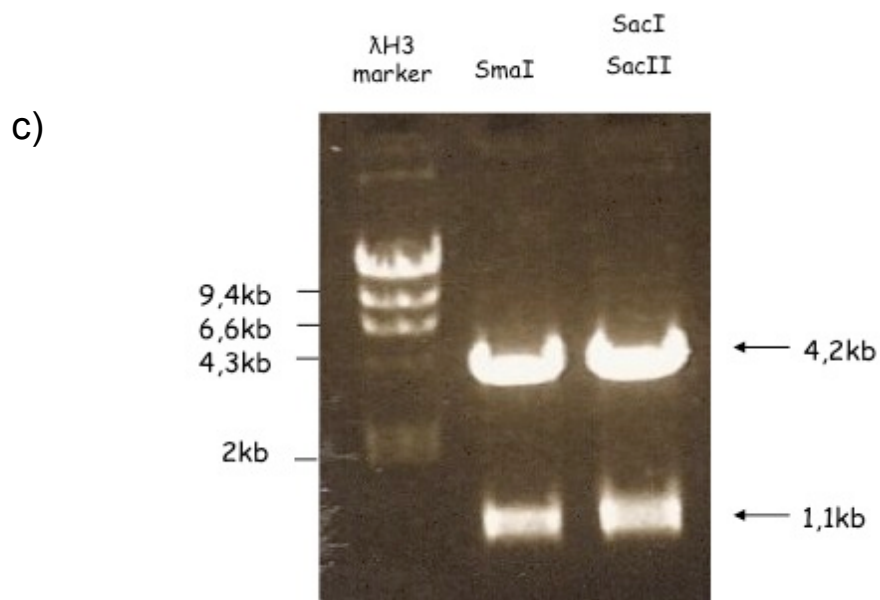
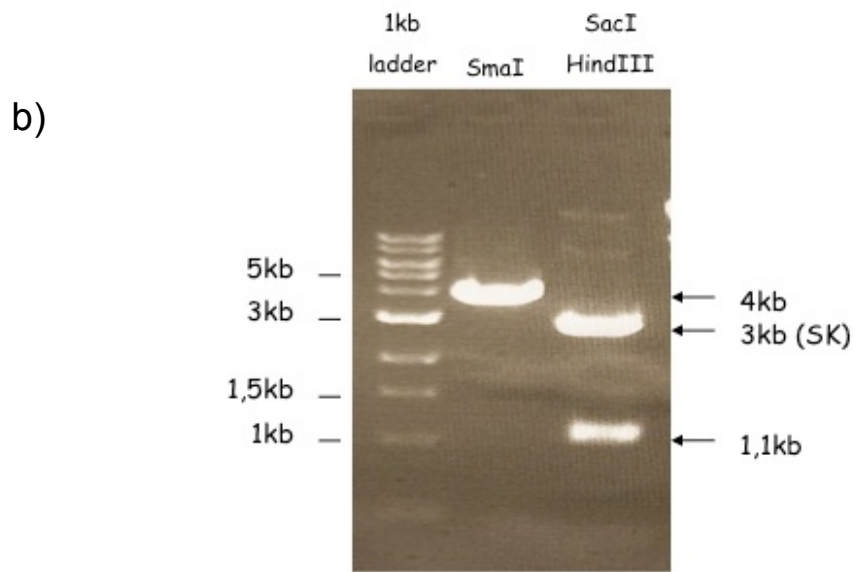
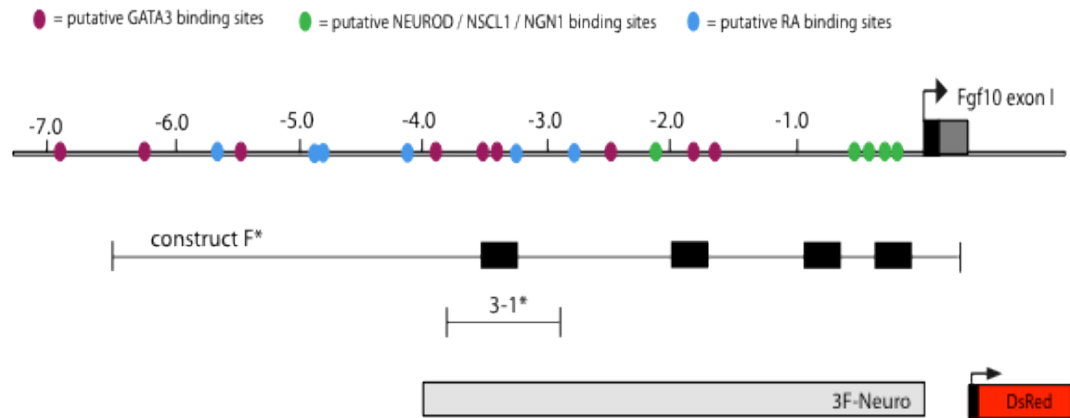


Figure 4.18

Neuro1.1 was then subcloned in pDsRed in reverse orientation as a *SacI-HincII* fragment (Figure 4.18d) and cloning confirmed by restriction analysis. *SmaI* and *SacI/SacII* double digest both resulted in the generation of two fragments of 4.2kb and 1.1kb (Figure 4.18c), as expected from the clone restriction map (Figure 4.18d)

### **3F-Neuro construct**

The discovery of potential *Fgf10* regulatory region not included in the 7F7R enhancer also prompted a new detailed comparison with the full *Fgf10* enhancer previously delimited by Ohuchi et al. (2005). This revealed that two out of four conserved elements upstream *Fgf10* were not included in 7F7R: elements c and d are lacking (Figure 4.2). Conserved elements b, c and d are thought to be involved in *Fgf10* regulation in the developing limb (Sasaki et al., 2002), and thus are less likely to contain ear regulatory elements if we assume that regulatory modules are discrete entities that do not overlaps (Davidson, 2006). However, these results were mostly based on transient mouse embryos, that is to say embryos resulting from injected eggs that are harvested at specific developmental stage following implantation in a pseudopregnant mother. This does not allow an analysis as detailed as with a stable transgenic line, where the embryos are instead brought to term and then used to generate as many litters as necessary for a full analysis of the transgene pattern in several embryos for each founder. Furthermore, the position of these conserved elements suggests 3F-Neuro rather than 7F7R contains all the elements to recapitulate *Fgf10* expression (Figure 4.19). The generation of *Fgf10*-reporter mouse line able to recapitulate *Fgf10* pattern of expression in all endogenous areas being one of the aims of this project, 3F-Neuro was cloned.



**Figure 4.19 The 3F-Neuro-DsRed reporter construct.** The 3F-Neuro enhancer is indicated in grey. Above it the 7kb upstream *Fgf10* are represented, along with putative binding sites for GATA3 (in red), NEUROD/NSCL1/NGN1 (in green), and retinoic acid (in blue). Enhancer fragments previously tested by Ohuchi (2005) are indicated with asterisks (construct F and 3-1). Dark boxes a, b, c and d are conserved elements, with these 4 regions being highly homologous in mouse, chick and human.

In order to generate a 3F-Neuro-DsRed construct; 3F7R and Neuro2.5 were first ligated together. Briefly, 3F7R and Neuro2.5 overlaps (Figure 4.2) and a single *Afl*III restriction site is located in the overlapping region between the two fragments (Figure 4.20a). Neuro2.5 was digested with *Afl*III and *Sac*I and cloned into a 3F7R-SK clone digested with the same enzyme, thus recreating the full length 3F-neuro (Figure 4.20a). Restriction analysis confirmed the cloning had been successful, with *Eco*RI giving rise to two DNA fragments of 5.4kb and 1.2kb and *Eco*RI/*Sac*I to three fragments of 3kb, 2.5kb and 1.2kb (Figure 4.20b). 3F-Neuro was then subcloned into pDsRed in reverse orientation as a *Sac*I-*Spe*I fragment (Figure 4.20d). Cloning was confirmed by restriction analysis with *Bgl*II that linearizes the 7.9kb clone and *Bgl*II/*Pvu*II double digest that generates two fragments of 4.3kb and 3.6kb (Figure 4.20c)

a)

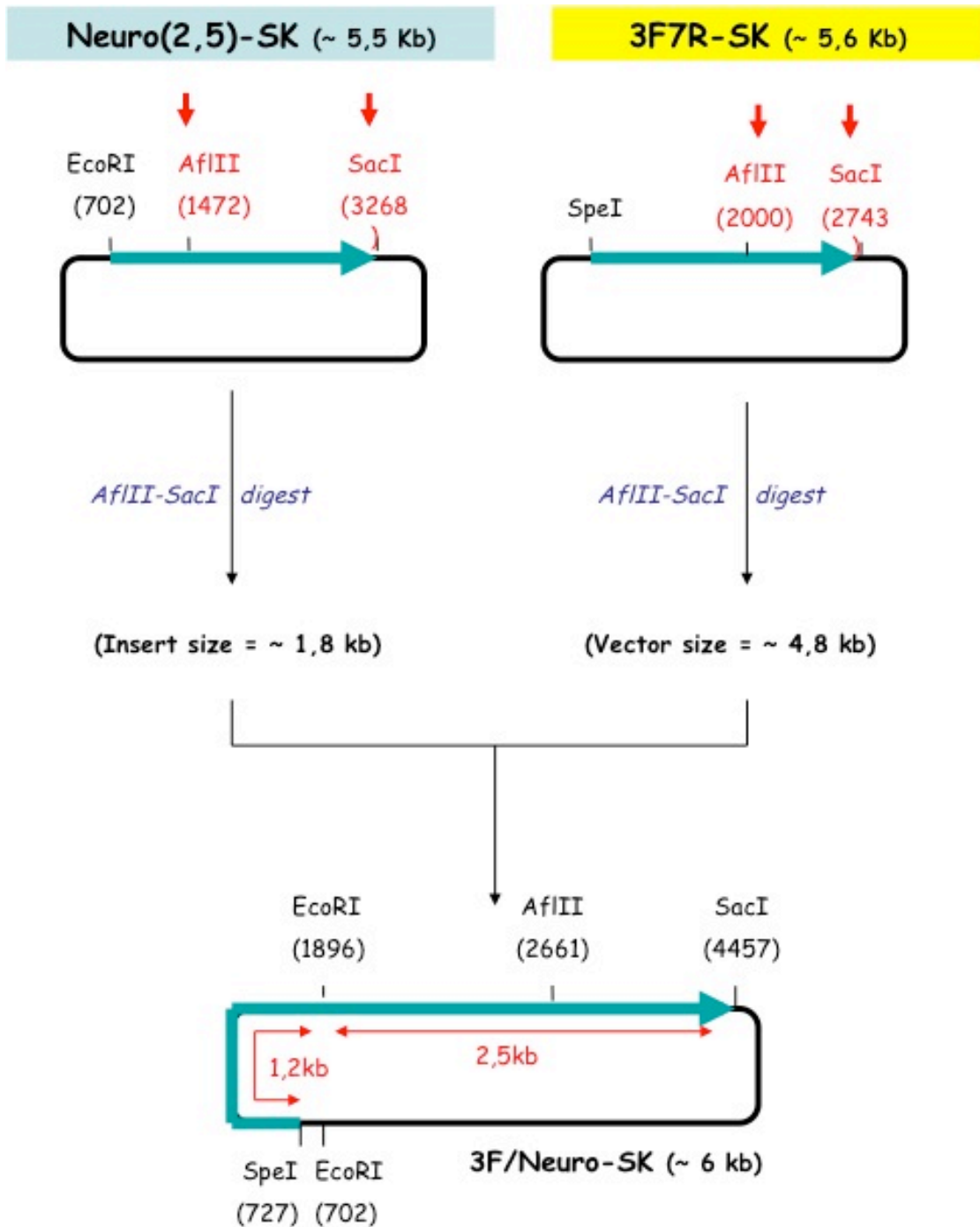


**Figure 4.20 Generation of a 3F-Neuro-DsRed reporter construct.** a) Overview of the cloning strategy used. 3F-neuro was reconstructed by directional cloning of Neuro2.5 as a *AfIII-SacI* fragment into the 3F7R-SK clone. b) Restriction analysis was performed using *EcoRI* that generates two fragments of 5.4kb and 1.2kb and *EcoRI/SacI* that generates three fragments of 3kb, 2.5kb and 1.2kb. c) 3F-neuro was then subcloned in reverse orientation in pDsRed as a *SacI-SpeI* fragment. Restriction analysis confirmed cloning with *BglII* that linearizes the 7.9kb clone and *BglII/PvuII* that generates two fragments of 4.3 and 3.6kb



### 7F-Neuro construct

Eventually, a construct including both 7F7R and the potential neuroenhancer, and hereafter 7F-Neuro (Figure 4.21) was also generated. 7F-Neuro was reconstructed by directional cloning of 7F7R in the Neuro2.5-*DsRed* clone as a *SpeI-EcoRI* digest (Figure 4.22a). Restriction analysis confirms cloning with *AflIII* generating two fragments of 6kb and 4.9kb, *BglII* two fragments of 5.5kb and *HindIII* generating one 10.9kb fragment (Figure 4.22b). This is consistent with the restriction map of the expected construct (Figure 4.22a)

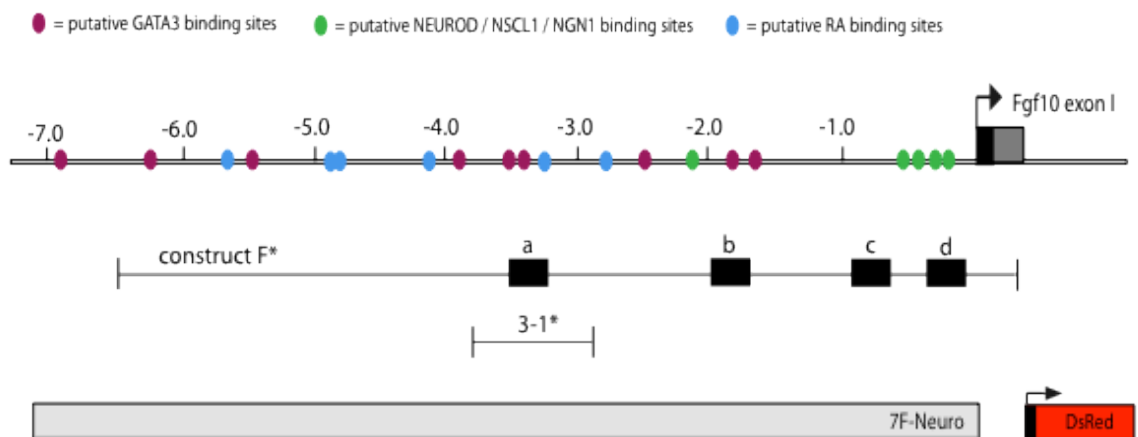
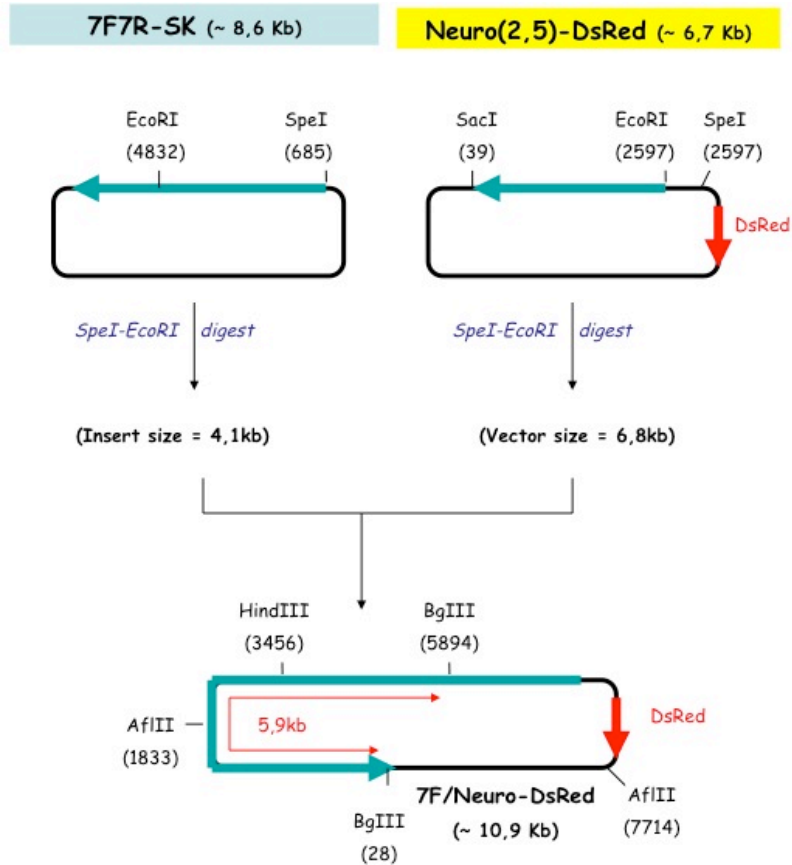


**Figure 4.21 The 7F-Neuro-DsRed reporter construct.** The 7F-Neuro enhancer is indicated in grey. Above it the 7kb upstream *Fgf10* are represented, along with putative binding sites for GATA3 (in red), NEUROD/NSCL1/NGN1 (in green), and retinoic acid (in blue). Enhancer fragments previously tested by Ohuchi (2005) are indicated with asterisks (construct F and 3-1). Dark boxes a, b, c and d are conserved elements, with these 4 regions being highly homologous in mouse, chick and human.

a)



b)

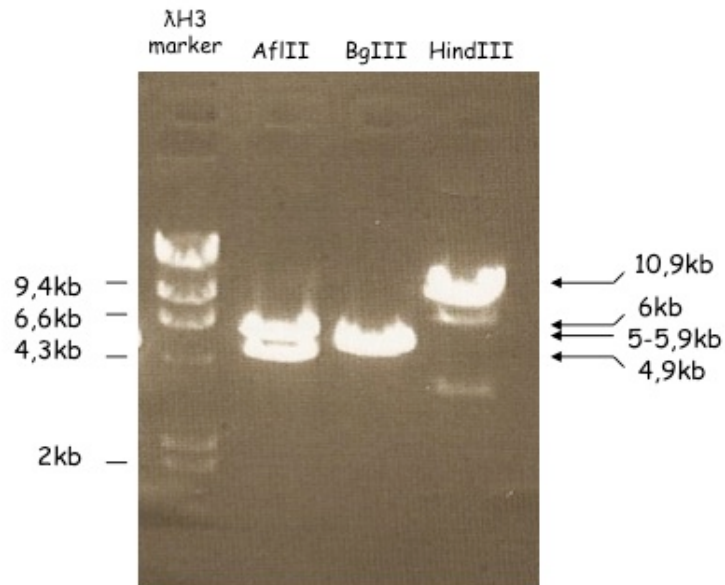


**Figure 4.22 Generation of 7F-Neuro-DsRed reporter construct.** a) Overview of the cloning strategy used. 7F-neuro was reconstructed by directional cloning of 7F7R in the Neuro2.5-DsRed clone as a *SpeI-EcoRI* digest. Restriction analysis confirm cloning with *AflIII* generating two fragments of 6kb and 4.9kb, *BglIII* two fragment of 5-5.9kb (appears as a single band on gel) and *HindIII* linearises the construct generating one 10.9kb fragment.

## 4.5 Generation and analysis of transgenic mouse lines

In vivo analysis of *Fgf10* regulation in the mouse was started with the injection of 7F7R-*DsRed*, the large enhancer fragment expected to recapitulate the full *Fgf10* endogenous inner ear pattern. Two independent transgenic lines containing the 7F7R-*DsRed* constructs were generated. Mice that had integrated the transgene were identified by PCR (Figure 4.23a) and selected for further breeding. For instance, one of the injection sessions leads to the generation of a female founder (2084; Figure 4.23b). This founder was then crossed with wild-type males to increase the colony. The first litter consisted of 6 pups, and included 1 male and 2 female carrying the 7F7R-*DsRed* transgene (Figure 4.23b). This 2<sup>nd</sup> generation of transgenics were crossed either with wild-type mice or with other 7F7R transgenics, and embryos were harvested at 9.5dpc. PCR analysis for detection of the transgene in embryos was carried out on yolk sac DNA to identify embryos carrying the transgene, and embryos positive for the 7F7R-*DsRed* transgene were analysed for fluorescence. However no fluorescence could be detected in any of the embryos analysed (n=6; data not shown).

In the experiments described by Ohuchi et al. (2005), the smaller enhancer (~800bp) only drove expression of *Fgf10* from 11.5dpc onwards. In order to determine if *Fgf10* expression was maybe just delayed with the 7F7R transgene, with essential elements missing for earlier expression, embryos were also analysed at later stages, at 10.5dpc and 11.5dpc. Unfortunately, here again, *Dsred* fluorescence was not detected in any of the embryos analysed, despite positive genotyping PCR results (data not shown).



This lack of fluorescence from the reporter could be explained in several ways:

- 1) The reporter gene may not be expressed. This could be due to a technical issue in generating the construct, such as inadvertently picking up a mutation in the promoter, or in crucial binding sites in the enhancer that would prevent or at least drastically reduce reporter gene expression
- 2) A mutation could have been introduced in the reporter gene itself leading to a non-functional DSRED protein and thus no fluorescence
- 3) The reporter transgene may have integrated into the genome in a region that is quiescent and refractory to expression.
- 4) The level of fluorescence may be too low and not be suitable for direct in vivo imaging at this stage in the mouse. Thus the signal may need to be amplified to be visible.

A sample of the purified 7F7R-*DsRed* construct that had been used for the injection was sent for sequencing to check the sequence integrity of the fragment used, to confirm the presence of the promoter in the right orientation and the absence of mutations in the promoter/*DsRed* reporter gene.

Sequence data from different reads using different primers were compared not only to mouse genome database ([www.ensembl.org/mus\\_musculus](http://www.ensembl.org/mus_musculus)), but also blasted against sequence data from other constructs generated in this lab that had been shown to drive expression in vivo. For instance the *βglobin* promoter from the *DsRed* construct was found to be perfectly aligned with the *βglobin* sequence from a functional *βglobin-ZsGreen* transgene. *DsRed* coding sequence was also perfectly aligned with the

sequence of a different but functional reporter in a CMV-*DsRed* plasmid. Sequence analysis confirmed the *βglobin* promoter was in the correct orientation and free from mutations. No mutations were detected from the sequence expected in *DsRed* either. The part of the enhancer sequenced corresponding to 7F7R did not reveal the presence of any mutations either. Although the entire 5.7kb of the enhancer was not sequenced, it is unlikely that even a few spontaneous mutations would totally shut down enhancer activity, as these would have to occur inadvertently in essential binding sites, and that *DsRed* expression in all endogenous areas of expression in vivo would have to be affected. These data suggested that the construct should be functional on the basis of the sequences analysed.

A second testable hypothesis was that the transgene was functional and *DsRed* is expressed, but at a level too low to be detected without amplification. In order to test this, two different DSRED antibodies were used in immunolabelling experiments. Following immunolabelling against whole transgenic embryos (9.5dpc and 10dpc) both wholemount and flatmounts were analysed using fluorescent microscopy. Again expression was not detected (Figure 4.23c). Thus in the absence of reporter detection, none of the two lines generated could be used for further regulatory studies of *Fgf10*.

Another hypothesis is that 7F7R does not contain some of the elements requires for *Fgf10* expression and/or contains negative regulatory elements. Comparison with the enhancer used by Ohuchi indeed revealed the presence of additional sequences in 5' of the 7F7R enhancer. These sequences might contain binding sites for negative regulators of *Fgf10*. In addition, as discussed in the previous subchapter the 7F7R

enhancer lacks 2 conserved elements. However, the 3F3R fragment was shown to drive the early and late patterns of expression (Economou et al., 2012). Thus, whilst additional neural domains that have never been intensively studied for any of these reporters could be present in these missing domains, the ability of 3F3R to drive early inner ear expression suggests that 7F7R transgene should have worked and this will be discussed later.

#### **4.6 Investigation of mouse *Fgf10* regulation in the developing chicken inner ear**

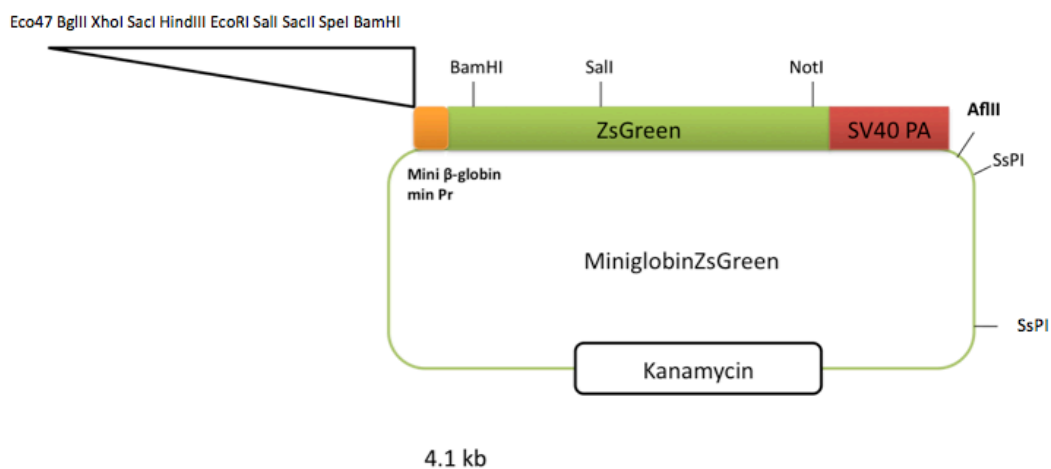
The time required to generate further stable lines of transgenic mice did not allow for the testing of the additional *Fgf10*-reporter constructs generated in mice. Therefore an alternative animal model, the chicken embryo, was chosen to assess the regulatory activity of the mouse *Fgf10* enhancer constructs. The chicken embryo has been shown to be a really useful model to quickly identify and at low cost, mouse regulatory regions (Timmer et al., 2001). In addition, experiments in this laboratory had shown that 3F3R could drive expression of *ZsGreen* in the chicken inner ear following otic placode electroporation (A.Economou, personal communication). However, the  $\beta$ globin minimal promoter used in the mouse reporter constructs unfortunately appeared to drive constitutive reporter expression in chick i.e. in the absence of enhancer elements (A. Economou, personal communication). Therefore a different reporter system was required for the regulatory analysis of test enhancers from mouse *Fgf10* in the developing chicken inner ear.

An independent project in the lab had led to the generation of a new  $\beta$ globin minimal promoter, where sequences driving constitutive expression were removed but still able to drive reporter expression in presence of functional enhancer elements. This newly engineered minimal promoter is termed the “miniglobin” promoter. This was used to generate two different base reporter vectors, one solely composed of the new miniglobin promoter and the *ZsGreen* reporter gene (MiniglobinZsGreen, see Figure 4.17a), and a second vector also harbouring an internal CMV-*DsRed* control cassette (MiniZsGreen-DsRed, see Figure 4.24b). This dual reporter vector should allow for the detection of both red fluorescence as a transfection control and green fluorescence for testing enhancer activity in the same cells. This is different from a co-electroporation system where experimental and control reporters cassettes are introduced via two different vectors and there is thus no assurance that the cells expressing the control also contain the enhancer-reporter vector and vice versa. A similar dual construct system had been successfully used for chick electroporation in another laboratory (Jung et al., 2009).

### **Regulatory analysis of *Fgf10* using the dual reporter system**

The dual reporter system was first used to test the regulatory activity of four *Fgf10* enhancer fragments: 7F7R, 7F3F-3R7R, 3F-Neuro and 3F3R (Figure 4.2). 3F3R has already been shown to drive reporter expression when cloned in miniglobin-*ZsGreen*. Therefore, it was used as a positive control for the dual reporter system. All fragments were cloned as *XhoI-EcoRV* fragments, 3F3R and 7F7R in a forward orientation and 3F-Neuro in the reverse orientation since it might contain part of the *Fgf10* promoter.

a)



b)

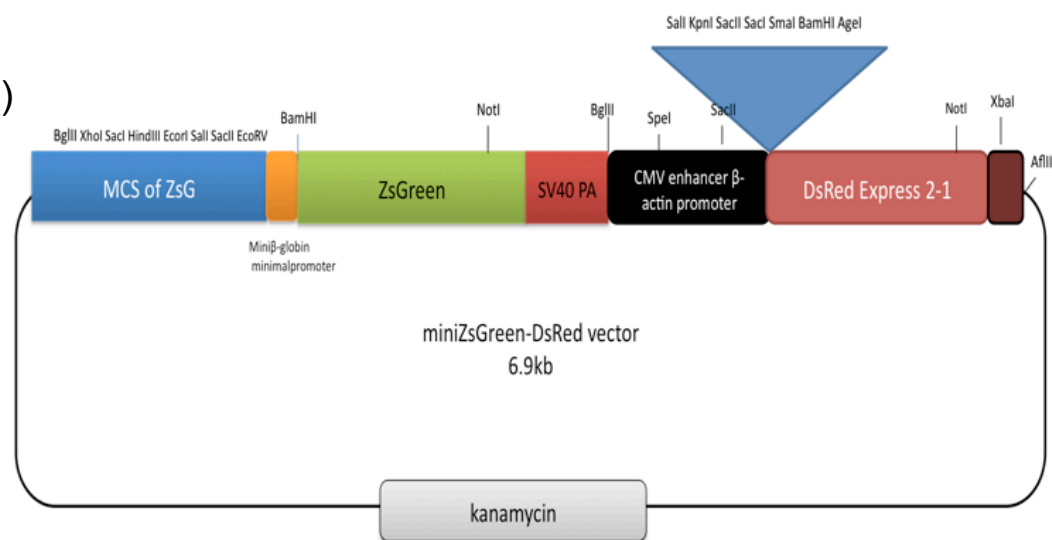
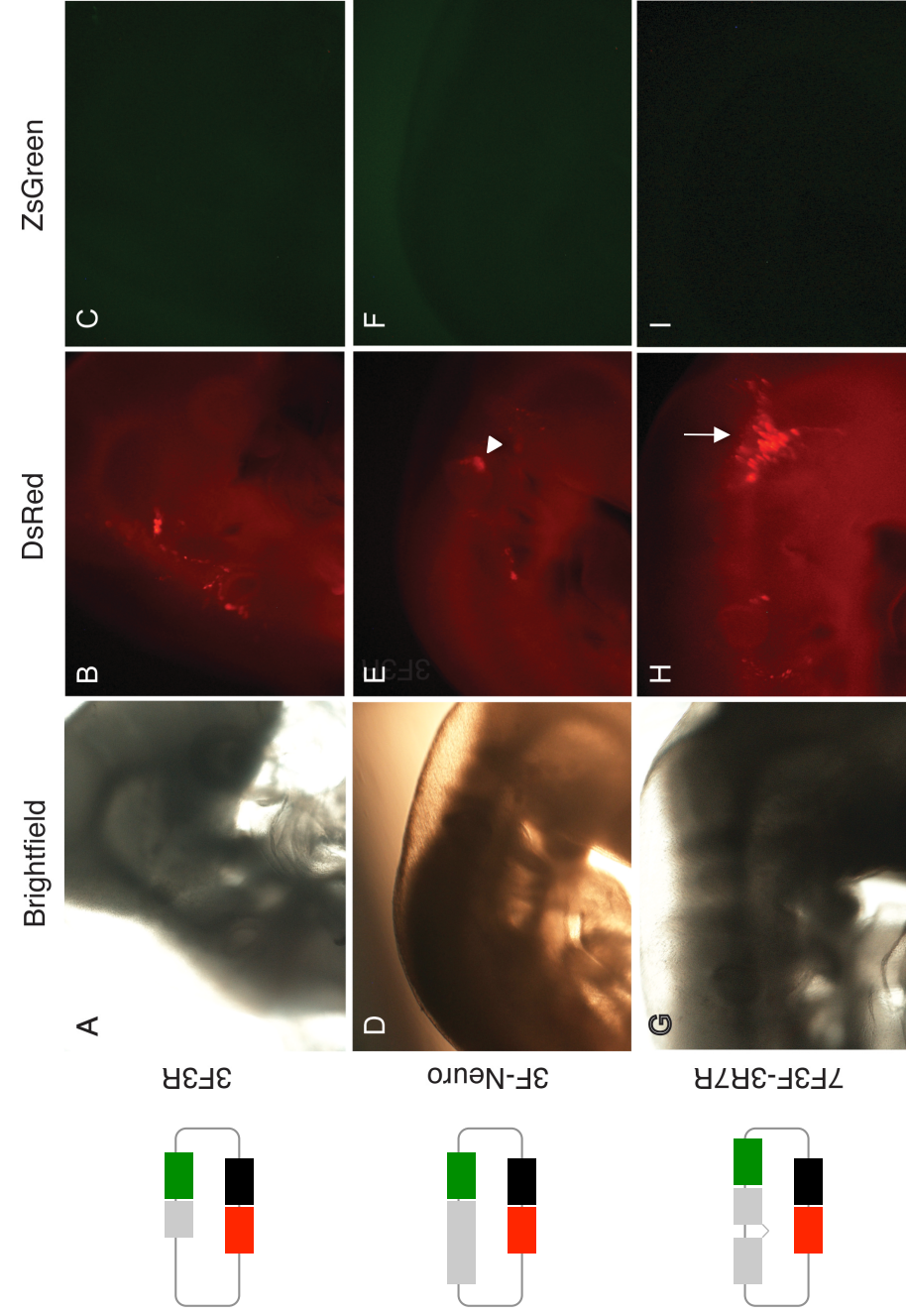


**Figure 4.24 Miniβglobin-ZsGreen and MiniZsGreen-DsRed reporter vectors.** Map of the Miniβglobin-ZsGreen reporter (a) and MiniZsGreen-DsRed dual reporter are (b). The dual reporter consists in the Miniβglobin-ZsGreen construct cloned into a CMV-DsRed control plasmid. Clone maps were taken from Shrivani dissertation (Msc, 2011)

Analysis of embryos electroporated with the 7F7R-dual reporter did not reveal any fluorescence for *DsRed* or *ZsGreen* in any of the embryos examined (n=9, data not shown). With other constructs, CMV-*DsRed* expression was detected in 3F3R (n=8/14; Figure 4.25B), 3F-Neuro (n=2/4; Figure 4.25C) and 7F3F-3R7R (n=3/6; Figure 4.25H) embryos. Interestingly, there was apparently no decrease in the number of DSRED positives cells from one construct to another despite their increasing size: 3F3R-dual is 8.3kb, 3F-Neuro is 9.4kb and 7F3F-3R7R is 11.1kb (compare Figure 4.25B,E,H). However, despite this good electroporation efficiency, *ZsGreen* expression was not seen in any of the cells that had successfully taken the reporter construct, with all the constructs tested (Figure 4.25C,F). Since in 3F3R-*ZsGreen* mice reporter gene expression is restricted to the inner ear (Economou, 2012), the lack of *ZsGreen* expression in chick embryos, electroporated with 3F3R-dual reporter, could be explained by the CMV-*DsRed* positive cells being all outside the otic vesicle (as seen in Figure 4.25B). However, the lack of expression reported with the larger 3F-Neuro fragments, despite CMV-*DsRed* being expressed in the anterior otic vesicle, suggests they may be a technical issue with the mini $\beta$ globin-*ZsGreen* part of the construct.

DNA samples from the plasmids used for electroporation were sent for sequencing to check that the three different enhancers had been cloned successfully and that there wasn't any mutation in the  *$\beta$ globin* promoter. No sequence anomalies were detected. Perhaps the use of a strong CMV promoter preferentially sequesters general and/or specific transcription factors and cofactors and thus out competes expression from the enhancer-reporter module of the construct. This might reflect the close proximity of the two promoters to one another in this artificial dual reporter system.

**Figure 4.25 Electroporation of mouse *Fgf10* constructs in chick using a dual reporter system.** Embryos were electroporated with 3 different *Fgf10*-dual reporter constructs as indicated on the cartoon representations on the left (grey represents the *Fgf10* enhancer; green, ZsGreen; black, CMV and red, DsRed). *DsRed* is a positive control of cells electroporation. An embryo electroporated with the 3F3R-Dual construct shows *DsRed* expression close to the developing otocyst, as well as in few additional pre and post-otic locations (B). An embryo, electroporated with the 3F-Neuro construct, shows *DsRed* expression in the anterior part of the otic vesicle, as well as in a couple cells surrounding the otic vesicle (E). An embryo electroporated with the 7F3F-3R7R construct shows strong *DsRed* expression in the brain (arrow) as well as in a few of cells around the otic vesicle (H). This demonstrates that the dual reporter was successfully electroporated, and, thus that the mini-*ZsGreen* construct is inside all the cells fluorescing in red. However, no *ZsGreen* expression could be detected, neither in the area around the otic vesicle (C) nor within the anterior wall of otic vesicle (F, compare with arrowhead in E).



To conclude the dual reporter system did not seem to allow a quick analysis of the *Fgf10* test regions, and would require further experiments to identify the underlying problems. Unfortunately there was insufficient time to identify the underlying cause for these reporter construct inabilities to drive *ZsGreen* expression. Interestingly however, these experiments do show that constructs up to 11.1kb are able to successfully be electroporated in the chicken embryo. This is larger than described in other studies that reported 10kb as being the upper limit of circular plasmid length that can be used for electroporation (Uchikawa, 2008).

#### **Regulatory analysis of *Fgf10* using co-electroporation**

Instead, a co-electroporation approach was next attempted. *Fgf10*-Mini-*ZsGreen* reporters were co-electroporated with a CMV-*DsRed* reporter control. Co-electroporations were performed for 7F7R-Mini*ZsGreen* and 3F3R-Mini*ZsGreen* (as positive control of *Fgf10* expression). For the 3F3R-Mini*ZsGreen* construct, co-electroporations appeared unsuccessful, with none of the chick embryo expressing either *DsRed* or *ZsGreen* (n=0/8, data not shown). For 7F7R, one embryo was expressing weakly the *DsRed* control (n=1/5). In this embryo there also appeared to be an isolated cell expressing *ZsGreen* at the level of the forebrain (data not shown). Another embryo not positive for *DsRed* control, also seemed to have one/few cells positives for *ZsGreen* reporter expression, and moreover in the region of the otic vesicle (data not shown). Overall the number of cells electroporated was quite low compared to the results usually obtained with the same parameters in the lab. In addition, the electroporation efficiency with mini*ZsGreen* reporter construct seemed to be lower than when using the large dual reporter construct. Eventually,

electroporations were also repeated with the help of another researcher in the lab (A.Economou), who electroporated the constructs with myself carrying out the embryo analysis. The 3F3R-*MiniZsGreen*, 3F7R-*MiniZsGreen* and 7F7R-*MiniZsGreen* constructs were all co-electroporated with *CMV-DsRed*.

The first *Fgf10* enhancer fragment to be tested was 3F3R (Figure 4.2). Out of the 3 embryos still alive 24 hours after electroporation, 3/7 survived, one did not express either *DsRed* or *ZsGreen* and the second embryo only expressed *DsRed* (data not shown). The 3<sup>rd</sup> embryo (Figure 4.26A,B,C) showed expression of the *DsRed* control plasmid in the anterior part of the otic vesicle (arrowhead, Figure 4.26B) as well as in a cluster of cell located just rostrally to the otic vesicle. A few cells also seemed to express *ZsGreen* within this rostral cluster but weakly (arrowhead, Figure 4.26C,C'). 3F3R usually give rise to a stronger reporter expression, where *ZsGreen* is expressed not only in the otic vesicle but also throughout the head surface ectoderm (A.Economou. personal communication)

The second enhancer fragment tested was 3F7R (Figure 4.2). Out of 4 embryos still alive 24 hours after electroporation (n=4/6), three embryos demonstrated expression from the *DsRed* control plasmid and two embryos had a fluorescent green signal, showing the enhancer is able to drive *ZsGreen* reporter expression. One of these chicken embryos showed strong *DsRed* expression in the otic vesicle (arrowhead, Figure 4.26E) as well as in a cluster of cells located caudally. A few cells could also be seen weakly expressing *ZsGreen* in the dorsal wall of the otic vesicle (arrowhead, Figure 4.26F,F') and a patch of cells caudally to the otic vesicle (arrow).

**Figure 4.26 Regulation of *Fgf10* mouse enhancers in chick.** Embryos otic vesicles were electroporated with a mix of CMV-DsRed and either 3F3R-miniβglobin-ZsGreen (A,B,C), 3F7R-miniβglobin-ZsGreen (D,E,F) or 7F7R-miniβglobin-ZsGreen as indicated on the cartoon representations on the left (grey represents the *Fgf10* enhancer; green, ZsGreen, black, CMV and red, DsRed). Larger version of C,F and I are presented in the following page as C',F' and I' to allow better visualization of the weak ZsGreen expression. An embryo electroporated with 3F3R-miniβglobin-ZsGreen shows *DsRed* expression in the anterior otic vesicle region (arrowhead,B). Weak ZsGreen expression can also be seen in the otic vesicle (arrowhead,C,C'). An embryo electroporated with 3F7R-miniβglobin-ZsGreen shows *DsRed* expression in the otic vesicle (arrowhead, E) and caudally to the otic vesicle. A few cells are seen to express weakly ZsGreen in similar area : the otic vesicle (arrowhead, F,F') and in a small caudal patch (arrow, F,F'). The strongest ZsGreen expression was seen following 7F7R electroporation, with a strong patch of expression in the hindbrain (arrow,I,I') and a smaller patch of ZsGreen expression in the otic vesicle (arrowhead,I,I'). *DsRed* was expressed in similar areas (H)

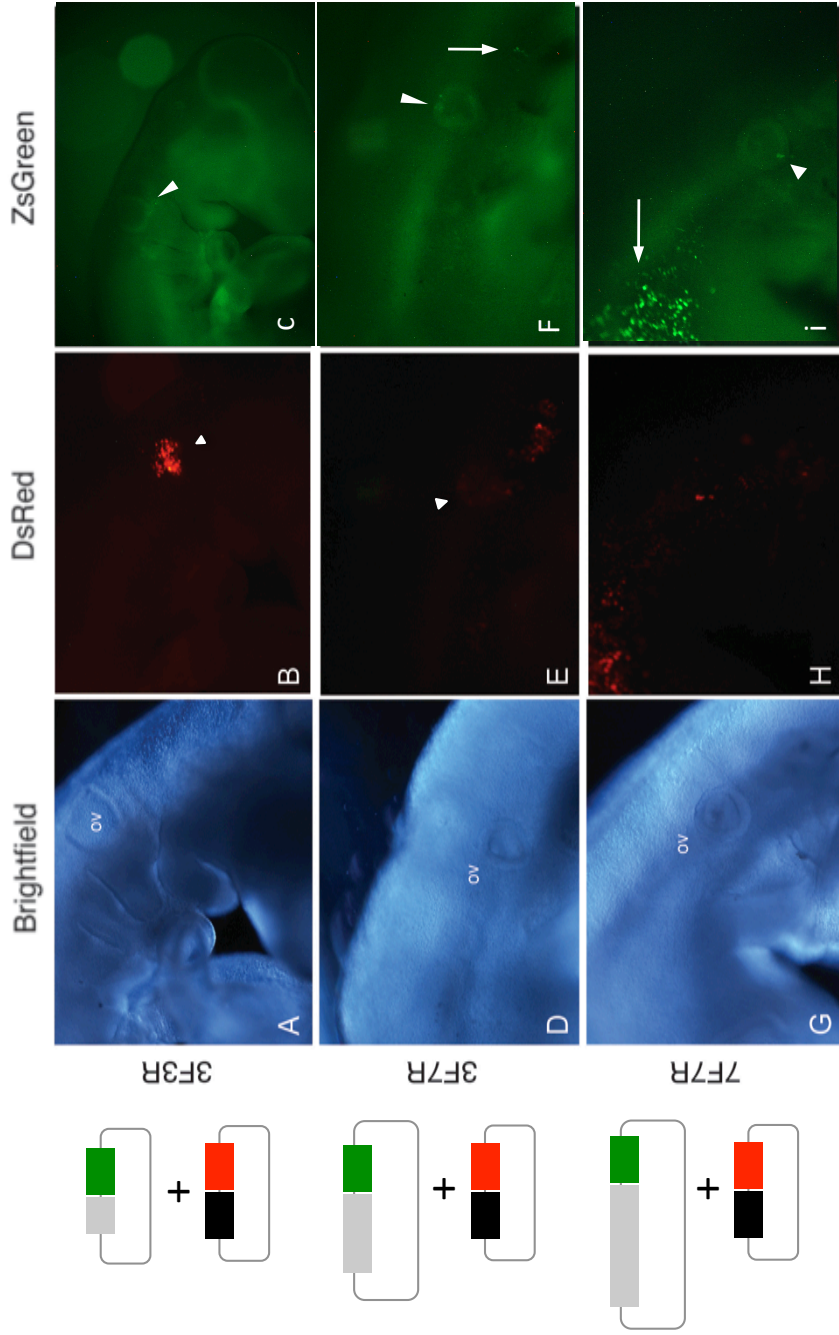
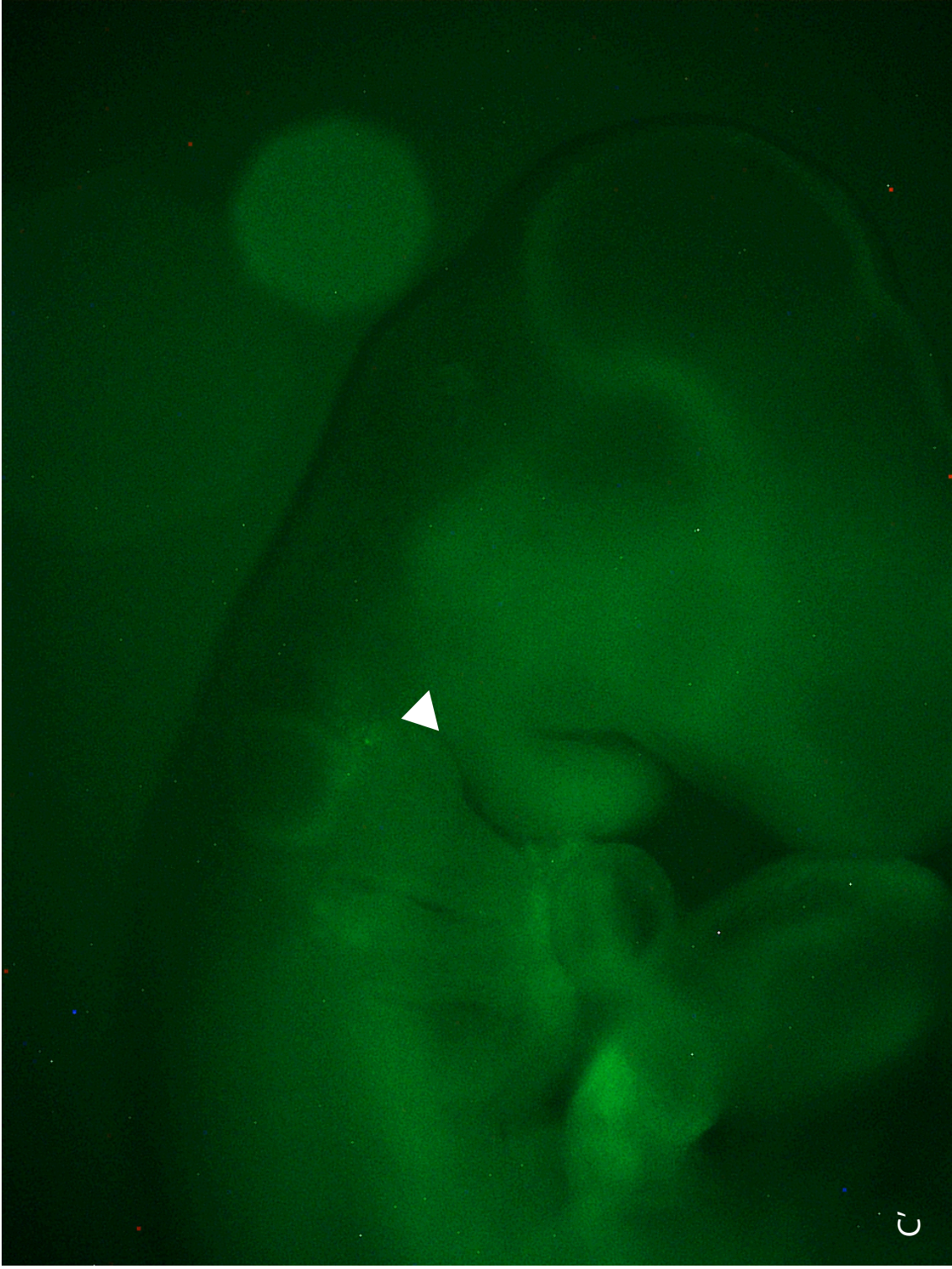


**Figure 4.19 (continues)**



C'

Figure 4.26 (continues)

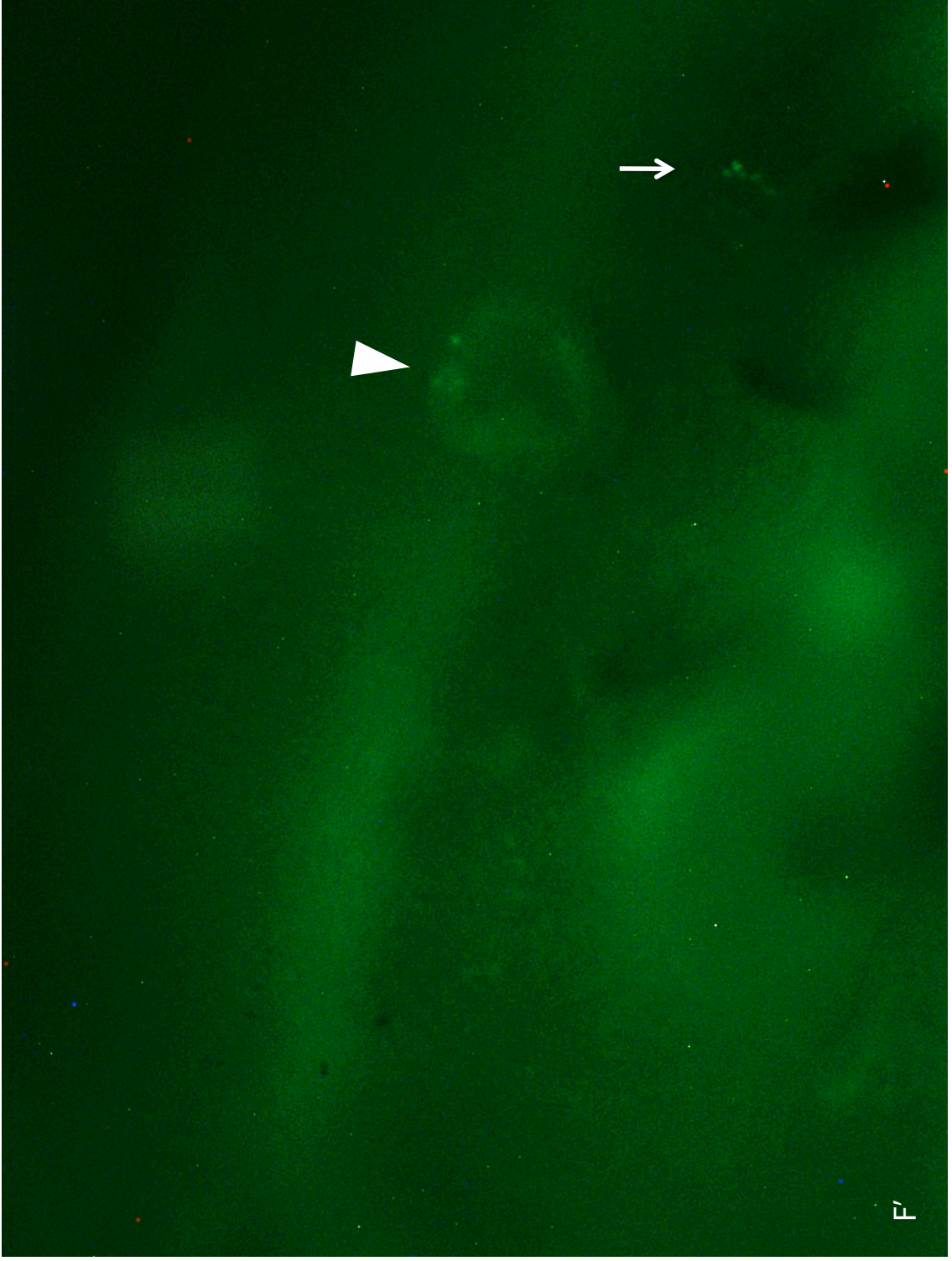


Figure 4.26 (continues)

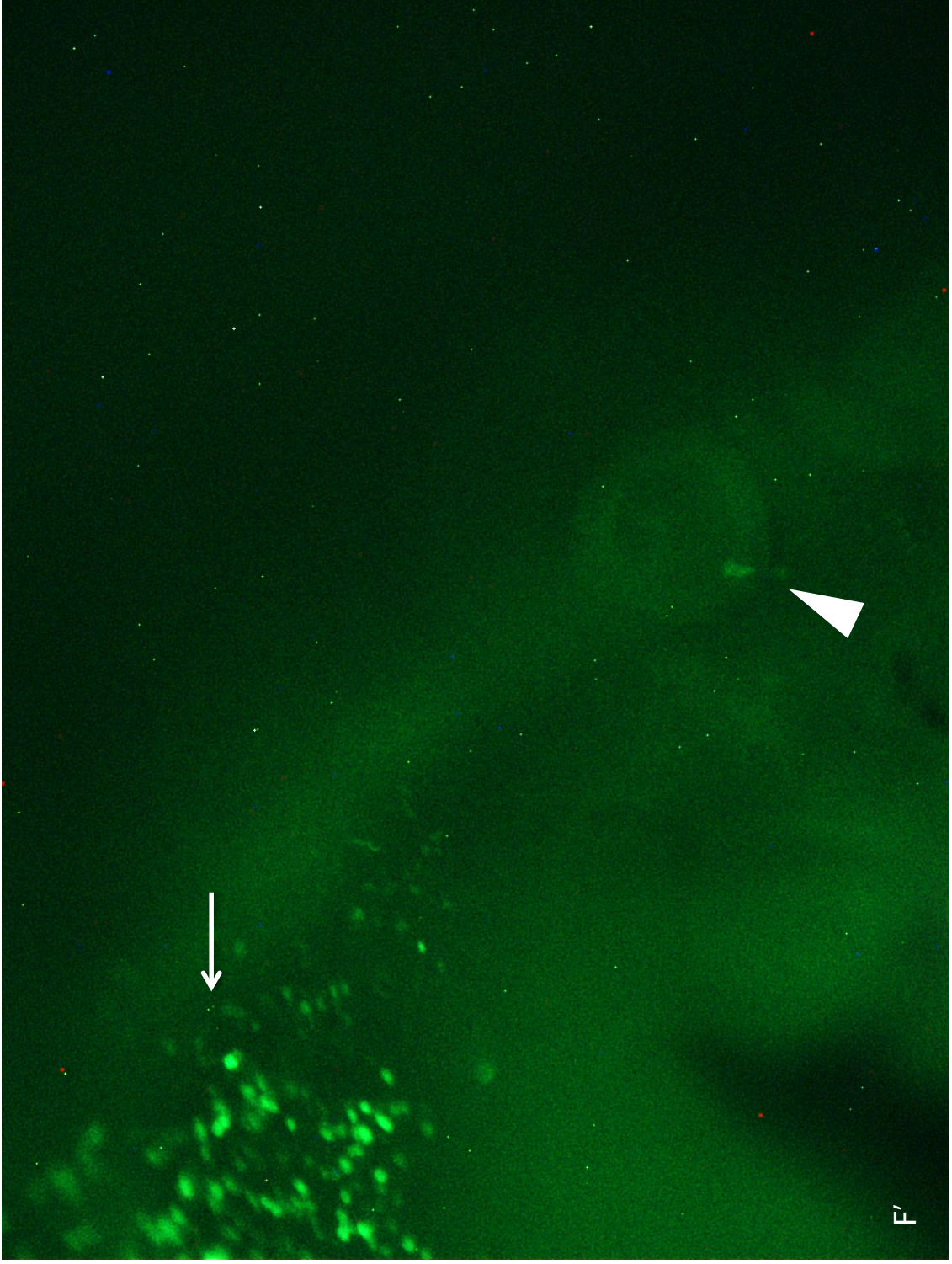


Figure 4.26

The third enhancer to be tested was 7F7R (Figure 4.2). Out of 6 embryos still alive 24 hours after electroporation (n=6/8), two did not show any expression and 4 showed both *DsRed* and *ZsGreen* fluorescent signals. One of the embryos strongly expressed CMV-*DsRed* in the hindbrain (Figure 4.26H), furthermore *DsRed* expression was also extending caudally to the otic vesicle from the forebrain to posterior otic domains. Expression of *ZsGreen* was also strong in the forebrain (arrow, Figure 4.26I,I') and there was a small patch of expression in the otic vesicle (arrowhead, Figure 4. 26I,I').

These results showed that all the *Fgf10* enhancer fragments tested were able to drive reporter expression in the chicken otic epithelium, as well as additional ectopic cells, with the 7F7R region apparently driving stronger and more widespread expression. However, only a small number of embryos were examined and further analysis would be required before drawing any conclusions. Importantly these experiments also demonstrate that the constructs I generated to investigate the regulation of *Fgf10*, and in particular 7F7R are functional in vivo. Future experiments will be needed to address why they do not work in the mouse. However there appear to be species differences in control outside the inner ear, including the regulatory input of *Gata3* (A.Economou, personal communication). Thus, this cannot replace the use of transgenic mice, but it can be use to test constructs functionality in vivo and maybe, in conjunction with mouse studies, to identify cross species conserved and non-conserved mechanisms.

## 4.7 Regulation of *Fgf10* by retinoic acid

Subsequently to the analysis of my series of *Fgf10*-reporter construct, the 3F3R enhancer was shown to contain all the elements required to recapitulate the full pattern of *Fgf10* expression in the inner ear (Economou et al., 2012). Thus, a stable line containing the 3F3R transgene was used to study the effect of RA on *Fgf10* inner ear expression. Frenz and colleagues (Frenz et al., 2010) had shown *Fgf3* and *Fgf10* downregulation in the inner ear following RA administration at 8.5dpc using RT-PCR, but these results lack the detailed cellular resolution required to detect any changes in expression pattern. For example is there a general downregulation of expression of *Fgf10* or is the *Fgf10* inner ear domain composed of RA-dependent and independent domains within the otic vesicle? To determine this, an in vivo analysis is required. Using the same method of self-ingestion of RA-laced sugar pellets developed for the analysis of *Fgf3*-regulation (section 3.1) and the 3F3R-transgenic line, a preliminary experiment was performed using 25mg of RA administered at 8.5dpc.

In half of the embryos examined (n=2/4), the pattern of *Fgf10*-expression was similar to control embryos (Figure 4.27E) with reporter expression evident throughout the otic vesicle, together with a strong patch of expression in the anterior wall (Figure 4.27D). In the other two embryos, the strong patch of *Fgf10* expression was shifted dorsally (Figure 4.27F,G). Interestingly these two embryos showed brain malformation suggesting a developmental delay. In particular one of the embryos had an open neural tube (Figure 4.27B), a phenotype characteristic of embryos exposed to RA prior to hindbrain patterning.

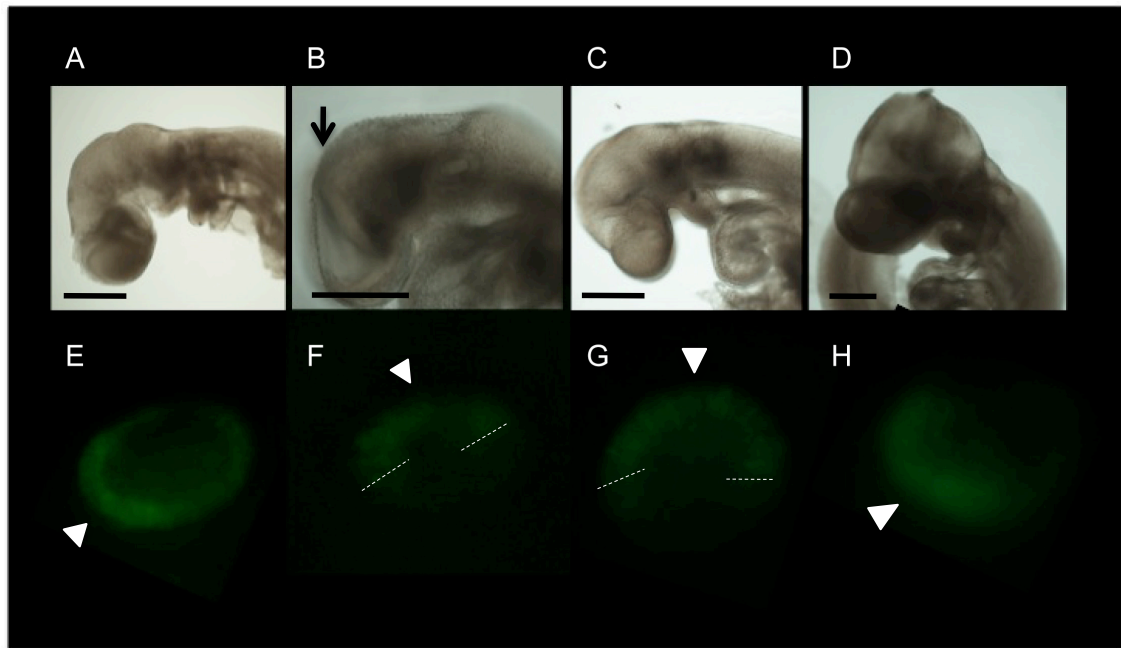


**Figure 4.27** Effect of exogenous RA administration on *Fgf10* expression in the 9.5dpc otic vesicle. (A) Brightfield pictures of control embryo. (B-D) Brightfield pictures of embryos exposed to RA. (E-F) Enlargements of the otic vesicles of embryos A to D. In untreated embryos, *Fgf10* is expressed throughout the otic vesicle with a stronger patch of expression located anteriorly (arrowhead, E). Following administration of 25mg/kg of RA at 8.5dpc, 2 embryos (n=4) presented a normal pattern of *Fgf10* expression (arrowhead, H). However, *Fgf10* was strongly downregulated in the two other embryos, as well as shifted dorsally (broken lines delimit the new area of expression, which is pointed out with an arrowhead (F,G)). Scale bar 500 $\mu$ m.

This suggested that the embryos with a dorsal shift of *Fgf10* expression might have been exposed to RA at a slightly earlier stage *in utero* than the ones with an unaltered expression. This might suggest that RA only affects *Fgf10* expression if embryos are exposed prior to hindbrain patterning. To conclude, the experiments here suggest that *Fgf10*, like *Fgf3* are under the regulatory control of RA signalling. Although 4 embryos with mixed phenotypes only weakly support this conclusion; further experiments performed as part of a separate project, but based on my working hypothesis, later confirmed these preliminary results (Ecomomou et al., 2012). This is discussed in more detailed in section 5.2.5.

## 5

## DISCUSSION

---

In this report, a novel, non-invasive method of retinoic acid administration via sugar pellets is developed and shown to be an efficient and reliable alternative to gavage delivery. Detailed analysis of *Fgf3-lacZ* embryos exposed to RA using this method shows that the timing of RA-administration is critical. Administration of RA at 8.5dpc only leads to a dose-dependant downregulation of otic *Fgf3* expression, whereas administration of RA at 7.75dpc lead to dowregulation of *Fgf3* expression as well as lateralization of *Fgf3* expression with increasing RA dose. This novel method of RA administration is also suitable for use in other organ systems, as shown by producing the same range of phenotypes obtained using gavage administration. Using this method the effect of RA on *Fgf10* expression using a 3f3r-transgenic line was also examined. Comparison of *Fgf3* and *Fgf10* control by RA, reveals both similarities and differences in the regulation of these two genes by RA.

### **5.1 Regulation of *Fgf3* by Retinoids**

#### ***5.1.1 An alternative method for RA delivery to pregnant mice***

In order to study the role of retinoids in embryonic development two methods have traditionally been used. The most widely used method is gavage feeding. For gavage administration, RA is first dissolved in DMSO or in a vegetable oil such as sesame seed

oil. The oily mix is then directly delivered to the oesophagus via a feeding needle and/or tube. This generates distress due to animal restraint and the insertion of the needle/tube, as shown by the elevated levels of plasma corticosterone following gavage administration in rat (Brown et al., 2000). A volume-dependent stress response was also reported in oil-based gavage (Brown et al., 2000). In addition to this general distress, gavage can directly cause damage to the trachea or worse, result in delivery of the solution into the lungs and therefore can only be performed by highly trained staff. A second, less used method to deliver RA, is via intraperitoneal (IP) injections (see references in Table 3.1). Although less invasive than the gavage method it still presents disadvantages. Here again, there is the general distress associated with mouse restraint (Hurst and West, 2010) and with the insertion of a needle into the abdomen (Meijer et al., 2006). In addition the exact injection site of RA cannot be exactly controlled. It could potentially damage internal organs or perforate the amniotic sac, leading to variation of the actual dose reaching the embryos in each separate injection. Therefore, in addition to the welfare burden imposed on the mice, this could also affect the experimental outcome. The stress imposed by both gavage and IP injection is another factor that can influence the RA effect. Indeed maternal restraint has been shown to enhance teratogenicity in mice (Rasco and Hood, 1995a, b). Thus reducing stress is likely to increase the reproducibility of RA phenotypes.

Refinement of the gavage method has been attempted in the rat, where gavage needles were coated in sucrose, and this appeared to reduce stress-related behaviours (Hoggatt et al., 2010). Administration of RA via food has also been carried out in mice with self-administration of food containing RA across several days (Niederreither et al.,

2001). However this method does not permit specific dose or timing of delivery to be carefully controlled, two criteria that dramatically impact on the severity and incidence of induced phenotypes.

This project looked to investigate and develop an alternative non-invasive method of RA administration that allows the delivery of specific doses of RA at a specific time during embryonic development. Pregnant mice were first trained with chocolate or sugar pellets, and it appeared that mice preferred sugar pellets to chocolate pellets. Chocolate/sugar pellets were then laced with RA and pregnant mice were found to still readily completely ingest them in less than 30min on average, ensuring delivery of specific RA doses at specific times. The sugar or the chocolate pellets were shown to not have teratogenic effects by themselves that could interfere with the presentation of the RA-induced phenotypes. This was an important parameter to assess since chocolate has been shown to be toxic to mice, with exposure during pregnancy leading to kidney (Patera et al., 2006) and limb (Skopinski et al., 2003) defects in the progeny. However doses used in these studies were 400mg daily throughout pregnancy, which is 500 times the amount used (0.8mg chocolate/pellet) in this study. In addition, pregnant mice were exposed to a maximum of two doses of 0.8mg, assuming they were trained once before the RA administration. Furthermore, the excess control experiments exposed to chocolate/sugar doses of 3x to 5x the single dose, and harvested 24h after administration, did not show any abnormal phenotype. Neither craniofacial malformations nor neural tube defects were detected, and Fgf3 expression was also unaltered. Altogether this demonstrates that chocolate and sugar are unlikely to be toxic at the doses used in this study.

The incidence of craniofacial malformations and altered *Fgf3* expression in mouse embryos at 9.5dpc was also scored in this study. The frequency of craniofacial phenotypes, such as anterior truncations and open neural tube phenotypes (Table 3.2), compares favourably following pellet delivery of RA with previously published data (Appendix Table S1) although a direct comparison between administration methods is not possible due to a slight difference in the exact timing of exposure.

The pellet delivery method is also applicable to studying other organ systems, such as the limb, palate and heart, where similar phenotypes were obtained using gavage or sugar pellet administration. In addition the incidence of these phenotypes were similar to those obtained using RA delivery by gavage (Appendix Table S1).

Therefore this new method is an effective delivery system to study the effect of the exposure to a specific dose of RA at a particular developmental time regardless of the organ system under investigation, while providing the best welfare outcome.

### **5.1.2 RA dosing regimes**

RA acts as a morphogen during development, with different doses giving rise to different cell fates. Due to this morphogenetic property, RA is thought to be involved in establishing pattern formation in the developing embryo in a number of contexts. The establishment of pattern formation in the hindbrain of differential *Hox* genes induction is one of the best examples of the morphogen properties of RA, where RA

from the paraxial mesoderm differentially induces *Hox* genes expression along the AP axis (White et al., 2007).

Since a small difference in the RA dose can have a tremendous effect on the phenotype, it is not surprising that a wide range of doses have been used in investigating the role of RA in the development of different organ systems such as the CNS, PNS, limb, palate, heart and eye (Table 3.1 and Appendix Table S1). A brief survey of the literature reveals that RA doses ranging from 0.3-200mg/kg have been used in gavage experiments and 1-70mg/kg in experiments using IP injection (Table 3.1). Furthermore, due to the morphogenetic influence of RA, it would seem appropriate to never restrict the analysis of retinoid function in an organ system, to just one concentration of RA.

This is commonly and easily performed in zebrafish studies, where the RA can be easily applied at different concentrations to the environment (Hans and Westerfield, 2007). RA can also be easily applied at specific concentration to chick embryos, using beads loaded with different nanomolar quantities of RA. However this suffers from the drawback of establishing the morphogen gradient from the bead itself rather than systemic delivery. In addition, the chick/RA bead system differs from the situation in mammals where in utero development doesn't allow direct exposure to RA. Delivery of RA to embryo indirectly via maternal administration means we can be less sure of the exact dose that reaches the target tissue/organ in the developing embryos. Therefore in this report a range of RA doses were applied, ranging from 4.5mg to 10mg/kg, and leads to the development of a variety of neural tube defects seen following gavage

treatment. Increasing doses lead to an increasing incidence of defects and an increase in their severity.

### **5.1.3 Effect of RA on *Fgf3* expression in embryos**

A range of RA doses and their effect on *Fgf3* regulation was investigated using the *Fgf3-lacZ* reporter line. Expression of *Fgf3* following RA administration at 7.75dpc, was first analysed in the developing CNS. Spinal cord expression is unaltered when exposed to doses up to 7mg/kg of RA, but is then downregulated with doses of 8-10mg/kg. In the hindbrain, rather than a straightforward downregulation with increasing dose of RA, interesting changes in the spatial expression of *Fgf3* were noted. Exposure to increasing doses of RA first led to an expansion of the rhombomere 1 domain of reporter expression, with loss of one or more rhombomeres boundaries, followed by a loss of expression at the highest dose. This is in agreement with the model in which the hindbrain is undergoing patterning at 7.75dpc, and excess RA applied during this period leads to a posteriorisation of hindbrain identity (reviewed in Glover et al., 2006). Comparison of 9.5dpc embryos exposed to 8mg/kg of RA with embryos exposed to 10mg/kg of RA suggest the loss of expression could be the result of the anterior truncation of the brain (and increasing posteriorisation) resulting in the loss of the rhombomere 1 domain. Interestingly, these results also suggest that an independent RA regulatory pathway governs *Fgf3* expression in rhombomere 1 and in the rhombomeres boundaries.

Administration of RA at 8.5dpc did not have any effect on *Fgf3* expression in the hindbrain until embryos were exposed to 25mg/kg of RA, and resulted in a general

downregulation of *Fgf3* expression without any changes in the boundaries of its spatial domain of expression. This is consistent with the neural tube having now completed patterning, thus preventing dramatic changes in rhombomeres boundaries/identity, although subtle modifications of other genes expression may still happen (Morriss-Kay et al., 1991).

#### **5.1.4 Dose-dependent effect of RA on *Fgf3* expression in the otic vesicle**

The dose-dependent teratogenicity of inner ear phenotypes following gavage delivery of RA has been previously investigated in the inner ear (Frenz et al., 1996). These authors showed that increasing doses of RA leads to an increase in the incidence of ear phenotypes when embryos are exposed to RA at 8.25-8.5dpc, but not when exposed at 7.25-7.5dpc when no phenotype was reported.

In agreement with this, the incidence of otic *Fgf3* alteration of expression was also found to be dose-dependent. However, considerably lower levels of RA than those required for teratogenicity are able to affect *Fgf3* expression. The teratogenic study looked at inner ear phenotypes at 11.5 and 13.5dpc whereas the gene expression analysis presented here was carried out at earlier stages (9.5 and 10.5dpc). Furthermore, the generation of an inner ear phenotype most probably requires the alteration in the expression of numerous genes in addition to *Fgf3*, that might require increased doses of RA and/or at different times. An alternative explanation could be an increased bioavailability of RA when administered through this new protocol.

In conclusion this study reveals a dose-dependent effect of RA on gene expression that is consistent with the dose-dependent otic phenotypes previously reported (Frenz, 1996). This likely reflects a dysregulation of inner ear patterning by RA excess.

### **5.1.5 Patterning in the otic vesicle**

Downregulation of *Fgf3* expression following exposure to increasing dose of RA shown here is consistent with previous RT-PCR studies (Frenz et al., 2010). However this study also reveals the differential downregulation of *Fgf3* expression in different areas of the inner ear. Following RA administration at 7.75dpc, *Fgf3* reporter expression is first downregulated in the antero-dorsal wall of the otic vesicle, with increasing doses of RA leading to the progressive restriction of *Fgf3* expression to a small medio-lateral domain. This contrasts with the effect of RA administration at 8.5dpc, which results in a general downregulation of *Fgf3* expression without any changes in the spatial expression of *Fgf3* in the otic vesicle.

These time-dependent differences in the alteration of *Fgf3* expression are similar to those reported in the hindbrain, which are thought to reflect the status of the patterning process at the time of RA administration. Interestingly RA has also been shown to be involved in early inner ear patterning (Bok et al., 2011; Hans and Westerfield, 2007; Radosevic et al., 2011; Romand et al., 2006). Thus, the lateralization of *Fgf3* expression following presomitic RA administration could be the result of reprogramming inner ear re-patterning at 7.75dpc, suggesting otic vesicle gene expression domains are still in the process of being established at this stage. Then following RA administration at 8.5dpc, the downregulated but otherwise unchanged

domain of *Fgf3* otic expression could reflect that otic patterning is now too advanced to allow the reprogramming of *Fgf3* spatial expression.

The responsiveness of otic tissue to RA has been previously investigated using a transgenic mouse line in which *LacZ* was placed under the control of RA responsive elements (RAREs), and reveals a progressive withdrawal of RA responsiveness first from the anterior region and moving posteriorly (Bok et al., 2011). In particular, the anterior border of *LacZ* activity was located rostrally to the otic placode at 8.25dpc, whereas half a day later, at 8.75dpc, only the posterior otic domain of the invaginating otic vesicle was still positive for *LacZ* reporter activity. This is consistent with a model where a gradient of RA would be involved in the patterning the inner ear up to at least 8.25dpc, with different RA doses eliciting different gene expression responses along the antero-posterior axis of the otic vesicle. Once the appropriate set of genes had been activated or repressed, RA responsiveness would progressively diminish reflecting that the otic vesicle pattern had been established in this structure.

Studies on pattern formation in invertebrates such as *Drosophila*, show that the organization of primordial larval structures depend on positional information in the form of morphogen gradients in delimiting compartments. Expression of intrinsic selector genes (e.g. the *homeobox* genes) would then determine the fate of cells within a specific compartment, as well as instruct them on how to interact with adjacent compartments (Lawrence and Struhl, 1996). A similar compartment-boundary model of cell fate specification has been proposed to explain patterning in the inner ear (Fekete, 1996). Regional expression in the otic vesicle can be induced and/or

maintained by signals emanating from surrounding tissues, such as FGFs signaling from the hindbrain, and RA from the presomitic mesoderm, resulting in the generation of otic compartments expressing different sets of genes (Figure 1.5). The boundaries between these compartments could then serve as sites of cell-cell interaction to mediate local patterning and cell fate specification in the inner ear (Fekete, 1996).

In the context of this model, the changes in the spatial expression domain of *Fgf3* could be interpreted as a disruption of otic boundaries by excess RA. This is in agreement with a recent study in mice showing a loss of another anterior domain of gene expression, *NeuroD1* from the antero-ventral region of the otocyst following gavage administration of RA at 7.75dpc, whereas *Tbx1* expression, which is normally only expressed posteriorly was detected both in the posterior and the anterior poles of the otic vesicle (Figure 5.1A; Bok et al., 2011). Thus it has been proposed that an excess of RA leads to a posteriorization of the otic vesicle (Bok et al., 2011).

Inner ear patterning by an anterior-posterior RA gradient is further supported by a series of experiments in chick embryos, where the effect of beads loaded either with retinoic acid or with citrate – that block RA signalling - was investigated. Increasing rostral RA signalling via the implantation of RA beads anteriorly to the otic vesicle lead to results similar to RA administration in mice with the anterior downregulation of *NeuroD1* and the ectopic expression of *Tbx1* in the anterior region of the otic vesicle (Figure 5.1A; Bok et al., 2011).

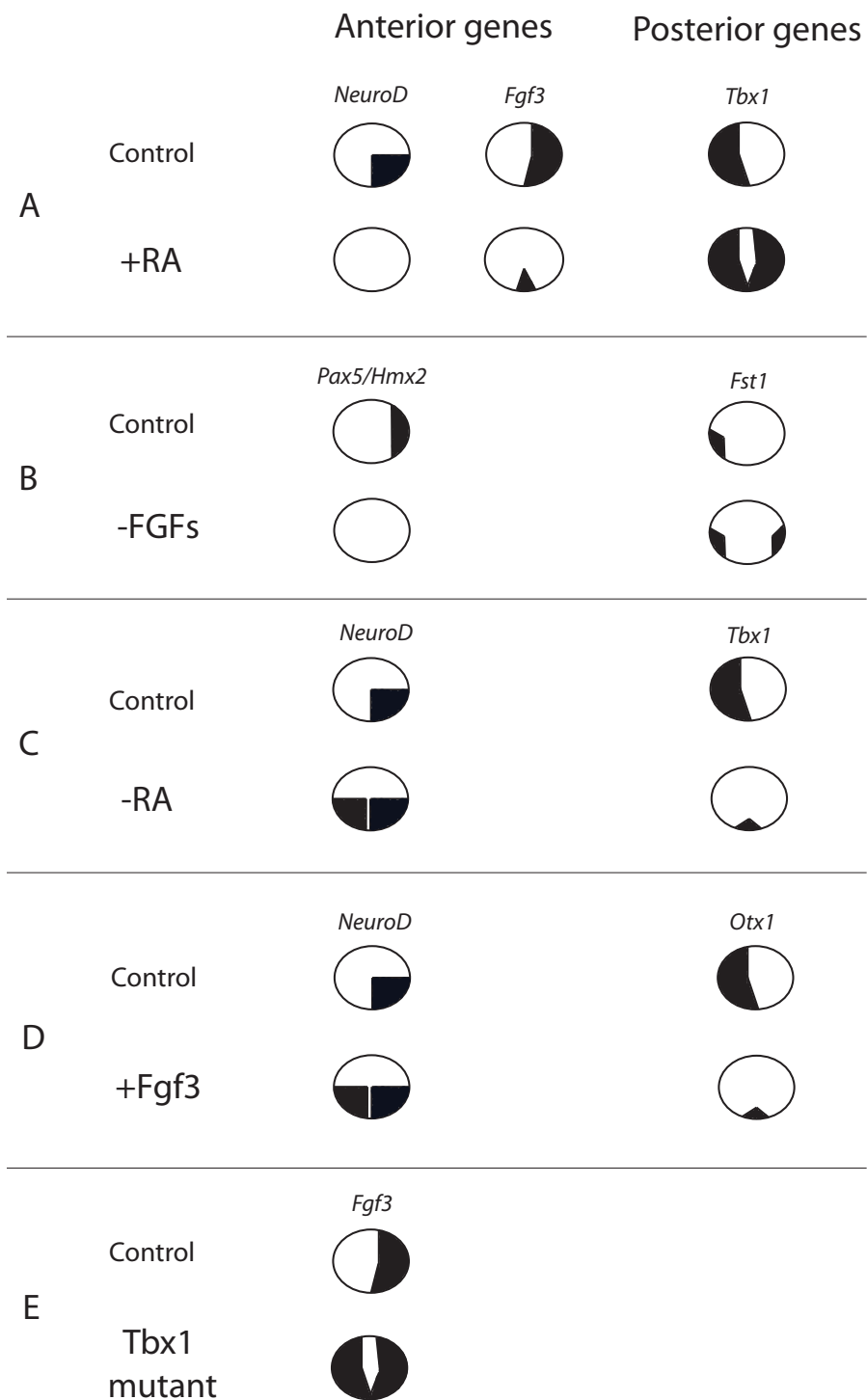


**Figure 5.1 Effects of RA and FGF signalling on the antero-posterior patterning of the otic vesicle.** Here are schematized some significant results from the analysis of RA and FGF signalling on the patterning of the otic vesicle (OV) in mouse, chicken and zebrafish (A-D). The pattern of expression of *Fgf3* in *Tbx1* mutant is also shown (E). Excess of RA (A), and blocking of FGF signalling (B), both lead to a loss/downregulation of anterior genes and a mirror duplication of posterior genes. Conversely, blocking RA signalling (C), or overexpressing *Fgf3* (D), both lead to a mirror duplication of anterior genes and a downregulation of posterior genes. Interestingly, lack of *Tbx1* also lead to a mirror duplication of the anterior gene *Fgf3* (E). See text (section 5.1.5) for details and references.

Blocking caudal RA signalling via the implantation of citrate beads posteriorly to the otic vesicle resulted in ectopic expression of *NeuroD1* expression posteriorly, with its normal expression in the antero-ventral wall of the otic vesicle unaltered (Figure 5.1C; Bok et al., 2011). In addition, blocking rostral RA signalling via the implantation of citrate beads rostrally to the otic vesicle results in the downregulation of *NeuroD1* expression. All together this shows that RA is an essential determinant of antero-posterior patterning with low concentrations and/or shorter exposure to RA inducing an anterior, neurosensory (*NeuroD+*) fate, whereas higher concentrations and/or longer exposure to RA would induce a posterior, non-sensory fate. In vivo this RA gradient is controlled by the precise spatio-temporal expression of RA synthesizing and catabolising enzymes (see section 1.4.1). *Tbx1* is one of the genes that mediate the effects of RA on A-P patterning, with an absence of *Tbx1* in mice resulting in the posterior expansion of the anterior neurosensory domain, and duplication of the vestibulo-cochlear ganglion. In contrast, *Tbx1* overexpression in humans results in a reduction of the neurogenic domain and in the size of the ganglion (Raft et al., 2004).

*NeuroD1* may be one of the neurosensory genes mediating the effect of RA on A-P patterning in the anterior part of the otic vesicle. Mice lacking *NeuroD1* are deaf and display a severe reduction of sensory neurons in the vestibulo-cochlear ganglion, a shortened and widened cochlear duct, and defects in hair cell organization in the organ of Corti, with duplication and ectopic addition of inner hair cells and misalignments of outer hair cells (Liu et al., 2000).

Downregulation and relocalisation of *Fgf3* expression following presomitic RA administration (Figure 5.1A) suggests that may also mediate the effects of RA on AP patterning, and in particular play a major role in the development of structures thought to emerge from the antero-ventral wall of the otic vesicle such as the sensory hair cells and neurons of the cochlear and vestibular system. In humans, homozygous mutation of *Fgf3* has been linked to deafness, suggesting a role in cochlear formation/function. However most individuals affected lack the entire inner ear, including cochlea, and the vestibule (Riazuddin et al., 2011) thus making unclear the exact role of *Fgf3* in inner ear patterning. Homozygous mutation of *Fgf3* in mice lead to less dramatic phenotypes, such as reduction in size and dorsal shift of the vestibulo-acoustic ganglion, poor cochlear coiling and abnormal vestibular structures (Hatch et al., 2007). In another *Fgf3* mutant, hearing and vestibular function was found to be completely unimpaired (Alvarez et al., 2003).

Variability in the phenotypes observed in *Fgf3* mutant mice could potentially be due to different factors. Firstly, the selection of strain for making a null mutant can have a significant effect on the phenotype (Thyagarajan et al., 2003) due to their different genetic backgrounds. This effect is due to 'modifier genes', which act in combination with the causative genes (Montagutelli, 2000). Some genetic backgrounds may include modifier genes that compensate for the missing genes, whereas in other genetic backgrounds there may be additional dysfunctional genes that will lead to a stronger phenotype. Secondly, the way the gene is targeted may also influence the phenotype. For example, the first *Fgf3* null mutant was generated by insertion of a *neomycin (neo)* resistance gene under the control of a phosphoglycerate kinase 1 (PGK) promoter in

the first exon of *Fgf3* (Wright et al, 2003) and the PGK-*neo* cassette has been reported to influence the expression of nearby genes, resulting in unusual phenotypes (Rijli et al., 1994; Wang et al., 1999). However Hatch et al. (2007) used two transgenic lines, one with a *neo* insertion in the exon 1 of *Fgf3* and a second one with a deletion of exon 2, who both exhibits similar phenotypes so we can here rule out an effect of the *neo* selector gene.

Interestingly, analysis of otic gene expression in *Fgf3* null mutants revealed that expression of ventral otic genes involved in cochlear development such as *Pax2* and *Otx2* was unaffected (Hatch et al., 2007) whereas the expression of dorsally expressed genes such as *Gbx2*, *Wnt2b*, *Dlx5* and *Hmx3* was absent or shifted. This is in agreement with a compartment/boundary model where formation of inner ear structures depends on signalling between compartments to mediate local patterning and cell fate specification.

Homozygous mutation of *Tbx1* also leads to an inner ear phenotype showing some similarities to homozygous *Fgf3* mutation, with *Tbx1* mutant also showing hypoplasia, and abnormal or lacking vestibular and cochlear structure (Arnold et al., 2006a; Arnold et al., 2006b). However instead of being reduced as in *Fgf3* mutants, the vestibulo-acoustic ganglion domain was expanded. Furthermore, *Fgf3* was ectopically expressed in the posterior otic vesicle domain (Figure 5.1E). This is consistent with the role of *Tbx1* in maintaining posterior non-neurogenic otic identity and suggests that at the opposite pole, *Fgf3* may be the mediator of anterior neurogenic fate.

This model is also consistent with the role of *Fgf3* in zebrafish where it has been demonstrated that blocking FGF signalling results in a loss of anteriorly expressed genes *Pax5* and *Hmx2*, whereas genes normally expressed in the posterior compartments such as *Fst1* and *Otx1* becomes ectopically expressed anteriorly. (see schematic of *Fst1* expression in Figure 5.1B; Hammond and Whitfield, 2011). These results are similar to what can be observed when altering RA signalling. As mentioned above, excess of RA results in the loss of anteriorly expressed genes such as *Lfng*, *NeuroD1* and *Fgf3* and the duplication of posteriorly expressed genes such as *Tbx1* anteriorly (see schematic of *NeuroD*, *Fgf3* and *Tbx1* expression in Figure 5.1A; Bok et al., 2011; Cadot et al., 2012). Interestingly the use of specifically localized RA bead and systemic RA administration lead to similar results. This suggests that otic patterning is highly sensitive to difference in effective RA concentration, regardless of the exact distribution of exogenous RA around the embryo. Conversely, blocking of RA signalling leads to a duplication of anterior gene expression domains such as *NeuroD1* that then starts to be expressed posteriorly in the chick otic vesicle; along with a downregulation of *Tbx1* expression in the posterior domain (Figure 5.1C; Bok et al., 2011).

Furthermore, when observed at later stages, the otic vesicles of Zebrafish in which FGF signalling was inhibited display a lack of anterior structures and a duplication of posterior regions (Hammond and Whitfield, 2011). Mirror duplication of the two posterior halves were also reported in chick embryo in which RA bead had been implanted next to the otic cup. Conversely, overexpression of *Fgf3* results in the loss of posterior otic structures and a duplication of anterior domains in Zebrafish (Hammond and Whitfield, 2011). In other words, inhibiting FGF signalling mimics the effect of

excess RA, whereas overexpression of *Fgf3* mimics the effect of blocking RA signalling, suggesting *Fgf3* may be one of the key gene by which RA regulates otic patterning. Patterns of gene expressions also supporting this hypothesis are schematised in Figure 5.1.

In conclusion, all together these studies suggest that AP otic patterning depends on an antero-posterior gradient of RA, with induction of *Tbx1* by high doses of RA playing a major role in the specification of the posterior part of the otic vesicle, and induction of *Fgf3* by low doses of RA playing a major part in the specification of the anterior part of the otic vesicle. The exact timing of axis fixation have not yet been established in mice, but the plasticity of gene expression such as *Fgf3* (Cadot et al., 2012), as well as *Tbx1* (Bok et al., 2011) following RA administration is consistent with ongoing AP patterning at 7.75dpc. On the other hand, *Fgf3* expression domains are not spatially altered by excess RA at 8.5dpc (Cadot et al., 2012), thus suggesting that the AP axis is fixed by 8.5dpc. This dual effect of RA in the early inner ear is discussed in more details in the following section.

### **5.1.6 Interpreting the dual effect of RA in the early inner ear**

The downregulation of *Fgf3* expression in embryos exposed to RA may be explained by direct regulation of *Fgf3* through RA-binding sites located in the enhancer region regardless of the stage of administration. However the lateralization of *Fgf3* expression that is only observed following exposure to RA at 7.75dpc requires an additional level of regulation. One possibility is that *Fgf3* is negatively regulated by other transcription factors responding to higher RA levels, with the loss of *Fgf3* expression in the antero-

dorsal part of the otic vesicle thus reflecting direct and indirect downregulation of RA. Another possibility is that the spatial change of the *Fgf3* expression domain in otic vesicle could be linked to the posteriorisation of the hindbrain.

In order to explain why *Fgf3* expression is first lateralized before becoming increasingly downregulated with increasing dose of RA, I propose the following model (Figure 5.2). A major source of RA involved in the patterning of the hindbrain and the otic vesicle comes from the caudal expression of *Raldh2* in the somites and lateral plate mesoderm (Romand et al, 2006; Bok et al. 2011). This generates a RA gradient along the AP axis that is accentuated across the otic vesicle through the action of several RA catabolizing enzymes, in particular CYP26C1, that is expressed rostrally to the otic vesicle at 8dpc. This RA source seems to generate a posteriorising signal since the expression of anterior neurogenic genes such as *NeuroD* is lost following administration of 50mg/kg of RA (Bok et al, 2011).

However, if the RA gradient were behaving like a simple sink and source model, with anterior genes such as *Fgf3* being downregulated at high RA concentration, we would predict an anterior shift or a general downregulation of *Fgf3* otic expression with increasing RA administration. Instead, this study shows that the expression of *Fgf3* at the boundary between anterior and posterior compartments stay unchanged, whereas the expression in the anterior and dorsal part of the otic vesicle becomes increasingly downregulated with increasing doses of RA.

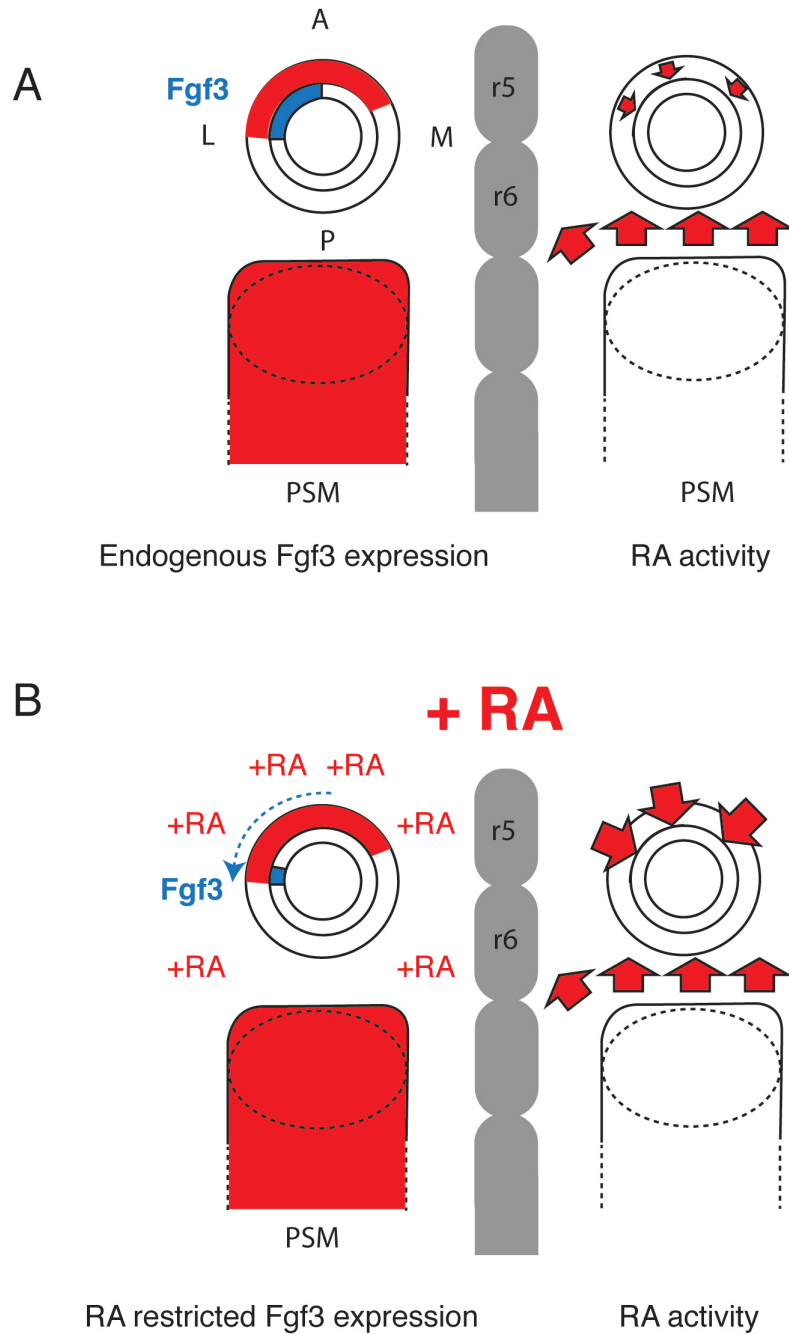


**Figure 5.2 Model of exogenous retinoic acid effect on otic patterning.** (A) On the left, endogenous RA sources are represented in red; on the right, the red arrows symbolized how these sources affect otic patterning. Endogenous sources of RA synthesis include the presomitic (PSM)/early somitic mesoderm, located caudally to the otic vesicle, and the anterior otic epithelium. During normal embryonic development, the developing inner ear is therefore in between two opposing gradients. I suggest that the strict localization of *Fgf3* to the anterior otic epithelium is due to his requirement for a lower RA threshold than posterior genes and its downregulation by high RA level (from the PSM) , thus preventing *Fgf3* expression to spread posteriorly. (B) Changes in RA signaling strength and *Fgf3* expression following RA systemic delivery of exogenous RA: combination of exogenous RA with endogenous RA results in an elevation of the two opposing RA gradients. The increasing anterior gradient would then progressively downregulate *Fgf3* expression, starting by the anterior pole.

Therefore, there must be a mechanism that maintains the boundary between anterior and posterior compartments, this could be the result of the source and sink interaction described by Bok et al., (2001), with relative concentrations of RA specifying the two poles of the otic vesicle. Then a second mechanism, based on effective RA concentrations, would specify the identity of each pole.

In our model, we believe this second mechanism reflects the presence of an additional RA source not considered by Bok et al. (2001). Retinoid synthesizing enzymes are also expressed in the otic epithelium in anterior/dorsal regions. *Raldh2* is expressed in the dorsal otic epithelium, and *Raldh3* in the dorsal and antero-ventral region of the otic epithelium (Romand et al., 2006), that together form a second RA source anteriorly and dorsally (Figure 5.2). Thus, when increasing doses of exogenous RA are applied, both the posterior signal and this second antero-dorsal source become more robust. A combination of raised systemic RA levels together with RA generated in the wall of the otic vesicle would expose *Fgf3* to abnormally high level of RA anteriorly and dorsally and therefore explain the gradual and increasing dorsal and anterior loss of reporter expression.

This model is complementary to the one proposed by Bok et al. (2001) as this additional source of RA also allows to explain the ectopic expression of *Tbx1* anteriorly following RA administration at 7.75dpc. It would be interesting to look at *NeuroD* expression following exposure to a range of RA doses to see whether it confirms this hypothesis by being first downregulated anteriorly before being completely lost.

In the introductory paragraph of this section, the possibility of an additional level of regulation by transcription factors responding to higher level of RA was also mentioned. *Tbx1* would be a good candidate since it starts being expressed where *Fgf3* expression is lost following exposure to RA. Furthermore, as discussed in section 5.1.5, *Fgf3* is ectopically expressed posteriorly in *Tbx1* mutant (Figure 5.1E; Raft et al., 2004). All together these results suggests that *Tbx1* represses *Fgf3* expression, although whether this regulation is direct or indirect remains to be determined.

Eventually, there is the possibility that the altered expression of otic genes reported does not reflect a direct regulation of otic patterning by RA, but a secondary effect of hindbrain posteriorization. This question has been addressed in chick by altering rhombomere patterns to mimic the effects of RA bead implantation (Bok et al., 2011). To do so, they replaced the rhombomeres normally adjacent to the ear (r4-r6) by a block of caudal tissues containing r7 and the spinal cord. This transplantation experiment did not result in the altered genes expression reported with RA (Bok et al., 2011). This suggests that, at least in chick, the effects of RA on otic patterning are independent of hindbrain signalling.

In summary, in the first part of this thesis I have proposed and developed a new method for retinoic acid administration, and used this to administer RA to *Fgf3*-reporter transgenic mice. This revealed a dose dependant downregulation of *Fgf3* in the developing inner ear and in the hindbrain. Reporter expression was also differentially downregulated according to the developmental stage of RA exposure. Furthermore, this study also highlights the value of transgenic reporter lines that allow

following in considerable detail subtle changes of expression that for many genes would not be readily detected via in situ hybridization alone.

## **5.2 Regulatory analysis of *Fgf10***

### ***5.2.1 Investigating *Fgf10* regulation in mice***

Hindbrain *Fgf10* and *Fgf3* have been shown to be redundantly required for otic placode induction (Zelarayan et al., 2007), and mutation in either *Fgf3* or *Fgf10* is linked to deafness in humans. Interestingly the two human deafness syndromes with which they are associated are phenotypically very similar. *Fgf3* mutations underlie LAMM syndrome (labyrinthine aplasia, microtia, and microdontia, OMIM 610706) that is characterized by lack of all inner ear structures (aplasia) and microdontia (Riazuddin et al., 2011). *Fgf10* mutations lead to LADD syndrome (Lacrimo-auriculo-dento-digital, OMIM 149730) that is characterized by hearing loss and microdontia (Shams et al., 2007). The ability of the two genes to compensate for each other during the otic induction in mice (Zelarayan et al., 2007) suggests they can trigger similar downstream pathways and may also be sharing the same upstream regulators in the hindbrain. Furthermore, they are also expressed in the developing inner ear itself, with expression in particular, overlapping in the antero-ventral wall of the otic vesicle, a region that is thought to give rise to the neurosensory components of the inner ear. This suggests *Fgf10* and/or *Fgf3* may be involved in the generation of neurons, hair cells or even both, and this has been brought out by phenotype analysis (section 1.3) making them potential factors to be used in future gene therapy to treat deafness. In

agreement with this, *Fgf3* and *Fgf10* were used in vitro to induce the differentiation of hair cell-like cells and auditory neurons (Chen et al., 2012). Furthermore, these otic neuroprogenitors were shown to differentiate and improve auditory-evoked response in gerbil.

In order to generate a *Fgf10*-reporter transgenic mice line, I first attempted to delimit an enhancer element that would recapitulate the full pattern of *Fgf10* expression in the inner ear, as well define any different *cis*-regulatory modules or units controlling *Fgf10* expression in different areas of the inner ear in either spatial and/or temporal terms. Previous studies had revealed that a 7kb region upstream *Fgf10* was able to recapitulate the full pattern of *Fgf10* expression whereas a smaller 800bp region within this enhancer was believed to control *Fgf10* expression from later stages (11.5dpc), and in restricted areas of the inner ear only (Ohuchi et al., 2005).

A series of constructs were prepared to generate an *Fgf10*-reporter line recapitulating the full pattern of *Fgf10* expression (7F7R-*DsRed*) and a variety of subfragment-reporter constructs that may reveal any distinct modular organization of the regulatory region. In addition, a cluster of *neurogenin*-related binding sites was detected and additional constructs prepared to test the potential input of this pathway in normal *Fgf10* regulation. Finally these would be compared with the *Fgf3* regulatory data, particularly the RA control of *Fgf3*.

However the generation of *Fgf10*-reporter mice containing a large upstream region proved to be difficult and delayed the generation of stable transgenic lines. Two

independent 7F7R-*DsRed* lines were eventually obtained but founders were female, and following breeding to increase the colony size, neither was found to exhibit fluorescent staining in the developing inner ear (nor in other embryonic domains examined at the same stages). The lack of reporter expression can be explained in several ways. First, a mutation may have been introduced in the promoter, reporter or enhancer. Sequencing of the promoter and reporter did not reveal any sequence mutations. Next, functionality of the 7F7R enhancer was confirmed by reporter expression in the chicken embryo following otic vesicle electroporation. Second, the transgene may have randomly integrated in a part of the genome that is quiescent. However, the likelihood that both independent integrations similarly integrated into such genomic regions is rather remote. Another possibility relates to plasmid vector sequences that were not removed prior to pronuclear injection, and that remaining plasmid sequences could inhibit gene transcription. Such negative regulatory effect of plasmid sequence have previously been reported. A last, possibility is that the enhancer is lacking DNA regions required for its expression and/or may contain repressor regions negatively regulating its ability to control expression.

Careful comparison of the restriction map of the 7F7R *Fgf10* enhancer to the map of the large enhancer Ohuchi identified (2005) revealed that the 7F7R enhancer fragment was lacking a 2kb 5' region, whilst including an additional promoter-proximal 700bp region (Figure 4.2). Analysis of this 700bp region revealed the presence of 8 repetitions of ETSF factors followed by 21 repetitions of VZF07 Zinc finger protein 263 sites, followed by 17 more sites for ETSF factors. Although a review of the literature did not reveal whether these factors could negatively regulate gene expression, it

cannot be ruled out that this apparently unusual stretch of DNA repeats might interfere with *Fgf10* expression. The presence of 2 conserved elements upstream *Fgf10* not included in 7F7R was also envisaged as a possibility to explain the lack of *DsRed* expression. However, the 3F3R fragment was later shown to drive the early and late patterns of inner ear expression (Economou et al., 2012). Thus, whilst additional neural domains that have never been intensively studied for any of these reporters could be present in these missing domains, the ability of 3F3R-*ZsGreen* to drive early inner ear expression suggests that the 7F7R-*DsRed* transgene should have worked. The technical issues raised in the previous paragraphs are thus the more likely to explain the lack of 7F7R-*DsRed* expression.

### **5.2.2 Investigating *Fgf10* regulation in chick**

A quick review of the literature shows that the chick has been successfully used for testing mouse enhancer regulatory activity (Saito et al., 2006). The ex-utero development of the chicken embryo makes it easy to incubate the embryo until an appropriate time of development, to access the embryo to electroporate reporter-constructs and subsequently analyse embryos for transgene expression after just 1 more day of incubation. Thus this method theoretically allows testing the regulatory potential of any enhancer in 4 days and at low cost. In addition, the analysis of mouse *Fgf10* regulation in the chicken inner ear also aimed at uncovering potential similarities and differences between *Fgf10* regulation in chick and in mouse.

Electroporation of 7F7R-*ZsGreen*, 3F3R-*Zgreen* and 3F7R-*ZsGreen* constructs lead to *ZsGreen* expression in a couple of embryos for each construct, showing that all the

enhancer fragments tested were able to drive *Fgf10* expression in the chicken inner ear. Importantly, this also demonstrates that the 7F7R fragment that had been used for the generation of the two transgenic mouse lines that did not exhibit any inner ear expression was however functional in the chicken. Although the relatively small number of chicken embryos expressing the transgene did not allow me to draw any firm conclusions, it seemed that the larger the construct, the stronger the fluorescence and the larger the area of expressing cells. This could be interpreted that 7F7R does contain additional domains positively regulating its expression in the chick embryo, and would be interesting to explore further.

In an independent project in the lab, the generation and characterization of a minimal *Fgf10* ear enhancer recapitulating most, if not all of *Fgf10* expression in the inner ear, was completed and shown to lie within the 3F3R enhancer (Economou et al., 2012). Furthermore, the *Fgf10* pattern of expression in electroporated chicken embryos was compared against mouse transgenic reporter embryos. In mice, the 3F3R-*ZsGreen* pattern of expression was strictly restricted to the inner ear, whereas in chick, 3F3R-*ZsGreen* is expressed in the otic epithelium and in addition other regions of surface ectoderm in (this study and A.Economou, personal communications). Also, mutation of the 3 GATA3 sites of 3F3R resulted in loss of *Fgf10* expression in all mouse lines examined (Economou et al., 2012), whereas reporter expression was still detected in chick (A. Economou personal communications). All together this suggests that some aspects of molecular mechanisms underlying *Fgf10* regulation are different between chick and mouse inner ear. It would be interesting to test the constructs containing all four conserved regions to see whether inner ear specificity is regained. But in the

opposite fashion, expression of the reporter does show that *Fgf10* reporter constructs can be tested for functionality in the chicken embryo, with the caveat that otic specificity may be lost.

Thus, the present work modulates what had been previously postulated (Timmer et al., 2001), and indicates that although chick electroporation may indeed be used to analyse the regulatory potential of enhancer regions for some mouse genes, this cannot be extended to all mouse genes. Therefore, an analysis of mouse enhancer regulation in chick should not stand on its own but always need to be corroborated by data in mice.

### **5.2.3 Regulation of *Fgf10* by the Neurogenin pathway**

In order to identify putative upstream regulators of *Fgf10*, bioinformatic analysis of the 6.9kb region upstream of *Fgf10* reported by Ohuchi et al. (2005) was performed using MatInspector (Quandt et al., 1995). This analysis showed the presence of 1294 putative transcription factor binding sites. Some of these factors were of particular interest, as they are known to be active in the early inner ear around the time of *Fgf10* onset of expression. This includes putative binding sites for members of the Neurogenin pathway, *Ngn1* and *NeuroD*. *Ngn1* and *NeuroD* are proneural genes expressed in the anteroventral wall of the otic vesicle and are required for neurogenesis in the inner ear (Abello and Alsina, 2007; Ma et al., 1998). Accordingly, *Ngn1* mutants fail to form the proximal cranial sensory ganglia and targeted mutation of *NeuroD* results in a severe loss of inner ear sensory neurons (Abello and Alsina, 2007; Ma et al., 1998). The number of otic neurons was also reduced in *Fgf10* null mice

(Pirvola et al., 2000), thus suggesting *Fgf10* may be one of the genes mediating the effect of the *Neurogenin* pathway.

The presence of a binding site alone is only a first step in the identification of an in vivo functional regulator of *Fgf10* expression, because consensus sequences may occur randomly within the genome by chance alone. However two additional organizational traits suggest functionality in vivo. First, the *Ngn1/NeuroD* sites lie in a region of homology conserved between mice, chick and humans (Ohuchi et al. 2005). In addition these sites form a cluster in the 3' region of the enhancer, and previous studies suggest that clustered binding sites identified by bioinformatic strategies are more likely to be functionally relevant in vivo (Gotea et al., 2010; Lifanov et al., 2003). Comparative analysis of *NeuroD* and *Fgf10* expression also supported the *Neurogenin* pathway as a candidate for direct regulation of *Fgf10*.

In order to test the functionality in vivo of these sites, several enhancer fragments containing all or part of the clustered neurogenic family of sites were constructed. At the time of writing they were not tested but they will likely be the starting point for further studies.

#### **5.2.4 Regulation of *Fgf10* by *Gata3***

The bioinformatic analysis of the 7.0kb region upstream *Fgf10* revealed the presence of 9 putative GATA3 binding sites. *Gata3* is a transcription factor expressed in the developing inner ear (Lawoko-Kerali et al., 2002; Lawoko-Kerali et al., 2004; Nardelli et al., 1999; Pauley et al., 2003) and, interestingly, *Fgf10* expression is downregulated in

*Gata3* null mice (Lillevali et al., 2006). All together these elements suggested that *Gata3* was a strong candidate for direct *Fgf10* regulation. As part of this project, the onset of *Gata3* and *Fgf10* expression were examined and compared. This comparative analysis revealed their expression is initiated in similar areas of the inner ear.

Other experiments performed independently in the lab then confirmed the direct regulation of *Fgf10* by *Gata3*. EMSA experiments were performed on the 3 GATA3 sites located in 3F3R and revealed the GATA3 protein could bind all three sites but with different affinity (Economou et al., 2012). The functional significance of these GATA3 binding sites was then tested in vivo, and GATA3 site2 was the only binding site absolutely required for *Fgf10* expression in the inner ear (Economou et al., 2012).

### **5.2.5 Regulation of *Fgf10* by Retinoids**

The 3F3R *Fgf10* enhancer contains two putative retinoic acid binding sites, and thus analysis of 3F3R-*ZsGreen* transgenic mice was used to gauge the response of *Fgf10* to RA. Using a dose that gave maximum response of *Fgf3*, 25mg/kg of RA at 8.5dpc lead to different spatial changes to *Fgf10* than those found for *Fgf3*. *Fgf10* expression appeared more dorsally localized, while lost and downregulated in the anteroventral wall of the otic vesicle in half of the embryos. In the remaining embryos, *Fgf10* expression appeared unchanged. Interestingly, embryos where expression was shifted and downregulated, also displayed abnormal brain phenotypes, such as open neural tube defects, that are characteristic of embryos exposed to RA prior to hindbrain patterning. Perhaps then exposure at 7.75dpc and during hindbrain patterning affects *Fgf10* expression, through dorsalisation and downregulation, but exposure at 8.5dpc

does not. Based on this hypothesis, I designed an additional set of RA treatments that were carried out by A. Economou during the writing of my thesis. When RA is administered at 7.75dpc, *Fgf10* expression becomes more dorsally localized in the otic vesicle and appears lost or downregulated in the anteroventral region, but when RA is administered at 8.5dpc the spatiotemporal pattern of *Fgf10* is no longer dorsalized but just downregulated (Economou et al., 2012). The downregulation of *Fgf10* expression following exposure to 25mg/kg of RA extends previous RT-PCR studies (Frenz et al., 2010) where the spatial dynamics of changes in expression are now revealed.

### **5.2.6 Differences and similarities in *Fgf10* and *Fgf3* regulation by Retinoids**

Regulation of *Fgf10* by retinoids shows similarities and differences with *Fgf3*. Similar to *Fgf3*, *Fgf10* expression is downregulated in the antero-ventral wall of the otocyst following RA administration. Both also exhibit spatial changes, although along different otic axes. Timing of administration appears to be important for both genes. *Fgf3* expression is shifted posteriorly and becomes lateralized in embryos exposed to RA before hindbrain patterning but is only downregulated in embryos exposed to RA after hindbrain patterning (Cadot et al., 2012). However, for *Fgf10*, the remaining patch of expression is dorsal whereas for *Fgf3* it is ventral. In addition, there were clear RA response differences in the incidence and extent of reporter downregulation, with only 30% of the *Fgf10* reporter embryos showing some downregulation when exposed to 25mg/kg of RA (Economou et al., 2012), whereas more than 90% of the embryos presented a downregulation of *Fgf3* expression when exposed to a similar RA dose (Cadot et al., 2012). However, these results may not be directly comparable since no

quantitative analysis of *Fgf3/Fgf10* expression was performed, the reporters are different and the dose-response of *Fgf10* to RA was not analysed in detail. Such experiments would be useful to confirm these conclusions.

The relocation of *Fgf10* expression following exposure of embryos at 7.75dpc (Economou et al., 2012) also confirms the plasticity of otic vesicle patterning at this stage of development as initially suggested following the detailed analysis of *Fgf3* expression. Reprogramming the spatial expression of two different *Fgfs* in the inner ear unequivocally demonstrates that at 7.75dpc the otic vesicle is able to reprogram its spatial gene expression pattern. This contrasts with the downregulated but spatially unaltered domain of *Fgf10* and *Fgf3* expression following RA administration at 8.5dpc, showing that at this stage, the otic vesicle seems to have become resistant to re-patterning.

Different spatial responses of *Fgf3* and *Fgf10* to RA may also reflect underlying differences in the regulation of the two ligands; and/or their functions within the otic epithelium that have not yet been fully defined. Indeed as part of this project, I also showed that the *Fgf3* pattern of expression is unchanged in *Fgf10* mutants and thus *Fgf3* could in part compensate for the lack of *Fgf10* in vivo at the ligand level, however the functionality of *Fgf3/Fgf10* redundancy within the otic epithelium and vestibulo-acoustic ganglion has not yet been investigated.

The major alteration in *Fgf3/Fgf10* spatial expression happens following exposure to RA during hindbrain patterning. Since otic vesicle formation is under the control of

signalling from the hindbrain (Alvarez et al., 2003) this raises the possibility that this repatterning may all or partly be due to the repatterning of the hindbrain. However, the presence of RAREs in both *Fgf* enhancers, and the ability of RA to bind *Fgf3* RAREs (Frenz et al., 2010) raise the possibility of a direct regulatory control. It will be interesting to define the extent of the RA response that is indirect, and due to alterations in hindbrain patterning, or direct through directly repressing *Fgf3* and *Fgf10* expression through binding the RAREs located in the two enhancers.

### 5.3 Conclusions

Regulatory mechanisms involved in the formation of sensory neurons and hair cells during inner ear development are still poorly understood and this is an obstacle to the generation of gene or stem cell therapies to treat deafness and hearing impairment. *Fgf3*, *Fgf10* and RA have long been known to play crucial roles in inner ear development and there has been accumulating evidence that they could be involved in hair cell differentiation (Kelley et al., 1993; Chen et al., 2012).

Using an *Fgf3-lacZ* transgenic line a detailed analysis of the effect of excess RA on *Fgf3* expression was performed (Cadot et al., 2012). This showed that RA differentially affects *Fgf3* expression depending on administration timing and dose. Administration of increasing doses of RA at 7.75dpc leads to a dose-dependent downregulation of *Fgf3* in the otic vesicle, as well as changes in hindbrain expression. Detailed analysis of the otic vesicle at 9.5dpc also showed a lateralization of *Fgf3* expression with increasing dose of RA. Administration of RA at 8.5dpc also leads to a dose-dependent downregulation of RA in the inner ear at higher doses than required at 7.75dpc but no

spatial changes of expression; otic *Fgf3* expression was evenly downregulated throughout the otic vesicle, suggesting that otic patterning is underway at 7.75dpc whereas the AP axis is fixed at 8.5dpc.

*Fgf10* enhancer-constructs were made and tested both in mice and chick embryos in order to identify fragments controlling all or part of *Fgf10* expression in the inner ear. Comparative analysis between electroporated chick inner ears and a *Fgf10-ZsGreen* transgenic mouse line (3F3R-*ZsGreen*; Economou et al., 2012) suggests that some of the molecular mechanisms underlying *Fgf10* regulation are different between mouse and chick inner ear. Using the 3F3R-*ZsGreen* transgenic mouse line shown to recapitulate *Fgf10* endogenous expression in all area of the inner ear (Economou et al., 2012). A preliminary analysis of *Fgf10* regulation by retinoids was performed and showed similarities with *Fgf3* regulation, with both time and dose differently affecting otic *Fgf10* expression. However, the change in spatial expression following RA administration at 7.75dpc and the dose required to induce it was different than for *Fgf3*. The differential responses of *Fgf3* and *Fgf10* to RA suggest these genes are unlikely to be fully redundant in the development of structures from the otic epithelium. The development of conditional double null alleles will be of some interest to explore functional redundancy and examine how this reflects the divergence of upstream molecular mechanisms. Moreover, the identification of whether the RA inputs to regulate *Fgf3/10* is direct or indirect is another goal that needs to be established in drawing up the molecular programme of early inner ear development.

# APPENDIX

---

**Figure S1 - Annotated sequence of the 7.4kb upstream *Fgf10*.** PCR primers delimiting the different *Fgf10* enhancer fragments cloned are indicated in yellow. Putative binding sites for GATA3 are highlighted in red; putative binding sites for neurogenic factors (NGN1, NEUROD, NSCL1) are highlighted in green, and putative binding sites for RA are highlighted in red.

caaaacaatttcacaagatgtaggttttcacacta **ggcacatgggccgg**

7F primer

**gggagatagct** → cagtggttaagaactcctattgctcctgtagaggattct

gttcagctcccagcactcttatggcagctcacaacttcctgtaattccat

ttccaggggattctcttctgccctccatgggttcttgcccacacatagta

tatacattctcctgtcagtctctctccatacaatacatttaaataagca

atattaataaatctgataaaaaattagaatatagcaggcaggttaggga

atTTTTatcagaaaatagttaatgtaatcatttagaacacactattgatt

catgattctggaagcaaaaggaaaagaagaacatcagggtacctggca

gagactttgcccaaaccctaagtctgtaggagaaatctggatcaaaggat — 7.0kb

tgtgcaattatcacagagtaggtgat **tatcaaatTTTT**TTTTTTTTTT

TTTTTTTggTTTTTTTggTTTTTTTgagacagggttctctgtatagccctg

gctgtactggaactcactttgtagaccaggctggccttgaactcagaaat

ccgcccgcgctgcctcccagtgctgggattaaaggcgtgcaccaccac

gcccggcttcaaattttaatccttcatgaagccagagagcagacgtgaca

gtctcccttgggtccttggtagagggtggacagcatagtttataggatcca

aatctttccaaacccttcttaggtcctgagacaattctagattcccatcc

ctaatgtcaataaaataaaataaaccaaagggtcacccatgtatatatgt

atgcatactctttatgagttaaatTTTcatatcttctttgtagatccaa

agtattgaaaattgcctactgcagcctagtagcacataataagtattcaa — 6.5kb

taaacagcactcgaattaaaaaacaattgagaaaatatacgaataatgac

cacctgtaaatatTTTcgtgtcaatgaaccaaattatataataattt

atgtatttaaatatgtatttgtatattaataagtaatacatatataat

atatacatatacatataatgtaatttctaacaaaatattacaaatatca

cccaactaagaactagaggccttgacgtggcaggagacagaggctctgtaa

agggtgaacaggaagcaccaaaaaactctt**caaagatcttaca**actttgt

caaggaaaggctgtctgtcagcatctcagagggtgacagatagcagctttg

tgaaaatatgttactgtgttttagcttcaagatacatagctcacatttct

ggaaatgtgctgatttatgtgagcgcatttccaatattccagtacagtta

cttttcttacaagatcccattcctttctaccttggccacatttctgttt — 6.0kb

ccagagttgatcgttgggtcattgaaaacaagagagctgaaaattcactt

tagtttcgaacttcaaaaaataaatgtttatatgaatgtgtatgctttg

aaggaccactctgtttagaaaaatctaacaatgatagtgtaaagaattaa

ctcaaattaatagattactttgtgggggtgcagacaggatttctctgtgt

agtcctggctgtctggaactcacctgtagagcaggcagg**gccttgaactc**

**agaaatctgcctgc**ctctacatccaagtgtgggattaaaggcatgcac

caccactgcctggctagattacttttctaaatagtatcattaattgcttg

agggagcaacttcaaaactcttattaaatcccaagaacccatgcttatc

ctgaaagtggtatggtataagttacttttaaatgt**attcatatcatt**tgaa

agagtctgctttcccaaaactacaaaaacccttattttttttgacctaatc — 5.5kb

aagtgatagttaatatttcaacacaaagccattttatagcttttctctgg

ctaatcaatggtagcaagatatgctggttttccataactaaagcctcct

aaggttccttatctcttcccttctggtaactcaggctatcggagcaagta

ggggatgataagaagaaaaaaaaaacagagaaaggaggaagaagaaaattg

gtagatgggtgtggtgagggtcacaagtaaggcctgtggctggcactcct

aactggtttctcattctgagtgactccagtctttctataaagtccaagag

ttgcatccagtttcaggctgaccatctttacttcagaaaagacccaaaga  
tattccagtcatccaaacttttcgagggatcatcatgacaccacaaaagaa  
aaattccaaagctgacttccaaagccatgttgcaagtgaagcagacacat  
actggaataagtaaacaatcctgtttgtgtgtgttcatgcatgaaggtgt — 5.0kb  
gagcgggctgtattgtatgaagtgtatagtgagttgtacataggtcaggg  
aaagacttgtcctatagtatccaagtctacctcattctcttaaccagcac  
gcccctgtgataccccacatcatcaggattgctggtgtccagagcaatac  
ctttcctttcctgtgtatggatgccagggattcaaattcaggccctcatg  
tttacatagtaagcactctgaccctcttagctatctccccaatttcctaa  
aacatcaaacaaaaagttcttttagactataggcatgacatttatatttga  
aatgtaatgtcatgcatagatttgattctgacagttggtgaccttgct  
tgtatatgcaattgtttaaaaaaaaaaaaatcaagagctttgaaaactaaa  
actaaactaaactctggttaattcaatgagggatgctcagttcctatggc  
tgggttgccactgttttgcaagtgttgagttcccactttctgtgagcta — 4.5kb  
aaaacctcttttcttttcattcggagctcttaatttgaaagcaataatga  
taaactactgtttctgtactgagctccaacgtggttgattgtatctatcc  
tttctagctgtagctttggaagagaaacgaacagaaaacaatgccttccta  
ctggcatttcctatatgtgaataggaaaataggcacacactcctactact  
acacagtaggcttaaaaaaaaaaaaaacaaaaaaaaacatggggcctgtgca  
tgtcgttaattgtcaaacagccttgctgacttttgacctgatttagcatta  
cttgaagcagctttctgacactgtcaatgccacctcatataatagaacat  
acatcttataactgaaccacagacagtgctgggccacataaagagcccag

gaaaggcatgcctcatctgtaaaccgct **cagagagcatagctactaaggc** — 3F primer

**atctg**ggagaaggccttcatggggccccgtttacacggaagtgccacatt — 4.0kb

tgagaggtcttttaaatgcttttcttcacaatcttgTTTTTaaaagttg

ataactcctcaaatacgtcgaatttaacagcagcttacctctctttctttc

aataaagatttag **actaatatcactg**gataggcttaggcatagaaacag

agcatgccttgcaaggatcggatgaaagagacagacagcctTTTTtagaat

agtgggtaccattctaatactgaagcttattctgccctttcaatcttaaca

gagaacaattaataaaggaaccattaagacctgattattgcagctaaa

aaaaaaaaaggaaggtaggtagaatttcagtcctttgaagtaactgagaa

tgattcaggcctcatta **cagagatataatc**tacattcatacatttatggt

agtg **attcaaatctatt**gggagagattggattccgttaaatagcgcacatct

ttcctgtggaacttttctcaggctttctggggctaagctaagaggtgact — 3.5kb

tcacaatgcaaagtgggtgggggatttagggattccactgggcctcagaaa

acaaggcagtacagagaagaaaaagaagaatgagatataatct **aaaaagc**

**tatgtcagcttttcct**ttgggcaatttagtaaagtgtcccgccctcct

gccatcacgctgtacagatgagaggcaaaaggactcgggaaccctcaaac

attgcacctgctgctgacaagttttaatgtgaaagttttgagaatgcct

ttacctcactataggtagaactaaaggcaaacTTTTtagctagaaaatctg

aacagctttgactggaataaaggatgatggagggttgggggtgggggtccg

gggaggagtggg **agtgttgggctgaagaagtgtc**tggtatgaatttaaaa

Neuro2.5  
Forward primer

aacagaaaagcactcaagttggcatcagtaatggttggtatccagtgtaaa

gaaaccccaaactaattacttcctgtgtttaataatTTTTTcacaaaagaa — 3.0kb

tctttattgtatggttccatcaaacaatTTTTTTTaaatgtaatttcaat

gggttgcaattcaaacatttgaattcttccttct**ttggagggtgtgactt**

**aaatccct**tagaaactgtctacccttcacttgcttgtctactcaggtat

aaaactgtgaagtaggaaattgaaattagcactgtgggctcatttttcaa

tatccatgctttaattaagaagcaagactttgtttgacgcatgctcttt

attgcttaacttttcaattaatagctacagaaatcagctaatacatatta

aagttagaaatct**gctgtgatggtcgtcacggttgtt****aaatctttt**gaat

3R primer

gagcattgcaatgagttataaataatgcaattaaaaatctcgattctggt

attattaagtagttctatttcaaaggcagtgaacacacagagaaatggaa

gagcatgcattcaaaccactaaaatgtatttggggaatcattaacaacgt — 2.5kb

ctatctctaagacttttgaattttaattgtctttctccagttcccagtga

agactgaaaccagtgcgcatgacagggttcctggcttgtgtgtgcaagc

tccttttgtaaattgtttctgaatcactatgccagttgctaactctcaaa

ttcaccttgaaacctctgcttctccctcagccatttaggttgaatcatgt

gaaatcaccaccaccgatgatat**tgaccatttgttt**tgcttagccagaa

cacagatgtctaactgcctcccacaacagagtaatatatgttcatgcaat

ccttccagccagccggttccttagttagatattttcttaaggaaatgat

ctctggtactcagaattgtatcatactcaggtaggaatggattattacia

tgtttcctcctggtacctttttgttttgggcaatagtttcctggtcttgt

gctgacttctgtctgtgtctgggtgaaagtttgtttctgagagcagggg — 2kb

tagagttgggggttgggtgtgcacaagagtgtttgtgaaaggtcggtaggt

agtgaagctgctgtgtaaagtagagccctttaacattaagtttgaagat

gggcggggacctcctctttatggtaaaatgcaaaggaaattgcatagagg

aaaaaaaaacaggcagcaggggatttgggtcaaactctgtgataaaaatctgc

gatcgcaggaaagtgcgtaggctttgaagccatgcggtgattctgtaaag

gactcgtgttaccaattagaaatcagtaacctgggtccctgatttcattt

gcgccaagagagaggctatgtttaaggggtgacgataaatctccctgagct

taaaaagacagagagggccaaagtgtgaactttttacttcagcaacggaa

gcgagaaatcaatgattcattaaaaccgagacctccttggaagctggca

ggagaggaggaaacgaagctagctcattatgtctcccttctcgattttag

cttctatcagtttataatctgttcttggagagagtttgcccagagcatcc

— 1.5kb  
Neuro1.1  
Forward primer

tcttctgccttctccccagccctcttccctgcttctgggatctggaaggc

7R primer

agaaacacatccacacacaaaagccaagctccaaactctattttcgcggc

caaaaggaaaaaaagaaaagaaaagaaaagaaaaggaaggaagga

aggaaggaaggaaggaaggaaggaaggaaggaaggaaggaaggaag

gaaggaaggaaggaaggaaggaagaaagaagaaaactacagtggaaaacaagt

gagcaaggggctccctgtaggggaggggagtggttcccgccggagggcag

caaaattcggaaagcacgcggacaactcgcgctggtggccagcgtgcga

gcacaggacgccggagccgcaattagcaggagctgcaggctgcggggcgg

ctgcgccacggaggcggcgaggaagggacccgcagccccagctcagag

— 1kb

caaaggcatcgcgcactcctctcgcccaagatcccccgccccctccccg

gtcccttccccctcccttttctctggcggtcccagcagcttagggtttc

agatgtcccaccgccgtttgacccccctcccccttctccaccctgcaa

atgaggtttgaccagcagaggcagagcccacctctggctgaaaagcactg

acatttagactccaggcttcaacctgtttacaagcggctttccaaggac

ttggaggtggagagaagggcccaacaaaacgccagccgccagccgcccc  
caaacaagaagtggctttcgggaagacttcacatcaacaggcaccaccaa  
aagagaaaggaaggagaagacaacagcgctgggcagctgcctccagttc  
tgacaactccaaagagacactttttaagtggccagcaggctgggactctg

cagagaaggaccagaaggtgccaaccgcagagggggcgcagatgtcttcct — 0.5kb

gcacccccacccccaccacttttgggttttggttcaccgctctgtcatctgt

tttcagacctcttttgcacatcaacatggtgaagaaaggagtgagaaga

gaacaaagtaacccccggggggagcgaagagctctggtgaccgacaccac

cagttcctactgccgcccaccacgtccactgttcaccctgagactgg

agagacgcaggcagcggatccgaggacggagcaggacaggcagccggtc

cttcctagaagttatgcatggttggtgcactcgcttctggccagatccgta

cccagagggagctatccagaagccaccacctccagctgtctctctcgctc

gcagcaggtcttacccttcagatgttccttctgatgagacaatttca

gtgccgagagtttcagtacaatgtggaatggatactgacacattgtgcc

Neuro1.1/Neuro2.5  
Reverse primer

**Table S1 – Range of *all-trans* retinoic acid doses administrated to pregnant mice via gavage or intraperitoneal injections (IP) in the study of various organs systems.** Data were adapted from the cited papers with the time of plug considered as 0dpc. The exact time of exposition during a specific day may then vary depending on the studies. In some cases embryos were exposed in the morning, at mid-day or at night. This usually triggers significant variation in the number of embryos expressing a phenotype, as we can see in studies marked with (\*), where several times of the day were tested. (--) indicates there was no data about the % of embryos expressing the phenotype but that the dose used successfully triggered a phenotype.

Organ system	Day of exposure	RA dose (mg/kg)	Incidence of defects	References
<b>PALATE</b>	7dpc	10	--	(Wang et al., 2009)
		100	--	(Wang et al., 2009)
	10dpc	25	0-17%*	(Kochhar et al., 1984)
		50	8-27%*	(Kochhar et al., 1984)
		100	28-46%* 40%	(Kochhar et al., 1984) (Abbott et al., 2005)
		200	54%	(Kochhar et al., 1984)
		2,5	0,5%	(Campbell et al., 2004)
	11dpc	10	7,6%	(Campbell et al., 2004)
		25	33%	(Kochhar et al., 1984)
		30	26,3%	(Campbell et al., 2004)
		50	82%	(Kochhar et al., 1984)
		60	42,4%	(Campbell et al., 2004)
		100	65-75% 73,7% 82%	(Abbott et al., 2005) (Campbell et al., 2004) (Kochhar et al., 1984)
		200	94%	(Kochhar et al., 1984)
	12dpc	70	-- --	(Degitz et al., 1998) (Zhang et al., 2003), (Dempsey, 1983)
100		0-50% 94,1%	(Abbott et al., 2005) (Wang et al., 2009)	
<b>HEART</b>	7dpc	10	60	(Wasiak and Lohnes, 1999)
		100	100	(Wasiak and Lohnes, 1999)
	8dpc	70 <sup>IP</sup>	51-67%	(Ratajska et al., 2005)
<b>FOREBRAIN</b>	6dpc	20	12-60%	(Simeone et al., 1995)
	7dpc	20	58-90% --	(Simeone et al., 1995) (Avantaggiato et al., 1996)
	8dpc	20	68-72%	(Simeone et al., 1995)

Organ system	Day of exposure	RA dose (mg/kg)	Incidence of defects	References	
<b>HINDBRAIN</b>	7dpc	10	--	(Morriss-Kay et al., 1991), (Mahmood et al., 1996)	
		12	--	(Morriss-Kay et al., 1991), (Mahmood et al., 1996) (Wood et al., 1994)	
		20	--	(Conlon and Rossant, 1992), (Marshall et al., 1992)	
		25	--	(Leonard et al., 1995)	
	8dpc	10	--	(Morriss-Kay et al., 1991), (Mahmood et al., 1996)	
		12	--	(Morriss-Kay et al., 1991), (Mahmood et al., 1996) (Wood et al., 1994)	
		20	--	(Folberg et al., 1999)	
	9dpc	20	--	(Folberg et al., 1999)	
	<b>LIMB</b>	9dpc	80	3%	(Kochhar, 1973)
		10dpc	25	0-15%*	(Kochhar et al., 1984)
50			7-76%*	(Kochhar et al., 1984)	
80			0%	(Kochhar, 1973)	
100			21-91%* 95,1% --	(Kochhar et al., 1984) (Cusic and Dagg, 1985) (Bynum, 1991)	
200			90%	(Kochhar et al., 1984)	
11dpc		20	64-82,6%	(Kwasigroch et al., 1984)	
		40	100%	(Kwasigroch et al., 1984)	
		60	100%	(Anson et al., 1991)	
		80	100%	(Kwasigroch et al., 1984), (Kochhar, 1973)	
		100	-- 87,6% 100%	(Hayes and Morriss-Kay, 2001) (Cusic and Dagg, 1985) (Kwasigroch and Neubert, 1980), (Alles and Sulik, 1989), (Anson et al., 1991)	
12dpc		80	84%	(Kochhar, 1973)	
13dpc		80	61%	(Kochhar, 1973)	
14-15dpc		80	0%	(Kochhar, 1973)	

Organ system	Day of exposure	RA dose (mg/kg)	Incidence of defects	References
<b>FORELIMB</b>		1 <sup>IP</sup>	0%	(Lee et al., 2006)
		3 <sup>IP</sup>	5,3%	(Lee et al., 2006)
	9dpc	5 <sup>IP</sup>	2,9%	(Lee et al., 2006)
		7,5 <sup>IP</sup>	5,3%	(Lee et al., 2006)
		50 <sup>IP</sup>	--	(Shimizu et al., 2007)
	10dpc	100	40%	(Abbott et al., 2005)
		2,5	4,9%	(Campbell et al., 2004)
		10	26,3%	(Campbell et al., 2004)
	11dpc	30	83%	(Campbell et al., 2004)
		60	93,3%	(Campbell et al., 2004)
		100	65-75% 93,2% 100%	(Abbott et al., 2005) (Campbell et al., 2004) (Kochhar et al., 1984)
	12dpc	100	0-50%	(Abbott et al., 2005)
<b>AXIAL SKELETON</b>	6dpc	20	--	(Kawanishi et al., 2003)
		30	--	(Kawanishi et al., 2003)
	7dpc	10	--	(Iulianella and Lohnes, 1997)
		20	--	(Kawanishi et al., 2003)
	8dpc	20	--	(Kawanishi et al., 2003)
		30	--	(Kawanishi et al., 2003)
	10-11dpc	100	--	(Iulianella and Lohnes, 1997)
	<b>EYE</b>		0,313	8,1%
7dpc		0,625	12,9%	(Sulik et al., 1995)
		1,25	32,4%	(Sulik et al., 1995)
		12,5 <sup>IP</sup>	95,5%	(Ozeki and Shirai, 1998)

Organ system	Day of exposure	RA dose (mg/kg)	Incidence of defects	References
<b>NEURAL TUBE CLOSURE, NTDs</b>	8dpc	5 <sup>IP</sup>	14-22%	(Juriloff et al., 1991)
		3 x 5	0%	(Ehlers et al., 1992)
		3 x 12,5	58%	(Ehlers et al., 1992)
		3 x 15	60%	(Ehlers et al., 1992)
		20 <sup>IP</sup>	25,7-100%*	(Kuno et al., 1999)
		30 <sup>IP</sup>	40,6-92%*	(Kuno et al., 1999)
		3 x 30	100%	(Ehlers et al., 1992)
		40 <sup>IP</sup>	57,1-94%*	(Kuno et al., 1999) -- (Yasuda et al., 1990)
		50 <sup>IP</sup>	94,4% --	(Kuno et al., 1999) (Dempsey and Trasler, 1983)
		60	--	(Yasuda et al., 1990)
		53 <sup>IP</sup>	--	(Kapron-Bras and Trasler, 1988)
		80	--	(Tibbles and Wiley, 1988)
<b>INNER EAR</b>	6dpc	20	0%	(Frenz et al., 1996)
		25	0%	(Frenz et al., 1996)
	7dpc	15	0%	(Frenz et al., 1996)
		20	0%	(Frenz et al., 1996)
		25	0%	(Frenz et al., 1996)
		50	--	(Bok et al., 2011)
		2 x 12,5	0%	(Frenz et al., 1996)
	8dpc	25	5%	(Frenz et al., 1996)
		2x25	95%	(Frenz et al., 1996), (Liu et al., 2008), (Frenz and Liu, 2000)
		50	-- 0%	(Bok et al., 2011) (Frenz et al., 1996)
	9dpc	25	--	(Frenz et al., 1996)

Organ system	Day of exposure	RA dose (mg/kg)	Incidence of defects	References
<b>PHARYNGEAL ARCHES</b>	7dpc	10	--	<i>(Mahmood et al., 1996)</i>
		12	--	<i>(Mahmood et al., 1996)</i>
		5	--	<i>(Taylor et al., 1995)</i>
	8dpc	10	--	<i>(Mahmood et al., 1996)</i>
		12	--	<i>(Mahmood et al., 1996)</i>
		60	--	<i>(Vanmuylder et al., 2004)</i>
		100	--	<i>(Abe et al., 2008)</i>
		60	--	<i>(Vanmuylder et al., 2004)</i>
	9dpc	60	--	<i>(Vanmuylder et al., 2004)</i>
	<b>NEURAL CREST</b>	7dpc	10	--
10			--	<i>(Mulder et al., 2000)</i>
9dpc		25	--	<i>(Mulder et al., 2000)</i>
		50	--	<i>(Mulder et al., 2000)</i>
		100	--	<i>(Mulder et al., 2000)</i>

## REFERENCES

Abbott, B.D., Best, D.S., Narotsky, M.G., 2005. Teratogenic effects of retinoic acid are modulated in mice lacking expression of epidermal growth factor and transforming growth factor-alpha. *Birth Defects Res A Clin Mol Teratol* 73, 204-217.

Abe, M., Maeda, T., Wakisaka, S., 2008. Retinoic acid affects craniofacial patterning by changing Fgf8 expression in the pharyngeal ectoderm. *Dev Growth Differ* 50, 717-729.

Alles, A.J., Sulik, K.K., 1989. Retinoic-acid-induced limb-reduction defects: perturbation of zones of programmed cell death as a pathogenetic mechanism. *Teratology* 40, 163-171.

Anson, J.F., Laborde, J.B., Pipkin, J.L., Hinson, W.G., Hansen, D.K., Sheehan, D.M., Young, J.F., 1991. Target tissue specificity of retinoic acid-induced stress proteins and malformations in mice. *Teratology* 44, 19-28.

Avantaggiato, V., Acampora, D., Tuorto, F., Simeone, A., 1996. Retinoic acid induces stage-specific repatterning of the rostral central nervous system. *Dev Biol* 175, 347-357.

Bok, J., Raft, S., Kong, K.A., Koo, S.K., Drager, U.C., Wu, D.K., 2011. Transient retinoic acid signaling confers anterior-posterior polarity to the inner ear. *Proc Natl Acad Sci U S A* 108, 161-166.

Bynum, S.V., 1991. Morphogenesis of retinoic acid-induced postaxial polydactyly in mice. *Teratology* 43, 1-9.

Campbell, J.L., Jr., Smith, M.A., Fisher, J.W., Warren, D.A., 2004. Dose-response for retinoic acid-induced forelimb malformations and cleft palate: a comparison of computerized image analysis and visual inspection. *Birth Defects Res B Dev Reprod Toxicol* 71, 289-295.

Conlon, R.A., Rossant, J., 1992. Exogenous retinoic acid rapidly induces anterior ectopic expression of murine Hox-2 genes in vivo. *Development* 116, 357-368.

Cusic, A.M., Dagg, C.P., 1985. Spontaneous and retinoic acid-induced postaxial polydactyly in mice. *Teratology* 31, 49-59.

Degitz, S.J., Morris, D., Foley, G.L., Francis, B.M., 1998. Role of TGF-beta in RA-induced cleft palate in CD-1 mice. *Teratology* 58, 197-204.

Dempsey, E.E., Trasler, D.G., 1983. Early morphological abnormalities in splotch mouse embryos and predisposition to gene- and retinoic acid-induced neural tube defects. *Teratology* 28, 461-472.

Ehlers, K., Sturje, H., Merker, H.J., Nau, H., 1992. Spina bifida aperta induced by valproic acid and by all-trans-retinoic acid in the mouse: distinct differences in morphology and periods of sensitivity. *Teratology* 46, 117-130.

Folberg, A., Nagy Kovacs, E., Luo, J., Giguere, V., Featherstone, M.S., 1999. RARbeta mediates the response of Hoxd4 and Hoxb4 to exogenous retinoic acid. *Dev Dyn* 215, 96-107.

Frenz, D.A., Liu, W., 2000. Treatment with all-trans-retinoic acid decreases levels of endogenous TGF-beta(1) in the mesenchyme of the developing mouse inner ear. *Teratology* 61, 297-304.

Frenz, D.A., Liu, W., Galinovic-Schwartz, V., Van De Water, T.R., 1996. Retinoic acid-induced embryopathy of the mouse inner ear. *Teratology* 53, 292-303.

- Hayes, C., Morriss-Kay, G.M., 2001. Retinoic acid specifically downregulates Fgf4 and inhibits posterior cell proliferation in the developing mouse autopod. *J Anat* 198, 561-568.
- Iulianella, A., Lohnes, D., 1997. Contribution of retinoic acid receptor gamma to retinoid-induced craniofacial and axial defects. *Dev Dyn* 209, 92-104.
- Juriloff, D.M., Harris, M.J., Tom, C., MacDonald, K.B., 1991. Normal mouse strains differ in the site of initiation of closure of the cranial neural tube. *Teratology* 44, 225-233.
- Kapron-Bras, C.M., Trasler, D.G., 1988. Histological comparison of the effects of the splotch gene and retinoic acid on the closure of the mouse neural tube. *Teratology* 37, 389-399.
- Kawanishi, C.Y., Hartig, P., Bobseine, K.L., Schmid, J., Cardon, M., Massenburg, G., Chernoff, N., 2003. Axial skeletal and Hox expression domain alterations induced by retinoic acid, valproic acid, and bromoxynil during murine development. *J Biochem Mol Toxicol* 17, 346-356.
- Kochhar, D.M., 1973. Limb development in mouse embryos. I. Analysis of teratogenic effects of retinoic acid. *Teratology* 7, 289-295.
- Kochhar, D.M., Penner, J.D., Tellone, C.I., 1984. Comparative teratogenic activities of two retinoids: effects on palate and limb development. *Teratog Carcinog Mutagen* 4, 377-387.
- Kuno, N., Kadomatsu, K., Muramatsu, T., 1999. Determination of the optimal time and dosage of all-trans retinoic acid for induction of murine exencephaly. *Teratology* 60, 63-67.
- Kwasigroch, T.E., Neubert, D., 1980. Estimation of creatine phosphokinase and hydroxyproline in the developing limb: its use in evaluating the effect of teratogens on myogenesis and chondrogenesis. *Teratog Carcinog Mutagen* 1, 181-191.
- Kwasigroch, T.E., Skalko, R.G., Church, J.K., 1984. Mouse limb bud development in submerged culture: quantitative assessment of the effects of in vivo exposure to retinoic acid. *Teratog Carcinog Mutagen* 4, 311-326.
- Lee, G.S., Liao, X., Cantor, R.M., Collins, M.D., 2006. Interactive effects of cadmium and all-trans-retinoic acid on the induction of forelimb ectrodactyly in C57BL/6 mice. *Birth Defects Res A Clin Mol Teratol* 76, 19-28.
- Leonard, L., Horton, C., Maden, M., Pizzey, J.A., 1995. Anteriorization of CRABP-I expression by retinoic acid in the developing mouse central nervous system and its relationship to teratogenesis. *Dev Biol* 168, 514-528.
- Liu, W., Levi, G., Shanske, A., Frenz, D.A., 2008. Retinolic acid-induced inner ear teratogenesis caused by defective Fgf3/Fgf10-dependent Dlx5 signaling. *Birth Defects Res B* 83, 134-144.

- Mahmood, R., Mason, I.J., Morriss-Kay, G.M., 1996. Expression of Fgf-3 in relation to hindbrain segmentation, otic pit position and pharyngeal arch morphology in normal and retinoic acid-exposed mouse embryos. *Anat Embryol* 194, 13-22.
- Mallo, M., Brandlin, I., 1997. Segmental identity can change independently in the hindbrain and rhombencephalic neural crest. *Dev Dyn* 210, 146-156.
- Marshall, H., Nonchev, S., Sham, M.H., Muchamore, I., Lumsden, A., Krumlauf, R., 1992. Retinoic acid alters hindbrain Hox code and induces transformation of rhombomeres 2/3 into a 4/5 identity. *Nature* 360, 737-741.
- Morriss-Kay, G.M., Murphy, P., Hill, R.E., Davidson, D.R., 1991. Effects of retinoic acid excess on expression of Hox-2.9 and Krox-20 and on morphological segmentation in the hindbrain of mouse embryos. *EMBO J* 10, 2985-2995.
- Mulder, G.B., Manley, N., Grant, J., Schmidt, K., Zeng, W., Eckhoff, C., Maggio-Price, L., 2000. Effects of excess vitamin A on development of cranial neural crest-derived structures: a neonatal and embryologic study. *Teratology* 62, 214-226.
- Ozeki, H., Shirai, S., 1998. Developmental eye abnormalities in mouse fetuses induced by retinoic acid. *Jpn J Ophthalmol* 42, 162-167.
- Ratajska, A., Zlotorowicz, R., Blazejczyk, M., Wasiutynski, A., 2005. Coronary artery embryogenesis in cardiac defects induced by retinoic acid in mice. *Birth Defects Res A Clin Mol Teratol* 73, 966-979.
- Shimizu, H., Lee, G.S., Beedanagari, S.R., Collins, M.D., 2007. Altered localization of gene expression in both ectoderm and mesoderm is associated with a murine strain difference in retinoic acid-induced forelimb ectrodactyly. *Birth Defects Res A Clin Mol Teratol* 79, 465-482.
- Simeone, A., Avantaggiato, V., Moroni, M.C., Mavilio, F., Arra, C., Cotelli, F., Nigro, V., Acampora, D., 1995. Retinoic acid induces stage-specific antero-posterior transformation of rostral central nervous system. *Mech Dev* 51, 83-98.
- Sulik, K.K., Dehart, D.B., Rogers, J.M., Chernoff, N., 1995. Teratogenicity of Low-Doses of All-Trans-Retinoic Acid in Persomite Mouse Embryos. *Teratology* 51, 398-403.
- Taylor, L.E., Bennett, G.D., Finnell, R.H., 1995. Altered gene expression in murine branchial arches following in utero exposure to retinoic acid. *J Craniofac Genet Dev Biol* 15, 13-25.
- Tibbles, L., Wiley, M.J., 1988. A comparative study of the effects of retinoic acid given during the critical period for inducing spina bifida in mice and hamsters. *Teratology* 37, 113-125.
- Vanmuylder, N., Evrard, L., Glineur, R., Salmon, I., Gashegu, J., Rooze, M., Louryan, S., 2004. [Histologic and ultrastructural features of cell death both physiological and

induced by two different teratogens in branchial arches of mouse embryo]. *Rev Med Brux* 25, 14-20.

Wang, M., Huang, H., Chen, Y., 2009. Smad2/3 is involved in growth inhibition of mouse embryonic palate mesenchymal cells induced by all-trans retinoic acid. *Birth Defects Res A Clin Mol Teratol* 85, 780-790.

Wasiak, S., Lohnes, D., 1999. Retinoic acid affects left-right patterning. *Dev Biol* 215, 332-342.

Wood, H., Pall, G., Morriss-Kay, G., 1994. Exposure to retinoic acid before or after the onset of somitogenesis reveals separate effects on rhombomeric segmentation and 3' HoxB gene expression domains. *Development* 120, 2279-2285.

Yasuda, Y., Konishi, H., Kihara, T., Tanimura, T., 1990. Discontinuity of primary and secondary neural tube in spina bifida induced by retinoic acid in mice. *Teratology* 41, 257-274.

Zhang, Y., Liu, K., Gao, Y., Li, S., 2007. Modulation of Dishevelled and Vangl2 by all-trans-retinoic acid in the developing mouse central nervous system and its relationship to teratogenesis. *Acta Biochim Biophys Sin (Shanghai)* 39, 684-692.

Zhang, Y., Mori, T., Iseki, K., Hagino, S., Takaki, H., Takeuchi, M., Hikake, T., Tase, C., Murakawa, M., Yokoya, S., Wanaka, A., 2003. Differential expression of decorin and biglycan genes during palatogenesis in normal and retinoic acid-treated mice. *Dev Dyn* 226, 618-626.

## BIBLIOGRAPHY

---

Abbott, B.D., Best, D.S., Narotsky, M.G., 2005. Teratogenic effects of retinoic acid are modulated in mice lacking expression of epidermal growth factor and transforming growth factor- $\alpha$ . *Birth Defects Res A Clin Mol Teratol* 73, 204-217.

Abello, G., Alsina, B., 2007. Establishment of a proneural field in the inner ear. *Int J Dev Biol* 51, 483-493.

Adamska, M., Herbrand, H., Adamski, M., Kruger, M., Braun, T., Bober, E., 2001. FGFs control the patterning of the inner ear but are not able to induce the full ear program. *Mech Dev* 109, 303-313.

Alles, A.J., Sulik, K.K., 1989. Retinoic-acid-induced limb-reduction defects: perturbation of zones of programmed cell death as a pathogenetic mechanism. *Teratology* 40, 163-171.

Alles, A.J., Sulik, K.K., 1992. Pathogenesis of retinoid-induced hindbrain malformations in an experimental model. *Clin Dysmorphol* 1, 187-200.

Alsina, B., Abello, G., Ulloa, E., Henrique, D., Pujades, C., Giraldez, F., 2004. FGF signaling is required for determination of otic neuroblasts in the chick embryo. *Dev Biol* 267, 119-134.

Alsina, B., Giraldez, F., Pujades, C., 2009. Patterning and cell fate in ear development. *International Journal of Developmental Biology* 53, 1503-1513.

Alvarez, Y., Alonso, M.T., Vendrell, V., Zelarayan, L.C., Chamero, P., Theil, T., Bosl, M.R., Kato, S., Maconochie, M., Riethmacher, D., Schimmang, T., 2003. Requirements for FGF3 and FGF10 during inner ear formation. *Development* 130, 6329-6338.

Arnold, J.S., Braunstein, E.M., Ohyama, T., Groves, A.K., Adams, J.C., Brown, M.C., Morrow, B.E., 2006a. Tissue-specific roles of Tbx1 in the development of the outer, middle and inner ear, defective in 22q11DS patients. *Hum Mol Genet* 15, 1629-1639.

Arnold, J.S., Werling, U., Braunstein, E.M., Liao, J., Nowotschin, S., Edelmann, W., Hebert, J.M., Morrow, B.E., 2006b. Inactivation of Tbx1 in the pharyngeal endoderm results in 22q11DS malformations. *Development* 133, 977-987.

Ashmore J.F., Kolston P.J., 1994. Hair cell based amplification in the cochlea. *Curentr Opinion in Neurobiology*. Volume 4, Issue 4, August 1994, Pages 503-508

Bok, J., Chang, W., Wu, D.K., 2007. Patterning and morphogenesis of the vertebrate inner ear. *Int J Dev Biol* 51, 521-533.

Bok, J., Raft, S., Kong, K.A., Koo, S.K., Drager, U.C., Wu, D.K., 2011. Transient retinoic acid signaling confers anterior-posterior polarity to the inner ear. *Proc Natl Acad Sci U S A* 108, 161-166.

Bok, J.W., Bronner-Fraser, M., Wu, D.K., 2005. Role of the hindbrain in dorsoventral but not anteroposterior axial specification of the inner ear. *Development* 132, 2115-2124.

Bottcher, R.T., Niehrs, C., 2005. Fibroblast growth factor signaling during early vertebrate development. *Endocr Rev* 26, 63-77.

Brigande, J.V., Heller, S., 2009. Quo vadis, hair cell regeneration? *Nat Neurosci* 12, 679-685.

Brown, A.P., Dinger, N., Levine, B.S., 2000. Stress produced by gavage administration in the rat. *Contemp Top Lab Anim Sci* 39, 17-21.

Burton, Q., Cole, L.K., Mulheisen, M., Chang, W., Wu, D.K., 2004. The role of Pax2 in mouse inner ear development. *Dev Biol* 272, 161-175.

Cadot, S., Frenz, D., Maconochie, M., 2012. A novel method for retinoic acid administration reveals differential and dose-dependent downregulation of Fgf3 in the developing inner ear and anterior CNS. *Dev Dyn* 241, 741-758.

Campbell, J.L., Jr., Smith, M.A., Fisher, J.W., Warren, D.A., 2004. Dose-response for retinoic acid-induced forelimb malformations and cleft palate: a comparison of computerized image analysis and visual inspection. *Birth Defects Res B Dev Reprod Toxicol* 71, 289-295.

Chacon-Heszele M.F., Dongdong D., Reynolds A.B., Chi F., Chen P., 2012. Regulation of cochlear convergent extension by the vertebrate planar cell polarity pathway is dependent on p120-catenin. *Development* 139, 968-978

Chang, W., Brigande, J.V., Fekete, D.M., Wu, D.K., 2004. The development of semicircular canals in the inner ear: role of FGFs in sensory cristae. *Development* 131, 4201-4211.

Chen, W., Jongkamonwiwat, N., Abbas, L., Eshtan, S.J., Johnson, S.L., Kuhn, S., Milo, M., Thurlow, J.K., Andrews, P.W., Marcotti, W., Moore, H.D., Rivolta, M.N., 2012. Restoration of auditory evoked responses by human ES-cell-derived otic progenitors. *Nature* 490, 278-282.

Choo, D., Sanne, J.L., Wu, D.K., 1998. The differential sensitivities of inner ear structures to retinoic acid during development. *Dev Biol* 204, 136-150.

Davidson, E.H., 2006. The regulatory genome : gene regulatory networks in development and evolution. Academic, Burlington, MA ; San Diego.

De Luca, A., Maiello, M.R., D'Alessio, A., Pergameno, M., Normanno, N., 2012. The RAS/RAF/MEK/ERK and the PI3K/AKT signalling pathways: role in cancer pathogenesis and implications for therapeutic approaches. *Expert Opin Ther Targets* 16 Suppl 2, S17-27.

Dempsey, E.E., Trasler, D.G., 1983. Early morphological abnormalities in splotch mouse embryos and predisposition to gene- and retinoic acid-induced neural tube defects. *Teratology* 28, 461-472.

Dorey, K., Amaya, E., 2010. FGF signalling: diverse roles during early vertebrate embryogenesis. *Development* 137, 3731-3742.

Economou, A., Datta, P., Georgiadis, V., Cadot, S., Frenz, D., Maconochie, M., 2013. Gata3 directly regulates early inner ear expression of Fgf10. *Dev Biol* 374, 210-222. <http://dx.doi.org/10.1016/j.ydbio.2012.11.028>

Emmanouil-Nikoloussi, E.N., Goret-Nicaise, M., Foroglou, C.H., Katsarma, E., Dhem, A., Dourov, N., Persaud, T.V., Thliveris, J.A., 2000. Craniofacial abnormalities induced by retinoic acid: a preliminary histological and scanning electron microscopic (SEM) study. *Exp Toxicol Pathol* 52, 445-453.

Fekete, D.M., 1996. Cell fate specification in the inner ear. *Curr Opin Neurobiol* 6, 533-541.

Fortnum HM, Summerfield AQ, Marshall DH, Davis AC, Bamford JM. Prevalence of permanent childhood hearing impairment in the United Kingdom and implications for universal neonatal hearing screening: questionnaire based ascertainment study. *British Medical Journal* 2001;323:536-40.

Frenz, D.A., Doan, T.M., Liu, W., 1998. Regulation of chondrogenesis in the developing inner ear: a role for sonic hedgehog. *Ann N Y Acad Sci* 857, 252-255.

Frenz, D.A., Liu, W., 2000. Treatment with all-trans-retinoic acid decreases levels of endogenous TGF-beta(1) in the mesenchyme of the developing mouse inner ear. *Teratology* 61, 297-304.

Frenz, D.A., Liu, W., Cvekl, A., Xie, Q., Wassef, L., Quadro, L., Niederreither, K., Maconochie, M., Shanske, A., 2010. Retinoid signaling in inner ear development: A "Goldilocks" phenomenon. *Am J Med Genet A* 152A, 2947-2961.

Frenz, D.A., Liu, W., Galinovic-Schwartz, V., Van De Water, T.R., 1996. Retinoic acid-induced embryopathy of the mouse inner ear. *Teratology* 53, 292-303.

Frisina, R.D., 2009. Age-related hearing loss: ear and brain mechanisms. *Ann N Y Acad Sci* 1170, 708-717.

Fritzsche, B., Jahan, I., Pan, N., Kersigo, J., Duncan, J., Kopecky, B., 2011. Dissecting the molecular basis of organ of Corti development: Where are we now? *Hear Res* 276, 16-26.

Gale, E., Zile, M., Maden, M., 1999. Hindbrain respecification in the retinoid-deficient quail. *Mech Dev* 89, 43-54.

Gilbert, 2006. *Developmental Biology*, 8th edition ed. Sinauer Associates, Sunderland, Massachusetts.

Glavic, A., Maris Honore, S., Gloria Feijoo, C., Bastidas, F., Allende, M.L., Mayor, R., 2004. Role of BMP signaling and the homeoprotein Iroquois in the specification of the cranial placodal field. *Dev Biol* 272, 89-103.

Glover, J.C., Renaud, J.S., Rijli, F.M., 2006. Retinoic acid and hindbrain patterning. *J Neurobiol* 66, 705-725.

Gospodarowicz, D., Moran, J.S., 1975. Mitogenic effect of fibroblast growth factor on early passage cultures of human and murine fibroblasts. *J Cell Biol* 66, 451-457.

Gotea, V., Visel, A., Westlund, J.M., Nobrega, M.A., Pennacchio, L.A., Ovcharenko, I., 2010. Homotypic clusters of transcription factor binding sites are a key component of human promoters and enhancers. *Genome Res* 20, 565-577.

Guillemot, F., Zimmer, C., 2011. From cradle to grave: the multiple roles of fibroblast growth factors in neural development. *Neuron* 71, 574-588.

Hamburger, V., Hamilton, H.L., 1951. A series of normal stages in the development of the chick embryo. 1951. *Dev Dyn* 195, 231-272.

Hammond, K.L., Whitfield, T.T., 2011. Fgf and Hh signalling act on a symmetrical pre-pattern to specify anterior and posterior identity in the zebrafish otic placode and vesicle. *Development* 138, 3977-3987.

Hans, S., Westerfield, M., 2007. Changes in retinoic acid signaling alter otic patterning. *Development* 134, 2449-2458.

Hatch, E.P., Noyes, C.A., Wang, X.F., Wright, T.J., Mansour, S.L., 2007. Fgf3 is required for dorsal patterning and morphogenesis of the inner ear epithelium. *Development* 134, 3615-3625.

Haugas, M., Lillevali, K., Hakanen, J., Salminen, M., 2010. Gata2 is required for the development of inner ear semicircular ducts and the surrounding perilymphatic space. *Dev Dyn* 239, 2452-2469.

Hoggatt, A.F., Hoggatt, J., Honerlaw, M., Pelus, L.M., 2010. A spoonful of sugar helps the medicine go down: a novel technique to improve oral gavage in mice. *J Am Assoc Lab Anim Sci* 49, 329-334.

Hurst, J.L., West, R.S., 2010. Taming anxiety in laboratory mice. *Nat Methods* 7, 825-826.

Itoh, N., Ornitz, D.M., 2008. Functional evolutionary history of the mouse Fgf gene family. *Dev Dyn* 237, 18-27.

Iwahori, A., Fraidenraich, D., Basilico, C., 2004. A conserved enhancer element that drives FGF4 gene expression in the embryonic myotomes is synergistically activated by GATA and bHLH proteins. *Dev Biol* 270, 525-537.

Jacobson, A.G., 1963. The Determination and Positioning of the Nose, Lens and Ear. Iii. Effects of Reversing the Antero-Posterior Axis of Epidermis, Neural Plate and Neural Fold. *J Exp Zool* 154, 293-303.

Jahan, I., Kersigo, J., Pan, N., Fritsch, B., 2010. Neurod1 regulates survival and formation of connections in mouse ear and brain. *Cell and Tissue Research* 341, 95-110.

Jung, S., Choi, J.H., Hong, C., Lee, H., Park, Y.K., Shin, J.H., Park, J.W., Park, S.H., 2009. A new reporter vector system based on flow-cytometry to detect promoter activity. *Immune Netw* 9, 243-247.

Karis, A., Pata, I., van Doorninck, J.H., Grosveld, F., de Zeeuw, C.I., de Caprona, D., Fritsch, B., 2001. Transcription factor GATA-3 alters pathway selection of olivocochlear neurons and affects morphogenesis of the ear. *Journal of Comparative Neurology* 429, 615-630.

Kelley, M.W., Xu, X.M., Wagner, M.A., Warchol, M.E., Corwin, J.T., 1993. The Developing Organ of Corti Contains Retinoic Acid and Forms Supernumerary Hair-Cells in Response to Exogenous Retinoic Acid in Culture. *Development* 119, 1041-1053.

Kiecker, C., Lumsden, A., 2005. Compartments and their boundaries in vertebrate brain development. *Nat Rev Neurosci* 6, 553-564.

Kil, S.H., Streit, A., Brown, S.T., Agrawal, N., Collazo, A., Zile, M.H., Groves, A.K., 2005. Distinct roles for hindbrain and paraxial mesoderm in the induction and patterning of the inner ear revealed by a study of vitamin-A-deficient quail. *Dev Biol* 285, 252-271.

Kim, W.Y., Fritsch, B., Serls, A., Bakel, L.A., Huang, E.J., Reichardt, L.F., Barth, D.S., Lee, J.E., 2001. NeuroD-null mice are deaf due to a severe loss of the inner ear sensory neurons during development. *Development* 128, 417-426.

Kingsley, R. E., 1999, "The Auditory System," in *Concise Text of Neuroscience*, 2 edn, Lippincott Williams & Wilkins, Baltimore, pp. 393-432.

Kochhar, D.M., Penner, J.D., Tellone, C.I., 1984. Comparative teratogenic activities of two retinoids: effects on palate and limb development. *Teratog Carcinog Mutagen* 4, 377-387.

Kumano, G., Ezal, C., Smith, W.C., 2001. Boundaries and functional domains in the animal/vegetal axis of *Xenopus gastrula* mesoderm. *Dev Biol* 236, 465-477.

Kurokawa, H. & Goode, R. L. 1995, "Sound pressure gain produced by the human middle ear", *Otolaryngol Head Neck Surg*, vol. 113, no. 4, pp. 349-355.

Lammer, E.J., Chen, D.T., Hoar, R.M., Agnish, N.D., Benke, P.J., Braun, J.T., Curry, C.J., Fernhoff, P.M., Grix, A.W., Jr., Lott, I.T., et al., 1985. Retinoic acid embryopathy. *N Engl J Med* 313, 837-841.

Lawoko-Kerali, G., Rivolta, M.N., Holley, M., 2002. Expression of the transcription factors GATA3 and Pax2 during development of the mammalian inner ear. *Journal of Comparative Neurology* 442, 378-391.

Lawoko-Kerali, G., Rivolta, M.N., Lawlor, P., Cacciabue-Rivolta, D.I., Langton-Hewer, C., van Doorninck, J.H., Holley, M.C., 2004. GATA3 and NeuroD distinguish auditory and vestibular neurons during development of the mammalian inner ear. *Mechanisms of Development* 121, 287-299.

Lawrence, P.A., Struhl, G., 1996. Morphogens, compartments, and pattern: lessons from *Drosophila*? *Cell* 85, 951-961.

Lifanov, A.P., Makeev, V.J., Nazina, A.G., Papatsenko, D.A., 2003. Homotypic regulatory clusters in *Drosophila*. *Genome Res* 13, 579-588.

Lillevali, K., Haugas, M., Matilainen, T., Pussinen, C., Karis, A., Salminen, M., 2006. Gata3 is required for early morphogenesis and Fgf10 expression during otic development. *Mechanisms of Development* 123, 415-429.

Lillevali, K., Matilainen, T., Karis, A., Salminen, M., 2004. Partially overlapping expression of Gata2 and Gata3 during inner ear development. *Developmental Dynamics* 231, 775-781.

Liu, M., Pereira, F.A., Price, S.D., Chu, M.J., Shope, C., Himes, D., Eatock, R.A., Brownell, W.E., Lysakowski, A., Tsai, M.J., 2000. Essential role of BETA2/NeuroD1 in development of the vestibular and auditory systems. *Genes & Development* 14, 2839-2854.

Lott, I.T., Bocian, M., Pribram, H.W., Leitner, M., 1984. Fetal hydrocephalus and ear anomalies associated with maternal use of isotretinoin. *J Pediatr* 105, 597-600.

Ma, Q., Anderson, D.J., Fritsch, B., 2000. Neurogenin 1 null mutant ears develop fewer, morphologically normal hair cells in smaller sensory epithelia devoid of innervation. *J Assoc Res Otolaryngol* 1, 129-143.

- Mahmood, R., Mason, I.J., Morriss-Kay, G.M., 1996. Expression of Fgf-3 in relation to hindbrain segmentation, otic pit position and pharyngeal arch morphology in normal and retinoic acid-exposed mouse embryos. *Anatomy and Embryology* 194, 13-22.
- Mallo, M., 2001. Formation of the middle ear: recent progress on the developmental and molecular mechanisms. *Dev Biol* 231, 410-419.
- Marshall, H., Nonchev, S., Sham, M.H., Muchamore, I., Lumsden, A., Krumlauf, R., 1992. Retinoic acid alters hindbrain Hox code and induces transformation of rhombomeres 2/3 into a 4/5 identity. *Nature* 360, 737-741.
- McCaffery, P.J., Adams, J., Maden, M., Rosa-Molinar, E., 2003. Too much of a good thing: retinoic acid as an endogenous regulator of neural differentiation and exogenous teratogen. *European Journal of Neuroscience* 18, 457-472.
- Meijer, M.K., Spruijt, B.M., van Zutphen, L.F., Baumans, V., 2006. Effect of restraint and injection methods on heart rate and body temperature in mice. *Lab Anim* 40, 382-391.
- Min, H., Danilenko, D.M., Scully, S.A., Bolon, B., Ring, B.D., Tarpley, J.E., DeRose, M., Simonet, W.S., 1998. Fgf-10 is required for both limb and lung development and exhibits striking functional similarity to Drosophila branchless. *Genes Dev* 12, 3156-3161.
- Moeller, M.P., 2007. Current state of knowledge: psychosocial development in children with hearing impairment. *Ear Hear* 28, 729-739.
- Montagutelli X., 2000. Effect of the Genetic Background on the Phenotype of Mouse Mutations. *J Am Soc Nephrol* 11: S101-S105, 2000
- Morriss, G.M., 1972. Morphogenesis of the malformations induced in rat embryos by maternal hypervitaminosis A. *J Anat* 113, 241-250.
- Morriss-Kay, G.M., Murphy, P., Hill, R.E., Davidson, D.R., 1991. Effects of retinoic acid excess on expression of Hox-2.9 and Krox-20 and on morphological segmentation in the hindbrain of mouse embryos. *EMBO J* 10, 2985-2995.
- Mulrow CD, Aguilar MD, Endicott JE, VelezR, Tuley MR, Charlip WS, Hill JA., 1990. Association between hearing impairment and the quality of life of elderly individuals. *J Am Geriatr Soc* 38: 45-50.
- Nakada, Y., Parab, P., Simmons, A., Omer-Abdalla, A., Johnson, J.E., 2004. Separable enhancer sequences regulate the expression of the neural bHLH transcription factor neurogenin 1. *Dev Biol* 271, 479-487.
- Nardelli, J., Thiesson, D., Fujiwara, Y., Tsai, F.Y., Orkin, S.H., 1999. Expression and genetic interaction of transcription factors GATA-2 and GATA-3 during development of the mouse central nervous system. *Dev Biol* 210, 305-321.

- Niederreither, K., Subbarayan, V., Dolle, P., Chambon, P., 1999. Embryonic retinoic acid synthesis is essential for early mouse post-implantation development. *Nat Genet* 21, 444-448.
- Niederreither, K., Vermot, J., Messaddeq, N., Schuhbaur, B., Chambon, P., Dolle, P., 2001. Embryonic retinoic acid synthesis is essential for heart morphogenesis in the mouse. *Development* 128, 1019-1031.
- Ohuchi, H., Yasue, A., Ono, K., Sasaoka, S., Tomonari, S., Takagi, A., Itakura, M., Moriyama, K., Noji, S., Nohno, T., 2005. Identification of cis-element regulating expression of the mouse *Fgf10* gene during inner ear development. *Developmental Dynamics* 233, 177-187.
- Ohyama, T., Groves, A.K., 2004. Generation of Pax2-Cre mice by modification of a Pax2 bacterial artificial chromosome. *Genesis* 38, 195-199.
- Ohyama, T., Groves, A.K., Martin, K., 2007. The first steps towards hearing: mechanisms of otic placode induction. *Int J Dev Biol* 51, 463-472.
- Park, B.K., Sperber, S.M., Choudhury, A., Ghanem, N., Hatch, G.T., Sharpe, P.T., Thomas, B.L., Ekker, M., 2004. Intergenic enhancers with distinct activities regulate *Dlx* gene expression in the mesenchyme of the branchial arches. *Dev Biol* 268, 532-545.
- Patera, J., Chorostowska-Wynimko, J., Slodkowska, J., Borowska, A., Skopinski, P., Sommer, E., Wasiutynski, A., Skopinska-Rozewska, E., 2006. Morphometric and functional abnormalities of kidneys in the progeny of mice fed chocolate during pregnancy and lactation. *Folia Histochem Cytobiol* 44, 207-211.
- Patient, R.K., McGhee, J.D., 2002. The GATA family (vertebrates and invertebrates). *Curr Opin Genet Dev* 12, 416-422.
- Patuzzi, R. 1996, "Cochlear Micromechanics and Macromechanics," in *The Cochlea*, P. Dallos, A. N. Popper, & R. R. Fay, eds., Springer-Verlag, New York, pp. 186-257.
- Pauley, S., Wright, T.J., Pirvola, U., Ornitz, D., Beisel, K., Fritzsche, B., 2003. Expression and function of FGF10 in mammalian inner ear development. *Dev Dyn* 227, 203-215.
- Perron, M., Opdecamp, K., Butler, K., Harris, W.A., Bellefroid, E.J., 1999. X-*ngnr-1* and X-*ath3* promote ectopic expression of sensory neuron markers in the neurula ectoderm and have distinct inducing properties in the retina. *Proc Natl Acad Sci U S A* 96, 14996-15001.
- Pfeffer, P.L., Payer, B., Reim, G., di Magliano, M.P., Busslinger, M., 2002. The activation and maintenance of Pax2 expression at the mid-hindbrain boundary is controlled by separate enhancers. *Development* 129, 307-318.

Pickles, J. O. 1988, "The Outer and Middle Ears," in *An Introduction to the Physiology of Hearing*, 2 edn, Academic Press Limited, London, pp. 12-25.

Pirvola, U., Spencer-Dene, B., Xing-Qun, L., Kettunen, P., Thesleff, I., Fritzschn, B., Dickson, C., Ylikoski, J., 2000. FGF/FGFR-2(IIIb) signaling is essential for inner ear morphogenesis. *J Neurosci* 20, 6125-6134.

Powles, N., Marshall, H., Economou, A., Chiang, C., Murakami, A., Dickson, C., Krumlauf, R., Maconochie, M., 2004. Regulatory analysis of the mouse *Fgf3* gene: control of embryonic expression patterns and dependence upon sonic hedgehog (Shh) signalling. *Dev Dyn* 230, 44-56.

Purves, D., Williams, S.M., 2001. *Neuroscience*, 2nd ed. Sinauer Associates, Sunderland, Mass.

Quandt, K., Frech, K., Karas, H., Wingender, E., Werner, T., 1995. MatInd and MatInspector: new fast and versatile tools for detection of consensus matches in nucleotide sequence data. *Nucleic Acids Res* 23, 4878-4884.

Radosevic, M., Robert-Moreno, A., Coolen, M., Bally-Cuif, L., Alsina, B., 2011. Her9 represses neurogenic fate downstream of *Tbx1* and retinoic acid signaling in the inner ear. *Development* 138, 397-408.

Raft, S., Nowotschin, S., Liao, J., Morrow, B.E., 2004. Suppression of neural fate and control of inner ear morphogenesis by *Tbx1*. *Development* 131, 1801-1812.

Rasco, J.F., Hood, R.D., 1995a. Enhancement of the teratogenicity of all-trans-retinoic acid by maternal restraint stress in mice as a function of treatment timing. *Teratology* 51, 63-70.

Rasco, J.F., Hood, R.D., 1995b. Maternal restraint stress-enhanced teratogenicity of all-trans-retinoic acid in CD-1 mice. *Teratology* 51, 57-62.

Rhinn, M., Dolle, P., 2012. Retinoic acid signalling during development. *Development* 139, 843-858.

Riazuddin, S., Ahmed, Z.M., Hegde, R.S., Khan, S.N., Nasir, I., Shaukat, U., Butman, J.A., Griffith, A.J., Friedman, T.B., Choi, B.Y., 2011. Variable expressivity of *FGF3* mutations associated with deafness and LAMM syndrome. *BMC Med Genet* 12, 21.

Rijli FM, Dolle P, Fraulob V, LeMeur M, Chambon P, 1994. Insertion of a targeting construct in a *Hoxd-10* allele can influence the control of *Hoxd-9* expression. *Dev Dyn* 201:366-377.

Romand, R., Dolle, P., Hashino, E., 2006. Retinoid signaling in inner ear development. *J Neurobiol* 66, 687-704.

Roth, N.T., Hanebuth, D., Probst R., 2011. Prevalence of age-related hearing loss in Europe: a review. *Eur Arch Otorhinolaryngol.* 268(8): 1101-1107

Sahara, S., O'Leary, D.D., 2009. Fgf10 regulates transition period of cortical stem cell differentiation to radial glia controlling generation of neurons and basal progenitors. *Neuron* 63, 48-62.

Saitsu, H., Shiota, K., Ishibashi, M., 2006. Analysis of Fibroblast growth factor 15 cis-elements reveals two conserved enhancers which are closely related to cardiac outflow tract development. *Mech Dev* 123, 665-673.

Sanchez-Calderon, H., Milo, M., Leon, Y., Varela-Nieto, I., 2007. A network of growth and transcription factors controls neuronal differentiation and survival in the developing ear. *International Journal of Developmental Biology* 51, 557-570.

Schimmang, T., 2007. Expression and functions of FGF ligands during early otic development. *International Journal of Developmental Biology* 51, 473-481.

Shams, I., Rohmann, E., Eswarakumar, V.P., Lew, E.D., Yuzawa, S., Wollnik, B., Schlessinger, J., Lax, I., 2007. Lacrimo-auriculo-dento-digital syndrome is caused by reduced activity of the fibroblast growth factor 10 (FGF10)-FGF receptor 2 signaling pathway. *Mol Cell Biol* 27, 6903-6912.

Shield B., 2006. Evaluation of the Social and Economic Costs of Hearing Impairment, October, *Hear-it AISBL* ([www.hear-it.org](http://www.hear-it.org))

Simeone, A., Avantaggiato, V., Moroni, M.C., Mavilio, F., Arra, C., Cotelli, F., Nigro, V., Acampora, D., 1995. Retinoic acid induces stage-specific antero-posterior transformation of rostral central nervous system. *Mech Dev* 51, 83-98.

Skopinski, P., Skopinska-Rozewska, E., Sommer, E., Chorostowska-Wynimko, J., Rogala, E., Cendrowska, I., Chrystowska, D., Filewska, M., Bialas-Chromiec, B., Bany, J., 2003. Chocolate feeding of pregnant mice influences length of limbs of their progeny. *Pol J Vet Sci* 6, 57-59.

Sprinzi, G.M., Riechelmann, H., 2010. Current trends in treating hearing loss in elderly people: a review of the technology and treatment options - a mini-review. *Gerontology* 56, 351-358.

Streit, A., 2007. The preplacodal region: an ectodermal domain with multipotential progenitors that contribute to sense organs and cranial sensory ganglia. *Int J Dev Biol* 51, 447-461.

Sulik, K.K., Dehart, D.B., Rogers, J.M., Chernoff, N., 1995. Teratogenicity of Low-Doses of All-Trans-Retinoic Acid in Persomite Mouse Embryos. *Teratology* 51, 398-403.

Takahashi, K., Yamanaka, S., 2006. Induction of pluripotent stem cells from mouse embryonic and adult fibroblast cultures by defined factors. *Cell* 126, 663-676.

Tekin, M., Akay, H.O., Fitoz, S., Birnbaum, S., Cengiz, F.B., Sennaroglu, L., Incesulu, A., Konuk, E.B.Y., Bayrak, A.H., Senturk, S., Cebeci, I., Utine, G., Tuncbilek, E., Nance,

W.E., Duman, D., 2008. Homozygous FGF3 mutations result in congenital deafness with inner ear agenesis, microtia, and microdontia. *Clinical Genetics* 73, 554-565.

Thyagarajan T., Totey S., Danton, M.J.S., Kulkarni A.B., 2003. Genetically Altered Mouse Models: the Good, the Bad, and the Ugly *Crit Rev Oral Biol Med* 14(3):154-174

Timmer, J., Johnson, J., Niswander, L., 2001. The use of in ovo electroporation for the rapid analysis of neural-specific murine enhancers. *Genesis* 29, 123-132.

Tumpel, S., Maconochie, M., Wiedemann, L.M., Krumlauf, R., 2002. Conservation and diversity in the cis-regulatory networks that integrate information controlling expression of *Hoxa2* in hindbrain and cranial neural crest cells in vertebrates. *Dev Biol* 246, 45-56.

Uchikawa, M., 2008. Enhancer analysis by chicken embryo electroporation with aid of genome comparison. *Dev Growth Differ* 50, 467-474.

Umemori, H., Linhoff, M.W., Ornitz, D.M., Sanes, J.R., 2004. FGF22 and its close relatives are presynaptic organizing molecules in the mammalian brain. *Cell* 118, 257-270.

Vander, A., Sherman, J., & Luciano, D. 2001, "The Sensory Systems," in *Human Physiology*, 8 edn, McGraw-Hill, New York, pp. 227-262.

Wasiak, S., Lohnes, D., 1999. Retinoic acid affects left-right patterning. *Dev Biol* 215, 332-342.

White, J.C., Highland, M., Kaiser, M., Clagett-Dame, M., 2000. Vitamin A deficiency results in the dose-dependent acquisition of anterior character and shortening of the caudal hindbrain of the rat embryo. *Dev Biol* 220, 263-284.

White, R.J., Nie, Q., Lander, A.D., Schilling, T.F., 2007. Complex regulation of *cyp26a1* creates a robust retinoic acid gradient in the zebrafish embryo. *PLoS Biol* 5, e304.

Wood, H., Pall, G., Morriss-Kay, G., 1994. Exposure to retinoic acid before or after the onset of somitogenesis reveals separate effects on rhombomeric segmentation and 3' *HoxB* gene expression domains. *Development* 120, 2279-2285.

Wright, T.J., Mansour, S.L., 2003. *Fgf3* and *Fgf10* are required for mouse otic placode induction. *Development* 130, 3379-3390.

Wu, D.K., Nunes, F.D., Choo, D., 1998. Axial specification for sensory organs versus non-sensory structures of the chicken inner ear. *Development* 125, 11-20.

Xu, H., Viola, A., Zhang, Z., Gerken, C.P., Lindsay-Illingworth, E.A., Baldini, A., 2007. *Tbx1* regulates population, proliferation and cell fate determination of otic epithelial cells. *Dev Biol* 302, 670-682.

Yasuda, Y., Okamoto, M., Konishi, H., Matsuo, T., Kihara, T., Tanimura, T., 1986. Developmental anomalies induced by all-trans retinoic acid in fetal mice: I. Macroscopic findings. *Teratology* 34, 37-49.

Zelarayan, L.C., Vendrell, V., Alvarez, Y., Dominguez-FrutoS, E., Theil, T., Alonso, M.T., Maconochie, M., Schimmang, T., 2007. Differential requirements for FGF3, FGF8 and FGF10 during inner ear development. *Developmental Biology* 308, 379-391.